8-24-2020 2:00 PM

Characterization of Mechanotransduction in Annulus Fibrosus Cells

Min Kyu M. Kim, *The University of Western Ontario*

Supervisor: Séguin, Cheryle A., *The University of Western Ontario*

A thesis submitted in partial fulfillment of the requirements for the Doctor of Philosophy degree in Physiology and Pharmacology

Abstract

IVD degeneration is a multifactorial pathological process associated with back pain. While biomechanical factors are important regulators of IVD homeostasis, mechanical loading also contribute to the onset of IVD degeneration. Importantly, the mechanotransduction pathways that mediate cell type-specific responses to mechanical loading are not well understood. Transient receptor potential vanilloid 4 (TRPV4) is a multimodally activated cell surface cation channel implicated as a mechanoreceptor regulating the mechano-response in other musculoskeletal cell types. Using both *in vitro* and *in vivo* models, the current study aimed to characterize the role of TRPV4 in annulus fibrosus (AF) cell mechanotransduction. Using a mechanically dynamic bioreactor system, AF cells were exposed to cyclic tensile strain (CTS) to assess mechanically-induced changes in gene expression and mitogen activated protein kinase (MAPK) pathway activation. Next, a novel transgenic *Trpv4*-reporter mouse model was used to determine the expression pattern of *Trpv4* during mouse spine development and aging. TRPV4 function in AF cells was then characterized using live cell calcium imaging and treatment with pharmacological modulators of TRPV4 during CTS. Lastly, conditional *Trpv4* knockout mice (*Col2-Cre;Trpv4*$^{fl/fl}$) were used to determine the role of TRPV4 signalling in IVD health and injury-induced degeneration. These studies demonstrated that the mechano-response of AF cells was frequency-dependent, showing increased stress fibre formation, ERK1/2 pathway activation, and gene expression changes (i.e. Extracellular matrix (ECM) genes, matrix remodelling genes, mechano-sensitive genes, inflammatory cytokine genes, and mechanoreceptor genes). *Trpv4* expression was first detected during spine development, was maintained in NP and inner AF tissues and subsequently decreased with age. Activation of

TRPV4 elicited intracellular calcium response in AF cells that was shown to regulate cytoskeletal remodelling and CTS-induced changes in *Acan*, *Col1a1*, and *Prg4* expression. Furthermore, loss of *Trpv4* led to decreased proteoglycan staining and the attenuation of degenerative changes in IVDs experiencing aberrant load following injury. Taken together, our findings suggest the existence of mechanical threshold that regulates IVD health and degeneration through TRPV4-mediated mechanotransduction pathways.

Keywords

Intervertebral Disc; Annulus Fibrosus; Cyclic Tensile Strain; Actin Cytoskeleton; Gene Expression; Transient Receptor Potential Vanilloid 4; Fate-Mapping; Needle Puncture Injury; Mouse Models

Summary for Lay Audience

Back pain is a major global health challenge and one of the most common causes of disability worldwide, imposing high socioeconomic burden on individuals and healthcare systems. In North America, four out of five adults will experience back pain at some point in their lives. Currently, back pain is treated mostly with pain management strategies and disc surgery, but the outcomes are disappointing, as the causes of back pain are rarely addressed. Back pain is a complex condition with multiple causes but is typically associated with intervertebral disc (IVD) degeneration. The IVD is a joint found between the spinal column that acts as a shock absorber during movement. Similar to muscles and bones, the force experienced by IVD is important for maintaining joint health, but abnormal levels can cause damage. This adaptive response to mechanical load is regulated at the cellular level by a process called mechanotransduction, in which cells sense and change external mechanical force into biological chemical signals. However, this cellular mechanism is not well understood. Using different experimental approaches, we aimed to determine how IVD cells adapt and respond to mechanical stimulation. Our studies showed that IVD cells respond to mechanical stimulation by changing their stiffness, activating specific biochemical signals, and regulating gene expression. Interestingly, the cellular responses differed depending on the frequency of the mechanical stimulation applied to the cells. These responses were found to be mediated by a receptor protein found on the cell surface that is activated by normal and abnormal levels of mechanical loading, serving to regulate IVD health and degeneration. Our findings contribute to an important biological question in the field of spine and IVD research regarding how mechanical forces regulate joint health.

Co-Authorship Statement

Co-authorship statements are included at the beginning of each chapter.

Acknowledgments

First and foremost, and with humble sincerity, I would like to thank my supervisor, Dr. Cheryle Séguin, for your fervent support and guidance throughout my Ph.D. training. I remember our first encounter after your seminar presentation, seeing me missing the bus, you gladly offered to give me a ride back to campus from Victoria Hospital. Since then, all the support and encouragement you have given me has helped me to be where I am now. If it wasn't for your patience and belief in me, I would not have had the opportunity to develop my passion for science and teaching. You were always inviting and willing to listen to your students and organize our thoughts and concerns in such a way that seemed more manageable. Meetings with you were always a huge encouragement and motivation that refueled my confidence and passion for research. You taught me how to do research "the right way" and to present the work as clearly as possible. Aside from these skills, I thank you for opening many doors of opportunities for me during my training. I was, am, and will always be grateful for your mentorship.

I would also like to thank my advisory committee members, Dr. S. Jeff Dixon, Dr. Dean Betts, Dr. Lauren Flynn, and Dr. Rithwik Ramachandran. Dr. Dixon, thank you so much for encouraging and challenging me to be more intricate and meticulous in my thinking and approach to science and research. Dr. Betts, thank you for your kind words of encouragement at every meeting, and for handling all of my big administrative work as my Graduate Studies Committee Representative. Dr. Flynn, thank you so much for inviting me into NSERC CREATE! research cluster to expand my research perspective through different opportunities in such a collaborative environment. Dr. Ramachandran, thank you for your enthusiasm and invitation for collaboration, which helped me to diversify my research scope. To all my

advisory committee members, your presence and mentorship over the years made such a positive impact on my experience throughout this program.

I would also like to extend my deepest gratitude to Diana Quinonez and Courtney Brooks, two stellar lab technicians and the pillars of the Séguin Lab. Diana, it has been a huge blessing and pleasure working with you. Thank you so much for all of your help with maintaining the mouse colonies and helping me with tail puncture experiments. Also, thank you so much for being the best lab bench buddy – I will always treasure the countless fun talks and debates we got to have over the years. Courtney, thank you for teaching me everything I know about cell culture systems and techniques. Thank you for always being so organized and keeping all of us in-check. I am always encouraged by your passion for research and love for art. Thank you both for all that you do – none of this project would have been possible without your help.

Special thanks to my past and present lab members who brought a sense of family into my experience in the Séguin Lab. You have made coming to lab a fun and enjoyable experience. Particularly, I would like to thank Dr. Matthew McCann and Dr. Neil Tenn who helped me to settle and adjust when I was starting as a new graduate student. Dr. McCann, thank you for sitting down with me for a coffee to answer all of my questions about the lab even before I started, and for all the science advices when in need. Dr. Tenn, thank you for helping me to get set up and start my experiments with CellScale bioreactor system. I really appreciate your help in optimizing the culture protocol with me. To my labmates, thank you for all the stimulating science talks, support in research, and fun memories in and out of the lab. You all have been there in my good and bad days, sharing in achievements and helping me during hardships. Thank you for being a colleague, a friend, and a family.

To the extended cousin on the floor, the Beier Lab, thank you for your open atmosphere and willing spirits throughout the years. Special thanks to Dr. Mike Pest, Dr. Mellina Bellini, Dawn Bryce, and Holly Dupuis. Thank you for constantly answering my questions and for sharing your expertise in imaging, histology, and embryology. It has been a great pleasure working with you all.

To my friends in London and Toronto, I cannot thank you enough for always being there for me. Special thanks to members of London First Korean Presbyterian Church, who shared my decade of living in London. Thank you for all of your prayers and encouragements. Particularly, I would like to thank all the members who journeyed with me to Haiti, Guatemala, and Peru. It is a blessing to have you all in my life.

Finally, to my caring and loving family. Mom and Dad, thank you for all the sacrifices you made to support the family. Thank you for always praying for me and challenging me to live a vision-inspired life. Your support, love, and encouragement has helped me to be where I am now. To my grandmother, thank you for always believing in me and greeting me with smiles and hugs every time I come visit. I would also like to thank my cousins, Ryan, Danny, and Brian, who I grew up with. Thank you for being the most outrageous gang of brothers who I can always rely on. And to my dearest sister, Mindy, thank you for all the fun memories living together in London. I am grateful for your positive, cheerful, and loving spirit, that brightens people around you. Words cannot describe how blessed I am to have you all in my life.

I reflect on my 10 years at The University of Western Ontario and am reminded that all the people I met, memories I created, amazing mentorship I received, and exciting opportunities I came across have shaped who I am now. It has been a huge privilege and honour to have worked with such talented, bright people who strive for and invite others to excellence. I am

grateful for the Department of Physiology and Pharmacology, the Collaborative Training Program in Musculoskeletal Health Research, and many others who have contributed to my success.

Many are often humbled as normal human scales and perhaps, even existence, become miniscule amidst the grandeur of nature. On the contrary, for me, my time at Western have taught me that it is rather the finest complexity of nature, the engineered details in the micro-cellular realm of life, that reveals how great our existence is. Therefore, I praise and glorify my God, who created me and has walked with me to learn the beauty of His creation and be in awe of His creativity. Blessings!

Table of Contents

List of Tables

List of Figures

List of Supplementary Figures

List of Appendices

List of Abbreviations

Acan	aggrecan
Acta2	actin alpha 2, smooth muscle
ADAMTS	a disintegrin and metalloproteinase with thrombospondin motifs
AF	annulus fibrosus
ANOVA	analysis of variance
ATP	adenosine triphosphate
BCA	bicinchoinic acid
Bgn	biglycan
BDNF	brain derived neurotrophic factor
BMP	bone morphogenic protein
$CaCl_2$	calcium chloride
Cd24	signal transducer CD24
CDH	cadherin
cDNA	complementary deoxyribonucleic acid
CEP	cartilage endplate
CGRP	calcitonin gene-related peptide
Cilp	cartilage intermediate layer protein
CO_2	carbon dioxide
Col1a1	collagen, type I, alpha 1
Col2a1	collagen, type II, alpha1
Col10a1	collagen, type X, alpha 1
Cox2	cyclooxygenase 2

Cre	cre recombinase
CREB	cAMP response element-binding protein
C_T	cycle threshold
CTS	cyclic tensile strain
DAPI	4,6'-diamidino-2-phenylindole
Dcn	decorin
DMEM	Dulbecco's modified Eagle's medium
DMSO	dimethyl sulfoxide
DNA	deoxyribonucleic acid
E	embryonic day
ECM	extracellular matrix
EDTA	ethylenediaminetetraacetic acid
EGTA	ethylene glycol-bis(β-aminoethyl ether)-N,N,N',N'-tetraacetic acid
ERK	extracellular signal-regulated kinase
EUCOMM	The European Conditional Mouse Mutagenesis Program
F12	Ham's factor 12
Fap	fibroblast activation protein
FBS	fetal bovine serum
Fos	c-Fos proto-oncogene
Fura2-AM	Fura-2-acetoxymethyl ester
GAG	glycosaminoglycan
Gdf10	growth differentiation factor 10
GFP	green fluorescence protein

GTP	guanosine triphosphate
HEPES	4-(2-hydroxyethyl)-1-piperazineethanesulfonic acid
Hprt	Hypoxanthine-guanine phosphoribosyltransferase
IAF	inner annulus fibrosus
IgG	immunoglobulin G
IL-1β	interleukin 1 beta
IL-6	interleukin 6
IL-8	interleukin 8
IRES	internal ribosome entry site
Itgβ1	integrin subunit beta 1
Itgα5	integrin subunit alpha 5
IM	intervertebral mesenchyme
IP3	inositol triphosphate
IVD	intervertebral disc
JNK	c-Jun N-terminal kinases
KCl	potassium chloride
$K_3Fe(CN)_6$	potassium ferricyanide
$K_4Fe(CN)_6$	potassium ferrocyanide
KIF3B	kinesin-like protein member 3B
KO	knock out
KOH	potassium hydroxide
Krt	cytokeratin
LPM	lateral plate mesoderm

MAPK	mitogen activated protein kinase
MCB1	MechanoCulture B1
$MgCl_2$	magnesium chloride
MKII	MAP kinase-activated protein kinase 2
MMP	metalloproteinase
MPa	Megapascal
MRI	magnetic resonance imaging
mRNA	messenger ribonucleic acid
MSC	mesenchymal stem cell
NaCl	sodium chloride
NC	notochord
N-CDH	N-cadherin
NEO	neomyocin
NGF	nerve growth factor
NOS	nitric oxide synthase
Noto	notochord homeobox
NP	nucleus pulposus
OCT	optimal cutting temperature
P2X	P2X purinoreceptor
P2Y	P2Y purinoreceptor
p38	cytokinin specific binding protein
PAR	protease activated receptor
PBS	phosphate buffered saline

PCR	polymerase chain reaction
PI3K	phosphoinositide 3-kinase
PN	postnatal day
Prg4	proteoglycan 4, lubricin
PV	prevertebrae
R26	ROSA26
RFP	red fluorescent protein
RGD	arginylglycylaspartic acid
RIPA	radioimmunoprecipitation assay buffer
RNA	ribonucleic acid
ROCK	rho-associated protein kinase
ROI	region of interest
ROS	reactive oxygen species
RUNX	runt-related transcription factor
SAPK	stress activated protein kinase
SEM	standard error of the mean
Shh	sonic hedgehog
SMA	smooth muscle actin
SOX9	SRY-Box transcription factor 9
T	brachyury
TBST	tris-buffered saline
TGF	transforming growth factor
TIMP1	tissue inhibitor of metalloproteinase

TLR	toll-like receptor
Tnfα	tumor necrosis factor alpha
TRP	transient receptor potential
TRPA	transient receptor potential ankyrin
TRPC	transient receptor potential canonical
TRPM	transient receptor potential melastatin
TRPML	transient receptor potential mucolipin
TRPN	transient receptor potential NOMP-C
TRPP	transient receptor potential polycystin
TRPV	transient receptor potential vanilloid
TRPV4	transient receptor potential vanilloid 4
VB	vertebral bone
VEGF	vascular endothelial growth factor
WBV	whole body vibration
WT	wild-type
X-Gal	5-bromo-4-chloro-3-indolyl-β-D-galactopyranoside

Chapter 1

1 Introduction and Review of the Literature

1.1 Overview

Musculoskeletal disorders are the second most common cause of disability worldwide, with disability-adjusted life years and prevalence increasing exponentially annually[1]. Among them, back pain is the leading cause of years lived with disability in more than half of the world. The etiology of back pain is not fully understood; it can originate from different anatomical structures of the spine including, ligaments, paravertebral musculatures, vertebral bones, spinal nerve roots, facet joints, but is most commonly associated with intervertebral disc (IVD) degeneration[2,3]. While pain management treatments are available, they do not adequately improve clinical outcomes and no disease modifying treatments exist for IVD degeneration. The current lack of therapeutic interventions for IVD degeneration is related to our limited understanding of the mechanisms regulating IVD development, homeostasis, and degeneration.

This chapter provides an overview of the current understanding of IVD biology, discussing topics ranging from spine development to the structural and molecular characteristics of normal and degenerative IVDs. Also described are the different experimental models used to study the molecular, cellular, and tissue-level effects of mechanical loading on the IVD as well as our knowledge of cellular mechanosensing and mechanotransduction in the musculoskeletal system.

1.2 Spine as a Joint Complex

The term spine describes a collection of vertebral bones (vertebrae) articulated in an interlocking stacked column[4]. This structure is found at the posterior midline of the body acting as the primary structural support for the torso. In taxonomic hierarchy, the vertebral column defines the subphylum *Vertebrata* of the phylum *Chordata*[5]. Specifically, the human spine is composed of 33 vertebrae divided into five anatomical regions: 7 cervical, 12 thoracic, 5 lumbar, 5 sacral, and 4 coccygeal[6] (**Figure 1.1A**). The zygapophyseal joints between the superior and inferior facets of the vertebral articular processes (commonly referred to as facet joints), as well as the intervertebral discs (IVDs) located between the vertebral bodies are the two major joints that form the articulations and serve as shock-absorbers for the 24 presacral vertebrae (**Figure 1.1B**). Functionally, the facet joints maintain vertebral alignment and allow for flexion-extension of the spine, while partially limiting axial rotation, lateral bending, as well as translation (glide) motions enabled by IVDs[7].

1.3 The Intervertebral Disc

The IVD is a connective tissue structure located between the vertebral bodies essential for spine stabilization, load bearing and movement. Anatomically, IVDs are composed of three distinct yet interdependent tissues: the gelatinous, highly hydrated central nucleus pulposus (NP), the outer fibrous annulus fibrosus (AF) encapsulating the NP, and the cartilage endplates (CEP) that anchor the disc to the adjacent vertebrae[8] (**Figure 1.1C**). Accordingly, IVDs are not uniform in their composition, possessing the components of both fibrous and cartilaginous connective tissues, and are therefore considered as fibrocartilage tissue[9]. The cells of the NP and AF have distinct developmental origins and produce a distinct

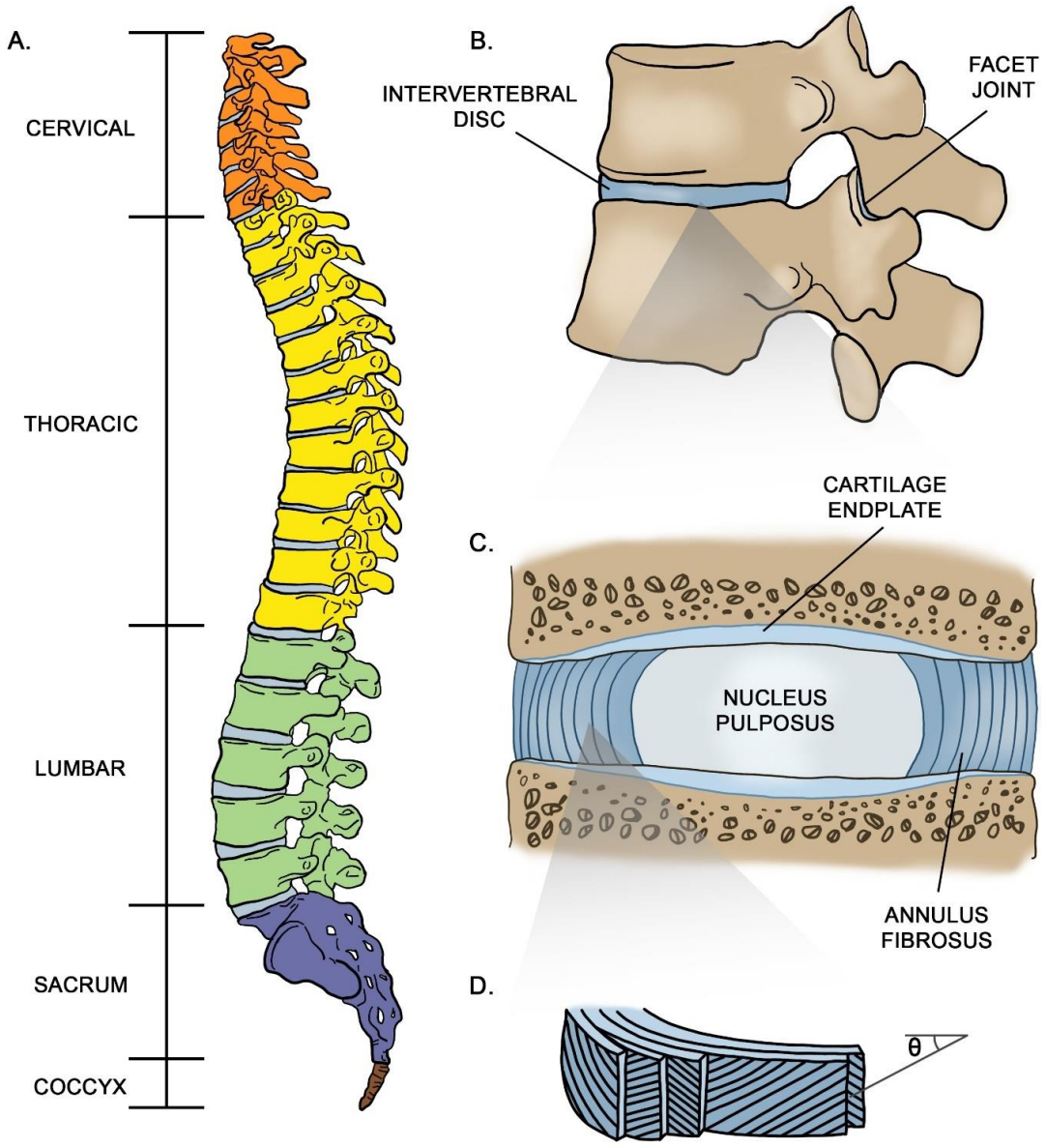

Figure 1.1. Schematic representation of the human spine, joint structure and intervertebral disc.

A) Illustration of the human spine highlighting the different anatomical regions. The human spine is made up of 33 vertebrae: 7 cervical (orange), 12 thoracic (yellow), 5 lumbar (green), 5 sacral (purple; sacral vertebrae are fused and collectively known as sacrum), and 4 coccygeal (brown; vertebrae fused and collectively called coccyx). B) Intervertebral discs are the joints between the vertebral bodies while the facet joints articulate the vertebral spinous processes. C) The intervertebral disc is composed of three tissues: the central nucleus pulposus that is contained radially by the annulus fibrosus and superiorly/inferiorly by the cartilage endplates. D) The annulus fibrosus is formed by concentric lamellae with parallel bundles of type I collagen which form an angle-ply structure, allowing for the annulus fibrosus to resist tensile strain.

extracellular matrix (ECM) compatible with the mechanical function of each tissue, that together form the complex microarchitecture required for proper disc function[10]. The interdependency of these tissue types requires maintenance of the integrity of all three disc tissues, as the breakdown of any one will functionally impact the others. Within each tissue, the cellular activity, including ECM production and the cellular response to mechanical loading, shapes the physiological and biomechanical functions of the IVD.

1.3.1 The Nucleus Pulposus

The NP is an aneural, avascular gelatinous tissue that forms the innermost core of the IVD. It is composed of water (70-90%), proteoglycans (50% of dry weight) and type II collagen (20% of dry weight)[11–13]. Proteoglycans found in the NP can be divided into two distinct classes: aggregating and non-aggregating proteoglycans. Large aggregating proteoglycans (i.e. aggrecan and versican) are monomers that form large aggregates through cross-linking with hyaluronan[14–17]. These monomers contain protein cores covalently linked to numerous sulphated glycosaminoglycans (GAG) side chains (i.e. chondroitin sulphate and keratan sulphate)[18,19]. Almost 90% of aggrecan's mass is attributed to GAG chains, each containing ~100 chondroitin sulphate chains and up to 60 keratan sulphate chains[20]. These sulphated side chains confer a strong negative charge which allows them to attract water molecules and provides viscoelastic properties to the tissue[21]. Non-aggregating proteoglycans include members of the small leucine-rich proteoglycans (i.e. biglycan, decorin, and fibromodulin) and other matrix proteoglycans that are important in the control of collagen fibrillogenesis, growth factor binding and sequestration, and interact with signalling molecules controlling proliferation, differentiation and ECM homeostasis[22,23]. In addition to proteoglycans, fibrillar proteins, such as type II collagen, are irregularly arranged and distributed

throughout the NP, providing a three-dimensional mesh-like microarchitecture to support both the proteoglycans and resident cell populations[12,22].

A feature that distinguishes the NP from other IVD tissues is its drastic change in cellular composition over time. In some species (e.g. rodents, cats and non-chondrodystrophoid dogs), the NP is formed and populated at birth by large vacuolated notochordal cells (30-40 μm in diameter) that persist through most of adulthood. In contrast, in other species (e.g. horses, and humans), the notochordal cells that initially populate the NP are progressively lost within the first decade after birth[24–28] and the NP becomes instead populated by small chondrocyte-like NP cells[24,25]. Historically, there have been two hypotheses regarding the origin of the cartilage-like cells of the NP. It was originally suggested that these NP cells were of mesenchymal origin, populating the NP following migration from the surrounding cartilage endplates[29]. Notochordal cells were thought to direct mesenchymal cell migration, stimulate matrix synthesis, and then undergo apoptosis[30,31]. Alternatively, it was suggested that notochord cells act as progenitors of the NP cells, and undergo terminal differentiation to produce cartilage-like cells (notochord cell maturation model)[32–34]. Previous fate mapping studies demonstrated that, at least in mice, chondrocyte-like NP cells are derived from the embryonic notochord[35,36]. Notably, the loss of notochordal cells is associated with the initiation of early degenerative changes in the IVD, suggesting that this cell population is crucial for the maintenance of the NP[37–39]. Recent studies also reported that hypertrophic cells detected in the NP during age-associated IVD degeneration are also of notochordal origin, formed by fusion of chondrocyte-like NP cells to form nested lacunae[40].

1.3.2 The Annulus Fibrosus

The AF is a highly organized tissue that circumferentially surrounds the NP. In contrast to the NP, the AF is composed of water (60-80%), with a greater proportion of collagen (50-70% dry weight) than proteoglycan (10-20% dry weight)[12,41]. The AF is formed by 15-25 concentric lamellae (in humans), each composed of parallel bundles of collagen fibres in an angle-ply fibre orientation[22,42]. Specifically, collagen fibres are oriented at 25-30° from the transverse plane in alternating orientation with each subsequent lamella[42] (**Figure 1.1D**). Individual lamellae are separated by an interlamellar proteoglycan-rich ECM (i.e. aggrecan, versican, lubricin, and elastin) produced by its resident cells[42,43]. It is thought that the interlamellar network formed by elastin fibres maintains the integrity of the lamellar structure, enabling the structure to recoil after deformation[43,44]. The AF is further divided into inner and outer regions, distinguishable by differences in cell shape and interlamellar ECM composition. The outer AF lamellae are primarily made up of tightly arranged bundles of type I collagen with resident cells exhibiting an elongated fibroblast-like morphology and adhering to collagen fibres within the lamellae[45,46]. The inner AF serves as a transition between the NP and AF tissues. Its matrix contains decreased levels of type I collagen compared to the outer AF, with increased concentration of type II collagen, and increased proteoglycan-rich interlamellar matrix produced by cells that show more rounded morphology[42,45,46]. This heterogeneity in the profile of the AF ECM may be due to different types and magnitudes of load experienced in different regions of AF tissues *in vivo*[45–48].

1.3.3 The Cartilage Endplate

IVDs are bordered at the superior and inferior ends by cartilage endplates, thin layers of hyaline cartilage that cover the vertebral bone creating an interface with the AF and NP[12]. The ECM of the CEP is composed of proteoglycans and type II collagen, populated by chondrocytes with a similar phenotype to those found in articular cartilage[49]. The orientation of the collagen fibres varies regionally across the CEP, with fibres running parallel to the vertebral bodies in the centre of the CEP (NP interfacing region) but are curved closer to the inner AF region. These curved collagen fibres merge with the collagen fibres of the AF (along with elastin fibres oriented parallel to collagen fibres) to structurally anchor the inner AF to the CEPs[50,51]. The collagen fibres in the outer AF penetrate the thinner layer of CEP and become interwoven with fibrillar matrix of vertebral bone to form a stable anchor[52].

The CEP serves important structural, load bearing, and barrier functions in the IVD. First, it acts as a structural barrier to separate the IVD from the adjacent vertebrae and contain the NP[10,49]. Secondly, the ECM composition and structure of the CEP allow it to evenly distribute compressive load originating from the IVD onto the vertebral body [53,54]. Lastly, the CEP functions as a semi-permeable barrier through which small molecules and solutes diffuse into the primarily avascular IVD. Although a blood supply is present in the outer AF, the inner AF and NP are avascular. As such, these tissues rely on solute diffusion as the primary source of nutrients from the capillary beds located in the bony endplate of the vertebrae [50]. The central zone of the CEP allows for the highest diffusion of small molecules such as oxygen and glucose, owing to the higher tissue porosity and GAG content in the central region[55–58]. With age, the CEP becomes thinner and other defects

such as fissures or calcification may prevent adequate nutrient supply, contributing to IVD degeneration[22,54].

1.4 Spine Development

As detailed above, the IVD is a heterogeneous structure formed by different tissues with distinct cell types, specific ECM composition, and tissue architecture. As such, complex mechanisms regulate embryonic IVD development. Previous studies have used different animal models to understand IVD development, including frogs (*Xenopus laevis*)[59,60], zebrafish[61,62], chick[63,64], and mice[35,36]. This section will provide an overview of the current understanding of murine IVD development since the studies outlined in the current thesis exclusively use the mouse as a model system.

1.4.1 Node and Notochord Development

In the early mouse embryo, the key event required for subsequent development of the spine is initiated at embryonic day (E)7.5, when the node is formed near the anterior end of the primitive streak (**Figure 1.2A**)[65]. The node is a transient structure located at the distal tip of the early embryo, responsible for establishing a left asymmetry of embryo patterning[66–68]. Monocilia that protrude from cells located on the apical surface of the node generate a rotation (clockwise rotation when viewed from the ventral size) to drive a leftward flow of extra-embryonic fluid containing morphogens, such as *Nodal* and *Cerl-2*, secreted by the epithelial cells found at the ventral node[66,68–70]. This unidirectional flow (referred to as nodal flow) regulates left side patterning via two possible mechanisms: i) through direct induction of differentiation on the left side of the embryo by morphogens carried through

the leftward nodal flow (formation of morphogen gradient) (**Figure 1.2B**)[69,71], or ii)

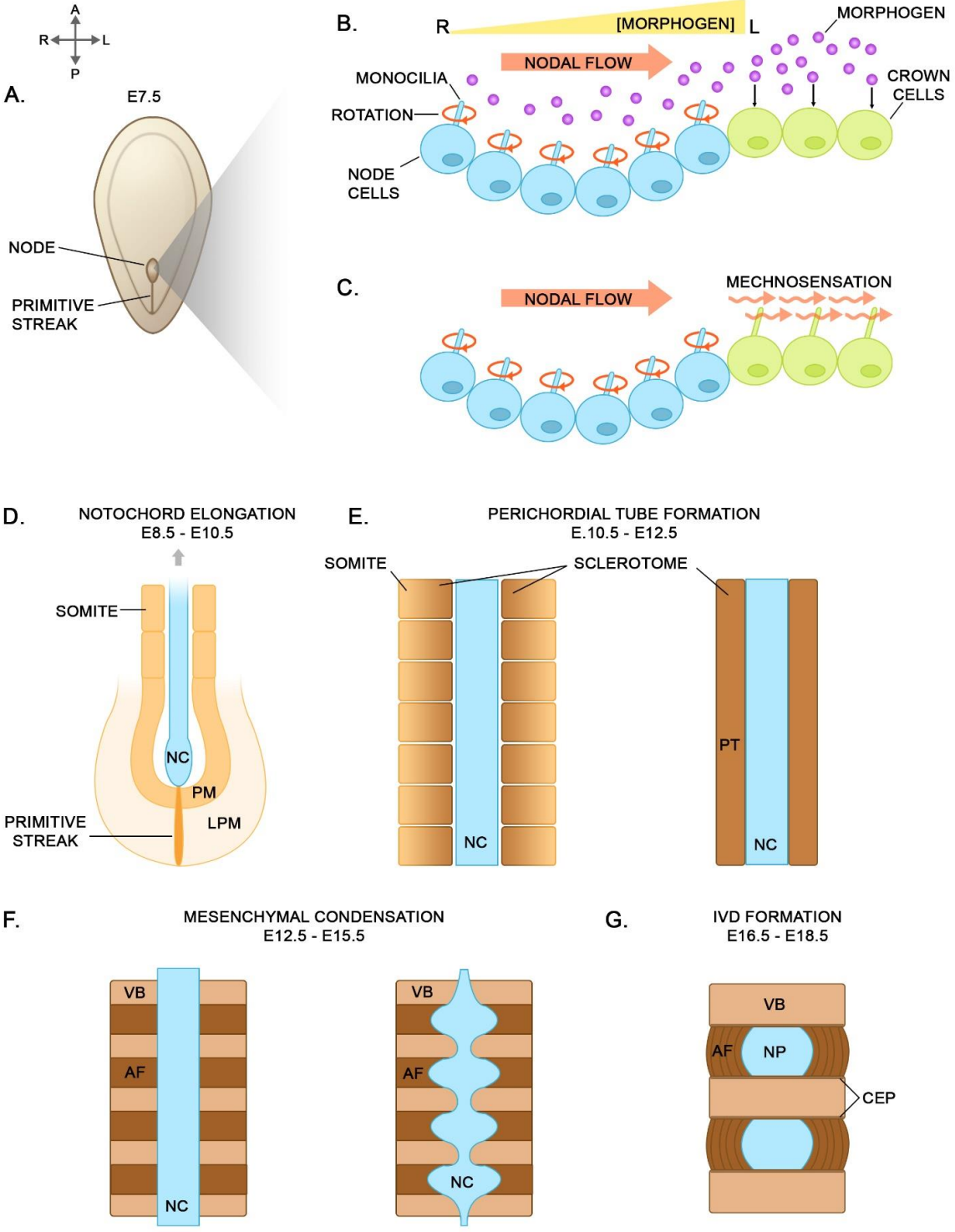

Figure 1.2. Schematic illustration of nodal flow models and key stages of murine spine development.

A) Node cells found within the node at embryonic day (E)7.5 create a nodal flow that is essential for left/right patterning of the embryo. A, anterior. P, posterior. L, left. R, right. Node cells contain monocilia that rotate in a clockwise direction, creating a leftward flow of extra-embryonic fluid, called nodal flow (B, C). In the mouse embryo, two possible mechanisms have been proposed to explain the contribution of nodal flow to embryo patterning. B) The nodal flow transports morphogens to the left side of the embryo, creating a gradient of signals. C) The leftward fluid flow is sensed by crown cells, leading to activation of mechano-sensitive calcium signalling. D) After node formation, by E9.0, notochord (NC) is formed flanked by paraxial mesoderm (PM) laterally. The cells of the notochord migrate, and the notochord elongates. The PM then undergoes segmentation to form the somites. LPM, lateral plate mesoderm. E) By E12.5, inner regions of the somites differentiate into sclerotome and aggregate around the NC for form perichordal tube (PT). F) Mesenchymal cells, found at the inner layer of PT, condense around the NC, acquiring a metameric pattern of condensed and non-condensed regions, which will form the annulus fibrosus (AF) and vertebral bone (VB), respectively, leading to NC segmentation. Metameric patterning is followed by segmentation of the NC. G) Formation of primitive intervertebral discs is associated with disappearance of NC within the VB regions, after which immature structures of nucleus pulposus (NP), AF, VB, and cartilage endplate (CEP) can be detected.

through fluid flow induction of mechanosensitive calcium signalling in peri-nodal crown cells that promote cells specification (physical stimulation) (**Figure 1.2C**)[72]. Although the underlying mechanisms remain to be elucidated, nodal flow creates left-right symmetry during development. By E9.0, mesodermal cells ingress through the primitive streak to form a solid rod-like structure called the notochord (axial mesoderm), flanked laterally by the paraxial mesoderm, which will go on to form the somites (**Figure 1.2D**)[67]. The cells that form the notochord migrate from the node and elongate along the central midline of the embryo to form the notochord[52,62]. In a developing embryo, the notochord serves two important functions. First, the notochord acts as a primitive axial support resisting compression along the primitive longitudinal (anterior/posterior) axis as the embryo grows[52]. Second, the notochord serves as a signalling centre, secreting morphogens, such as sonic hedgehog (*Shh*) and noggin, responsible for patterning of surrounding tissues[35,73].

1.4.2 The Patterning of the Axial Skeleton

Development of axial skeleton is a complex, stepwise process that requires intricate coordination of cell signalling and differentiation. At E6.0 gastrulation establishes three germ layers of the embryo: the ectoderm, which forms the skin and nervous system, the endoderm, which forms the digestive, respiratory, and urinary system, and the mesoderm, which forms the circulatory system, muscles, bones, and connective tissues[74]. The mesoderm is further divided into three compartments: lateral plate mesoderm, intermediate mesoderm, and paraxial mesoderm[74]. From E7.5-E11.5, the paraxial mesoderm undergoes segmentation to form the somites (**Figure 1.2D**)[75]. Somites are transient structures that pattern and segment the embryo along the anterior-posterior axis[76]. At E12.5 *Shh* released from the notochord directs the somites to a sclerotomal fate by inducing paired box 1

(*Pax1*) gene expression, facilitating sclerotome cells to aggregate and condense around the notochord to form a perichordal tube (**Figure 1.2E**)[77,78]. These sclerotome gives rise to the ribs, vertebral bodies, CEP and AF of the IVD[76]. By E13.5, mesenchymal cells from the inner layer of perichordal tube accumulate around the notochord and acquire a metameric pattern of condensed and non-condensed segments that later give rise to the AF and vertebral bodies, respectively (**Figure 1.2F**)[35,36,77]. Concurrent with mesenchymal condensation, the notochord regresses in the regions where the vertebral bodies will develop, but expands within the prospective IVD regions, exhibiting the "moniliform" shape (**Figure 1.2F**)[76]. The processes that control notochord segmentation are unclear. One possible mechanism is biomechanical force exerted by the developing vertebral bodies, squeezing the notochord cells toward the prospective IVD regions[79,80]. In support of proposed mechanical force model of notochord segmentation, pan-*Col2a1* knockout mice (*Col2a1*$^{-/-}$) showed defects in vertebral bone formation and retention of the notochord in developing spine, leading to either the absence or reduced size of the NP in the IVD[79]. The segmented notochord can be detected at E15.5, after which immature structures of NP, AF, and vertebral bodies begins to form (E16.5-E18.5) (**Figure 1.2G**)[77].

1.5 Back Pain and Intervertebral Disc Degeneration

The most recent *Global Burden of Disease Study* reports that low back pain is the leading cause of years lived with disability in 126 of 195 countries and territories studied[1]. In fact, low back pain has been one of the top three causes of years lived with disability globally since 1990, with the over 245 million newly reported cases in 2017[1]. Clinically, low back pain is one of the most common reasons for doctor visits, with a reported lifetime prevalence of 84% in North America, making it the most prevalent medical condition [81–

[84]. On a socioeconomic level, back pain is associated with a substantial economic burden on the healthcare system, as well as indirect costs decreased productivity and work absence among affected individuals[84,85]. In the United States alone, back pain accounts for more than $100 billion in annual health care costs[86,87]. Although back pain may manifest and affect individuals at all ages, the debilitating impact on quality of life is more severe in the older population[88]. With the aging population and increased life expectancy, the socioeconomic burden of back pain is expected to rise globally.

Back pain can originate from a single or combination of different anatomical structures of the spine, including muscles, ligaments, vertebral bones, spinal nerve roots, facet joints, and IVDs[81,82]. However, approximately 30% of cases of chronic back pain are associated with radiographic findings of IVD degeneration[89]. Currently, there are no disease-modifying treatments for IVD degeneration or its associated back pain. Treatment options are limited to pain management and, in severe cases, surgical approaches such as spinal fusion or artificial disc replacement that show limited efficacy, stressing the need for the development of novel therapeutic interventions[90–92]. Such treatment strategies for IVD degeneration should not only aim to eliminate painful symptoms, but should target the restoration of tissue structure and function. Although the etiology and pathophysiology of IVD degeneration is still unclear, multiple interdependent factors, including altered mechanical loading[22,93,94], reduced nutrient supply[38,56], and genetics[95,96], have been implicated in the initiation and progression of this degenerative cascade.

IVD degeneration, has been perhaps best defined as a progressive cell-mediated response to aberrant mechanical load that activates a non-reversible cascade of changes in the cells and their microenvironment, ultimately leading to structural and functional failure[22]. The

pathogenesis of IVD degeneration is marked by loss of the balance between anabolic and catabolic processes in the tissue, associated with increased matrix degradation and abnormal matrix synthesis[9]. In the IVD, matrix remodelling is mediated by the matrix metalloproteinase (MMP) and disintegrin and metalloproteinase with thrombospondin motifs (ADAMTS) families of catabolic enzymes that break down major ECM components such as collagens and proteoglycans[97]. These enzymes are expressed in healthy IVD tissues, playing an important role in adaptive tissue matrix remodelling. However, IVD tissue degeneration initiates when there is an imbalance between ECM degradation and new matrix synthesis. In the human IVD, proteoglycan fragmentation is first detected during childhood, and with increasing age, there is a gradual decrease in proteoglycan content (i.e. aggrecan)[97,98]. Cleaved aggrecan fragments do not aggregate, making them less effective in attracting water molecules[97,98]. In addition to the overall degradation of the ECM during IVD degeneration, altered matrix synthesis and composition are observed. Along with decreased aggrecan, the inner AF and the NP show increased biglycan production, while the outer AF show decreased decorin and increased biglycan and fibromodulin production[99]. In addition, the relative proportions of chondroitin sulphate and keratan sulphate decrease in the NP[100]. The collagen synthesis pattern is also altered, with more type II collagen appearing in the outer AF and type I collagen expression increased in the inner AF and NP[97,101]. These alterations in ECM composition lead to reduced water content in the NP[98,101,102], reducing its ability to absorb and redistribute compressive forces during axial loading[98,101,102]. Due to a loss of intradiscal pressure, the AF deforms by in- and out-ward bulging and buckling, leading to structural defects such as rim lesions, circumferential tears, and radial fissures, which may lead to IVD herniation[94,103].

Furthermore, with age, the CEP undergoes progressive thinning and calcification, leading to reduced nutrient diffusion, acidic pH, and complete oxygen deprivation[56,104–106]. This degenerative cascade is also associated with increased levels of proinflammatory cytokines, such as interleukin 1 (*IL-1*) and tumor necrosis factor α (*TNF-α*) in the IVD that can upregulate catabolic enzymes, exacerbating the degenerative changes[22,97]. In advanced IVD degeneration, such as disc herniation, increased levels of inflammatory cytokines can stimulate NP cells to produce neurotropic and angiogenic factors, such as nerve growth factor (NGF), brain derived neurotrophic factor (BDNF), and vascular endothelial growth factor (VEGF), that can promote neuronal and vascular ingrowth[107]. Sensory neurons that are found in degenerated IVDs are often NGF-dependent neurons immunoreactive for calcitonin gene-related peptide (CGRP), involved in pain perception related to inflammatory pain, leading to discogenic back pain[108].

1.6 Mechanical Load and Intervertebral Disc Degeneration

1.6.1 Mechanical Environment of Intervertebral Disc

The primary function of the IVD is to act as a shock absorber for the spine. The mechanism by which the IVD accommodates such mechanical demands was first described in the 'hydrostatic model' by Schmorl[109]. When a healthy IVD is under load, the compressive load is absorbed by the highly hydrated, aggrecan-rich NP. The resulting pressure within the NP is redistributed radially to the surrounding AF and vertically to the CEP. The consequent radial pressure exerted by the NP is then balanced by the elastic tension that develops in the concentric lamellae of the AF[8,22,48] (**Figure 1.3**). Accordingly, during axial loading, NP cells experience hydrostatic and osmotic pressure, while AF cells experience tensile and shear stress[110]. Similar to other musculoskeletal tissues, the IVD is sensitive to

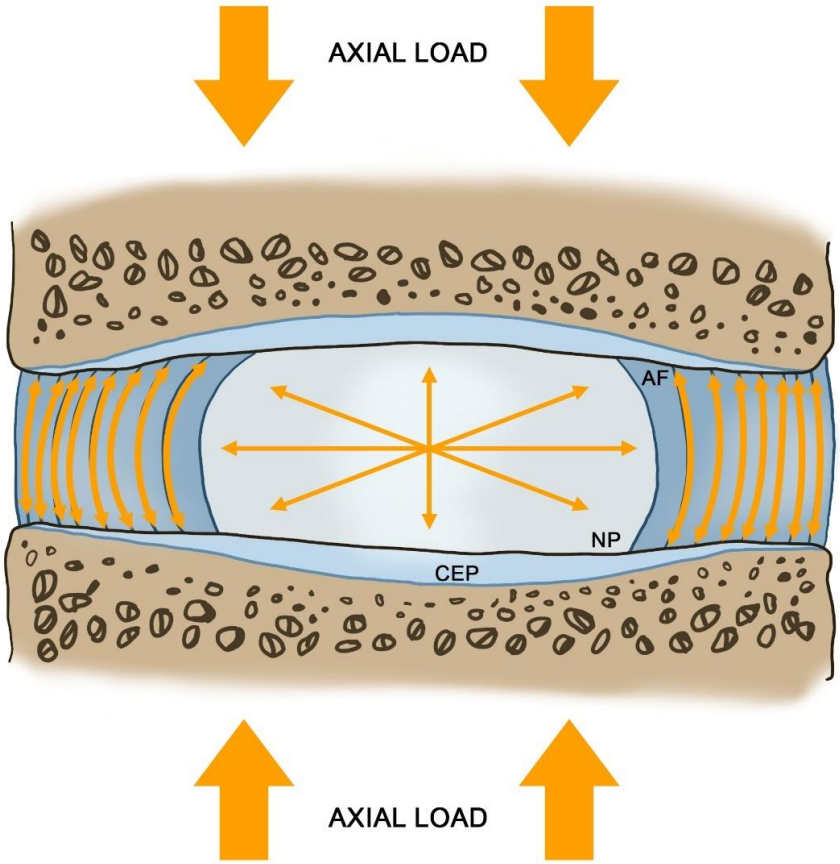

Figure 1.3. Schematic illustration depicting mechanical forces experienced by the intervertebral disc (IVD) during axial load.

The interdependent tissues of the IVD work together to absorb mechanical load in the spine. Upon load, the compressive forces are absorbed by the highly hydrated nucleus pulposus (NP). The NP contains a high concentration of negatively charged proteoglycans that imbibe water. The compressive load absorbed by the NP creates an intradiscal pressure around the surrounding annulus fibrosus (AF). The AF accommodates this pressure by stretching radially, creating tension along its concentric lamellae.

its mechanical environment and depends on these mechanical cues for maintenance of its structural integrity. Cells of the IVD respond to mechanical stimuli by changing gene expression and other cellular processes that enable the tissue to adapt to their environment[48,110].

Information on mechanical stresses experienced by human IVDs *in vivo* are limited to a few studies that reported intradiscal pressure measured by inserting needle pressure transducers into the lumbar IVDs of healthy subjects performing various activities[111–113]. These studies reported a baseline intradiscal pressure of 0.1-0.2 MPa in supine bedrest and 0.5 MPa in a standing posture. High pressure was measured while performing various activities, peaking at 2.3 MPa during heavy lifting. Furthermore, loading frequencies were found to rage between 0.1 – 1.0 Hz when performing normal daily activities (bed rest to walking)[53]. With recent studies reporting increased risk of IVD degeneration by the use of needle disc puncture[114], more recent studies used *ex vivo* models to characterize the strain profile of the human IVDs. These studies demonstrated that the AF experiences tissue strain ranging from 1-26% during compressive loading that generated physiologically relevant pressure in the IVD (0.74±0.15 MPa) [53,115,116].

1.6.2 Altered Mechanical Load and Intervertebral Disc Degeneration

Mechanical loading is one of the risk factors that contribute to the onset of IVD degeneration. Previous studies reported that IVD degeneration is most frequently detected in the lower lumbar IVDs (i.e. L3/L4 and L4/L5)[117,118] – sites experiencing higher mechanical stress compared to IVDs in other lumbar levels[119]. In humans, over-loading either through exposure to occupational hazards[120,121] or intense recreational activities such as weightlifting[122] are associated with IVD degeneration. On the other hand, under-loading

due to extended bedrest[123] or exposure to microgravity[124,125] also contribute to IVD degeneration. A number of studies investigating the effects of mechanical stimulation on IVD cells have proposed that a physiological 'window' of loading parameters exists that elicits anabolic response in the IVD cells. Indeed, studies demonstrate that mechanical stimulation of physiologically relevant parameters induces anabolic response, such as up-regulated matrix gene expression, while aberrant 'non-physiological' loading parameters (i.e. under- and over-load) leads to catabolic response, including increased matrix degrading enzyme expression and cell death.

1.7 Mechanotransduction in the Intervertebral Disc

Mechanotransduction refers to the process by which cells sense and convert a mechanical input (i.e. physical force) into intracellular biochemical signalling pathways to elicit biological responses[126]. In the context of the IVD, cells not only respond to mechanical cues through interaction with their ECM, but also to direct mechanical stimulation, causing cell deformation, cell membrane stretching and cell volume changes[110]. Importantly, mechanisms by which IVD cells sense mechanical loads are still poorly understood. The mechanical environment, and thus, type of strain, experienced is cell type and region specific[127]. Given the complex loading environment of the IVD, studies have used different models to understand the mechano-response and identify candidate mechanotransduction pathways in the IVD at the cell or tissue level.

1.7.1 *In Vitro* Models of Mechanobiology in the Intervertebral Disc

In vitro studies using mechanically dynamic bioreactor systems have been extensively used to study the effects of mechanical stimulation on IVD cells. Although human cells are

optimal for translation of findings, access to human IVD cells is limited to surgical or post-mortem samples where the age, gender, and levels of degeneration influence the results observed. In particular, access to 'healthy' controls is limited in human tissues. In comparison, animal models are more readily available to study the pathobiology of IVD degeneration. IVD cells from large (cows, pigs, and sheep) and small (mice, rats, and rabbits) animals have been used to study the cellular response to different types of mechanical load, including tensile, compressive, and fluid shear strains. *In vitro* loading parameters used are generally based on values reported in human IVDs. For example, tensile loading at 10% strain and 1.0 Hz is generally used to recapitulate the strain profile experienced by the human AF during daily activity.

Bioreactor systems have been widely used to characterize the mechano-response of AF cells to tensile load. Several studies used the commercially available Flexcell® tension bioreactor that uses a pneumatic system to deliver biaxial cyclic tensile strain (CTS) to flexible culture surfaces. Using this system, exposure of bovine AF to 10% CTS at 1.0 Hz for 60 min induced remodelling of F-actin filaments and microtubules, with increased gene and protein expression of β-actin and β-tubulin. CTS-stimulated bovine AF cells showed increased type I collagen and type II collagen gene expression compared to the unloaded control. Interestingly, this CTS protocol increased *MMP2*, *MMP3* and *ADAMTS5* gene expression, but decreased *MMP1* and *MMP9* gene expression[128]. Moreover, studies using these devices stablished that rabbit AF cells respond differently based on the magnitude, frequency, and duration of the applied load as well as in the presence of interleukin 1 beta (IL-1β)[129]. Rabbit AF cells stimulated with IL-1β in static culture showed increased expression of catabolic genes, including, inducible nitric oxide synthase (*iNOS*),

cyclooxygenase 2 (*COX-2*), *MMP3*, and *MMP1*. However, mechanical stimulation at physiological range (3% - 6% at 0.1 Hz - 1.0 Hz) decreased the expression levels of *iNOS, COX2,* and *MMP3*. Notably, exposure of rabbit AF cells to high mechanical loading (18% CTS at 0.1 Hz for 24 h) upregulated the expression of all catabolic genes increased by IL-1β and downregulated *TIMP1,* a natural inhibitor of MMP proteins. Complementing studies using the commercial bioreactor system, previous work by Gawri *et al*[130] used a bioreactor systems to deliver low-frequency high-magnitude strains[131] to IVD cells. These studies demonstrated that prolonged exposure of human NP and AF cells to 20% CTS at 0.001 Hz promoted the secretion of factors detected in IVD degeneration that promote neurite outgrowth and cell death, including toll-like receptor 2 and 4, neuronal growth factor, and tumor necrosis factor α[130]. Building on these findings, recent studies have investigated the mechanosensitive signalling pathways mediating the response of AF cells to tensile load. In human AF cells, α5β1 integrin receptor activation and mitogen-activated protein kinase (MAPK) signalling (i.e. extracellular signal regulated kinase 1/2 (ERK1/2), c-Jun N-terminal kinase JNK, and p38) have been shown to mediate CTS-induced inflammatory cytokine gene expression changes(i.e. *COX-2*, *IL-6*, *IL-8*)[132,133].

To date, the study of NP cell mechanotransduction has focused on bioreactor systems that delivers cyclic compression to NP cells in 3-dimensional (3D) culture. Exposure of rat NP cells to cyclic compression (10% scaffold deformation at 1.0 Hz; 6 h per day) for 10 days increased aggrecan and type II collagen gene and protein expression, while maintaining phenotypic NP markers (i.e. *Krt19*, *Foxf1*, and *Pax1*)[134,135]. Moreover, human NP cells exposed to hydrostatic pressure using parameters that model *in vivo* loading (0.25 MPa at 0.1 Hz) for 30 min showed decreased matrix degrading enzyme gene expression, including

MMP2 and *MMP3*. In contrast, increased loading of rat NP cells at 1.3 MPa at 1.0 Hz induced a catabolic response marked by decreased aggrecan and type II collagen gene expression, increased reactive oxygen species generation, and the expression of markers of cell senescence (i.e. p16 and p53)[136]. Studies by Li *et al*[137] demonstrated that the response of porcine NP cells to mechanical load was dependent on the magnitude, frequency, and duration of loading – a cellular behaviour also detected in CTS-induced AF cells. Specifically, these studies showed increased GAG content and type II collagen staining, as well as decreased cell death in porcine NP cells exposed to 0.4 MPa compression at 1.0 Hz. The opposite effect was observed in porcine NP cells exposed to 1.3 MPa compression at 5.0 Hz, with decreased aggrecan and type II collagen gene expression and increased MMP3 and ADAMTS4 gene expression[137]. Using a 3D culture system, dynamic compression induction of *Krt19*, *Foxf1*, and *Pax1* gene expression was shown to be driven by N-Cadherin mediated PI3K/Akt pathway activation. Dynamic compression also increased the expression of N-Cadherin (*Cdh2*), suggesting potential role for the N-Cadherin adhesion molecule in NP mechanotransduction[135]. Moreover, hyperosmotic stress elicited an intracellular calcium transient in rat NP cells that mediated aquaporin2 (*Aqp2*) gene expression[138]. Interestingly, intracellular calcium transients were only detected in porcine NP cells exposed to hyperosmotic stress after actin cytoskeleton destabilization[139].

Taken together, these studies establish the existence of a range of mechanical loading parameters that promote an anabolic response in IVD cells, however they also demonstrate the existence of a threshold beyond which mechanical loading induces tissue catabolism. However, it is important to acknowledge that *in vitro* models do not recapitulate the

complex loading environment experienced *in vivo*, nor the direct interaction between IVD cell types that may contribute to the cellular response.

1.7.2 *Ex Vivo* Models of Mechanobiology in the Intervertebral Disc

Ex vivo organ culture models allow the preservation of tissue architecture and biochemical components to study IVD mechanotransduction in cells within their innate environment. Early studies on an IVD explant organ culture system investigated the effects of static culture in rabbit IVDs within alginate gels, and found that IVDs embedded in alginate gel maintained higher sulphated GAG, antigenic keratan sulphate, hyaluronan, and collagen compared to the free swelling controls, suggesting that cellular activity in the explant can be modulated by tuning culture conditions[139]. Subsequent studies introduced static compression (0, 0.2, 0.4, 0.8, and 1.0 MPa) to mouse caudal IVDs, and demonstrated dose-dependent increased cell apoptosis[140]. To improve cell viability in explant, ovine caudal IVDs were anticoagulated to allow for adequate CEP permeability and cultured in cyclic uniaxial diurnal loading (0.2 MPa for 8 h and 0.8 MPa for 16 h) for up to 7 days[141]. These studies showed increased solute diffusion through the endplate by cyclic loading, leading to improved cell viability and increased GAG synthesis. Moreover, studies simulating physiological load (cyclic compression alternating in magnitude ranging from 0.1 - 0.6 MPa at 1 Hz for 16 h per day, followed by 8 h of low cyclic load of 0.1 - 0.2 MPa) on caprine lumbar IVD showed that after 21-day of culture, increased cell viability and increased *ACAN* and *COL2A1* gene expression were detected in both NP and AF compared to static controls[142]. Among the matrix remodelling genes assessed, *TIMP1* and *ADAMTS4* were up-regulated in the NP, suggesting simulated physiological load preserved the native properties of caprine IVDs in culture.

Another advantage of organ culture system is the ability to investigate drivers of IVD degeneration in the microenvironment. Previous studies cultured bovine caudal IVDs under static or dynamic loading with or without exogenous TNFα in culture, simulating an inflammatory state of surrounding spinal tissues[143]. In IVDs under dynamic loading, exogenous TNFα increased the production and secretion of inflammatory cytokines (TNFα, IL-1β and IL-6) as well as increased tissue stiffness compared to the controls. In addition, *ex vivo* organ culture has been used to study IVD mechanical injury. Acute mechanical injury was induced in healthy human IVDs by rapid compression by 30%, inducing CEP cracks[144]. Compared to uninjured controls (received 5% compression), IVD injury caused significantly increase in cell death. Proteoglycan content within the injured IVD was reduced, but its content in the matrix was increased. Increased matrix metalloproteinase and aggrecanase activity were detected in injured tissue, and injured IVDs secreted elevated levels of inflammatory cytokines and nerve growth factors. Other injury models such as needle puncture or burst fractures in bony endplate have also been adopted to study their effects on IVD mechanical properties and degenerative progression *ex vivo*[145–147].

1.7.3 *In Vivo* Models to Study Mechanobiology in the Intervertebral Disc

In order to study the effects of mechanical loading *in vivo*, two general categories of animal models have been used, with load induced by either exercise or IVD injury.

Exercise-induced models aim to increase joint tissue loading through the introduction of specific forms of exercise, typically designed to model human activities. Previous work by our group developed a whole-body vibration platform suitable for small rodents to deliver high-frequency low-amplitude whole body vibration (WBV), mimicking parameters used

in clinical and commercial settings for whole-body vibration[148–150]. 10-week-old CD1 male mice were exposed to WBV (45 Hz, 0.3 g, 30 min/day, 5 days/week) for 4 weeks to study the effects of whole-body vibration on IVD health. Following 4 weeks of vibration, mice showed signs of IVD degeneration with disrupted AF structure, increased cell death, and up-regulated *Mmp3* gene expression, which correlated with increased staining of MMP-cleaved collagen and aggrecan fragments[148]. With longer exposure to vibration (8 weeks), IVD tissues showed increased expression of *Mmp3*, *Mmp13*, *Adamts5* and *Il-1β*[149].

IVD injury models disrupt IVD structure to alter mechanical loading both at the site of injury as well as at adjacent IVDs and allow for reproducible and inducible IVD degeneration. In the context of the mouse, three models have been established, all of which target the caudal (tail) spines: Tail Compression, Tail Looping, and AF Needle Puncture. First, the tail compression model first developed by Lotz *et al*[151], involves the insertion of pins into two adjacent caudal vertebrae which are then fixed to external rings connected by spring-suture system to deliver static compressive load to the IVD between the two vertebrae. The system can be adjusted to control the magnitude of static compression delivered. Previous work showed that with increasing compressive stress, the inner and middle AF became progressively more disorganized with increased cell death and decreased aggrecan and type II collagen gene expression[151]. A similar model was developed in the rat to immobilize or deliver cyclic compression loading to caudal IVDs[152]. Rats that underwent 72 h of immobilization and subsequent 1.5 h cyclic compression (1.0 MPa at 2.0 Hz) showed catabolic response, with decreased type I collagen, and type II collagen gene expression and increased *Mmp3* and *Adamts4* gene expression[152].

Secondly, the tail looping model developed by Sakai *et al*[153] is a procedure where the tail is looped and caudal vertebra (Co)5 and Co13 are fixed together using wire, followed by removal of distal tail from Co14. In this model, the IVDs upstream of Co5 (Co2/Co3 and Co3/Co4) are used as internal control. The caudal IVDs within the loop are subjected to chronic compressive load and assume a wedged shape and histological signs of severe degeneration marked by NP fibrosis and loss of AF lamellar structure are detected within 4 weeks[153].

Lastly, AF needle puncture models cause acute mechanical instability following decompression (i.e. herniation) of the NP. Loss of the NP impairs the ability of the punctured IVD to withstand compression during normal tail movement, and aberrant loads are transferred to adjacent IVD tissues proximal and distal to punctured IVD. Yang *et al*[154] first adopted the AF puncture model in mice, showing advanced degeneration in punctured caudal IVDs. More recently, the IVDs adjacent to the punctured IVD were used to study tissue response to aberrant load following injury[155,156].

Together, *in vitro* and *in vivo* models have informed our current understanding of cellular mechano-response and mechanically induced degeneration in the IVD. Despite the growing evidence that mechano-regulatory processes regulate IVD health and degeneration, the mechanisms by which cells respond to normal and aberrant load is unknown. Accordingly, cellular mechanosensation in the IVD must be considered.

1.8 Mechanoreceptors: Mechanosensation at the Cell Membrane

All cells of the body are subjected to external mechanical forces from their environment. The detailed molecular mechanisms that underlie mechanotransduction processes can be complex and specific to cell types and their pericellular environments. However, central aspects of cell mechanotransduction are shared in all cells. First, mechanical force is sensed by mechanoreceptors. Mechanoreceptors are cell surface molecules that usually undergo force-induced conformational changes to couple a biochemical event directly or allosterically[157]. Second, activated mechanoreceptors then interact with 'mechano-transmitters' to transduce activation signals, initiated near cell membrane, via specific cytoplasmic signalling pathways[158]. Third, these signalling cascades then act on downstream mechano-targets to regulate cellular processes, including gene expression, proliferation, and cytoskeletal remodelling[159]. Importantly, the emergence of these mechanosensitive "receptorome" allows for studies of mechanosensation and mechanoadaptation at the cellular level.

Within a biological system, mechanical stimuli can function as a ligand similar to a biochemical molecule. Types of mechanical load include hydrostatic pressure, compression, tension, shear stress, osmotic forces, or matrix stiffness, all leading to cellular deformation[160]. Moreover, similar to how the effect of a biochemical ligand is regulated by ligand concentration, receptor concentration and frequency of action, a mechanical force can vary in magnitude, frequency, and duration. Finally, given the significance of mechanical input to proper physiological function, receptor-ligand specificity exists, with specific cell surface receptors capable of receiving different mechanical inputs. These

mechanical inputs can directly change receptor conformation through distinct mechanisms depending on the receptor type.

1.8.1 Integrins

Integrins are a class of cell adhesion molecules that regulate interactions between a cell and its surrounding ECM[161]. Mechanical activation of integrins occur through a hinge movement mechanism[126] (**Figure 1.4A**). Structurally, integrin receptors are heterodimers consisting one alpha (α) and one beta (β) subunit bound non-covalently. Currently, 18 α and 8 β subunits are known to exist in humans, which are reported to form 24 distinct heterodimers[162]. Integrins participate in various signalling events, controlling gene expression, cell cycle, and apoptosis[161,163]. Among the known heterodimers, the α5β1 and α5β3 are used ubiquitously by cells to interact with fibronectin within the ECM[161,164]. Under physiological conditions, α5β1 and α5β3 integrins assume a bent conformation, which represents an inactive state with low to moderate affinities for ligands[162]. As a transmembrane mechanical link between the intracellular and extracellular environment, integrins are often subjected to tensile forces applied externally at the head or internally at the cytoplasmic tail where the cytoskeleton is attached. During mechanical stimulation, this tension can cause a conformational change from the bent to the extended state, leading to receptor activation[165–167]. Force-induced receptor activation has been shown to strengthen integrin-mediated adhesion, increase fibronectin production and reinforce integrin-ligand bond[165,168,169].

In the context of the IVD, integrin subunit expression profile studies reported α1, α5, αv, α6, β1, β3, β4, β5 subunits to be expressed in human and porcine IVDs[170]. Specifically, α5β1 integrin signalling has been reported to mediate the mechano-response of human NP

and AF cells to dynamic compression, resulting in decreased aggrecan (*ACAN*) and *ADAMTS4* gene expression[171]. Furthermore, studies using mechanically dynamic organ

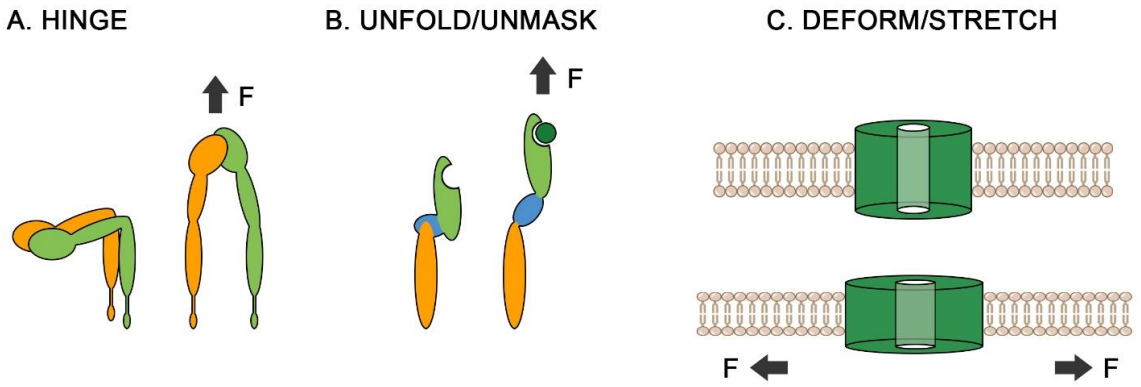

Figure 1.4. Schematic illustration depicting the different mechanisms of mechanosensation by mechanoreceptors.

Mechanosensitive receptor proteins have the ability to change their structure in response physical forces. Different receptors, potentially due to their physical structure or secondary mechanism of signal transduction, adopt different force-induced rearrangement for their activation. A) Hinge activation describes when receptors in a bent position (inactive state) are extended by mechanical force, resulting in receptor activation. B) The unfolding/unmasking mechanism is a force-gated process that involves mechanical force changing the conformation of a receptor to reveal specific activation sites that are otherwise auto-inhibited (buried). C) Deformation by stretch is a common mechanism adopted by pore-forming ion channel receptors, in which membrane stretch leads to direct conformational change leading to receptor activation (channel opening).

culture system reported that α5β1 integrin signalling mediates mechanically-induced apoptosis and induces *Mmp3, Mmp13* expression in rat IVD cells[172].

1.8.2 Cell-Cell Receptors

A specific example of a cell-cell receptor, the Notch receptor, is mechanically activated by an unfolding/unmasking mechanism[157] (**Figure 1.4B**). Notch receptors are transmembrane receptors that regulate cell-cell communication. Notch signalling affects diverse cellular processes, from cell fate decisions during development to the regulation of tissue homeostasis in mature tissues. Notch receptor activation occurs in a juxtacrine manner by cell surface ligands from neighbouring cells[173]. Notch ligands are single-pass transmembrane proteins that are members of the DSL (Delta/Serrate/LAG-2) family[173,174]. Upon activation, the Notch receptor exposes S2 site where ADAM metalloprotease-mediated proteolytic cleavage occurs[174]. Cleavage at this site leads to intracellular cleavage to release the Notch intracellular domain that localizes to the nucleus and regulates gene expression[175]. Interestingly, although ligand binding relieves Notch receptor of its auto-inhibited conformation, this conformational change alone is not sufficient for unmasking the S2 site. A tensile force created by the neighbouring cell through ligand-receptor binding further unmasks the S2 site for cleavage[173,176–179]. Hence, Notch activation is mechanically regulated and requires a pulling force to expose an otherwise buried S2 cleavage site.

In the IVD, activation of Notch signalling induces cell type-specific effects. Activation of Notch signalling in healthy AF cells from the rat model suppressed *Acan* and *Col1a1* gene expression while promoted expression of *Adamts4* gene. In contrast, Notch activation in healthy NP cells did not induce any change in ECM gene expression, but suppressed catabolic gene expression (*Mmp3, Mmp13, Adamts4*, and *Adamts5*)[180]. Furthermore, in

human IVDs, Notch signalling was increased in AF and NP cells of degenerated human IVDs compared to healthy controls, with proinflammatory cytokines inducing Notch signalling in the NP cells [181,182].

1.8.3 Ion Channels

The activation of mechanically gated pore-forming ion channels occur through deformation due to membrane stretch[157] (**Figure 1.4C**). The transient receptor potential (TRP) ion channels are a family of cation channels that serve as sensors for a broad spectrum of stimuli[183]. TRP ion channels are mechanosensitive, responding to tension, cell swelling, cell shrinkage, compression, and shear stress[184–189]. It is important to note that in all mechanical stimuli reported to activate TRP channels, the force experienced at the site of ion channel activation, is membrane deformation. Two distinct models of mechanical gating have been proposed for TRP channels. The membrane tension model states that tensile force applied to the lipid bilayer generates membrane tension to gate the channel[190]. For example, using a strategy based on detergent solubilization of frog oocyte membrane proteins followed by liposome reconstitution and evaluation by patch-clamp, studies reported that TRPC1 channel activation was achieved by direct membrane stretch[189]. Alternatively, the tether model involves applied force being transmitted through a tether connecting the channel with cytoskeleton and other periphery proteins to gate the channel[190]. Studies demonstrated that the cytosolic domain of TRPN channels acts as a membrane-microtubule connectors that serve as tethering sites for the channel, microtubule and cell membrane[191]. TRPN channels were found to co-localize with the microtubule cytoskeleton and pharmacological disassembly of the microtubules impaired TRPN mechano-activation[192]. Given that TRP channels are diverse in their types and modes of

activation, they may appropriate different mechanisms of channel activation depending on type and sensitivity to stimuli. Nevertheless, both models demonstrate force-induced gating mechanism for TRP ion channels.

Since the first reports of mammalian TRP channels[193,194], they have been widely implicated in the regulation of tissue homeostasis and disease in many organ systems. In recent years, TRP ion channels have been studied in the context of musculoskeletal health research, as detailed in the following section.

1.9 Transient Receptor Potential Vanilloid 4 in the Musculoskeletal System

The TRP channels are a family of membrane bound non-selective cation channel proteins involved in different homeostatic functions in mammals[183]. The discovery of TRP channels revealed a potential mechanisms by which cells are able to sense their environment, as TRP channels are activated by a diverse array of physical and chemical stimuli, including osmolarity, heat, cold, pH, metabolites, and mechanical loading[195,196]. The TRP superfamily is divided into seven subfamilies by sequence homology: TRPC (canonical), TRPV (vanilloid), TRPM (melastatin), TRPP (polycystin), TRPML (mucolipin), TRPA (ankyrin), and TRPN (NOMP-C)[197,198]. Given their diversity in both activation and function in cell physiology, TRP channel dysfunction contributes to wide array of diseases, which were identified through point mutations (channelopathies) or genetic modification of TRP channels in mouse models[195,199]. Accordingly, TRP channels have emerged as novel pharmacological targets for treating disease in major organ systems.

Specifically, TRPV4 is a calcium (Ca^{2+})-permeable, nonselective cation channel that transduces environmental cues into cellular responses by generating intracellular Ca^{2+} transients[196]. TRPV4 contains 6 transmembrane spanning α helix domains with a pore loop that acts as a selectivity filter allowing for Ca^{2+} permeability[200,201] (**Figure 1.5A**). TRPV4 was first isolated from rat kidney, reported to be activated by exposure of cells to hypotonicity[202]. The hypotonic osmotic stress caused cell swelling, leading to activation of phospholipase A2 (PLA2)[203]. PLA2 was found to hydrolyze cell membrane lipids to produce arachidonic acid, which is metabolized to epoxyeicosatrienoic acids that directly activate TRPV4 channel through cytochrome P450[203,204]. Later, TRPV4 was found to be multi-modally activated, mediating signalling pathways following thermal, chemical, mechanical stimuli, as well as pain and inflammation[197,202,205,206]. Recent studies have shown that TRPV4 is expressed and functionally relevant in musculoskeletal tissues including cartilage and bone[207,208].

In murine chondrogenic cells, pharmacological activation of TRPV4 increased *Sox9* gene expression, which is critical for chondrocyte differentiation[207]. In the context of mechanotransduction, TRPV4 was shown to regulate the metabolic response of porcine chondrocytes to dynamic compressive loading, specifically the induction of *Tgf-β3* expression[206]. Moreover, TRPV4 activation by hypo-osmotic stimulation enhanced chondrocyte Ca^{2+} signalling, which was necessary for regulatory cell volume decrease and prostaglandin E2 production[209]. Mice with global deletion of *Trpv4* (*Trpv4*$^{-/-}$) show accelerated osteoarthritis and increased subchondral bone volume compared to wild-type[210]. In addition to accelerated age-associated osteoarthritis, *Trpv4*$^{-/-}$ mice fed high-fat diet had increased weight gain, adiposity, and more severe osteoarthritis compared to wild-

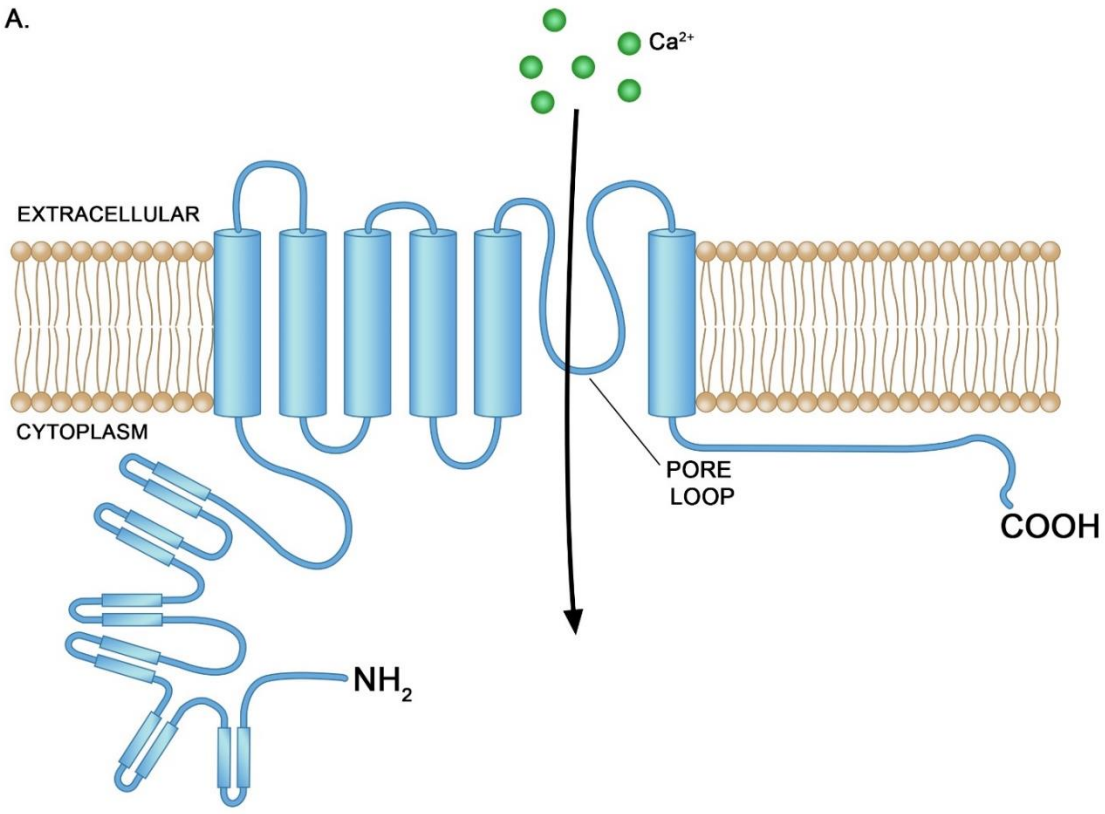
A.
Ca^{2+}
EXTRACELLULAR
CYTOPLASM
PORE
LOOP
COOH
NH_2

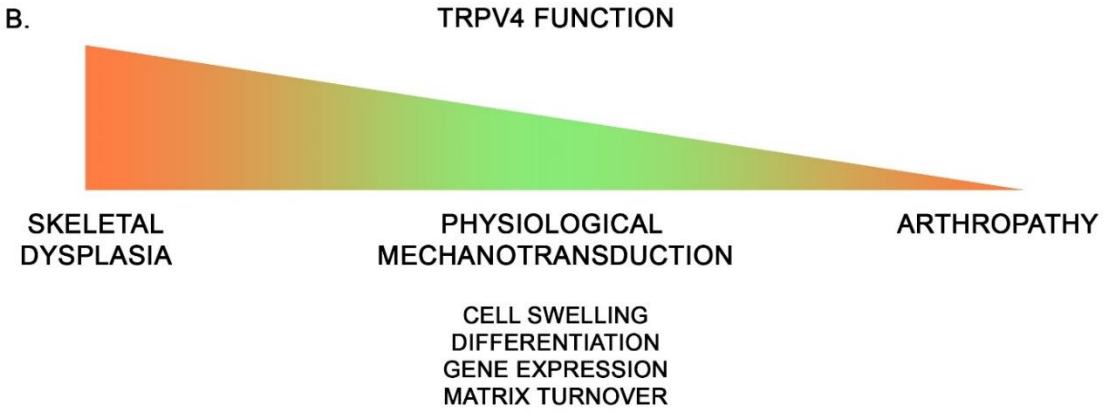
B.
TRPV4 FUNCTION
SKELETAL
DYSPLASIA
PHYSIOLOGICAL
MECHANOTRANSDUCTION
ARTHROPATHY
CELL SWELLING
DIFFERENTIATION
GENE EXPRESSION
MATRIX TURNOVER

Figure 1.5. Transient receptor potential vanilloid 4 structure and function.

A) TRPV4 is a membrane spanning cation channel with 6 transmembrane domains, a pore loop region, and intracellular C- and N-terminus ends. B) TRPV4 ion channels are multi-modally activated calcium (Ca^{2+})-permeable cation channels that regulate numerous cellular processes. Specifically, TRPV4 acts as a mechanoreceptor in bone and cartilage tissues. Mechanically induced TRPV4 signalling regulates cell swelling, differentiation, gene expression and matrix turnover (i.e. bone formation and resorption). In the musculoskeletal system, expression and activity of TRPV4 is tightly regulated as demonstrated by channelopathies associated with alterations in channel activity. TRPV4 gain-of-function mutations cause skeletal dysplasia whereas loss of TRPV4 accelerates arthropathic changes.

type mice on the same diet[211]. Recently, using an inducible, cartilage-specific *Trpv4* knockout mouse model (*Col2a1-CreER^{T2}; Trpv4$^{lox/lox}$*), O'Conor et. al[212] showed that loss of TRPV4-mediated signalling in chondrocytes at skeletal maturity reduced the severity of age-associated osteoarthritis.

Mechanical stimulation and Ca^{2+} signalling are important for bone homeostasis. TRPV4 is expressed by both osteoblasts and osteoclasts and serves to regulate bone formation and resorption[213]. In osteoblastic cells, BMP2-mediated signalling enhances TRPV4 expression, thereby regulating cell differentiation. In differentiated osteoblasts, TRPV4 activation is necessary for fluid flow-induced Ca^{2+} oscillations[214]. In *Trpv4$^{-/-}$* mice, osteoclast cell number and bone resorption activity are decreased compared to wild-type mice, leading to increased bone mass and trabecular bone volume[208]. The opposite phenotype was observed in mice carrying osteocyte-specific gain-of-function TRPV4 mutation, which showed increased osteoclast numbers and resorptive activity compared to wild-type, leading to overall bone loss. Clinically, gain-of-function TRPV4 mutations have been associated with a range of skeletal dysplasias, such as brachyolmia and metatropic dwarfism[215,216].

Recently, TRP channels have been studied in the context of the IVD. Studies using gene array analysis to compare healthy and degenerate human IVDs identified 26 out of 28 currently known TRP genes to be expressed irrespective of health status[217]. Among the 26 TRP genes identified, *TRPV4*, *TRPC6*, *TRPM2* and *TRPML1* expression was increased in degenerate IVDs compared to the healthy controls[217,218]. Furthermore, work by Walter *et al*[219] demonstrated that in an IVD organ culture model, decreased osmolarity induced TRPV4 expression and activity, leading to increased TRPV4-mediated intracellular Ca^{2+}

influx, regulating inflammatory cytokine gene expression. While previous studies have begun exploring the expression and function of TRP channels in degenerative IVDs, the role of TRPV4 in IVD mechanobiology and tissue homeostasis remains largely unexplored.

1.10 Rationale, Hypotheses and Objectives

Aim 1: Quantify the Effects of Mechanical Loading on Annulus Fibrosus Cells

Rationale: Previous studies examining the effects of mechanical loading on AF cells were limited to the analysis of extracellular matrix and matrix remodelling genes[47,128,132,133,220,221]. Information characterizing the effects of mechanical load on other biologically relevant genes (i.e. mechanosensitive genes, inflammatory cytokines, mechanoreceptor proteins) in AF cells is limited. Furthermore, the characterization of MAPK signalling in mechanically stimulated human AF cells was limited to cells derived from degenerative tissue, which has been reported to affect the cellular response to mechanical loading[133]. To address these limitations, we used the commercially available *MechanoCulture* device to deliver bi-axial cyclic tensile strain (CTS) to primary murine AF cells. Using this device, we quantified the effects of acute exposure of mechanical loading on AF cell gene expression and other cellular processes, using parameters of frequency, magnitude, and duration designed to recapitulate a range of physiological conditions.

Hypothesis: Exposure of AF cells to physiological loading will induce anabolic changes, specifically up-regulating the expression of anabolic genes and suppressing the expression of catabolic genes.

Objective 1: Validate mechanically-dynamic culture using the *MechanoCulture B1* bioreactor

Objective 2: Quantify the effects of acute exposure to CTS on AF cells

Objective 3: Identify mechanosensitive pathway(s) in AF cells following acute exposure to CTS

Aim 2: Characterize the Expression Pattern and Function of TRPV4 in the Murine IVD

Rationale: TRPV4 was identified as a potential target to examine how IVD cells sense external cues since it is known to be activated by many stimuli and mediates a wide range of physiological responses. For example, previous studies reported the physiological importance of TRPV4 as a multimodal receptor, osmosensor[202,209], puriceptor[222,223], thermosensor[224], and mechanosensory[206,208,214] in different tissues. Studies examining the role of TRPV4 in the musculoskeletal system have largely focused on articular cartilage and bone[206–209,213,214]. Our analysis of mechanically-induced gene expression in murine AF cells demonstrated increased *Trpv4* expression following acute exposure to CTS (Aim1). Importantly, the expression pattern and function of TRPV4 in the IVD remains unknown. Using a novel *Trpv4* reporter mouse we sought to examine the spatiotemporal localization of TRPV4 as well as its functional activation in the murine IVD to assess its potential role in regulating IVD biology.

Hypothesis: TRPV4 expression and activity is necessary for the development of the IVD and for mediating mechano-response of AF cells to cyclic tensile strain.

Objective1: Determine the spatiotemporal expression profile of *Trpv4* in the murine spine

Objective 2: Determine the function of TRPV in AF cell mechano-response

Aim 3: Determine the Role of TRPV4 in IVD Health and Injury

Rationale: Studies conducted in Aim 2 demonstrated that TRPV4 is expressed and functionally active in the murine IVD, mediating mechanically-induced expression of matrix genes. Previous studies have demonstrated that TRPV4 expression and activity are sensitive to changes in tissue osmolarity and inflammatory cytokines associated with IVD degeneration[219]. Importantly, the role of TRPV4 in regulating IVD health and degeneration is not well understood. Using *Col2-Cre* mice[225] , we deleted *Trpv4* in the IVD and performed histological analyses on the lumbar spines to characterize changes in IVD health and vertebral bone length. To study TRPV4 function in the context of IVD degeneration, we used a percutaneous AF needle puncture model to induce injury in caudal IVDs and assessed histopathological changes in punctured IVDs, IVDs adjacent to sites of injury, and control IVDs.

Hypothesis: Deletion of *Trpv4* in cells of the IVD will delay and/or prevent injury-induced IVD degeneration.

Objective 1: Determine the effects of *Trpv4* deletion on lumbar IVD health and vertebral bone growth

Objective 2: Determine the role of *Trpv4* in an injury-induced model of IVD degeneration

1.11 References

1. James SL, Abate D, Abate KH, et al. Global, regional, and national incidence, prevalence, and years lived with disability for 354 Diseases and Injuries for 195 countries and territories, 1990-2017: A systematic analysis for the Global Burden of Disease Study 2017. *Lancet*. 2018:1789-1858. doi:10.1016/S0140-6736(18)32279-7

2. Deyo RA. Early Diagnostic Evaluation of Low Back Pain. *N Engl J Med*. 2001;344(5):363-370. doi:10.1056/NEJM200102013440508.

3. Deyo RA, Weinstein JN. Low Back Pain. *N Engl J Med*. 2001;344(5):363-370. doi:10.1056/NEJM200102013440508

4. Mahadevan V. Anatomy of the vertebral column. *Surg (United Kingdom)*. 2018;36(7):327-332. doi:10.1016/j.mpsur.2018.05.006

5. Kershaw DR. *Introduction to the Sybphylum Vertebrata*. Springer; 1983.

6. Nedresky D, Singh G. *Anatomy, Back, Nucleus Pulposus*. StatPearls Publishing; 2019. http://www.ncbi.nlm.nih.gov/pubmed/30570994. Accessed July 5, 2020.

7. Shapiro IM, Vresilovic EJ, Risbud M V. Is the spinal motion segment a diarthrodial polyaxial joint: What a nice nucleus like you doing in a joint like this? *Bone*. 2012;50(3):771-776. doi:10.1016/j.bone.2011.12.004

8. Molladavoodi S, McMorran J, Gregory D. Mechanobiology of annulus fibrosus and nucleus pulposus cells in intervertebral discs. *Cell Tissue Res*. 2020;379(3):429-444. doi:10.1007/s00441-019-03136-1

9. Roughley PJ. Biology of intervertebral disc aging and degeneration: involvement of the extracellular matrix. *Spine (Phila Pa 1976)*. 2004;29(23):2691-2699. doi:10.1097/01.brs.0000146101.53784.b1

10. Chan WCW, Sze KL, Samartzis D, Leung VYL, Chan D. Structure and Biology of the Intervertebral Disk in Health and Disease. *Orthop Clin North Am*. 2011;42(4):447-464. doi:10.1016/j.ocl.2011.07.012

11. Buckwalter JA. Spine update: Aging and degeneration of the human intervertebral disc. *Spine (Phila Pa 1976)*. 1995;20(11):1307-1314. doi:10.1097/00007632-199506000-00022

12. Pattappa G, Li Z, Peroglio M, Wismer N, Alini M, Grad S. Diversity of intervertebral disc cells: Phenotype and function. *J Anat*. 2012;221(6):480-496. doi:10.1111/j.1469-7580.2012.01521.x

13. Tomaszewski KA, Saganiak K, Gładysz T, Walocha JA. The biology behind the human intervertebral disc and its endplates. *Folia Morphol*. 2015;74(2):157-168.

doi:10.5603/FM.2015.0026

14. Venn G, Mason RM. Biosynthesis and metabolism in vivo of intervertebral-disc proteoglycans in the mouse. *Biochem J*. 1983;215(2):217-225. doi:10.1042/bj2150217

15. Moreland LW. Intra-articular hyaluronan (hyaluronic acid) and hylans for the treatment of osteoarthritis: Mechanisms of action. *Arthritis Res Ther*. 2003;5(2):54-67. doi:10.1186/ar623

16. Adams P, Muir H. Qualitative changes with age of proteoglycans of human lumbar discs. *Ann Rheum Dis*. 1976;35(4):289-296. doi:10.1136/ard.35.4.289

17. Cole TC, Burkhardt D, Frost L, Ghosh P. The proteoglycans of the canine intervertebral disc. *BBA - Gen Subj*. 1985;839(2):127-138. doi:10.1016/0304-4165(85)90029-7

18. Chandran PL, Horkay F. Aggrecan, an unusual polyelectrolyte: Review of solution behavior and physiological implications. *Acta Biomater*. 2012;8(1):3-12. doi:10.1016/j.actbio.2011.08.011

19. Nap RJ, Szleifer I. Structure and interactions of aggrecans: Statistical thermodynamic approach. *Biophys J*. 2008;95(10):4570-4583. doi:10.1529/biophysj.108.133801

20. Kiani C, Chen L, Wu YJ, Yee AJ, Yang BB. Structure and function of aggrecan. *Cell Res*. 2002;12(1):19-32. doi:10.1038/sj.cr.7290106

21. Kraemer J, Kolditz D, Gowin R. Water and electrolyte content of human intervertebral discs under variable load. *Spine (Phila Pa 1976)*. 1985;10(1):69-71. doi:10.1097/00007632-198501000-00011

22. Adams MA, Roughley PJ. What is intervertebral disc degeneration, and what causes it? *Spine (Phila Pa 1976)*. 2006;31(18):2151-2161. doi:10.1097/01.brs.0000231761.73859.2c

23. DiFabio JL, Pearce RH, Caterson B, Hughes H. The heterogeneity of the non-aggregating proteoglycans of the human intervertebral disc. *Biochem J*. 1987;244(1):27-33. doi:10.1042/bj2440027

24. Roberts S. Disc morphology in health and disease. In: *Biochemical Society Transactions*. Vol 30. Biochem Soc Trans; 2002:864-869. doi:10.1042/BST0300864

25. Hunter CJ, Matyas JR, Duncan NA. The three-dimensional architecture of the notochordal nucleus pulposus: Novel observations on cell structures in the canine intervertebral disc. *J Anat*. 2003;202(3):279-291. doi:10.1046/j.1469-7580.2003.00162.x

26. Hunter CJ, Matyas JR, Duncan NA. Cytomorphology of notochordal and chondrocytic cells from the nucleus pulposus: A species comparison. *J Anat*. 2004;205(5):357-362. doi:10.1111/j.0021-8782.2004.00352.x

27. Butler WF. Comparative anatomy and development of the mammalian disc. In: Ghosh P, ed. *The Biology of the Intervertebral Disc*. CRC Press; 1989:88-108.

28. Urban JPG, Roberts S, Ralphs JR. The nucleus of the intervertébral disc from development to degeneration. *Am Zool*. 2000;40(1):53-61. doi:10.1668/0003-1569(2000)040[0053:tnotid]2.0.co;2

29. Vujovic S, Henderson S, Presneau N, et al. Brachyury, a crucial regulator of notochordal development, is a novel biomarker for chordomas. *J Pathol*. 2006;209(2):157-165. doi:10.1002/path.1969

30. Trout JJ, Buckwalter JA, Moore KC. Ultrastructure of the human intervertebral disc: II. Cells of the nucleus pulposus. *Anat Rec*. 1982;204(4):307-314. doi:10.1002/ar.1092040403

31. Kim KW, Lim TH, Kim JG, Jeong ST, Masuda K, An HS. The origin of chondrocytes in the nucleus pulposus and histologic findings associated with the transition of a notochordal nucleus pulposus to a fibrocartilaginous nucleus pulposus in intact rabbit intervertebral discs. In: *Spine*. Vol 28. Lippincott Williams and Wilkins; 2003:982-990. doi:10.1097/01.BRS.0000061986.03886.4F

32. Pazzaglia UE, Salisbury JR, Byers PD. Development and involution of the notochord in the human spine. *J R Soc Med*. 1989;82(7):413-415. doi:10.1177/014107688908200714

33. Boos N, Weissbach S, Rohrbach H, Weiler C, Spratt KF, Nerlich AG. Classification of age-related changes in lumbar intervertebral discs: 2002 Volvo award in basic science. *Spine (Phila Pa 1976)*. 2002;27(23):2631-2644. doi:10.1097/00007632-200212010-00002

34. Liebscher T, Haefeli M, Wuertz K, Nerlich AG, Boos N. Age-related variation in cell density of human lumbar intervertebral disc. *Spine (Phila Pa 1976)*. 2011;36(2):153-159. doi:10.1097/BRS.0b013e3181cd588c

35. Choi KS, Cohn MJ, Harfe BD. Identification of nucleus pulposus precursor cells and notochordal remnants in the mouse: Implications for disk degeneration and chordoma formation. *Dev Dyn*. 2008;237(12):3953-3958. doi:10.1002/dvdy.21805

36. McCann MR, Tamplin OJ, Rossant J, Seǵuin CA. Tracing notochord-derived cells using a Noto-cre mouse: Implications for intervertebral disc development. *DMM Dis Model Mech*. 2012;5(1):73-82. doi:10.1242/dmm.008128

37. Aguiar DJ, Johnson SL, Oegema TR. Notochordal cells interact with nucleus pulposus cells: Regulation of proteoglycan synthesis. *Exp Cell Res*.

1999;246(1):129-137. doi:10.1006/excr.1998.4287

38. Boos N, Weissbach S, Rohrbach H, Weiler C, Spratt KF, Nerlich AG. Classification of age-related changes in lumbar intervertebral discs: 2002 Volvo award in basic science. *Spine (Phila Pa 1976)*. 2002;27(23):2631-2644. doi:10.1097/00007632-200212010-00002

39. Hunter CJ, Matyas JR, Duncan NA. The notochordal cell in the nucleus pulposus: A review in the context of tissue engineering. *Tissue Eng*. 2003;9(4):667-677. doi:10.1089/107632703768247368

40. Mohanty S, Pinelli R, Pricop P, Albert TJ, Dahia CL. Chondrocyte-like nested cells in the aged intervertebral disc are late-stage nucleus pulposus cells. *Aging Cell*. 2019;18(5). doi:10.1111/acel.13006

41. Newell N, Little JP, Christou A, Adams MA, Adam CJ, Masouros SD. Biomechanics of the human intervertebral disc: A review of testing techniques and results. *J Mech Behav Biomed Mater*. 2017;69:420-434. doi:10.1016/j.jmbbm.2017.01.037

42. Marchand F, Ahmed AM. Investigation of the laminate structure of lumbar disc anulus fibrosus. *Spine (Phila Pa 1976)*. 1990;15(5):402-410. doi:10.1097/00007632-199005000-00011

43. Yu J, Tirlapur U, Fairbank J, et al. Microfibrils, elastin fibres and collagen fibres in the human intervertebral disc and bovine tail disc. *J Anat*. 2007;210(4):460-471. doi:10.1111/j.1469-7580.2007.00707.x

44. Michalek AJ, Buckley MR, Bonassar LJ, Cohen I, Iatridis JC. Measurement of local strains in intervertebral disc anulus fibrosus tissue under dynamic shear: Contributions of matrix fiber orientation and elastin content. *J Biomech*. 2009;42(14):2279-2285. doi:10.1016/j.jbiomech.2009.06.047

45. Bruehlmann SB, Rattner JB, Matyas JR, Duncan NA. Regional variations in the cellular matrix of the annulus fibrosus of the intervertebral disc. *J Anat*. 2002;201(2):159-171. doi:10.1046/j.1469-7580.2002.00080.x

46. Iu J, Santerre JP, Kandel RA. Inner and outer annulus fibrosus cells exhibit differentiated phenotypes and yield changes in extracellular matrix protein composition in vitro on a polycarbonate urethane scaffold. *Tissue Eng - Part A*. 2014;20(23-24):3261-3269. doi:10.1089/ten.tea.2013.0777

47. Rannou F, Richette P, Benallaoua M, et al. Cyclic tensile stretch modulates proteoglycan production by intervertebral disc annulus fibrosus cells through production of nitrite oxide. *J Cell Biochem*. 2003;90(1):148-157. doi:10.1002/jcb.10608

48. Neidlinger-Wilke C, Galbusera F, Pratsinis H, et al. Mechanical loading of the

intervertebral disc: From the macroscopic to the cellular level. *Eur Spine J*. 2014;23(SUPPL. 3). doi:10.1007/s00586-013-2855-9

49. Humzah MD, Soames RW. Human lntervertebral Disc: Structure and Function. *Anat Rec*. 1988;220(4):337-356.

50. Maroudas A, Stockwell RA, Nachemson A, Urban J. Factors involved in the nutrition of the human lumbar intervertebral disc: cellularity and diffusion of glucose in vitro. *J Anat*. 1975;120(Pt 1):113-130. http://www.ncbi.nlm.nih.gov/pubmed/1184452. Accessed July 6, 2020.

51. Yu J, Peter C, Roberts S, Urban JPG. Elastic fibre organization in the intervertebral discs of the bovine tail. *J Anat*. 2002;201(6):465-475. doi:10.1046/j.1469-7580.2002.00111.x

52. Corallo D, Trapani V, Bonaldo P. The notochord: Structure and functions. *Cell Mol Life Sci*. 2015;72(16):2989-3008. doi:10.1007/s00018-015-1897-z

53. Broberg KB. On the mechanical behaviour of intervertebral discs. *Spine (Phila Pa 1976)*. 1983;8(2):151-165. doi:10.1097/00007632-198303000-00006

54. Antoniou J, Goudsouzian NM, Heathfield TF, et al. The human lumbar endplate: Evidence of changes in biosynthesis and denaturation of the extracellular matrix with growth, maturation, aging, and degeneration. In: *Spine*. Vol 21. Spine (Phila Pa 1976); 1996:1153-1161. doi:10.1097/00007632-199605150-00006

55. Benneker LM, Heini PF, Alini M, Anderson SE, Ito K. 2004 Young investigator award winner: Vertebral endplate marrow contact channel occlusions and intervertebral disc degeneration. *Spine (Phila Pa 1976)*. 2005;30(2):167-173. doi:10.1097/01.brs.0000150833.93248.09

56. Urban JP, Holm S, Maroudas A NA. Nutrition of the Intervertebral Disk. *Clin Orthop Relat Res*. 1977;129:101-114. doi:10.1097/00003086-197711000-00012

57. Maroudas A, Stockwell RA, Nachemson A, Urban AJ. *Factors Involved in the Nutrition of the Human Lumbar Intervertebral Disc: Cellularity and Diffusion of Glucose in Vitro*. Vol 120.; 1975.

58. Wu Y, Cisewski SE, Wegner N, et al. Region and strain-dependent diffusivities of glucose and lactate in healthy human cartilage endplate. *J Biomech*. 2016;49(13):2756-2762. doi:10.1016/j.jbiomech.2016.06.008

59. Malacinski GM, Youn BW, Jurand A. Tissue interactions during axial structure pattern formation in amphibia. *Scan Electron Microsc*. 1981;(Pt 2):307-318. http://www.ncbi.nlm.nih.gov/pubmed/7034171. Accessed July 6, 2020.

60. Sánchez RS, Sánchez SS. Characterization of *pax1* , *pax9* , and *uncx* sclerotomal genes during *Xenopus laevis* embryogenesis. *Dev Dyn*. 2013;242(5):572-579.

doi:10.1002/dvdy.23945

61. Morin-Kensicki EM, Melancon E, Eisen JS. Segmental relationship between somites and vertebral column in zebrafish. *Development*. 2002;129:3851-3860.

62. Fleming A, Keynes R, Tannahill D. A central role for the notochord in vertebral patterning. *Development*. 2004;131(4):873-880. doi:10.1242/dev.00952

63. Pourquié O. Somite formation in the chicken embryo. *Int J Dev Biol*. 2018;62(1-3):57-62. doi:10.1387/ijdb.180036op

64. Shapiro F. Vertebral development of the chick embryo during days 3-19 of incubation. *J Morphol*. 1992;213(3):317-333. doi:10.1002/jmor.1052130305

65. Kinder SJ, Tsang TE, Wakamiya M, et al. The organizer of the mouse gastrula is composed of a dynamic population of progenitor cells for the axial mesoderm. *Development*. 2001;128(18):3623-3634.

66. Shiratori H, Hamada H. The left-right axis in the mouse: From origin to morphology. *Development*. 2006;133(11):2095-2104. doi:10.1242/dev.02384

67. Yamanaka Y, Tamplin OJ, Beckers A, Gossler A, Rossant J. Live Imaging and Genetic Analysis of Mouse Notochord Formation Reveals Regional Morphogenetic Mechanisms. *Dev Cell*. 2007;13(6):884-896. doi:10.1016/j.devcel.2007.10.016

68. Beckers A, Alten L, Viebahn C, Andre P, Gossler A. The mouse homeobox gene Noto regulates node morphogenesis, notochordal ciliogenesis, and left-right patterning. *Proc Natl Acad Sci U S A*. 2007;104(40):15765-15770. doi:10.1073/pnas.0704344104

69. Nonaka S, Tanaka Y, Okada Y, et al. Randomization of left-right asymmetry due to loss of nodal cilia generating leftward flow of extraembryonic fluid in mice lacking KIF3B motor protein. *Cell*. 1998;95(6):829-837. doi:10.1016/S0092-8674(00)81705-5

70. Marques S, Borges AC, Silva AC, Freitas S, Cordenonsi M, Belo JA. The activity of the Nodal antagonist Cerl-2 in the mouse node is required for correct L/R body axis. *Genes Dev*. 2004;18(19):2342-2347. doi:10.1101/gad.306504

71. Tanaka Y, Okada Y, Hirokawa N. FGF-induced vesicular release of Sonic hedgehog and retinoic acid in leftward nodal flow is critical for left-right determination. *Nature*. 2005;435(7039):172-177. doi:10.1038/nature03494

72. McGrath J, Somlo S, Makova S, Tian X, Brueckner M. Two populations of node monocilia initiate left-right asymmetry in the mouse. *Cell*. 2003;114(1):61-73. doi:10.1016/S0092-8674(03)00511-7

73. Tam PPL, Loebel DAF. Gene function in mouse embryogenesis: Get set for

gastrulation. *Nat Rev Genet*. 2007;8(5):368-381. doi:10.1038/nrg2084

74. Tam PPL, Behringer RR. Mouse gastrulation: The formation of a mammalian body plan. *Mech Dev*. 1997;68(1-2):3-25. doi:10.1016/S0925-4773(97)00123-8

75. Forsberg H, Crozet F, Brown NA. Waves of mouse Lunatic fringe expression, in four-hour cycles at two-hour intervals, precede somite boundary formation. *Curr Biol*. 1998;8(18):1027-1030. doi:10.1016/S0960-9822(07)00424-1

76. Williams S, Alkhatib B, Serra R. Development of the axial skeleton and intervertebral disc. In: *Current Topics in Developmental Biology*. Vol 133. Academic Press Inc.; 2019:49-90. doi:10.1016/bs.ctdb.2018.11.018

77. Dalgleish AE. A study of the development of thoracic vertebrae in the mouse assisted by autoradiography. *Cells Tissues Organs*. 1985;122(2):91-98. doi:10.1159/000145988

78. Fan CM, Tessier-Lavigne M. Patterning of mammalian somites by surface ectoderm and notochord: Evidence for sclerotome induction by a hedgehog homolog. *Cell*. 1994;79(7):1175-1186. doi:10.1016/0092-8674(94)90009-4

79. Aszódi A, Chan D, Hunziker E, Bateman JF, Fässler R. Collagen II is essential for the removal of the notochord and the formation of intervertebral discs. *J Cell Biol*. 1998;143(5):1399-1412. doi:10.1083/jcb.143.5.1399

80. Theiler K. Vertebral malformations. *Adv Anat Embryol Cell Biol*. 1988;112:1-99. doi:10.1007/978-3-642-73775-6

81. Maher C, Underwood M, Buchbinder R. Non-specific low back pain. *Lancet*. 2017;389(10070):736-747. doi:10.1016/S0140-6736(16)30970-9

82. Balagué F, Mannion AF, Pellisé F, Cedraschi C. Clinical update: low back pain. *Lancet*. 2007;369(9563):726-728. doi:10.1016/S0140-6736(07)60340-7

83. Thiese MS, Hegmann KT, Wood EM, et al. Prevalence of low back pain by anatomic location and intensity in an occupational population. *BMC Musculoskelet Disord*. 2014;15(1):283. doi:10.1186/1471-2474-15-283

84. Katz JN. Lumbar disc disorders and low-back pain: Socioeconomic factors and consequences. In: *Journal of Bone and Joint Surgery - Series A*. Vol 88. J Bone Joint Surg Am; 2006:21-24. doi:10.2106/JBJS.E.01273

85. Maetzel A, Li L. The economic burden of low back pain: A review of studies published between 1996 and 2001. *Best Pract Res Clin Rheumatol*. 2002;16(1):23-30. doi:10.1053/berh.2001.0204

86. Frymoyer JW, Cats-Baril WL. An overview of the incidences and costs of low back pain. *Orthop Clin North Am*. 1991;22(2):263-271.

87. Katz JN. Lumbar disc disorders and low-back pain: socioeconomic factors and consequences. *J Bone Jt Surg Am*. 2006;88(2):21-24.

88. Hurwitz EL, Randhawa K, Yu H, Côté P, Haldeman S. The Global Spine Care Initiative: a summary of the global burden of low back and neck pain studies. *Eur Spine J*. 2018;27(6):796-801. doi:10.1007/s00586-017-5432-9

89. Arnbak B, Jensen TS, Egund N, et al. Prevalence of degenerative and spondyloarthritis-related magnetic resonance imaging findings in the spine and sacroiliac joints in patients with persistent low back pain. *Eur Radiol*. 2016;26(4):1191-1203. doi:10.1007/s00330-015-3903-0

90. Fujii K, Yamazaki M, Kang JD, et al. Discogenic Back Pain: Literature Review of Definition, Diagnosis, and Treatment. *JBMR Plus*. 2019;3(5):e10180. doi:10.1002/jbm4.10180

91. Roelofs PDDM, Deyo RA, Koes BW, Scholten RJPM, Van Tulder MW. Non-steroidal anti-inflammatory drugs for low back pain. *Cochrane Database Syst Rev*. 2008;(1). doi:10.1002/14651858.CD000396.pub3

92. Friedman BW, O'Mahony S, Mulvey L, et al. One-week and 3-month outcomes after an emergency department visit for undifferentiated musculoskeletal low back pain. *Ann Emerg Med*. 2012;59(2). doi:10.1016/j.annemergmed.2011.09.012

93. Zhu Q, Gao X, Gu W. Temporal changes of mechanical signals and extracellular composition in human intervertebral disc during degenerative progression. *J Biomech*. 2014;47(15):3734-3743. doi:10.1016/j.jbiomech.2014.09.004

94. Vergroesen PPA, Kingma I, Emanuel KS, et al. Mechanics and biology in intervertebral disc degeneration: A vicious circle. *Osteoarthr Cartil*. 2015;23(7):1057-1070. doi:10.1016/j.joca.2015.03.028

95. Hanaei S, Abdollahzade S, Khoshnevisan A, Kepler CK, Rezaei N. Genetic aspects of intervertebral disc degeneration. *Rev Neurosci*. 2015;26(5):581-606. doi:10.1515/revneuro-2014-0077

96. Feng Y, Egan B, Wang J. Genetic factors in intervertebral disc degeneration. *Genes Dis*. 2016;3(3):178-185. doi:10.1016/j.gendis.2016.04.005

97. Le Maitre CL, Pockert A, Buttle DJ, Freemont AJ, Hoyland JA. Matrix synthesis and degradation in human intervertebral disc degeneration. In: *Biochemical Society Transactions*. Vol 35. Portland Press Ltd; 2007:652-655. doi:10.1042/BST0350652

98. Antoniou J, Steffen T, Nelson F, et al. The human lumbar intervertebral disc: Evidence for changes in the biosynthesis and denaturation of the extracellular matrix with growth, maturation, ageing, and degeneration. *J Clin Invest*. 1996;98(4):996-1003. doi:10.1172/JCI118884

99. Singh K, Masuda K, Thonar EJMA, An HS, Cs-Szabo G. Age-related changes in the extracellular matrix of nucleus pulposus and anulus fibrosus of human intervertebral disc. *Spine (Phila Pa 1976)*. 2009;34(1):10-16. doi:10.1097/BRS.0b013e31818e5ddd

100. Kääpä E, Holm S, Inkinen R, Lammi MJ, Tammi M, Vanharanta H. Proteoglycan chemistry in experimentally injured porcine intervertebral disk. *J Spinal Disord*. 1994;7(4):296-306.

101. Kepler CK, Ponnappan RK, Tannoury CA, Risbud M V., Anderson DG. The molecular basis of intervertebral disc degeneration. *Spine J*. 2013;13(3):318-330. doi:10.1016/j.spinee.2012.12.003

102. BRADFORD DS, OEGEMA TR, COOPER KM, WAKANO K, CHAO EY. Chymopapain, Chemonucleolysis, and Nucleus Pulposus Regeneration A Biochemical and Biomechanical Study. *Spine (Phila Pa 1976)*. 1984;9(2):135-147. doi:10.1097/00007632-198403000-00004

103. Adams MA, McNally DS, Dolan P. "Stress" distributions inside intervertebral discs. The effects of age and degeneration. *J Bone Jt Surg - Ser B*. 1996;78(6):965-972. doi:10.1302/0301-620X78B6.1287

104. Rajasekaran S, Babu JN, Arun R, Armstrong BRW, Shetty AP, Murugan S. ISSLS prize winner: A study of diffusion in human lumbar discs: A serial magnetic resonance imaging study documenting the influence of the endplate on diffusion in normal and degenerate discs. *Spine (Phila Pa 1976)*. 2004;29(23):2654-2667. doi:10.1097/01.brs.0000148014.15210.64

105. De Geer CM. Intervertebral Disk Nutrients and Transport Mechanisms in Relation to Disk Degeneration: A Narrative Literature Review. *J Chiropr Med*. 2018;17(2):97-105. doi:10.1016/j.jcm.2017.11.006

106. Horner HA, Urban JPG. 2001 Volvo award winner in basic science studies: Effect of nutrient supply on the viability of cells from the nucleus pulposus of the intervertebral disc. *Spine (Phila Pa 1976)*. 2001;26(23):2543-2549. doi:10.1097/00007632-200112010-00006

107. LA Binch A, Cole AA, Breakwell LM, et al. Expression and regulation of neurotrophic and angiogenic factors during human intervertebral disc degeneration. *Arthritis Res Ther*. 2014;16(5):416. doi:10.1186/s13075-014-0416-1

108. Ohtori S, Inoue G, Miyagi M, Takahashi K. Pathomechanisms of discogenic low back pain in humans and animal models. *Spine J*. 2015;15(6):1347-1355. doi:10.1016/j.spinee.2013.07.490

109. Schmorl G. Die pathologische anatomic der wirbelsaule. *Verh Stsch Ortho Ges*. 1927;21:3-41.

110. Fearing B V., Hernandez PA, Setton LA, Chahine NO. Mechanotransduction and cell biomechanics of the intervertebral disc. *JOR Spine*. 2018;1(3):e1026. doi:10.1002/jsp2.1026

111. H J Wilke, P Neef, M Caimi, T Hoogland LEC. New in vivo measurements of pressures in the intervertebral disc in daily life. *Spine (Phila Pa 1976)*. 1999;24(8):755-762.

112. Nachemson, Alf; Morris J. In Vivo Measurements of Intradiscal Pressure. *J Bone Jt Surg*. 1964;46(5):1077-1092. doi:10.2106/00004623-196446050-00012

113. Sato K, Kikuchi S, Yonezawa T. In vivo intradiscal pressure measurement in healthy individuals and in patients with ongoing back problems. *Spine (Phila Pa 1976)*. 1999;24(23):2468-2474. doi:10.1097/00007632-199912010-00008

114. Carragee EJ, Don AS, Hurwitz EL, Cuellar JM, Carrino J, Herzog R. 2009 ISSLS Prize Winner: Does Discography Cause Accelerated Progression of Degeneration Changes in the Lumbar Disc. *Spine (Phila Pa 1976)*. 2009;34(21):2338-2345. doi:10.1097/BRS.0b013e3181ab5432

115. Ebara S, Iatridis JC, Setton LA, Foster RJ, Van Mow C, Weidenbaum M. Tensile properties of nondegenerate human lumbar anulus fibrosus. *Spine (Phila Pa 1976)*. 1996;21(4):452-461. doi:10.1097/00007632-199602150-00009

116. O'Connell GD, Johannessen W, Vresilovic EJ, Elliott DM. Human Internal Disc Strains in Axial Compression Measured Noninvasively Using Magnetic Resonance Imaging. *Spine (Phila Pa 1976)*. 2007;32(25):2860-2868. doi:10.1097/BRS.0b013e31815b75fb

117. Miller JAA, Schmatz C, Schultz AB. Lumbar Disc Degeneration. *Spine (Phila Pa 1976)*. 1988;13(2):173-178. doi:10.1097/00007632-198802000-00008

118. Sabnis AB, Chamoli U, Diwan AD. Is L5–S1 motion segment different from the rest? A radiographic kinematic assessment of 72 patients with chronic low back pain. *Eur Spine J*. 2018;27(5):1127-1135. doi:10.1007/s00586-017-5400-4

119. Zahari SN, Latif MJA, Rahim NRA, Kadir MRA, Kamarul T. The Effects of Physiological Biomechanical Loading on Intradiscal Pressure and Annulus Stress in Lumbar Spine: A Finite Element Analysis. *J Healthc Eng*. 2017;2017. doi:10.1155/2017/9618940

120. Luoma K, Riihimäki H, Luukkonen R, Raininko R, Viikari-Juntura E, Lamminen A. Low back pain in relation to lumbar disc degeneration. *Spine (Phila Pa 1976)*. 2000;25(4):487-492. doi:10.1097/00007632-200002150-00016

121. Roy TC, Lopez HP, Piva SR. Loads Worn by Soldiers Predict Episodes of Low Back Pain During Deployment to Afghanistan. *Spine (Phila Pa 1976)*. 2013;38(15):1310-1317. doi:10.1097/BRS.0b013e31829265c4

122. Videman T, Sarna S, Battié MC, et al. The long-term effects of physical loading and exercise lifestyles on back-related symptoms, disability, and spinal pathology among men. *Spine (Phila Pa 1976)*. 1995;20(6):699-709. doi:10.1097/00007632-199503150-00011

123. Belavý DL, Bansmann PM, Böhme G, et al. Changes in intervertebral disc morphology persist 5 mo after 21-day bed rest. *J Appl Physiol*. 2011;111(5):1304-1314. doi:10.1152/japplphysiol.00695.2011

124. Sayson J V., Hargens AR. Pathophysiology of low back pain during exposure to microgravity. *Aviat Sp Environ Med*. 2008;79(4):365-373. doi:10.3357/ASEM.1994.2008

125. Johnston SL, Campbell MR, Scheuring R, Feiveson AH. Risk of herniated nucleus pulposus among U.S. astronauts. *Aviat Sp Environ Med*. 2010;81(6):566-574. doi:10.3357/ASEM.2427.2010

126. Pruitt BL, Dunn AR, Weis WI, Nelson WJ. Mechano-Transduction: From Molecules to Tissues. doi:10.1371/journal.pbio.1001996

127. O'Connell GD, Vresilovic EJ, Elliott DM. Human intervertebral disc internal strain in compression: The effect of disc region, loading position, and degeneration. *J Orthop Res*. 2011;29(4):547-555. doi:10.1002/jor.21232

128. Duance V, Blain EJ. The effects of cyclic tensile strain on the organisation and expression of cytoskeletal elements in bovine intervertebral disc cells: An in vitro study. *S Li Eur Cells Mater*. 2014;21:508-522. doi:10.22203/eCM.v021a38

129. Sowa G, Coelho P, Vo N, et al. Determination of annulus fibrosus cell response to tensile strain as a function of duration, magnitude, and frequency. *J Orthop Res*. 2011;29(8):1275-1283. doi:10.1002/jor.21388

130. Gawri R, Rosenzweig DH, Krock E, et al. High mechanical strain of primary intervertebral disc cells promotes secretion of inflammatory factors associated with disc degeneration and pain. *Arthritis Res Ther*. 2014;16(1):R21. doi:10.1186/ar4449

131. Majd H, Wipff P-J, Buscemi L, et al. A Novel Method of Dynamic Culture Surface Expansion Improves Mesenchymal Stem Cell Proliferation and Phenotype. *Stem Cells*. 2009;27(1):200-209. doi:10.1634/stemcells.2008-0674

132. Gilbert HTJ, Nagra NS, Freemont AJ, Millward-Sadler SJ, Hoyland JA. Integrin – Dependent Mechanotransduction in Mechanically Stimulated Human Annulus Fibrosus Cells: Evidence for an Alternative Mechanotransduction Pathway Operating with Degeneration. Tsilibary EC, ed. *PLoS One*. 2013;8(9):e72994. doi:10.1371/journal.pone.0072994

133. Pratsinis H, Papadopoulou A, Neidlinger-Wilke C, Brayda-Bruno M, Wilke HJ, Kletsas D. Cyclic tensile stress of human annulus fibrosus cells induces MAPK

activation: Involvement in proinflammatory gene expression. *Osteoarthr Cartil*. 2016;24(4):679-687. doi:10.1016/j.joca.2015.11.022

134. Neidlinger-Wilke C, Würtz K, Liedert A, et al. A three-dimensional collagen matrix as a suitable culture system for the comparison of cyclic strain and hydrostatic pressure effects on intervertebral disc cells. *J Neurosurg Spine*. 2005;2(4):457-465. doi:10.3171/spi.2005.2.4.0457

135. Xu Y, Yao H, Li P, et al. Cellular Physiology and Biochemistry Cellular Physiology and Biochemistry Dynamic Compression Promotes the Matrix Synthesis of Nucleus Pulposus Cells Through Up-Regulating N-CDH Expression in a Perfusion Bioreactor Culture Cellular Physiology and Biochemistry Cellular Physiology and Biochemistry. *Cell Physiol Biochem*. 2018;46:482-491. doi:10.1159/000488616

136. Li P, Hou G, Zhang R, et al. High-magnitude compression accelerates the premature senescence of nucleus pulposus cells via the p38 MAPK-ROS pathway. *Arthritis Res Ther*. 2017;19(1):1-14. doi:10.1186/s13075-017-1384-z

137. Li P, Gan Y, Wang H, et al. Dynamic compression effects on immature nucleus pulposus: A study using a novel intelligent and mechanically active bioreactor. *Int J Med Sci*. 2016;13(3):225-234. doi:10.7150/ijms.13747

138. Gajghate S, Hiyama A, Shah M, et al. Osmolarity and intracellular calcium regulate aquaporin2 expression through TonEBP in nucleus pulposus cells of the intervertebral disc. *J Bone Miner Res*. 2009;24(6):992-1001. doi:10.1359/jbmr.090103

139. Pritchard S, Erickson GR, Guilak F. Hyperosmotically Induced Volume Change and Calcium Signaling in Intervertebral Disk Cells: The Role of the Actin Cytoskeleton. *Biophys J*. 2002;83:2502-2510.

140. Ariga K, Yonenobu K, Nakase T, et al. Mechanical Stress-Induced Apoptosis of Endplate Chondrocytes in Organ-Cultured Mouse Intervertebral Discs. *Spine (Phila Pa 1976)*. 2003;28(14):1528-1533. doi:10.1097/01.BRS.0000076915.55939.E3

141. Gantenbein B, Grünhagen T, Lee CR, van Donkelaar CC, Alini M, Ito K. An In Vitro Organ Culturing System for Intervertebral Disc Explants With Vertebral Endplates. *Spine (Phila Pa 1976)*. 2006;31(23):2665-2673. doi:10.1097/01.brs.0000244620.15386.df

142. Paul CPL, Zuiderbaan HA, Zandieh Doulabi B, et al. Simulated-physiological loading conditions preserve biological and mechanical properties of caprine lumbar intervertebral discs in EX vivo culture. *PLoS One*. 2012;7(3). doi:10.1371/journal.pone.0033147

143. Walter BA, Likhitpanichkul M, Illien-Junger S, Roughley PJ, Hecht AC, Iatridis JC. TNFα Transport Induced by Dynamic Loading Alters Biomechanics of Intact Intervertebral Discs. 2015. doi:10.1371/journal.pone.0118358

144. Alkhatib B, Rosenzweig DH, Krock E, et al. Acute mechanical injury of the human intervertebral disc: link to degeneration and pain. *Eur Cells Mater*. 2014;28:98-111. doi:10.22203/eCM.v028a08

145. Iatridis JC, Michalek AJ, Purmessur D, Korecki CL. Localized intervertebral disc injury leads to organ level changes in structure, cellularity, and biosynthesis. *Cell Mol Bioeng*. 2009;2(3):437-447. doi:10.1007/s12195-009-0072-8

146. Korecki CL, Costi JJ, Iatridis JC. Needle puncture injury affects intervertebral disc mechanics and biology in an organ culture model. *Spine (Phila Pa 1976)*. 2008;33(3):235-241. doi:10.1097/BRS.0b013e3181624504

147. Dudli S, Haschtmann D, Ferguson SJ. Persistent degenerative changes in the intervertebral disc after burst fracture in an in vitro model mimicking physiological post-traumatic conditions. *Eur Spine J*. 2015;24(9):1901-1908. doi:10.1007/s00586-014-3301-3

148. McCann MR, Patel P, Pest MA, et al. Repeated exposure to high-frequency low-amplitude vibration induces degeneration of murine intervertebral discs and knee joints. *Arthritis Rheumatol*. 2015;67(8):2164-2175. doi:10.1002/art.39154

149. McCann MR, Veras MA, Yeung C, et al. Whole-body vibration of mice induces progressive degeneration of intervertebral discs associated with increased expression of Il-1β and multiple matrix degrading enzymes. *Osteoarthr Cartil*. 2017;25(5):779-789. doi:10.1016/j.joca.2017.01.004

150. McCann MR, Patel P, Beaucage KL, et al. Acute vibration induces transient expression of anabolic genes in the Murine intervertebral disc. *Arthritis Rheum*. 2013;65(7):1853-1864. doi:10.1002/art.37979

151. Lotz JC, Colliou OK, Chin JR, Duncan NA, Liebenberg E. Compression-induced degeneration of the intervertebral disc: An in vivo mouse model and finite-element study. *Spine (Phila Pa 1976)*. 1998;23(23):2493-2506. doi:10.1097/00007632-199812010-00004

152. MacLean JJ, Lee CR, Grad S, Ito K, Alini M, Iatridis JC. Effects of Immobilization and Dynamic Compression on Intervertebral Disc Cell Gene Expression In Vivo. *Spine (Phila Pa 1976)*. 2003;28(10):973-981. doi:10.1097/01.brs.0000061985.15849.a9

153. Sakai D, Nishimura K, Tanaka M, et al. Migration of bone marrow-derived cells for endogenous repair in a new tail-looping disc degeneration model in the mouse: A pilot study. *Spine J*. 2015;15(6):1356-1365. doi:10.1016/j.spinee.2013.07.491

154. Yang F, Leung VY, Luk KD, Chan D, Cheung KM. Injury-induced sequential transformation of notochordal nucleus pulposus to chondrogenic and fibrocartilaginous phenotype in the mouse. *J Pathol*. 2009;218(1):113-121. doi:10.1002/path.2519

155. Tian Z, Ma X, Yasen M, et al. Intervertebral Disc Degeneration in a Percutaneous Mouse Tail Injury Model. *Am J Phys Med Rehabil*. 2018;97(3):170-177. doi:10.1097/PHM.0000000000000818

156. Piazza M, Peck SH, Gullbrand SE, et al. Quantitative MRI correlates with histological grade in a percutaneous needle injury mouse model of disc degeneration. *J Orthop Res*. 2018;36(10):2771-2779. doi:10.1002/jor.24028

157. Chen Y, Ju L, Rushdi M, Ge C, Zhu C. Receptor-mediated cell mechanosensing. *Mol Biol Cell*. 2017;28(23):3134-3155. doi:10.1091/mbc.E17-04-0228

158. Wang N, Butler JP, Ingber DE. Mechanotransduction across the cell surface and through the cytoskeleton. *Science (80-).* 1993;260(5111):1124-1127. doi:10.1126/science.7684161

159. Ingber DE. Cellular mechanotransduction: putting all the pieces together again. *FASEB J*. 2006;20(7):811-827. doi:10.1096/fj.05-5424rev

160. Gasparski AN, Beningo KA. Mechanoreception at the cell membrane: More than the integrins. *Arch Biochem Biophys*. 2015;586:20-26. doi:10.1016/j.abb.2015.07.017

161. Hynes RO. Integrins: A family of cell surface receptors. *Cell*. 1987;48(4):549-554. doi:10.1016/0092-8674(87)90233-9

162. Hynes RO. Integrins: Bidirectional, allosteric signaling machines. *Cell*. 2002;110(6):673-687. doi:10.1016/S0092-8674(02)00971-6

163. Luo BH, Springer TA. Integrin structures and conformational signaling. *Curr Opin Cell Biol*. 2006;18(5):579-586. doi:10.1016/j.ceb.2006.08.005

164. Puklin-Faucher E, Sheetz MP. The mechanical integrin cycle. *J Cell Sci*. 2009;122(2):179-186. doi:10.1242/jcs.042127

165. Clark K, Pankov R, Travis MA, et al. A specific α5β1-integrin conformation promotes directional integrin translocation and fibronectin matrix formation. *J Cell Sci*. 2005;118(2):291-300. doi:10.1242/jcs.01623

166. Chen Y, Lee H, Tong H, Schwartz M, Zhu C. Force regulated conformational change of integrin αVβ3. *Matrix Biol*. 2017;60-61:70-85. doi:10.1016/j.matbio.2016.07.002

167. Chen W, Lou J, Hsin J, Schulten K, Harvey SC, Zhu C. Molecular dynamics simulations of forced unbending of integrin αVβ3. *PLoS Comput Biol*. 2011;7(2):1001086. doi:10.1371/journal.pcbi.1001086

168. Friedland JC, Lee MH, Boettiger D. Mechanically activated integrin switch controls α5β 1 function. *Science (80-).* 2009;323(5914):642-644.

doi:10.1126/science.1168441

169. Kong F, García AJ, Mould AP, Humphries MJ, Zhu C. Demonstration of catch bonds between an integrin and its ligand. *J Cell Biol*. 2009;185(7):1275-1284. doi:10.1083/jcb.200810002

170. Nettles DL, Richardson WJ, Setton LA. Integrin expression in cells of the intervertebral disc. *J Anat*. 2004;204(6):515-520. doi:10.1111/j.0021-8782.2004.00306.x

171. Le Maitre CL, Frain J, Millward-Sadler J, Fotheringham AP, Freemont AJ, Hoyland JA. Altered integrin mechanotransduction in human nucleus pulposus cells derived from degenerated discs. *Arthritis Rheum*. 2009;60(2):460-469. doi:10.1002/art.24248

172. Kurakawa T, Kakutani K, Morita Y, et al. Functional impact of integrin α5β1 on the homeostasis of intervertebral discs: A study of mechanotransduction pathways using a novel dynamic loading organ culture system. *Spine J*. 2015;15(3):417-426. doi:10.1016/j.spinee.2014.12.143

173. Henrique D, Schweisguth F. Mechanisms of notch signaling: A simple logic deployed in time and space. *Dev*. 2019;146(3). doi:10.1242/dev.172148

174. Gordon WR, Arnett KL, Blacklow SC. The molecular logic of Notch signaling - A structural and biochemical perspective. *J Cell Sci*. 2008;121(19):3109-3119. doi:10.1242/jcs.035683

175. Struhl G, Adachi A. Nuclear access and action of Notch in vivo. *Cell*. 1998;93(4):649-660. doi:10.1016/S0092-8674(00)81193-9

176. Fehon RG, Kooh PJ, Rebay I, et al. Molecular interactions between the protein products of the neurogenic loci Notch and Delta, two EGF-homologous genes in Drosophila. *Cell*. 1990;61(3):523-534. doi:10.1016/0092-8674(90)90534-L

177. Wang X, Ha T. Defining single molecular forces required to activate integrin and Notch signaling. *Science (80-).* 2013;340(6135):991-994. doi:10.1126/science.1231041

178. Gordon WR, Vardar-Ulu D, Histen G, Sanchez-Irizarry C, Aster JC, Blacklow SC. Structural basis for autoinhibition of Notch. *Nat Struct Mol Biol*. 2007;14(4):295-300. doi:10.1038/nsmb1227

179. Gordon WR, Zimmerman B, He L, et al. Mechanical Allostery: Evidence for a Force Requirement in the Proteolytic Activation of Notch. *Dev Cell*. 2015;33(6):729-736. doi:10.1016/j.devcel.2015.05.004

180. Zheng Y, Liu C, Ni L, et al. Cell type-specific effects of Notch signaling activation on intervertebral discs: Implications for intervertebral disc degeneration. *J Cell*

Physiol. 2018;233(7):5431-5440. doi:10.1002/jcp.26385

181. Wang H, Tian Y, Wang J, et al. Inflammatory cytokines induce NOTCH signaling in nucleus pulposus cells: Implications in intervertebral disc degeneration. *J Biol Chem*. 2013;288(23):16761-16774. doi:10.1074/jbc.M112.446633

182. Hiyama A, Skubutyte R, Markova D, et al. Hypoxia activates the notch signaling pathway in cells of the intervertebral disc: Implications in degenerative disc disease. *Arthritis Rheum*. 2011;63(5):1355-1364. doi:10.1002/art.30246

183. Samanta A, Hughes TET, Moiseenkova-Bell VY. Transient receptor potential (TRP) channels. In: *Subcellular Biochemistry*. Vol 87. Springer New York; 2018:141-165. doi:10.1007/978-981-10-7757-9_6

184. Liu C, Montell C. Forcing open TRP channels: Mechanical gating as a unifying activation mechanism. *Biochem Biophys Res Commun*. 2015;460(1):22-25. doi:10.1016/j.bbrc.2015.02.067

185. Numata T, Kiyonaka S, Kato K, Takahashi N, Mori Y. Activation of TRP channels in mammalian systems. In: *TRP Channels*. CRC Press; 2016:43-90. https://www.ncbi.nlm.nih.gov/books/NBK92819/. Accessed July 8, 2020.

186. Liedtke W, Choe Y, Martí-Renom MA, et al. Vanilloid receptor-related osmotically activated channel (VR-OAC), a candidate vertebrate osmoreceptor. *Cell*. 2000;103(3):525-535. doi:10.1016/S0092-8674(00)00143-4

187. Ciura S, Bourque CW. Transient receptor potential vanilloid 1 is required for intrinsic osmoreception in organum vasculosum lamina terminalis neurons and for normal thirst responses to systemic hyperosmolality. *J Neurosci*. 2006;26(35):9069-9075. doi:10.1523/JNEUROSCI.0877-06.2006

188. Oancea E, Wolfe JT, Clapham DE. Functional TRPM7 channels accumulate at the plasma membrane in response to fluid flow. *Circ Res*. 2006;98(2):245-253. doi:10.1161/01.RES.0000200179.29375.cc

189. Maroto R, Raso A, Wood TG, Kurosky A, Martinac B, Hamill OP. TRPC1 forms the stretch-activated cation channel in vertebrate cells. *Nat Cell Biol*. 2005;7(2):179-185. doi:10.1038/ncb1218

190. Jin P, Jan LY, Jan Y-N. Structural Features Relevant to Mechanotransduction Mechanisms. *Annu Rev Neurosci*. 2020;43:207-229. doi:10.1146/annurev-neuro-070918

191. Liang X, Madrid J, Gärtner R, et al. A NOMPC-dependent membrane-microtubule connector is a candidate for the gating spring in fly mechanoreceptors. *Curr Biol*. 2013;23(9):755-763. doi:10.1016/j.cub.2013.03.065

192. Zhang W, Cheng LE, Kittelmann M, et al. Ankyrin Repeats Convey Force to Gate

the NOMPC Mechanotransduction Channel. *Cell*. 2015;162(6):1391-1403. doi:10.1016/j.cell.2015.08.024

193. Wes PD, Chevesich J, Jeromin A, Rosenberg C, Stetten G, Montell C. TRPC1, a human homolog of a Drosophila store-operated channel. *Proc Natl Acad Sci U S A*. 1995;92(21):9652-9656. doi:10.1073/pnas.92.21.9652

194. Zhu X, Chu PB, Peyton M, Birnbaumer L. Molecular cloning of a widely expressed human homologue for the Drosophila trp gene. *FEBS Lett*. 1995;373(3):193-198. doi:10.1016/0014-5793(95)01038-G

195. Benemei S, Patacchini R, Trevisani M, Geppetti P. TRP channels. *Curr Opin Pharmacol*. 2015;22:18-23. doi:10.1016/j.coph.2015.02.006

196. Shibasaki K. TRPV4 ion channel as important cell sensors. *J Anesth*. 2016;30:1014-1019. doi:10.1007/s00540-016-2225-y

197. Darby WG, Grace MS, Baratchi S, McIntyre P. Modulation of TRPV4 by diverse mechanisms. *Int J Biochem Cell Biol*. 2016;78:217-228. doi:10.1016/j.biocel.2016.07.012

198. White JPM, Cibelli M, Urban L, Nilius B, McGeown JG, Nagy I. TRPV4: Molecular conductor of a diverse orchestra. *Physiol Rev*. 2016;96(3):911-973. doi:10.1152/physrev.00016.2015

199. Mcnulty AL, Leddy HA, Liedtke W, Guilak F. TRPV4 as a Therapeutic Target for Joint Diseases. doi:10.1007/s00210-014-1078-x

200. Strotmann R, Semtner M, Kepura F, Plant TD, Schöneberg T. Interdomain Interactions Control Ca2+-Dependent Potentiation in the Cation Channel TRPV4. Koch K-W, ed. *PLoS One*. 2010;5(5):e10580. doi:10.1371/journal.pone.0010580

201. Voets T, Prenen J, Vriens J, et al. Molecular determinants of permeation through the cation channel TRPV4. *J Biol Chem*. 2002;277(37):33704-33710. doi:10.1074/jbc.M204828200

202. Liedtke W, Choe Y, Martí-Renom MA, et al. Vanilloid receptor-related osmotically activated channel (VR-OAC), a candidate vertebrate osmoreceptor. *Cell*. 2000;103(3):525-535. doi:10.1016/S0092-8674(00)00143-4

203. Ryskamp DA, Jo AO, Frye AM, et al. Swelling and eicosanoid metabolites differentially gate TRPV4 channels in retinal neurons and glia. *J Neurosci*. 2014;34(47):15689-15700. doi:10.1523/JNEUROSCI.2540-14.2014

204. Watanabe H, Vriens J, Prenen J, Droogmans G, Voets T, Nillus B. Anandamide and arachidonic acid use epoxyeicosatrienoic acids to activate TRPV4 channels. *Nature*. 2003;424(6947):434-438. doi:10.1038/nature01807

205. Alessandri-Haber N, Joseph E, Dina OA, Liedtke W, Levine JD. TRPV4 mediates pain-related behavior induced by mild hypertonic stimuli in the presence of inflammatory mediator. *Pain*. 2005;118(1-2):70-79. doi:10.1016/j.pain.2005.07.016

206. O'Conor CJ, Leddy HA, Benefield HC, Liedtke WB, Guilak F. TRPV4-mediated mechanotransduction regulates the metabolic response of chondrocytes to dynamic loading. *Proc Natl Acad Sci U S A*. 2014;111(4):1316-1321. doi:10.1073/pnas.1319569111

207. Muramatsu S, Wakabayashi M, Ohno T, et al. Functional gene screening system identified TRPV4 as a regulator of chondrogenic differentiation. *J Biol Chem*. 2007;282(44):32158-32167. doi:10.1074/jbc.M706158200

208. Masuyama R, Vriens J, Voets T, et al. TRPV4-Mediated Calcium Influx Regulates Terminal Differentiation of Osteoclasts. *Cell Metab*. 2008;8(3):257-265. doi:10.1016/j.cmet.2008.08.002

209. Phan MN, Leddy HA, Votta BJ, et al. Functional characterization of TRPV4 as an osmotically sensitive ion channel in porcine articular chondrocytes. *Arthritis Rheum*. 2009;60(10):3028-3037. doi:10.1002/art.24799

210. Clark AL, Votta BJ, Kumar S, Liedtke W, Guilak F. Chondroprotective role of the osmotically sensitive ion channel transient receptor potential vanilloid 4: Age- and sex-dependent progression of osteoarthritis in Trpv4-deficient mice. *Arthritis Rheum*. 2010;62(10):2973-2983. doi:10.1002/art.27624

211. O'Conor CJ, Griffin TM, Liedtke W, Guilak F. Increased susceptibility of Trpv4-deficient mice to obesity and obesity-induced osteoarthritis with very high-fat diet. *Ann Rheum Dis*. 2013;72(2):300-304. doi:10.1136/annrheumdis-2012-202272

212. O'Conor CJ, Ramalingam S, Zelenski NA, et al. Cartilage-Specific Knockout of the Mechanosensory Ion Channel TRPV4 Decreases Age-Related Osteoarthritis. *Sci Rep*. 2016;6(June):1-10. doi:10.1038/srep29053

213. Mizoguchi F, Mizuno A, Hayata T, et al. Transient receptor potential vanilloid 4 deficiency suppresses unloading-induced bone loss. *J Cell Physiol*. 2008;216(1):47-53. doi:10.1002/jcp.21374

214. Suzuki T, Notomi T, Miyajima D, et al. Osteoblastic differentiation enhances expression of TRPV4 that is required for calcium oscillation induced by mechanical force. *Bone*. 2013;54(1):172-178. doi:10.1016/j.bone.2013.01.001

215. Nishimura G, Lausch E, Savarirayan R, et al. TRPV4-associated skeletal dysplasias. *Am J Med Genet Part C Semin Med Genet*. 2012;160C(3):190-204. doi:10.1002/ajmg.c.31335

216. Kang SS, Shin SH, Auh CK, Chun J. Human skeletal dysplasia caused by a

constitutive activated transient receptor potential vanilloid 4 (TRPV4) cation channel mutation. *Exp Mol Med*. 2012;44(12):707-722. doi:10.3858/emm.2012.44.12.080

217. Sadowska A, Hitzl W, Karol A, et al. Differential regulation of TRP channel gene and protein expression by intervertebral disc degeneration and back pain. *Sci Rep*. 2019;9(1):1-16. doi:10.1038/s41598-019-55212-9

218. Sadowska A, Touli E, Hitzl W, et al. Inflammaging in cervical and lumbar degenerated intervertebral discs: analysis of proinflammatory cytokine and TRP channel expression. *Eur Spine J*. 2018;27(3):564-577. doi:10.1007/s00586-017-5360-8

219. Walter BA, Purmessur D, Moon A, et al. Reduced tissue osmolarity increases trpv4 expression and pro-inflammatory cytokines in intervertebral disc cells. *Eur Cells Mater*. 2016;32:123-136. doi:10.22203/eCM.v032a08

220. Gilbert HTJ, Hoyland JA, Millward-Sadler SJ. The response of human anulus fibrosus cells to cyclic tensile strain is frequency-dependent and altered with disc degeneration. *Arthritis Rheum*. 2010;62(11):3385-3394. doi:10.1002/art.27643

221. Gilbert HTJ, Hoyland JA, Freemont AJ, Millward-Sadler SJ. The involvement of interleukin-1 and interleukin-4 in the response of human annulus fibrosus cells to cyclic tensile strain: An altered mechanotransduction pathway with degeneration. *Arthritis Res Ther*. 2011;13(1):R8. doi:10.1186/ar3229

222. Bonvini S, Birrell M, Dubuis E, et al. Activation of TRPV4 triggers ATP release and mast cell dependent contraction of airway smooth muscle (ASM). In: *European Respiratory Journal*. Vol 46. European Respiratory Society (ERS); 2015:OA3253. doi:10.1183/13993003.congress-2015.oa3253

223. Rajasekhar P, Poole DP, Liedtke W, Bunnett NW, Veldhuis NA. P2Y1 receptor activation of the TRPV4 ion channel enhances purinergic signaling in satellite glial cells. *J Biol Chem*. 2015;290(48):29051-29062. doi:10.1074/jbc.M115.689729

224. Güler AD, Lee H, Iida T, Shimizu I, Tominaga M, Caterina M. Heat-evoked activation of the ion channel, TRPV4. *J Neurosci*. 2002;22(15):6408-6414. doi:10.1523/jneurosci.22-15-06408.2002

225. Terpstra L, Prud'Homme J, Arabian A, et al. Reduced chondrocyte proliferation and chondrodysplasia in mice lacking the integrin-linked kinase in chondrocytes. *J Cell Biol*. 2003;162(1):139-148. doi:10.1083/jcb.200302066

Chapter 2

2 The Mechano-Response of Murine Annulus Fibrosus Cells to Cyclic Tensile Strain is Frequency-Dependent

2.1 Co-Authorship Statement

All data presented in this chapter were collected and analyzed by Kim, M.K.M., Burns, M.J., and Serjeant, M.E. in the laboratory of Dr. Séguin, C.A. Serjeant, M.E. performed Western blot analysis and Burns, M.J. performed real-time PCR for inflammatory cytokine genes. All other experiments were performed by Kim, M.K.M. Manuscript was written by Kim, M.K.M. with suggestions from Dr. Séguin, C.A.

2.2 Chapter Summary

The intervertebral disc (IVD) is a composite structure essential for spine stabilization, load bearing, and movement. Biomechanical factors are important contributors to the IVD microenvironment regulating joint homeostasis; however the cell type-specific effectors of mechanotransduction in the IVD are not fully understood. The current study aimed to determine the effects of cyclic tensile strain (CTS) on annulus fibrosus (AF) cells and identify mechano-sensitive pathways. Using a cell-type specific reporter mouse to differentiation NP and AF cells from the murine IVD, we characterized AF cells in dynamic culture exposed to CTS (6% strain) at specific frequencies (0.1 Hz, 1.0 Hz, or 2.0 Hz). We demonstrate that our culture model maintains the phenotype of primary AF cells and that the bioreactor system delivers uniform biaxial strain across the cell culture surface. We show that exposure of AF cells to CTS induces cytoskeleton reorganization resulting in stress fibre formation, with acute exposure to CTS at 2.0 Hz inducing a significant yet transient increase ERK1/2 pathway activation. Using SYBR-based qPCR to assess the

expression of extracellular matrix (ECM) genes, ECM-remodeling genes, candidate mechano-sensitive genes, inflammatory cytokines and cell surface receptors, we demonstrated that exposure of AF cells to CTS at 0.1 Hz increased *Acan, Prg4, Col1a1* and *Mmp3* expression. AF cells exposed to CTS at 1.0 Hz showed a significant increase in the expression of *Acan, Myc,* and *Tnfα*. Exposure of AF cells to CTS at 2.0 Hz induced a significant increase in *Acan, Prg4, Cox2, Myc, Fos,* and *Tnfα* expression. Among the cell surface receptors assessed, AF cells exposed to CTS at 2.0 Hz showed a significant increase in *Itgβ1, Itgα5,* and *Trpv4* expression. Our findings demonstrate that the response of AF cells to CTS is frequency-dependent, and suggest that mechanical loading may directly contribute to matrix remodelling and the onset of local tissue inflammation in the murine IVD.

2.3 Introduction

According to the most recent *Global Burden of Disease Study*, back pain is the leading cause of years lived with disability worldwide[1]. Although the etiology of chronic back pain remains largely unknown, persistent back pain has been associated with magnetic resonance imaging (MRI) findings of lumbar intervertebral disc (IVD) degeneration in ~30% of patients[2]. The pathophysiology of IVD degeneration involves progressive cell-mediated changes to the IVD microenvironment, including extracellular matrix (ECM) breakdown, altered matrix synthesis, and local tissue inflammation, ultimately resulting in structural and functional tissue failure[3-6]. Although the etiology of IVD degeneration is unclear, initiation and progression of the degenerative cascade involves multiple interdependent factors including altered mechanical loading[7-10], reduced nutrient supply[9-12], altered cellular composition[3, 13], and hereditary factors[5, 14-15].

The IVD is a fibrocartilaginous connective tissue structure essential for spine load bearing and movement. Anatomically, IVDs consist of three distinct tissues: the central gelatinous nucleus pulposus (NP), the outer collagenous annulus fibrosus (AF) that circumferentially encapsulates the NP, and the cartilage endplates that anchor the disc to the adjacent vertebrae and allow for passive diffusion of nutrients to the IVD[8,12,16-17]. As such, IVDs are heterogenous composite structures with each tissue having a unique structure and specific ECM composition that together form the complex microarchitecture of the IVD required for joint function[17].

Similar to other musculoskeletal tissues, mechanical loading poses an interesting dichotomy in IVD biology: while physiological levels of mechanical loading during moderate locomotive activities are essential for IVD health and tissue homeostasis[10,18-19], mechanical stimuli due to high and low degrees of physical activities (overloading and immobilization) can contribute to tissue degeneration[18-20]. IVDs are subjected to various types of mechanical forces, including hydrostatic pressure, compressive, tensile and shear forces[21-24]. Within this dynamic microenvironment, NP cells are primarily exposed to compressive and hydrostatic loading, while AF cells are exposed to multi-directional deformation resulting in tensile strain[21-24]. Previous studies investigating the mechanical forces experienced by human IVDs reported that in performing daily activities, intradiscal pressures are predicted to range from 0.1 MPa (bedrest) to 2.5 MPa (heavy lifting)[25]. Furthermore, studies characterizing the mechanical properties and strain profiling of human IVDs reported that the AF experiences 1-13% strain during daily activities[26], with tissue strain reaching up to 26% during physiological compressive loading[27].

To better understand how the dynamic environment of the IVD regulates cell function, studies have examined the effects of cyclic tensile strain (CTS) on AF cells to model their exposure to tensile loading *in vivo.* In response to uniaxial CTS (2%, 1.0 Hz), human AF cells in 3D culture show increased aggrecan gene expression and decreased expression of matrix degrading enzymes[28]. Using the same model system, exposure of AF cells to 4% CTS (1.0 Hz) induced a modest increase in matrix gene expression, dependent on osmotic potentials[29]. In contrast, exposure of human AF cells to high levels of bi-axial strain (20% CTS, 0.001 Hz) induced catabolic responses, including upregulation of inflammatory cytokine production and cell death[30]. Studies using the Flexcell tension system reported that human AF cells exposed to 10% CTS at 1.0 Hz showed increased expression of matrix genes and decreased expression of matrix degrading enzymes, whereas 10% CTS frequency at 0.33 Hz shifted the mechano-response toward matrix catabolism[31-32]. Of note, application of either loading protocol to human AF cells from degenerate IVDs increased catabolic gene expression[30].

To date, reports on the mechano-sensory mechanism of AF cells have focused on the role of integrin-ECM interactions in CTS sensing[32-33]; however, a specific signalling pathway involved in mechanotransduction remains largely unexplored. Mitogen-activated protein kinases (MAPKs) are a family of highly conserved protein kinases that serves as intermediates in signal transduction pathways[34]. MAPKs are grouped into three subfamilies – extracellular signal-regulated kinases (ERKs), p38, and c-jun N-terminal or stress-activated kinases (JNK/SAPK) – based on their sequence, sensitivity to activation and mechanisms of action[35]. Functionally, ERKs regulate cell survival and proliferation[36], whereas p38 kinases regulate inflammatory responses, cell cycle control, and

differentiation[37]. Interestingly, AF cells isolated from degenerative human IVDs show activation of all three MAPK subfamilies (ERK1/2, p38, JNK) upon mechanical stimulation[38].

The current study used a transgenic mouse model to genetically label and isolate AF cells from the murine IVD, and employed an *in vitro* culture system to deliver acute bi-axial CTS. Bi-axial multi-directional load was chosen to model complex circumferential tensile load experienced by the AF cells *in vivo* when the tissue is subjected to multi-axial load constrained by the adjacent vertebral bodies (axial and radial load)[23, 27]. The study aimed to quantify the mechano-response of healthy murine AF cells to different loading conditions, focusing on cytoskeletal adaptation, changes in gene expression, and the identification of CTS-induced signalling pathways.

2.4 Methods

2.4.1 Animals

To differentiate cell types within the IVD, the notochord-specific Noto^{Cre} mouse strain reported by our group[39] was mated to the conditional *ROSA26 (R26) mT/mG* reporter mouse (*Gt(ROSA)26Sor*$^{tm4(ACTB-tdTomato,-EGFP)Luo}$/J)[40]. Genotyping was performed as previously described[39]. IVD tissues from *Noto*$^{Cre/WT}$*;Rosa*$^{mTmG/mTmG}$ mice, in which notochord-derived NP cells are marked by green fluorescent protein (GFP) and AF cells express tdTomato, were used for all experiments. Mice were housed in standard cages and maintained on a 12-hour light/dark cycle, with rodent chow and water available *ad libitum.* Mice were euthanized by CO_2 asphyxiation at 2 months-of-age for tissue isolation. All animal experiments were performed in accordance with the policies and guidelines set forth

by the Canadian Council on Animal Care and were approved by the Animal Use Subcommittee of the University of Western Ontario (protocol 2017-154, **Appendix A**).

2.4.2 Tissue isolation and culture of AF cells

Lumbar spines from 2-month-old mice were dissected, followed by microdissection of NP and AF tissues using a fluorescent stereo microscope (Leica M165 FC). Isolated tissues were immediately fixed for RNA extractions. For primary cell culture (overview in **Figure 2.1A**), intact IVDs were dissected from 2-month-old mice (cervical to caudal) and the AF tissues were microdissected (Leica M165 FC). Isolated AF tissues were transferred to a sterile 3 mm culture dish with 2 mL of Type II collagenase (3 mg/ml; Worthington, NJ, USA) in Dulbecco's modified Eagle's medium/Ham's F-12 medium (DMEM/F12) and incubated for 20 minutes at 37ºC. AF tissues were then minced and further digested for 1 hour at 37ºC. Digested tissues were triturated and filtered using a 70 micron cell strainer and cells were pelleted by centrifugation (1,100 rpm for 5 min). Cells were plated at an initial density of ~400,000 cells/cm^2 and cultured in DMEM/F12 supplemented with 10% Fetal Bovine Serum (FBS) and 1% penicillin and streptomycin (Thermo Fisher Scientific, MA, USA) at 37°C in a humidified atmosphere of 5% CO_2. Media was changed every 2 days until cells reached 80% confluency. AF cells isolated from IVD tissues of two mice were pooled together and used for each experimental replicate.

2.4.3 Mechanical stimulation

The MechanoCulture B1 (MCB1) device (CellScale Biomaterials Testing, Waterloo, Ontario, Canada) was used to deliver bi-axial multi-directional cyclic tensile strain to monolayer cultures (**Figure 2.1B, C**)[41]. The MCB1 device included an actuator chamber, housing a programmable circuit board and motor (**Figure 2.1B**, top), connected

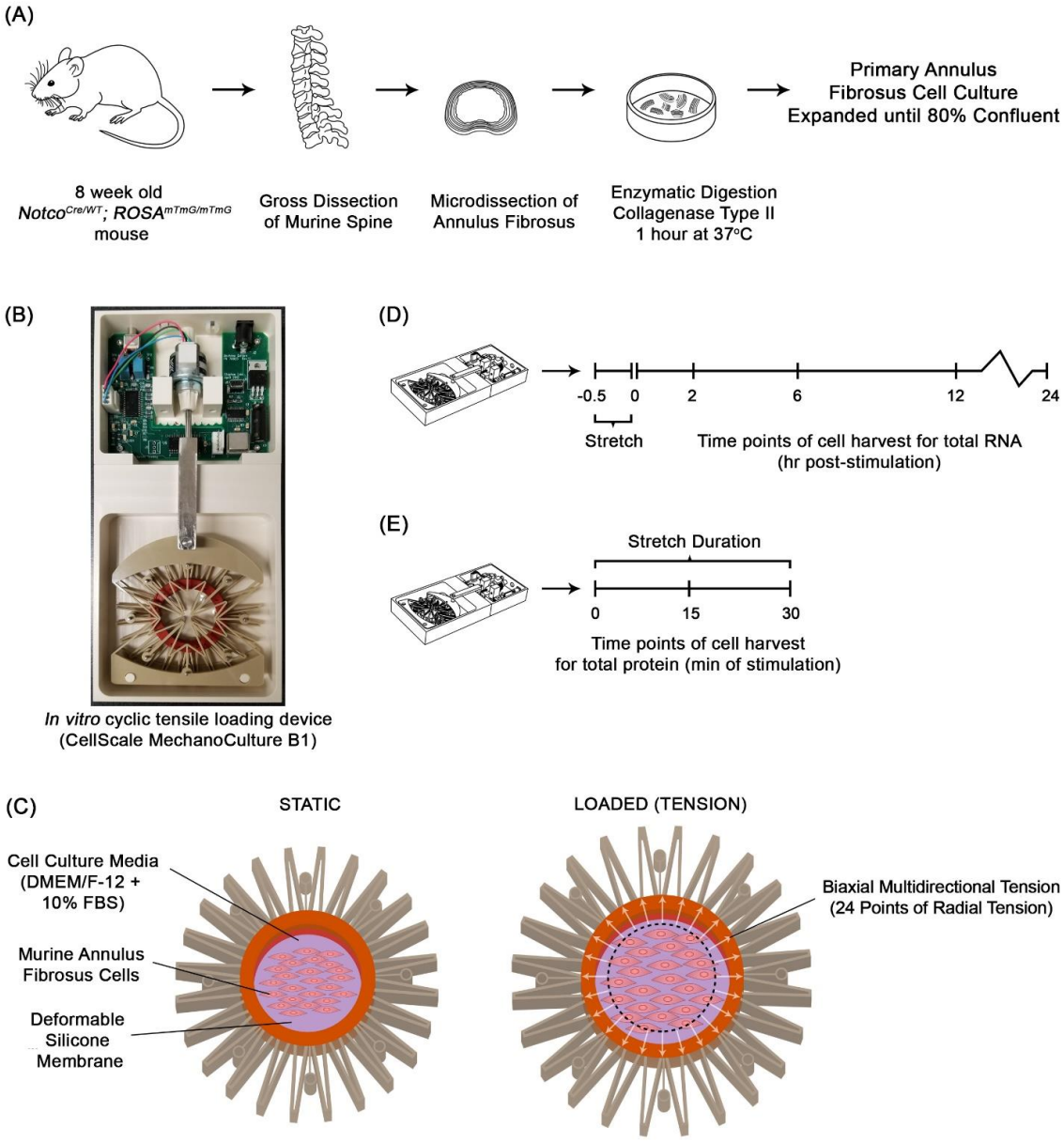

Figure 2.1. Experimental design and mechanical stimulation of murine annulus fibrosus cells.

A) Schematic representation of the protocol used for the isolation and culture of primary murine annulus fibrosus cells. B) Images of the MechanoCulture B1 device inside the cell culture incubator. C) Schematic depicting the *in vitro* model used to deliver cyclic tensile strain. Cells were seeded on a deformable silicone membrane puncture mounted on a 24-pin mounting ring designed to generate radial motion from a linear motion input, resulting in the delivery of biaxial stretch. D, E) Schematic representations of the experimental procedures used to deliver 6% cyclic tensile strain at frequencies of 0.1, 1.0, or 2.0 Hz to investigate gene expression (C) and signal transduction (D) in mechanically stimulated annulus fibrosus cells.

by a stainless steel arm to a loading chamber containing the deformable construct on which the cells were grown (**Figure 2.1B**, bottom). Three deformable polyether ether ketone plastic layers were assembled in order to transfer the linear motion of the steel arm into a radial stretch of an inner circle (35 mm diameter) of 24 pins. Clear silicone membranes (0.005" thickness, ultimate tensile strength 8.62 MPa, McMaster-Carr, Aurora, USA, #87315K71) were puncture-mounted on the device's 24-pin mounting ring and the assembled constructs were sterilized by standard gravity displacement steam autoclave cycle (30 min sterilization, 20 min cool; temperature during sterilization = 121.1°C – 123.3°C). Sterilized silicone membranes were then coated with 2 mL of 50% FBS DMEM/F12 overnight. Primary AF cells were seeded at a density of 48,000 cells/cm^2 onto the FBS-coated silicone membrane and cultured for 2 days in culture media supplemented with 50 ng/μL L-ascorbic acid. Once monolayers reached 80% confluency, the assemblies were transferred to the loading chamber of the device within the culture incubator. AF cells were exposed to 6% CTS, at sinusoidal frequencies of either 0.1 Hz, 1.0 Hz, or 2.0 Hz for 30 min. AF cells cultured on FBS-coated silicone membranes without mechanical stimulation served as time-matched unloaded controls. After 30 min of CTS, cells were incubated for additional 2, 6, 12, or 24 hours before harvesting for total RNA, with time-matched unloaded cells serving as control.

2.4.4 Motion tracking analysis

To quantify the magnitude and uniformity of the strain applied to the silicone membrane by the MCB1 device, motion tracking analysis was performed. Fine graphite powder was used to pattern the silicone membrane in order to quantify the motion of specific points during mechanical stretch. The patterned surface was imaged at 0.5 mm intervals using a

DMK 41AU02 Monochrome Camera (Imaging Source, Charlotte, NC, USA) until the programmed displacement (3.5 mm) was reached. Using commercially available image tracking software, (LabJoy, CellScale), four different regions of the membrane were tracked and the strains experienced in these regions were calculated based on pixel displacement.

2.4.5 Immunofluorescence analysis

Immediately following mechanical stimulation, AF cells on the silicone membranes were fixed with 4% paraformaldehyde for 10 min and then permeabilized with 0.1% Triton X-100 (in Phosphate Buffered Saline; PBS) for 10 min at room temperature. After blocking in 1% Bovine Serum Albumin (in PBS) for 30 min, Alexa Fluor 488 Phalloidin (Life Technologies, Carlsbad, CA, USA) was used to detect F-actin according to manufacturer's protocol and the nuclei detected using Hoechst 33258 stain (Thermo Fisher). Images were acquired using a Zeiss Axio Observer 7 with AxioVision software (Carl Zeiss, Jena, Germany). In each of the 4 biological replicates, cells within 3 non-overlapping regions of interest (ROIs) were imaged for each experimental group (unloaded, 0.1 Hz, 1.0 Hz, and 2.0 Hz) for a total of 12 images for each experimental group. Each image was analyzed by counting total number of cells (5 – 9 cells per ROI) and categorizing each cell as either stress fibre-negative (cells with intense F-actin staining localized near cell periphery with either punctate or weak fibre staining in cytoplasm) or stress fibre-positive (condensed F-actin fibre staining). For each experimental group, total of 63 – 84 cells were examined. Cells staining positive for stress fibres are presented as percentage of total cells counted for each experimental group.

2.4.6 Protein isolation and Western blot analysis

AF cells were cultured on the silicone membranes in the MCB1 device as described above and transferred to serum-free DMEM/F12 media 24 h prior to loading. AF cells were subjected to 6% CTS at frequencies of either 1.0 Hz, 2.0 Hz, for either 15 or 30 min (n=3). Immediately following mechanical loading, AF cells were scraped from silicone membranes and lysed using RIPA buffer containing protease inhibitor (cOmplete^{TM} Mini, EDTA-free Protease Inhibitor Cocktail, Sigma-Aldrich Canada). Samples were centrifuged at 14,000 x g for 15 min at 4^{o}C. The supernatant was collected, and protein concentration was determined using the BCA Protein Assay Kit (Pierce Biotechnology, Rockford, IL, USA) according to the manufacturer's protocol. For each sample, 21 μg of protein was loaded and resolved by sodium dodecyl sulfate polyacrylamide gel electrophoresis (10% gels) and proteins were transferred to Immobilon® Polyvinylidene fluoride membranes (Sigma-Aldrich) using the Trans-Blot® Turbo^{TM} Blotting System (Bio-Rad). Membranes were blocked with 5% w/v non-fat dried milk in Tris-Buffered Saline-Tween (TBST) and incubated with primary antibody against Phospho-p38 MAPK Thr180/Tyr182 (Cell Signaling Technology, #4511, 1:1000), p38 MAPK (Cell Signaling Technology, #8690, 1:1000), Phospho-p44/42 MAPK Erk1/2 Thr202/Tyr204 (Cell Signaling Technology, #4370, 1:1000), or p44/42 MAPK Erk1/2 (Cell Signaling Technology, #4370, 1:1000) in TBST with 5% milk (Cell Signaling Technology, Danvers, MA, USA). After washing with TBST, membranes were incubated with anti-rabbit horseradish peroxidase-linked secondary antibody (Santa Cruz Biotechnology, Dallas, TX, USA, sc-2004; 1:2000). Protein bands were visualized by chemiluminescence using the Enhanced Chemiluminescence Kit (Bio-Rad, Hercules, CA, USA) and imaged using the ChemiDOC

XRS+ System (Bio-Rad). Densitometric analysis was performed using ImageLab software (Bio-Rad). Levels of phospho-proteins were quantified and presented normalized to corresponding total protein levels.

2.4.7 RNA extraction and gene expression analysis

Total RNA was extracted from IVD tissues, primary AF cells cultured on standard tissue culture plastic or silicone membrane (passage 1) or CTS-treated and unloaded AF cells 2, 6, 12, or 24 hour post-stimulation (n=4-7) using Trizol reagent (Life Technologies) according to the manufacturer's protocol. RNA was quantified using a NanoDrop 2000 spectrophotometer (Thermo Fisher Scientific). Complementary DNA was synthesized from 150 ng of RNA using the Bio-Rad iScript cDNA synthesis kit. Gene expression was determined by SYBR-based real-time PCR using the Bio-Rad CFX384 thermocycler. PCR reactions were run in triplicate using 470 nM forward and reverse primers (primer sequences in **Table 2.1**) with 2x SsoFast EvaGreen Supermix (Bio-Rad). The PCR program consisted of the following: initial 2 min enzyme activation at 95^{o}C, 10 sec denaturation at 95^{o}C, 30 sec annealing/elongation at 60^{o}C, for total of 40 cycles. For cell phenotype characterization, transcript levels were determined relative to a six-point calibration standard curve made from pooled cDNA generated from wild type murine heart, brain, kidney, muscle, IVD, and mouse embryonic fibroblasts. For CTS experiments, gene expression values were calculated using $\Delta\Delta$Ct, normalized for input based on hypoxanthine quinine phosphoribosyl transferase (*Hprt*) expression and expressed relative to the time-matched unloaded controls within each trial.

Table 2.1. Sequences of the primers used in the real-time PCR analysis.

Gene	Forward (5' → 3')	Reverse (5' → 3')
Acan	CCTGCTACTTCATCGACCCC	AGATGCTGTTGACTCGAACCT
Acta2	GTCCCAGACATCAGGGAGTAA	TCGGATACTTCAGCGTCAGGA
Adamts4	GAGGAGGAGATCGTGTTTCCAG	CAAACCCTCTACCTGCACCC
Bgn	ACGAATCCATGACAACCGTATC	GCTCCTGGTTCAAAGCCACT
Cd24	ACCCACGCAGATTTACTGCAA	CCCCTCTGGTGGTAGCGTTA
Cilp	ATGGCAGCAATCAAGACTTGG	AGGCTGGACTCTTCTCACTGA
Col1a1	CTGGCGGTTCAGGTCCAAT	TCCAGGCAATCCAGGAGC
Col2a1	GCACATCTGGTTTGGAGAGACC	TAGCGGTGTTGGGAGCCA
Col10a1	GGGACCCCAAGGACCTAAAG	GCCCAACTAGACCTATCTCACCT
Cox2	GGCGCAGTTTATGTTGTCTGT	CAAGACAGATCATAAGCGAGGA
Dcn	TCTTGGGCTGGACCATTTGAA	CATCGGTAGGGGCACATAGA
Fap	GTCACCTGATCGGCAATTTGT	CCCCATTCTGAAGGTCGTAGAT
Fos	CGGGTTTCAACGCCGACTA	TTGGCACTAGAGACGGACAGA
Gdf10	GAAGTACAACCGAAGAGGTGC	AGGCTTTTGGTCGATCATTTCC
Hprt	CAGGCCAGACTTTGTTGGAT	TTGCGCTCATCTTAGGCTTT
Il-1β	CCCTGCAGCTGGAGAGTGTGGA	TGTGCTCTGCTTGTGAGGTGCTG
Il-6	TCTCTGCAAGAGACTTCCATCCAGT	AGTAGGGAAGGCCGTGGTTGTCA
Itgβ1	ACTGATTGGCTGGAGGAATGTTAC	CTGGACAAGGTGAGCAATAGAAGG
Itgα5	CTTCTCCGTGGAGTTTTACCG	GCTGTCAAATTGAATGGTGGTG
Mmp3	TTGTCCCGTTTCCATCTCTCTC	TTGGTGATGTCTCAGGTTCCAG
P2rx7	GGCACTGGAGGAAAATTTGA	TGAGCAAGTCAATGCACACA
Prg4	GGGTGGAAAATACTTCCCGTC	CAGGACAGCACTCCATGTAGT
Timp1	CTTGGTTCCCTGGCGTACTC	ACCTGATCCGTCCACAAACAG
Tlr2	CACCACTGCCCGTAGATGAAG	AGGGTACAGTCGTCGAACTCT
Tlr4	GCCTTTCAGGGAATTAAGCTCC	GATCAACCGATGGACGTGTAAA
Tnfα	TCGGGGTGATCGGTCCCCAA	GGTGGTTTGCTACGACGTGGGC
Trpv4	TTCGTAGGGATCGTTGGTCCT	TACAGTGGGGCATCGTCCGT

2.4.8 Statistical analysis

All statistical analyses were performed with GraphPad Prism 6 Software (GraphPad Software, San Diego, CA, USA). The analysis of data from stress fibre quantification and gene expression for cell phenotype characterization were analyzed using one-way analysis of variation (ANOVA) followed by Tukey's multiple comparison test. Western blot data were analyzed using Krustkal-Wallis and Dunn's post-hoc test. For CTS experiments, gene expression levels in AF cells exposed to CTS at varying frequencies were compared to unloaded controls at each time point using one-way ANOVA with Dunnett's post-hoc test. For each gene, differences in expression values between CTS-treated AF cells harvested at specific time points post-stimulation were compared using one-way ANOVA with Tukey's post-hoc test. In order to test if frequency is a source of variation for a given gene, differences in gene expression values between different CTS protocols at each time point were analyzed using two-way ANOVA followed by Tukey's post-hoc test. P values less than 0.05 were considered statistically significant.

2.5 Results

2.5.1 MechanoCulture B1 device delivers uniform cyclic tensile loading

To quantify the magnitude and uniformity of the strain applied to the silicone culture membrane, motion tracking analysis was performed. The device was programmed for a 3.5 mm linear displacement, a load translated into 24 points of radial motion by the device (**Figure 2.1B, C**). Regions of interest (ROIs) on the silicone membrane were tracked and imaged every 0.5 mm during the displacement and the strain calculated based on pixel displacement (**Figure 2.2A**). This analysis demonstrated that the average strain experienced by the ROIs on the silicone membrane at full displacement (3.5 mm) was

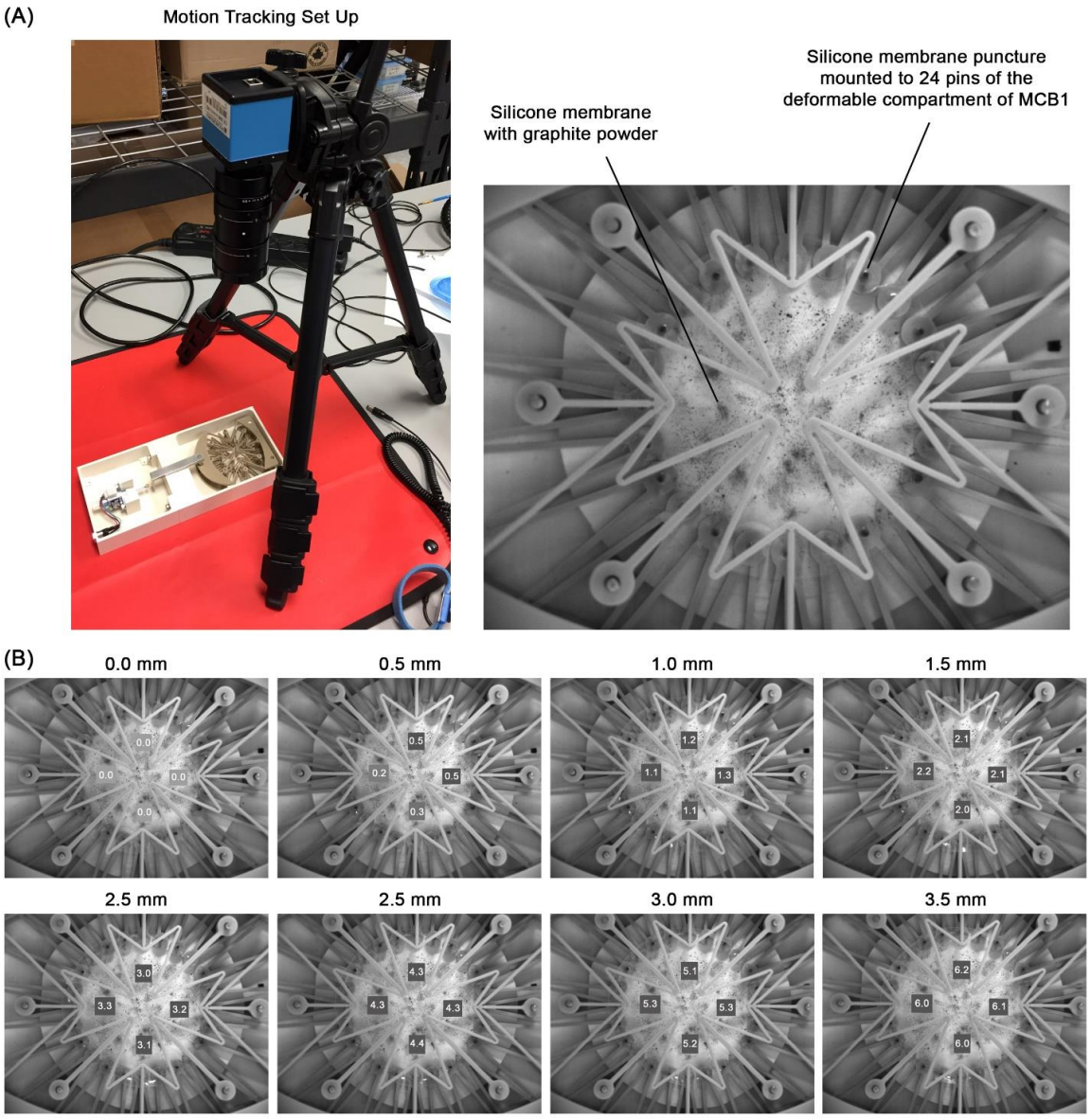

Figure 2.2. Motion tracking analysis of the MechanoCulture B1 device to validate strain profile.

A) Silicone membrane was textured using graphite powder and the membrane was stretched and imaged every 0.5 mm until the programmed total displacement (3.5 mm) was reached. B) Four different regions of interest (ROI) on the membrane were tracked and strains experienced in these regions were calculated based on pixel displacement (values indicate within ROIs at each displacement). The analysis demonstrated that a 3.5 mm displacement produced uniform 6% on the silicone cell culture membrane.

6.075 ± 0.096%. The small variability in strain measured between ROIs suggests that strain across the membrane at full displacement is uniform (**Figure 2.2B**).

Previous studies predicted that the AF experiences compressive tissue strains of 1-26%, radial tensile strain of 1-19%, and lamellar fibre strain of up to 13% when IVD is compressed with a load physiologically similar to that of walking[26,27,42]. Given such data, CTS of 6% was chosen as it falls within the physiological range of mechanical stimulation *in vivo*. Frequency of 1.0 Hz was chosen as being representative of physiologic locomotion, and frequencies of 0.1 Hz and 2.0 Hz were chosen as being less than and greater than physiologic locomotion, respectively[43]. (0.1 Hz = bed rest, 1.0 Hz = walking gait, 2.0 Hz = steady running gait).

2.5.2 Primary murine annulus fibrosus cells maintain an AF-like phenotype in culture

To allow cell type-specific isolation from the murine IVD, primary cells were isolated from the *Noto*^{cre}*;ROSA*$^{mTmG/mTmG}$ conditional reporter mice in which AF cells express red fluorescent protein (RFP) whereas notochord-derived NP cells express GFP (**Figure 2.3A**). In all AF cell preparations maintained in monolayer culture, only RFP-expressing cells were observed, confirming the absence of notochord-derived NP cells (**Figure 2.3A**).

To ensure that primary AF cells maintained their phenotype in our *in vitro* culture system, we quantified the expression of previously reported AF- and NP-associated markers[44-50] as well as fibroblast markers, and compared expression levels to those of the intact AF and NP tissues. Primary AF cells showed robust expression of the AF-associated markers, type I collagen (*Col1a1*), growth differentiation factor (*Gdf10*), paired box 1 (*Pax1*) and cartilage intermediate layer protein (*Cilp*), compared to expression of these genes in the

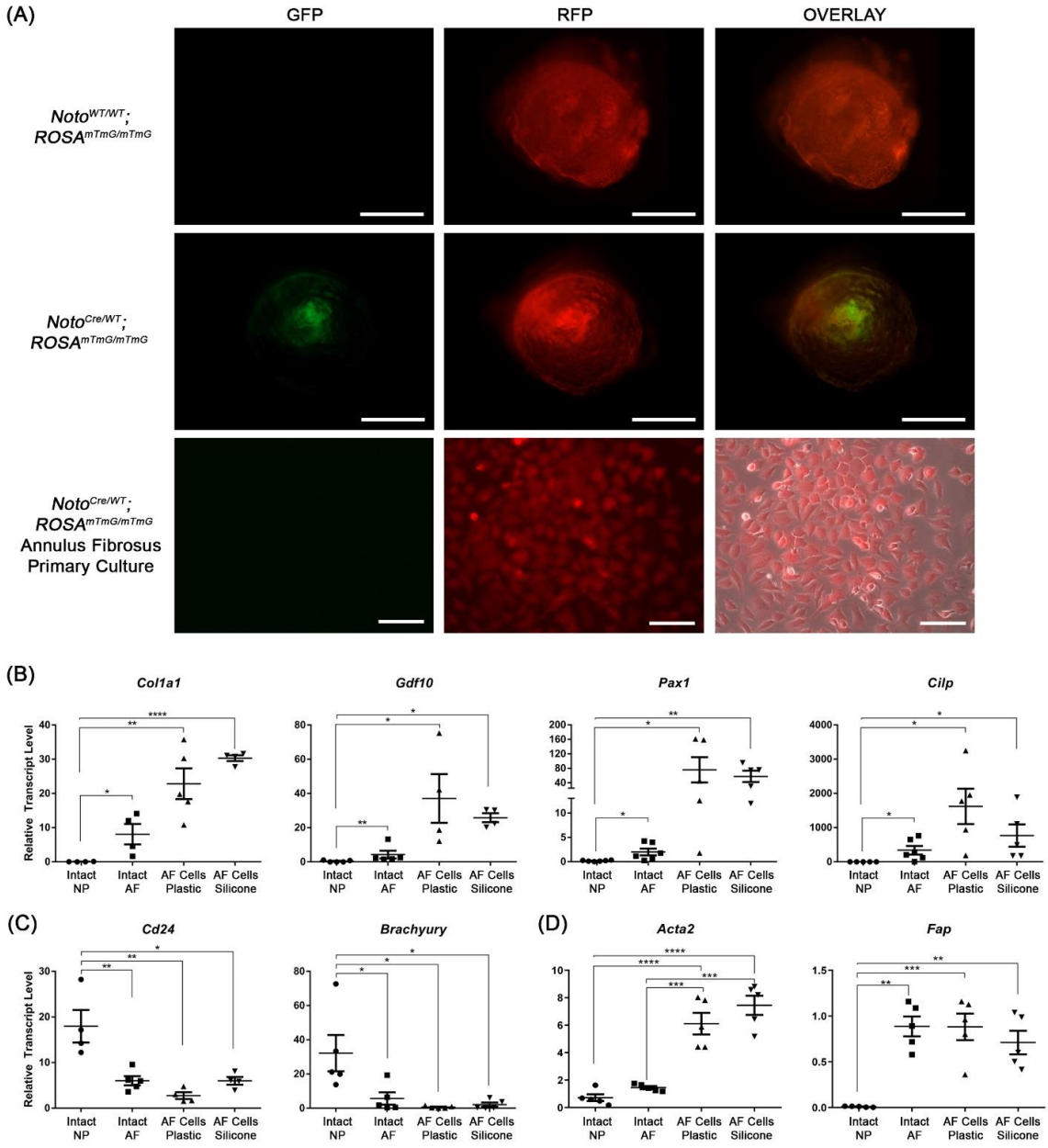
(A)
GFP
RFP
OVERLAY
Noto^WT/WT; ROSA^mTmG/mTmG
Noto^Cre/WT; ROSA^mTmG/mTmG
Noto^Cre/WT; ROSA^mTmG/mTmG
Annulus Fibrosus Primary Culture
(B)
Col1a1
Gdf10
Pax1
Cilp
Relative Transcript Level
Intact NP
Intact AF
AF Cells Plastic
AF Cells Silicone
(C)
Cd24
Brachyury
(D)
Acta2
Fap

Figure 2.3. Analysis of cell phenotype in primary AF cell cultures.

Primary AF cells were isolated from the *Noto*$^{Cre/WT}$*; ROSA*$^{mTmG/mTmG}$ conditional reporter mouse to allow for cell isolation based on fluorescence. A) Fluorescent micrograph of intact IVD isolated from *Noto*$^{WT/WT}$*; ROSA*$^{mTmG/mTmG}$ and *Noto*$^{Cre/WT}$*; ROSA*$^{mTmG/mTmG}$ mice showing NP-specific CRE activity. AF cells isolated from the conditional reporter show RFP but not GFP expression, indicating the absence of NP cell contamination. B-D) Gene expression analysis of primary annulus fibrosus cells compared to intact IVD tissues using panels of AF- and NP-associated markers and fibroblast markers. The expression of selected genes was quantified using qRT-PCR in primary AF cells grown on standard tissue culture plastic or silicone membranes (n=5) and compared to intact AF and NP tissues (n=6 mice; 5-6 IVDs pooled per mouse). Transcript levels were determined relative to a six-point calibration curve. B) AF cells cultured on tissue culture plastic and silicone membranes maintained expression of the AF markers, *Col1a1, Gdf10, Pax1,* and *Cilp* at levels comparable to intact AF tissue, significantly higher compared to NP tissue. C) AF cells cultured on tissue culture plastic and silicone membranes exhibited significantly lower expression of the NP markers, *Cd24* and *Brachyury* compared to NP tissues. D) AF cells cultured on tissue culture plastic and silicone membranes had significantly increased expression of *Acta2* compared to both intact IVD tissues; however, *Fap* expression was not significantly altered in AF cell cultures compared to intact AF tissue. Grubb's outlier test was used to identify outliers. Data presented as mean ± SEM. Data analyzed using one-way ANOVA followed by Tukey's post-hoc test. * = $P < 0.05$; ** = $P < 0.01$, *** = $P<0.001$; **** = $P<0.0001$. Scale bars = tissue micrograph = 200 μm; cell culture = 100 μm.

NP tissues (**Figure 2.3B**). No significant differences were detected in the expression of AF markers in primary cells cultured on tissue culture plastic or silicone membranes compared to the intact AF tissues. In contrast, AF cells showed minimal or no detectable expression of the NP-associated markers, *Cd24* and *Brachyury*, with no differences detected between AF tissue and primary cells cultured on either tissue culture plastic or silicone membranes (**Figure 2.3C**). Moreover, we quantified the expression of the markers of the myofibroblast / activated fibroblast phenotype, alpha smooth muscle actin (*Acta2)*[51] and fibroblast activation protein (*Fap)*[52]. Primary AF cells cultured on tissue culture plastic and silicone membranes showed significantly increased expression of *Acta2* compared to intact AF and NP tissues; however, expression of *Fap* was not altered in cultured AF cells compared to intact AF tissues (**Figure 2.3D**).

2.5.3 Mechanical stimulation induces cytoskeletal rearrangement in annulus fibrosus cells

To confirm that AF cells sense and respond to the CTS delivered by the MCB1 device, cytoskeletal rearrangement was examined since cytoskeletal reorganization has been shown to play a pivotal role in AF mechanotransduction[53]. In AF cells under static culture (unloaded control), F-actin was localized near the cell periphery in a predominantly punctate distribution with weak fibre staining. This pattern of F-actin staining was similar following 30 min exposure of cells to CTS at 0.1 Hz (**Figure 2.4A** solid arrow); however following exposure to CTS at 1.0 and 2.0 Hz, AF cells showed significantly increased stress fibre formation, which increased with higher frequency of loading (**Figure 2.4A** hollow arrow). Upon quantification, 61% of cells and 74% of cells were positive for stress fibres in AF cells exposed to CTS at 1.0 Hz and 2.0 Hz protocol, respectively (**Figure 2.4B**). The

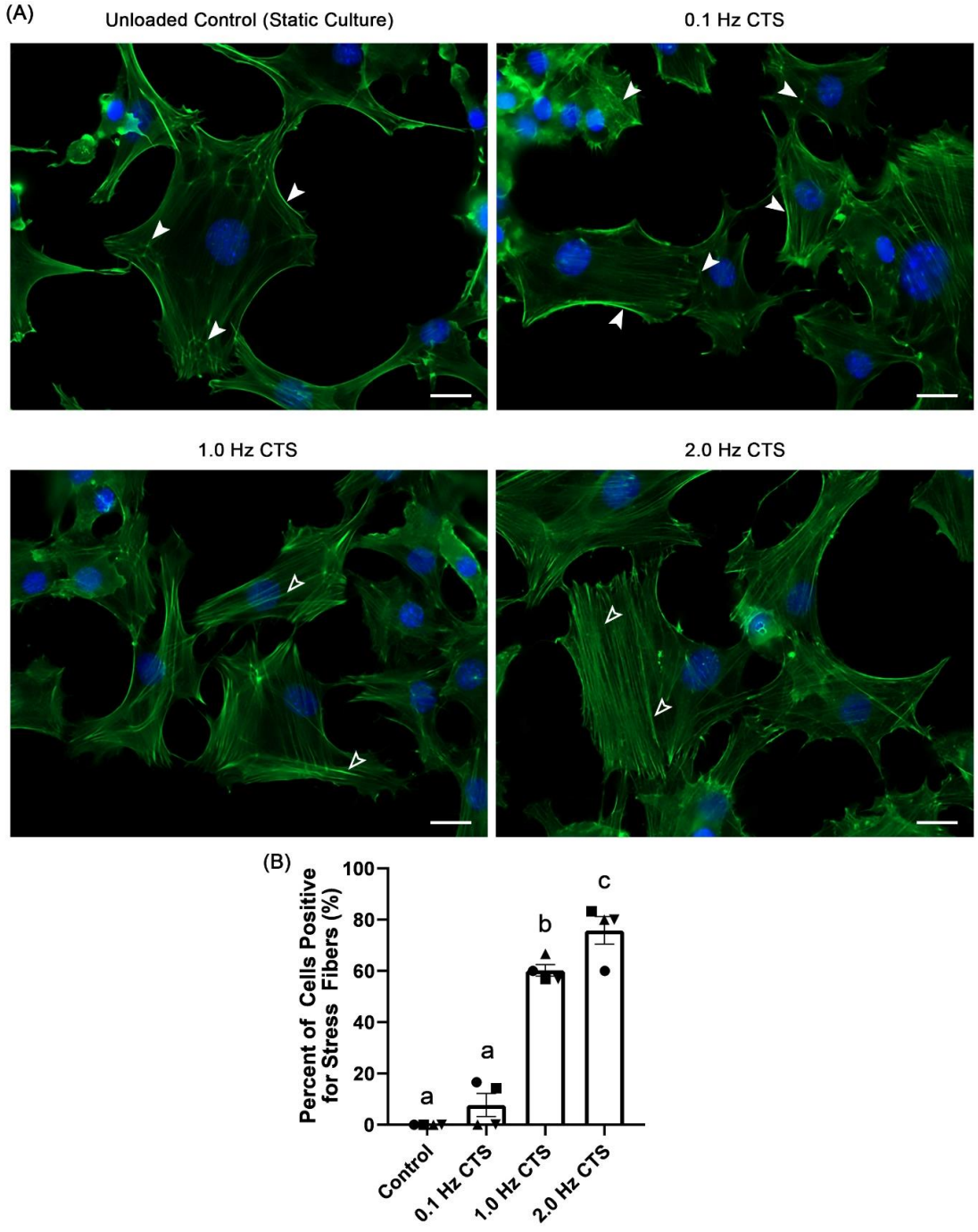
(A)
Unloaded Control (Static Culture)
0.1 Hz CTS
1.0 Hz CTS
2.0 Hz CTS
(B)
Percent of Cells Positive for Stress Fibers (%)
100
80
60
40
20
0
a
a
b
c
Control
0.1 Hz CTS
1.0 Hz CTS
2.0 Hz CTS

Figure 2.4. Cytoskeletal rearrangement in AF cells exposed to cyclic tensile strain.

A. Representative images of AF cells in which F-actin was visualized with alexa 488 phalloidin (counter stained with Hoechst stain to visualize nuclei) in AF cells grown in static culture (unloaded control) or following 30 min exposure to 6% cyclic tensile strain (CTS) at 0.1, 1.0, or 2.0 Hz. In the unloaded control and 0.1 Hz, F-actin was predominantly localized near the cell periphery with punctate distribution or weak fibre staining in the cytoplasm (white solid arrow). In contrast, AF cells exposed to CTS at 1.0 Hz and 2.0 Hz showed distinct stress fibre formations (hollow arrow). B) For each treatment group, the percentage of stress fibre-positive cells was assessed. Graphs present the average percentage of stress fibre-positive cells (calculated from 3 independent regions of interest) for each treatment group, for each of the 4 biological replicate experiments (presented as matching symbol). Compared to the unloaded control, exposure of AF cells to CTS at 1.0 or 2.0 Hz induced a significant increase in number of stress fibre-positive cells. Data presented as mean ± SEM from 4 independent experiments. Bars labelled with the same letter are not significantly different based on $p < 0.05$; one-way ANOVA followed by Tukey's post-hoc test.; Scale bar = 20 μm.

stress fibres formed in AF cells exposed to CTS at 1.0 and 2.0 Hz showed a random orientation.

2.5.4 Cyclic tensile strain activates ERK1/2 signalling in AF cells

After validating our model of dynamic cell culture, we first assessed the effects of CTS on MAPK pathway activation. Exposure of AF cells to 15 or 30 min CTS at 1.0 Hz did not induce a significant activation of either the ERK1/2 or p38 MAPK pathways, compared to static (unloaded) control (**Figure 2.5A**). Exposure of AF cells to CTS at 2.0 Hz induced a transient increase in ERK1/2 phosphorylation, significantly increased following 15 min of CTS but not significantly different from static control following 30 min CTS (**Figure 2.5B**). No statistical difference was detected in p38 activation in AF cells exposed to CTS at either time point (**Figure 2.5B**).

2.5.5 Acute exposure of AF cells to CTS induces frequency-dependent changes in gene expression

Since the effects of CTS on AF cell cytoskeletal rearrangement and MAPK pathway activation varied based on the frequency of load applied, we aimed to characterize the corresponding changes in gene expression using real-time PCR, focusing on expression of ECM genes, matrix degrading enzymes, inflammatory cytokines, candidate mechanosensitive genes, and cell surface receptors identified in related musculoskeletal cell types[9,30,32,54-61]. Given differences in the dynamic regulation of gene expression, cells were exposed to a single protocol of CTS (6% strain at 0.1, 1.0, or 2.0 Hz) and RNA was harvested following 2, 6, 12, or 24 h post stimulation.

AF cells exposed to acute (30 min) 6% CTS at 0.1 Hz showed a significant increase in the expression of multiple ECM genes, including type I collagen (*Col1a1*; significant increase

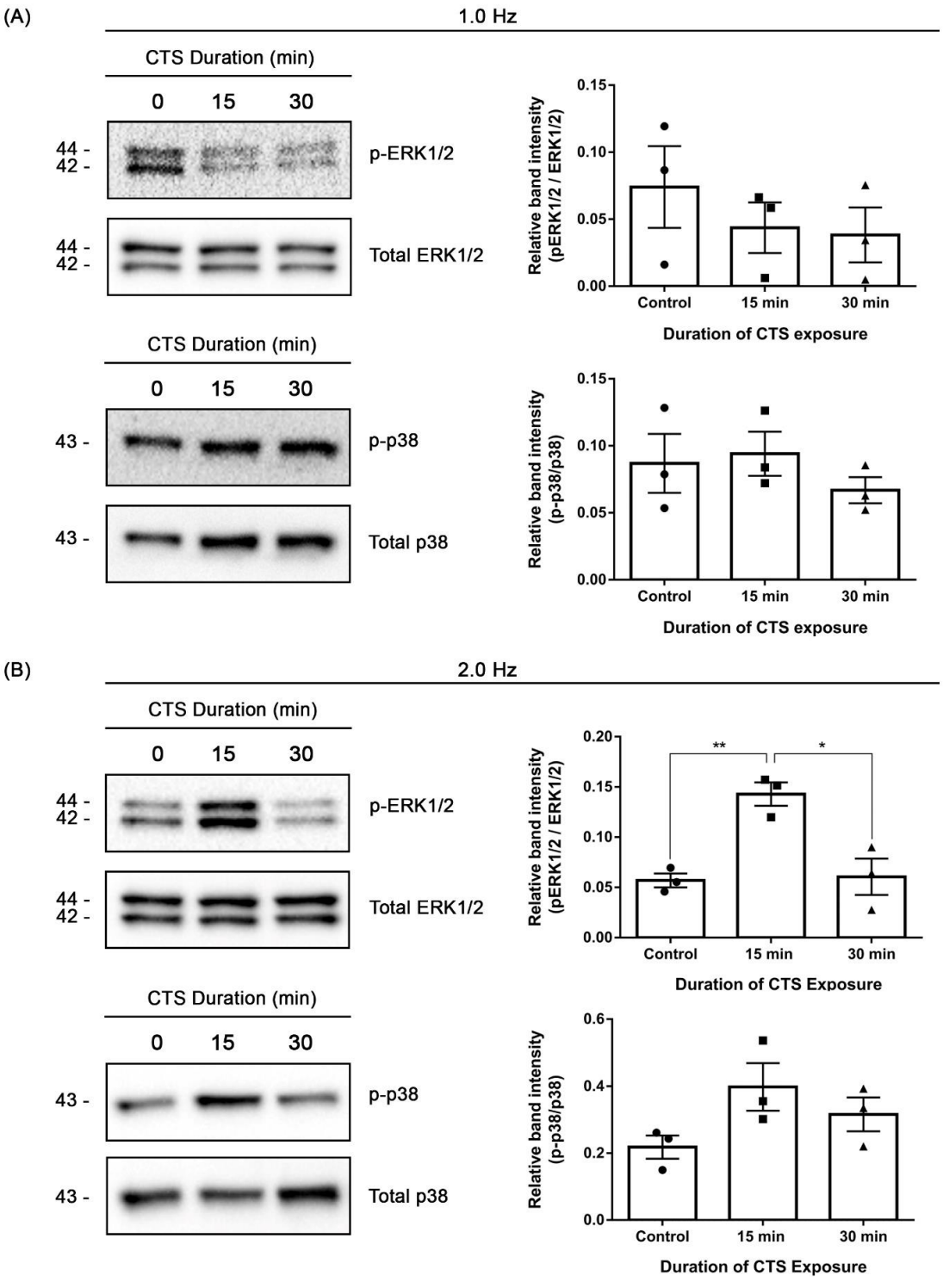
(A)
1.0 Hz
CTS Duration (min)
0
15
30
44 -
42 -
p-ERK1/2
Total ERK1/2
43 -
p-p38
Total p38
Relative band intensity (pERK1/2 / ERK1/2)
Relative band intensity (p-p38/p38)
0.15
0.10
0.05
0.00
Control
15 min
30 min
Duration of CTS exposure
(B)
2.0 Hz
**
*
0.20
0.6
0.4
0.2
0.0
Duration of CTS Exposure

Figure 2.5. ERK1/2 and p38 pathway activation in annulus fibrosus cells following cyclic tensile strain.

AF cells were subjected to 6% CTS for 15 or 30 min at frequencies of either 1.0 Hz (A) or 2.0 Hz (B). Cells cultured on silicone membranes in the absence of mechanical loading served as a control (0 CTS column). Total protein was harvested from AF cells immediately after loading and MAPK pathway activation was assessed through immunoblotting using antibodies for the phosphorylated forms (upper panels) or total (lower panels) ERK1/2 and p38 (bands representative of n=3 cell preparations, 2 animals per cell preparations). Quantification was performed by measurement of average relative density of bands corresponding to phosphoproteins, normalized to total protein. Data presented as a mean SEM; data were analyzed using Kruskal-Wallis test and Dunn's post-hoc test. * = $p < 0.05$; ** = $p < 0.01$.

at 2 h compared to unloaded controls; fold change = 1.6 ± 0.18), lubricin and aggrecan (*Prg4* and *Acan* respectively; both significantly increased at 2 h and 24 h compared to unloaded controls; fold change (*Prg4)* = 1.8 ± 0.16, fold change (*Acan*) = 1.6 ± 0.13) (**Figure 2.6A**); no significant differences were detected in the expression of type X collagen (*Col10a1*), biglycan (*Bgn*), or decorin (*Dcn*) (**Supplementary Figure 2.1**). We next assessed the expression of genes associated with matrix remodelling. Although no significant differences were detected in the expression of a disintegrin and metalloproteinase with thrombospondin type 1 motif 4 (*Adamts4*) or tissue inhibitor of metallopeptidase 1 (*Timp1*), mRNA levels of matrix metallopeptidase 3 (*Mmp3*) were increased in AF cells following acute exposure to CTS at 0.1 Hz (significantly increased at 2 h compared to unloaded controls; fold change = 1.6 ± 0.16) (**Figure 2.6B**). Acute exposure of AF cells to CTS at 0.1 Hz did not alter inflammatory cytokine gene expression (tumor necrosis factor alpha, *Tnfα*; interleukin 1 beta, *Il-1β*; interleukin 6, *Il-6*) or candidate mechanosensitive gene expression (cytochrome c oxidase subunit 2, *Cox2*; MYC proto-oncogene, *Myc*; Fos proto-oncogene AP-1 transcription factor subunit, *Fos*) compared to unloaded controls (**Figure 2.6C, D**).

AF cells were next subjected to acute (30 min) 6% CTS at 1.0 Hz. Compared to CTS at 0.1 Hz, AF cells showed fewer changes in the expression of ECM genes, with significant increases detected in the expression of *Acan* (6 h post-loading; fold change = 1.3 ± 0.05; **Figure 2.7A**) and no significant changes in the expression of matrix remodelling genes compared to unloaded controls (**Figure 2.7B**). No significant differences were detected in the expression of *Col10a1*, *Bgn*, or *Dcn* (**Supplementary Figure 2.1**). Interestingly, CTS at 1.0 Hz induced a significant increase in the expression of *Tnfα* (12 h post-loading; fold

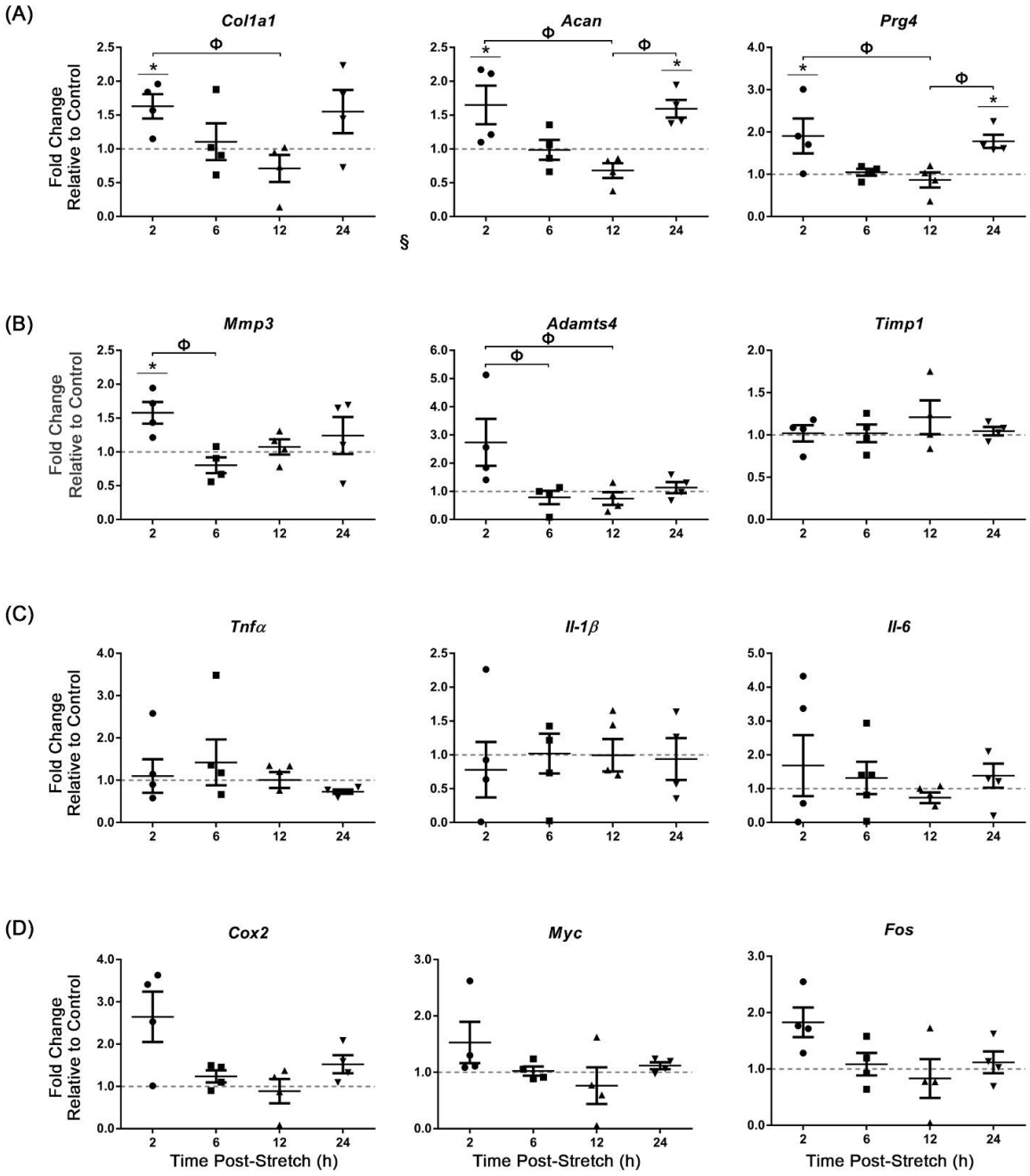
(A)
Col1a1
Acan
Prg4
(B)
Mmp3
Adamts4
Timp1
(C)
Tnfα
Il-1β
Il-6
(D)
Cox2
Myc
Fos
Fold Change Relative to Control
Time Post-Stretch (h)
2
6
12
24
Φ
*
§

Figure 2.6. Real-time PCR analysis of gene expression in AF cells following acute exposure to CTS at 0.1 Hz.

Primary AF cells were subjected to 6% CTS at 0.1 Hz for 30 min and RNA harvested following 2, 6, 12 or 24 h to assess the expression of extracellular matrix genes (A), matrix remodelling genes (B), inflammatory cytokines (C), and candidate mechanosensitive genes (D). AF cells showed a significant increase in the expression of *Col1A1* (2 h post-loading), *Prg4* (2h, 24 h post-loading), *Acan* (2h, 24 h post-loading) and *Mmp3* (2 h post-loading). Relative gene expression was calculated using ΔΔCt, normalized for input using the housekeeping gene *Hprt* and expressed relative to time-matched unloaded controls within each trial (control = 1; indicated as grey dotted lines). Data presented in mean ± SEM; n=4 cell preparations. Data were analyzed using one-way ANOVA followed by either Dunnett;s or Tukey's post-hoc test. Grubb's outlier test used to identify outliers. * = $P < 0.05$ versus unloaded control; Φ = $P < 0.05$ between fold changes at two time points.

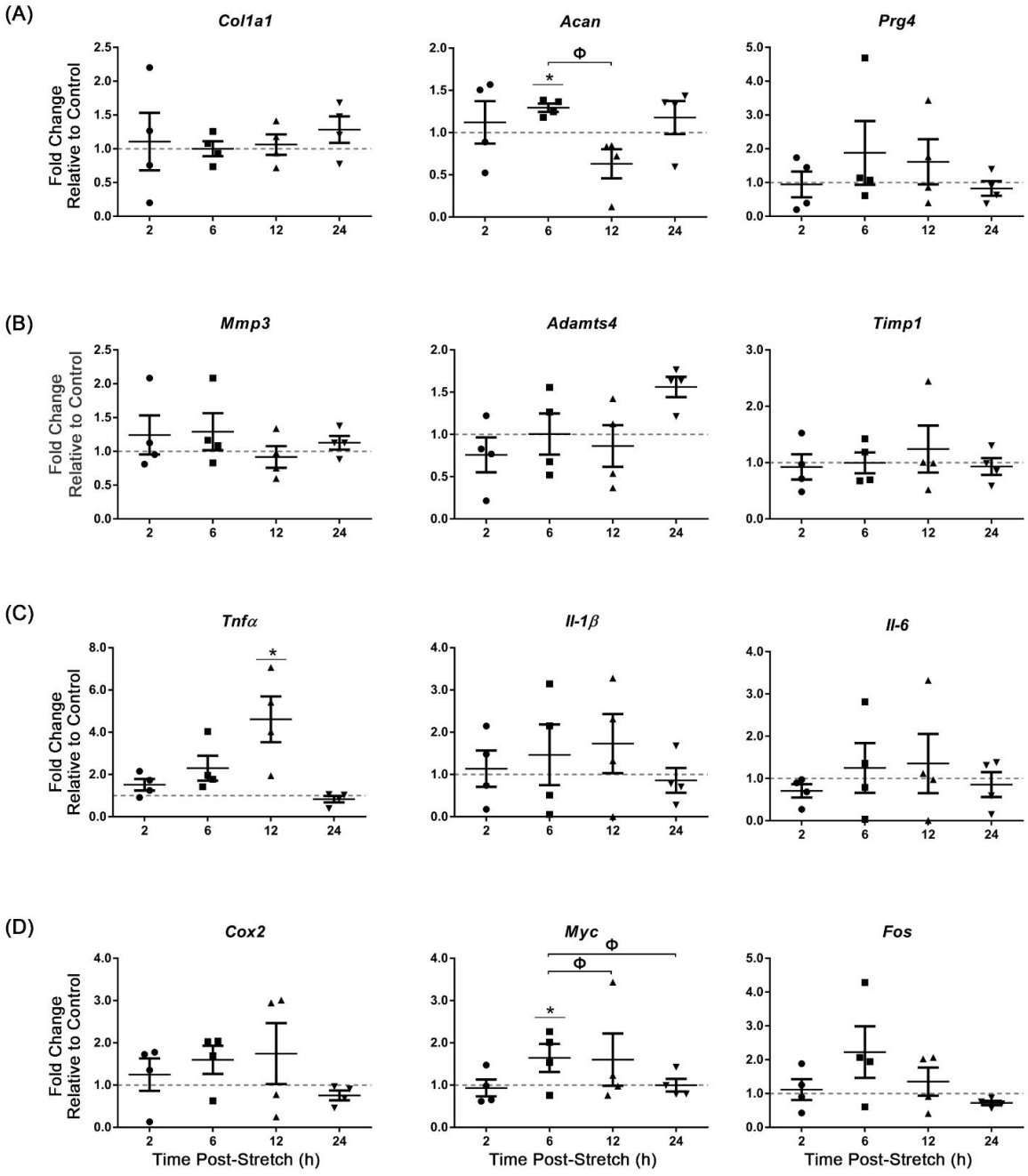
(A)
Col1a1
Acan
Prg4
(B)
Mmp3
Adamts4
Timp1
(C)
Tnfα
Il-1β
Il-6
(D)
Cox2
Myc
Fos
Fold Change Relative to Control
Time Post-Stretch (h)
2
6
12
24
*
Φ

Figure 2.7. Real-time PCR analysis of gene expression in AF cells following acute exposure to CTS at 1.0 Hz.

Primary AF cells were subjected to 6% CTS at 1.0 Hz for 30 min and RNA harvested following 2, 6, 12 or 24 h to assess the expression of extracellular matrix genes (A), matrix remodelling genes (B), inflammatory cytokines (C), and candidate mechanosensitive genes (D). AF cells showed a significant increase in the expression of *Acan* (6 h post-loading), *Tnfα* (12 h post-loading) and *Myc* (6 h post-loading). Relative gene expression was calculated using ΔΔCt, normalized for input using the housekeeping gene *Hprt* and expressed relative to time-matched unloaded controls within each trial (control = 1; indicated as grey dotted lines). Data presented in mean ± SEM; n=4 cell preparations. Data were analyzed using one-way ANOVA followed by either Dunnett;s or Tukey's post-hoc test. Grubb's outlier test used to identify outliers. * = $P < 0.05$ versus unloaded control; Φ = $P < 0.05$ between fold changes at two time points.

change = 4.36 ± 1.15; **Figure 2.7C**) in AF cells compared to unloaded controls. Among the candidate mechanosensitive genes, 30 min CTS at 1.0 Hz induced a significant increase in *Myc* expression (6 h post-loading; fold change = 1.6 ± 0.21) in AF cells compared to unloaded controls (**Figure 2.7D**).

Lastly, AF cells were exposed to acute (30 min) 6% CTS at 2.0 Hz showed a significant increase in the expression of the ECM genes *Acan* and *Prg4* (6 h and 2h post-loading, respectively; fold change (*Acan*) = 2.4 ± 0.12, fold change (*Prg4*) = 3.2 ± 0.89) compared to unloaded controls (**Figure 2.8A**). No significant differences were detected in the expression of *Col10a1*, *Bgn*, or *Dcn* (**Supplementary Figure 2.1**) or genes associated with matrix remodelling (**Figure 2.8B**). Acute CTS at 2.0 Hz induced a significant increase in *Tnfα* gene expression (2 h post-loading; fold change = 2.2 ± 0.52; **Figure 2.8C**) in AF cells compared to unloaded controls. Notably, all candidate mechanosensitive genes assessed (*Cox2*, *Myc*, *Fos*) were significantly upregulated compared to the unloaded controls at 6 h following exposure of AF cells to acute CTS at 2.0 Hz (fold change (*Cox2*) = 2.3 ± 0.45, fold change (*Myc*) = 1.5±0.07, fold change (*Fos*) = 1.6 ± 0.13; **Figure 2.8D**).

Given that CTS at 2.0 Hz elicited the most robust changes in the expression of ECM, pro-inflammatory cytokine, and mechanosensitive genes in AF cells compared to other loading protocols, we assessed if the expression of cell surface receptors would likewise be altered by these parameters of mechanical load. AF cells exposed to CTS at 2.0 Hz showed a significant increase in the gene expression of integrin subunits, *Itgα5* (12 h post-loading; fold change = 1.4 ± 0.12) and *Itgβ1* (12 h post-loading; fold change = 1.6±0.13) compared to unloaded controls (**Figure 2.9A**). Acute (30 min) exposure of AF cells to CTS at 2.0 Hz did not significantly alter the expression of both toll-like receptor 2 (*Tlr2*) and toll-like

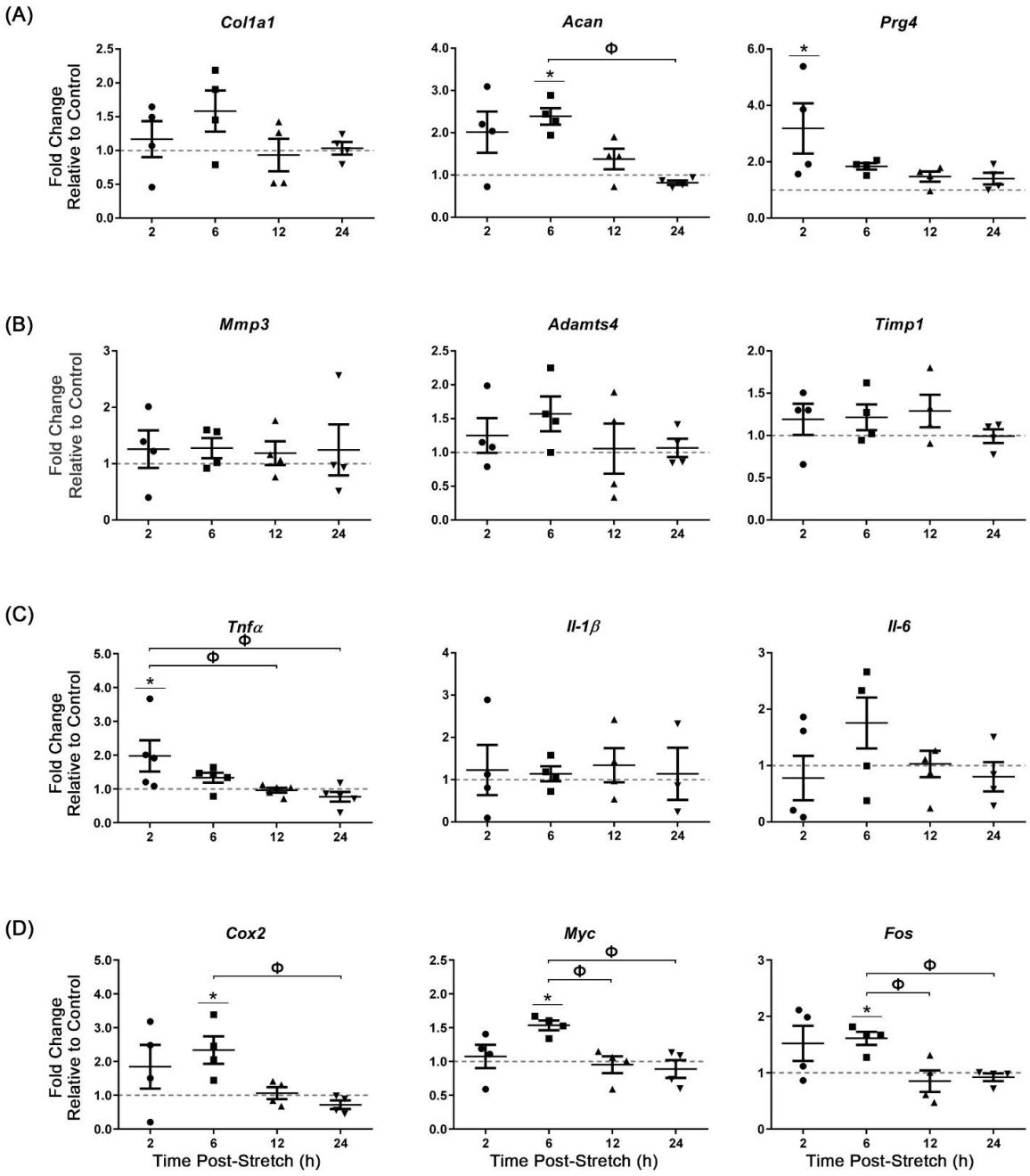
(A)
Col1a1
Acan
Prg4
(B)
Mmp3
Adamts4
Timp1
(C)
Tnfα
Il-1β
Il-6
(D)
Cox2
Myc
Fos
Fold Change Relative to Control
Time Post-Stretch (h)
2
6
12
24
*
Φ

Figure 2.8. Real-time PCR analysis of gene expression in AF cells following acute exposure to CTS at 2.0 Hz.

Primary AF cells were subjected to 6% CTS at 2.0 Hz for 30 min and RNA harvested following 2, 6, 12 or 24 h to assess the expression of extracellular matrix genes (A), matrix remodelling genes (B), inflammatory cytokines (C), and candidate mechanosensitive genes (D). AF cells showed a significant increase in the expression of *Acan* (6 h post-loading), *Prg4* (2 h post-loading), *Tnfα* (2 h post-loading), *Cox2* (6 h post-loading), *Myc* (6 h post-loading) and *Fos* (6h post-loading). Relative gene expression was calculated using ΔΔCt, normalized for input using the housekeeping gene *Hprt* and expressed relative to time-matched unloaded controls within each trial (control = 1; indicated as grey dotted lines). Data presented in mean ± SEM; n=4 cell preparations. Data were analyzed using one-way ANOVA followed by either Dunnett;s or Tukey's post-hoc test. Grubb's outlier test used to identify outliers. * = $P < 0.05$ versus unloaded control; Φ = $P < 0.05$ between fold changes at two time points.

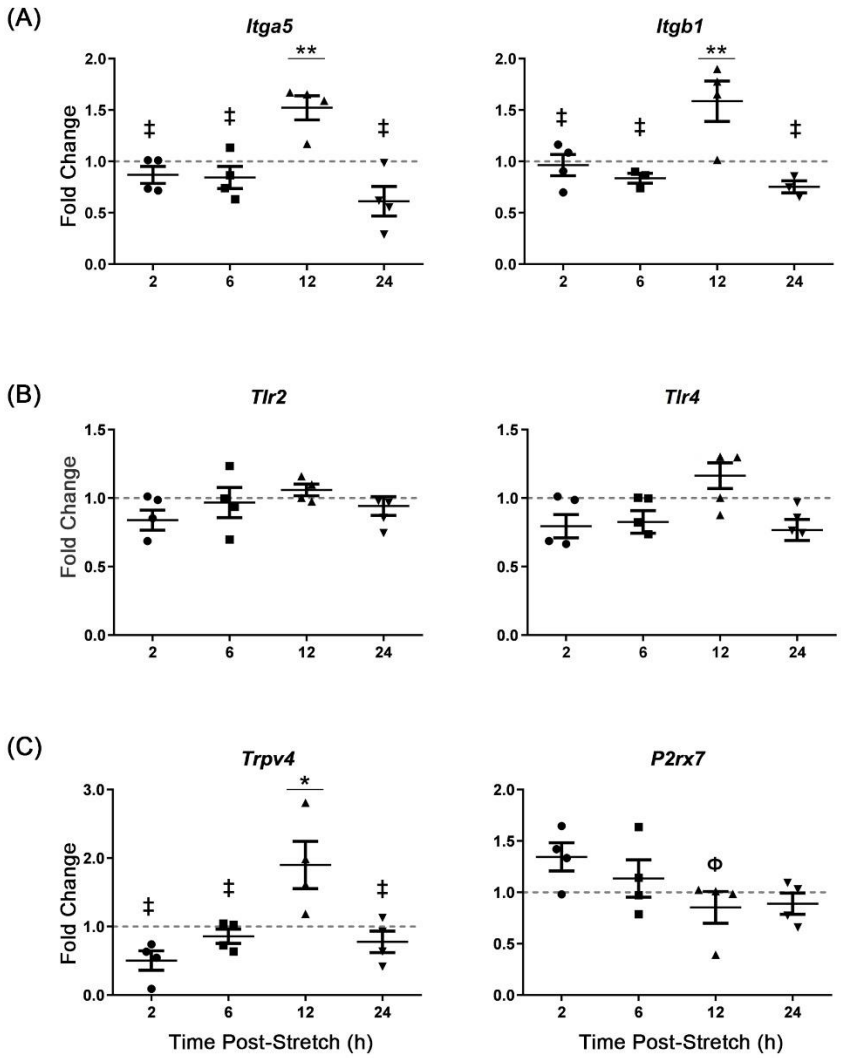

Figure 2.9. Real-time PCR analysis of candidate cell surface receptor gene expression in AF cells following acute exposure to CTS at 2.0 Hz.

Primary AF cells were subjected to 6% CTS at 2.0 Hz for 30 min and RNA harvested following 2, 6, 12 or 24 h to assess the expression of integrin subunits (A), Toll-like receptors (B), and membrane ion channel receptors (C). AF cells showed a significant increase in the expression of *Itgα5* (12 h post-loading), *Itgβ1* (12 h post-loading), and *Trpv4* (12 h post-loading). Relative gene expression was calculated using ΔΔCt, normalized for input using the housekeeping gene *Hprt* and expressed relative to time-matched unloaded controls within each trial (control = 1; indicated as grey dotted lines). Data presented in mean ± SEM; n=4 cell preparations. Data were analyzed using one-way ANOVA followed by either Dunnett;s or Tukey's post-hoc test. Grubb's outlier test used to identify outliers. * = $P < 0.05$ versus unloaded control; ** = $P < 0.01$ versus unloaded control; Φ = $P < 0.05$ between fold changes at two time points.

receptor 4 (*Tlr4*) genes (**Figure 2.9B**). In contrast, acute exposure of AF cells to CTS at 2.0 Hz significantly upregulated the expression of the transient receptor potential vanilloid 4 (*Trpv4)* gene at 12 h post-loading (fold change = 1.9 ± 0.34), with a trend towards increased purinoreceptor x subtype 7 (*P2rx7)* gene expression 2 h post-loading (fold change = 1.3 ± 0.14), compared to unloaded controls (**Figure 2.9C**).

All of the gene expression data from three different CTS protocols were compared at each time points to test if changes in gene expression are frequency-dependent. The analysis identified frequency as a significant source of variation in the expression of *Acan*, *Myc*, and *Tnfα* genes (**Supplementary Figure 2.2**).

2.6 Discussion

At the cellular level, mechanical loading in the IVD regulates a variety of biological processes in both cell type- and stimulus-dependent manner. Considering the dynamic nature of the loading environment in the IVD, previous studies examined the effects of CTS on AF cells, focusing on changes in the expression of genes related to ECM anabolism and catabolism[28-32]. Loading frequency, among other parameters of CTS, has been shown to be an important factor in determining cellular response to mechanical load[56]. Building upon these findings, the present study aimed to characterize the mechano-response of primary murine AF cells grown in a dynamic culture system that delivers bi-axial CTS. Using this model, we showed that AF cells adapted to different load frequencies by remodelling their cytoskeletal microarchitecture and activating intracellular signalling pathways dependent on the frequency of the applied load. Furthermore, we demonstrated that varying loading frequencies altered the mechano-response of AF cells at the level of gene expression, with notable changes in the expression of extracellular matrix, pro-

inflammatory cytokines, mechano-sensitive genes, and cell surface receptors. Taken together, these data provide further evidence for the existence of a "window" of loading parameters that may be beneficial to the IVD health.

The design of the present study incorporated two essential validation steps. First, we incorporated both IVD-specific genetic labeling strategies and gene expression analysis to assess and validate the AF cell phenotypes in our *in vitro* culture system. This analysis enabled us to confirm that primary cell preparations did not contain NP cells, and also enabled us to assess the effects of the culture substrate on cell phenotype, since fibroblasts have been shown to exhibit matrix stiffness adaptation[57]. Gene expression analysis demonstrated that on both tissue culture plastic and deformable silicone membranes, primary AF cells maintained robust expression of the AF-associated markers *Col1a1*[44], *Gdf10*[45], the marker of sclerotome development, *Pax1*[48], and *Cilp*[49] a gene recently reported by our group as enriched in the murine AF compared to the NP[50]. In addition, we assessed the expression of *Acta2* and *Fap*, two markers of the fibroblast phenotype[51,52]. Primary AF cells showed increased expression of *Acta2* and similar expression of *Fap* compared to intact AF tissues. Alpha smooth muscle actin (α-SMA), protein encoded by *Acta2*, is a contractile actin isoform found in myofibroblast[51]. In the context of the IVD, previous studies showed α-SMA expression in AF cells in both the canine and human IVD[62-63] as well as primary AF cells in 2D culture[62]. Buckley *et al*[63] and Desmouliere *et al*[64] independently showed that α-SMA plays a role in cell attachment, maintenance of cell shape, and may contribute to production and accumulation of ECM. *Fap* is a specific marker of the activated fibroblast phenotype and implicated in pathological tissue fibrosis[52]; no differences were detected in the current study between the expression of *Fap*

in primary AF cells compared to intact AF tissues. These data confirm that AF cells maintain their phenotype with increased expression of microarchitecture proteins for attachment and matrix production. Second, we confirmed the peak strain and strain uniformity of the MCB1 device by motion tracking analysis and showed that the CTS was being sensed by the AF cells by assessing stress fibre formation. Bioreactor systems described in previous studies were associated with limitations, including non-uniform strain patterns and heterogeneity in type of loading delivered (i.e. biaxial at central area, but approached pure uniaxial strain towards the edge)[66-68]. Our validation demonstrated that the MCB1 device overcame these limitations by incorporating a design mechanism that transfers linear motion into 24 points of radial stretch, which resulted in delivery of uniform biaxial strain on the silicone membrane.

One of the earliest responses we detected in AF cells exposed to CTS was transient activation of ERK1/2, but this was only observed at our highest frequency loading (6% CTS at 2.0 Hz). MAPKs are part of a phospho-relay signalling pathway known to mediate stress responses in different cell types, including IVD cells[33-38], making them potential mediators of mechanotransduction. Previous study by Pratsinis *et al* showed that in human AF cells derived from degenerate IVDs, 4% uniaxial CTS at 1.0 Hz induced the activation of all three MAPK pathways (ERK. P38, JNK) immediately after CTS, independent of strain magnitude of the applied load[38]. In contrast, the present study detected only significant activation of ERK1/2 in healthy murine AF cells. These differences may be due to the different species of origin of the AF cells used, differences in loading parameters, or differences associated with isolating cells from healthy or degenerate tissues. Functionally, integrin-dependent activation of ERK1/2, Src and RhoA has been found to regulate stress

fibre formation in other cell types, including endothelial cells and osteocytes[71-73]. Given that increased stress fibre formation in AF cells was induced by increasing frequency of CTS in our study, early activation of ERK1/2 may be required for cytoskeletal rearrangement in AF cells. Of note, a study by Hirata *et al* showed that phosphorylated ERK1/2 proteins localize to the stress fibres upon mechanical stretch, suggesting that stress fibres serve as a platform for tension-induced activation of biochemical mechanotransduction pathways[74]. As such, the link between cytoskeletal tension, stress fibre formation and the role of ERK1/2 activation should be further explored in AF cells.

Our findings are similar to previous studies reporting an anabolic response of matrix gene expression in AF cells subjected to CTS[28,29,31,32,58]. Interestingly, our study demonstrated that exposure of AF cells to CTS at low (0.1 Hz) and high (2.0 Hz) frequencies induced a significant increase in the gene expression of *Prg4*. Lubricin, the protein encoded by *Prg4*, is a large mucinous glycoprotein that serves as the primary boundary lubricant for articular cartilage[75] and its expression has been found to be protective against the development of osteoarthritis[76]. Previous studies reported lubricin expression in the interlamellar space of the annular lamellae in caprine IVDs[77]. Our data suggests that similar to chondrocytes in which *Prg4* expression is regulated by shear force[78], *Prg4* is mechanically regulated in the AF.

We also assessed the effects of CTS-exposure on AF cell expression of candidate mechano-sensitive genes identified in related musculoskeletal cell types. Previous studies reported that in osteoblasts, expression of *Cox2*, *Myc*, and *Fos* genes are induced by various modes of mechanical stimulation (vibration, fluid shear) and muscle cells also increase *Fos* gene expression following exposure to 20% cyclic tensile strain[53-55]. The most robust and

consistent changes were observed in AF cells exposed to CTS 2.0 Hz, which induced a significant upregulation of *Cox2*, *Myc*, and *Fos* gene expression. Given that expression of all three of these genes is required for transition from G1 to S phase of the cell cycle[55,56,57], these findings suggest that AF cells exposure to higher frequency CTS may promote cell proliferation. A previous study demonstrated that expression of a dominant negative form of Rho GTPase in osteoblasts blocked fluid shear stress-induced stress fibre formation and the expression of the immediate early genes *Cox2* and *Fos*[57]. Future studies using this model system will build on the characterization of the acute effects of CTS, and specifically assess the role of Rho GTPase and the changes in cell proliferation in AF cells following chronic exposure to CTS.

The pathophysiology of IVD degeneration is associated with alterations to the ECM due to imbalances between synthesis and degradation of ECM proteins. It has been hypothesized that ECM degradation fragments induce local inflammation driven by cells of the IVD[80]. However, the role of mechanical stimulation in either the initiation or propagation of local inflammation is largely unknown. Previous studies report that IVD cells exposed to high mechanical strain at low frequency (20% at 0.001 Hz) show increased gene expression of inflammatory receptors and cytokines[30]. In keeping with these findings, the present study showed that exposure of AF cells to CTS at 1.0 Hz and 2.0 Hz induced a significant upregulation of *Tnfα* gene expression, suggesting that mechanical stimulation alone can directly contribute to the initiation of local inflammation. We acknowledge, however, that these findings are limited to quantification of changes at the level of gene expression; more long-term experiments should explore how alterations in gene expression alter levels of secreted inflammatory cytokines. Although traditionally inflammation was viewed as

detrimental response involved in disease progression, recent reports suggest that a balanced inflammatory response may be required for matrix repair and maintaining tissue homeostasis in different cell types, including IVD cells[80,81]. Given that the loading parameters used in this study fall within the range of those experienced in a physiological context, the increased expression of *Tnfα* may be contributing to matrix homeostasis. Nonetheless, the data suggest a direct link between mechanical stimulation and inflammatory cytokine gene expression in AF cells.

At the cellular level, mechanical signals are transduced via cell surface receptors acting in concert to translate physical force into biologically relevant signals[32,72]. Previous studies using dynamic organ culture showed that expression of integrin subunits α5 and β1 genes was induced in both rat NP and AF tissues by cyclic compressive stress (1.3 MPa, 1.0 Hz) for 6 days[82]. Le Maitre *et al* [83] showed that compression-induced changes in matrix gene expression in human NP cells were mediated by α5β1 integrin signalling. Our findings of mechanically- induced *Itgα5* and *Itgβ1* expression suggest that α5β1 integrin signalling may likewise contribute to AF mechanotransduction in response to CTS, in keeping with the downstream activation of the ERK1/2 pathway we report. Gawri *et al*[30] showed increased expression of both the toll-like receptor 2 and 4 genes in human IVD cells exposed to high mechanical strain at low frequency (20% cyclical stretch at 0.001 Hz). The observed difference from the current study which showed no change in TLR expression in murine AF cells may be due to differences in loading parameters, such as strain percentage, frequency, and duration. Lastly, *Trpv4* and *P2rx7,* candidate mechano-sensitive channels studied in other musculoskeletal cell types[58-60] were upregulated in AF cells following exposure to CTS. Previous studies reported that the expression of both genes was regulated

by cyclic compression in chondrocytes[58,59]. Functionally, both TRPV4 and P2X7 have been shown to elicit intracellular calcium transient upon mechanical compression[58,59]. In the context of the IVD, TRPV4 is activated by changes in osmolarity[84], and a related purinoreceptor, P2X4, has been shown to mediate ATP-induced membrane potential response[85]. Taken together, the current study demonstrates that AF cells adapt to mechanical stimulation by regulating cell surface receptor gene expression, thereby potentially modulating the activation of intracellular signalling pathways.

A limitation of the current study is the examination of cellular responses to CTS in a cell culture system where cells were seeded onto silicone membranes; consequently, endogenous cell-matrix interactions present in the IVD microenvironment were not recapitulated. In order to minimize these issues, AF cells were pre-cultured on membranes in media supplemented with ascorbic acid to enable collagen production and secretion. To fully explore the effect of ECM in mediating mechanical strain, future studies could incorporate specific ECM protein coatings in the MCB1 device. We also acknowledge that our protocols for primary murine cell isolation may have introduced heterogeneity in the AF cell population studied. To maximize the yield of our primary cell isolation from the murine IVDs, we pooled AF tissues from all anatomical regions (cervical through caudal) and included cells from both inner and outer AF. Subtle differences in the phenotype of AF cells in each of these regions, or in the mechanical loading environment from which they were isolated may impact their response to mechanical stimulation *in vitro*.

2.7 Conclusions

Overall, our findings suggest that effects of CTS on healthy murine AF cells are frequency-dependent. The most anabolic effect marked by increased expression of extracellular

matrix genes was observed following exposure to 6% CTS at 0.1 Hz. At higher frequency (2.0 Hz), CTS induced mechanically sensitive genes (associated with the regulation of cell cycle progression) as well as proinflammatory cytokine gene expression in healthy AF cells. Taken together, these finding further suggests the existence of a range of loading parameters that are beneficial to IVD health, which may help to understand the pathophysiology of IVD degeneration in the context of mechanobiology. Moreover, the differences in MAPK activation we report in AF cells derived from healthy IVDs compared to previous findings from degenerate tissues suggest differences in the cellular signalling pathways activated by CTS in AF cells associated with tissue health. Further studies are needed to elucidate other mechanotransduction pathways and their involvement in regulating cellular function in the IVD.

2.8 Supplementary Figure

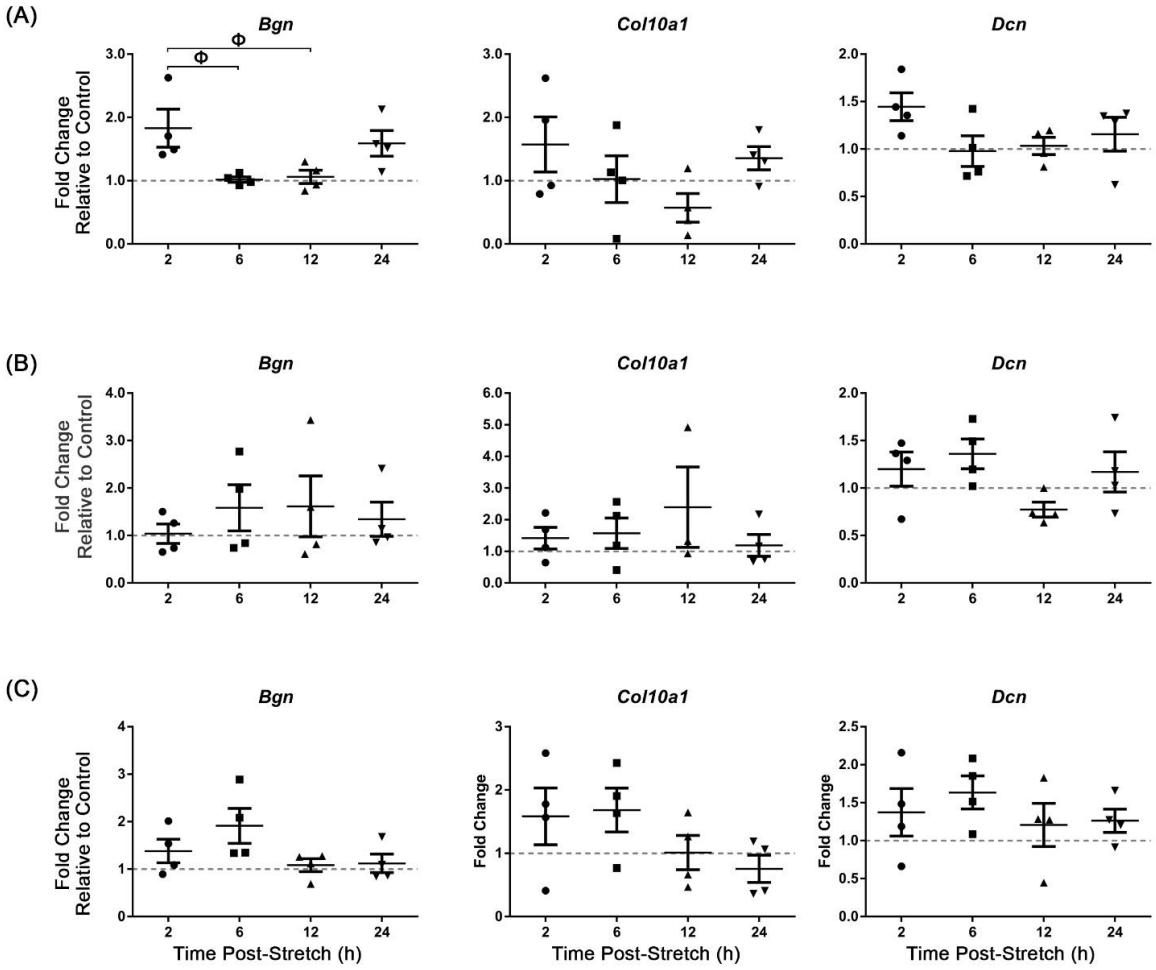

Supplementary Figure 2.1. Effects of CTS on the expression of additional candidate ECM genes in AF cells.

Biglycan (*Bgn*), type X collagen (*Col10a1*), and decorin (*Dcn*) gene expression was quantified in AF cells exposed to acute CTS at 0.1 Hz (A), 1.0 Hz (B), and 2.0 Hz (C). The expression levels of the three matrix genes did not change upon mechanical stimulation. Relative gene expression was calculated using the ΔΔCt method, normalized for input using the housekeeping gene *Hprt* and expressed relative to time-matched unloaded controls within each trial (control = 1; indicated as grey dotted lines). Data presented in mean ± SEM; n=4 cell preparations. Data were analyzed using one-way ANOVA followed by either Dunnett;s or Tukey's post-hoc test. Grubb's outlier test used to identify outliers. Φ = $P < 0.05$ between fold changes at two time points.

Gene	Source of Variation	F	p value	Significant?
Acan	Time	8.505	<0.0001	Yes
	Frequency	4.189	0.0215	Yes
Adamts4	Time	1.392	0.2519	No
	Frequency	1.425	0.2511	No
Col1a1	Time	2.982	0.0288	Yes
	Frequency	0.5803	0.5639	No
Cox2	Time	4.237	0.0054	Yes
	Frequency	0.3675	0.6946	No
Fos	Time	4.017	0.0072	Yes
	Frequency	0.2096	0.8117	No
Il-1β	Time	0.4179	0.7948	No
	Frequency	0.2114	0.8102	No
Il-6	Time	0.3325	0.8546	No
	Frequency	0.03311	0.9675	No
Mmp3	Time	1.147	0.3469	No
	Frequency	1.017	0.3697	No
Myc	Time	4.409	0.0043	Yes
	Frequency	3.506	0.0385	Yes
Prg4	Time	2.456	0.0592	No
	Frequency	2.622	0.0838	No
Timp1	Time	0.7253	0.5793	No
	Frequency	0.9733	0.3856	No
Tnfα	Time	3.137	0.0233	Yes
	Frequency	3.811	0.0296	Yes

Supplementary Figure 2.2. Two way ANOVA table with P and F value for each gene.

2.9 References

1. James SL, Abate D, Abate KH, et al. Global, regional, and national incidence, prevalence, and years lived with disability for 354 diseases and injuries for 195 countries and territories, 1990–2017: a systematic analysis for the Global Burden of Disease Study 2017. *The Lancet.* 2018;392(10159):1789-858.

2. Arnbak B, Jensen TS, Egund N, et al. Prevalence of degenerative and spondyloarthritis-related magnetic resonance imaging findings in the spine and sacroiliac joints in patients with persistent low back pain. *Eur Radiol.* 2016; 26(4): 1191-1203.

3. Smith LJ, Nerurkar NL, Choi KS, Harfe BD, Elliott DM. Degeneration and regeneration of the intervertebral disc: lessons from development. *Disease models & mechanisms.* 2011;4(1):31-41.

4. Adams MA, Roughley PJ. What is intervertebral disc degeneration, and what causes it?. *Spine.* 2006;31(18):2151-61.

5. Kepler CK, Ponnappan RK, Tannoury CA, Risbud MV, Anderson DG. The molecular basis of intervertebral disc degeneration. *The Spine Journal.* 2013;13(3):318-30.

6. Le Maitre CL, Pockert A, Buttle DJ, Freemont AJ, Hoyland JA. Matrix synthesis and degradation in human intervertebral disc degeneration. *Biochemical society transactions.* 2007;35(4):652-655.

7. Zhu Q, Gao X, Gu W. Temporal changes of mechanical signals and extracellular composition in human intervertebral disc during degenerative progression. *Journal of biomechanics.* 2014;47(15):3734-3743.

8. Vo NV, Hartman RA, Patil PR, Risbud MV, Kletsas D, Iatridis JC, Hoyland JA, Le Maitre CL, Sowa GA, Kang JD. Molecular mechanisms of biological aging in intervertebral discs. *Journal of orthopaedic research.* 2016;34(8):1289-1306.

9. Vergroesen PP, Kingma I, Emanuel KS, Hoogendoorn RJ, Welting TJ, van Royen BJ, van Dieën JH, Smit TH. Mechanics and biology in intervertebral disc degeneration: a vicious circle. *Osteoarthritis and cartilage*. 2015;23(7):1057-1070.

10. Setton LA, Chen J. Cell mechanics and mechanobiology in the intervertebral disc. *Spine*. 2004;29(23):2710-2723.

11. Urban JP, Roberts S. Degeneration of the intervertebral disc. *Arthritis Res Ther*. 2003;5(3):120.

12. Urban JP, Smith S, Fairbank JC. Nutrition of the intervertebral disc. *Spine.* 2004;29(23):2700-2709.

13. Wang SZ, Rui YF, Lu J, Wang C. Cell and molecular biology of intervertebral disc degeneration: current understanding and implications for potential therapeutic strategies. *Cell proliferation.* 2014;47(5):381-390.

14. Feng Y, Egan B, Wang J. Genetic factors in intervertebral disc degeneration. *Genes & diseases.* 2016;3(3):178-185.

15. Hanaei S, Abdollahzade S, Khoshnevisan A, Kepler CK, Rezaei N. Genetic aspects of intervertebral disc degeneration. *Reviews in the neurosciences*. 2015;26(5):581-606.

16. Marchand FR, Ahmed AM. Investigation of the laminate structure of lumbar disc anulus fibrosus. *Spine.* 1990;15(5):402-10.

17. Chan WC, Sze KL, Samartzis D, Leung VY, Chan D. Structure and biology of the intervertebral disk in health and disease. *Orthopedic Clinics.* 2011;42(4):447-64.

18. Gawri R, Moir J, Ouellet J, Beckman L, Steffen T, Roughley P, Haglund L. Physiological loading can restore the proteoglycan content in a model of early IVD degeneration. *PloS one.* 2014;9(7):e101233.

19. Iatridis JC, MacLean JJ, Roughley PJ, Alini M. Effects of mechanical loading on intervertebral disc metabolism in vivo. *The Journal of bone and joint surgery.* 2006;88(0 2):41-46.

20. Videman TA, Nurminen MA, Troup JD. 1990 Volvo Award in clinical sciences. Lumbar spinal pathology in cadaveric material in relation to history of back pain, occupation, and physical loading. *Spine.* 1990;15(8):728-740.

21. Gregory, D. E., & Callaghan, J. P. (2011). A comparison of uniaxial and biaxial mechanical properties of the annulus fibrosus: a porcine model. *Journal of biomechanical engineering*, *133*(2).

22. Shirazi-Adl SA, Shrivastava SC, Ahmed AM. Stress analysis of the lumbar disc-body unit in compression. A three-dimensional nonlinear finite element study. Spine. 1984;9(2):120-34.

23. Adams MA, McNally DS, Dolan P. 'Stress' distributions inside intervertebral discs. The effects of age and degeneration. *The Journal of bone and joint surgery.* British volume. 1996;78(6):965-72.

24. Neidlinger-Wilke C, Galbusera F, Pratsinis H, Mavrogonatou E, Mietsch A, Kletsas D, Wilke HJ. Mechanical loading of the intervertebral disc: from the macroscopic to the cellular level. *European Spine Journal.* 2014;23(3):333-43.

25. Wilke HJ, Neef P, Caimi M, Hoogland T, Claes LE. New in vivo measurements of pressures in the intervertebral disc in daily life. *Spine.* 1999;24(8):755-62.

26. Broberg KB. On the mechanical behaviour of intervertebral discs. Spine. 1983 Mar;8(2):151-65.

27. Ebara S, Iatridis JC, Setton LA, Foster RJ, Mow VC, Weidenbaum M. Tensile properties of nondegenerate human lumbar anulus fibrosus. *Spine.* 1996;21(4):452-61.

28. Neidlinger-Wilke C, Würtz K, Liedert A, Schmidt C, Börm W, Ignatius A, Wilke HJ, Claes L. A three-dimensional collagen matrix as a suitable culture system for the comparison of cyclic strain and hydrostatic pressure effects on intervertebral disc cells. *Journal of Neurosurgery: Spine.* 2005;2(4):457-65.

29. Wuertz K, Urban JP, Klasen J, Ignatius A, Wilke HJ, Claes L, Neidlinger-Wilke C. Influence of extracellular osmolarity and mechanical stimulation on gene expression of intervertebral disc cells. *Journal of Orthopaedic Research.* 2007;25(11):1513-22.

30. Gawri R, Rosenzweig DH, Krock E, Ouellet JA, Stone LS, Quinn TM, Haglund L. High mechanical strain of primary intervertebral disc cells promotes secretion of inflammatory factors associated with disc degeneration and pain. Arthritis research & therapy. 2014;16(1):R21.

31. Gilbert HT, Hoyland JA, Millward-Sadler SJ. The response of human anulus fibrosus cells to cyclic tensile strain is frequency-dependent and altered with disc degeneration. *Arthritis & Rheumatism.* 2010;62(11):3385-94.

32. Gilbert HT, Nagra NS, Freemont AJ, Millward-Sadler SJ, Hoyland JA. Integrin–Dependent mechanotransduction in mechanically stimulated human annulus fibrosus cells: evidence for an alternative mechanotransduction pathway operating with degeneration. *PloS one.* 2013;8(9):e72994.

33. Zhang K, Ding W, Sun W, Sun XJ, Xie YZ, Zhao CQ, Zhao J. Beta1 integrin inhibits apoptosis induced by cyclic stretch in annulus fibrosus cells via ERK1/2 MAPK pathway. *Apoptosis.* 2016;21(1):13-24.

34. Davis RJ. The mitogen-activated protein kinase signal transduction pathway. *Journal of biological chemistry*. 1993;268:14553-6.

35. Robinson MJ, Cobb MH. Mitogen-activated protein kinase pathways. *Current opinion in cell biology*. 1997;9(2):180-6.

36. Roux PP, Blenis J. ERK and p38 MAPK-activated protein kinases: a family of protein kinases with diverse biological functions. *Microbiol. Mol. Biol. Rev*. 2004;68(2):320-44.

37. Zarubin T, Jiahuai HA. Activation and signaling of the p38 MAP kinase pathway. Cell research. 2005;15(1):11.

38. Pratsinis H, Papadopoulou A, Neidlinger-Wilke C, Brayda-Bruno M, Wilke HJ, Kletsas D. Cyclic tensile stress of human annulus fibrosus cells induces MAPK activation: involvement in proinflammatory gene expression. Osteoarthritis and cartilage. 2016;24(4):679-87.

39. McCann MR, Tamplin OJ, Rossant J, Séguin CA. Tracing notochord-derived cells using a Noto-cre mouse: implications for intervertebral disc development. *Disease models & mechanisms.* 2012;5(1):73-82.

40. Muzumdar MD, Tasic B, Miyamichi K, Li L, Luo L. A global double-fluorescent Cre reporter mouse. *Genesis.* 2007;45(9):593-605.

41. Chen K, Vigliotti A, Bacca M, McMeeking RM, Deshpande VS, Holmes JW. Role of boundary conditions in determining cell alignment in response to stretch. *Proceedings of the National Academy of Sciences.* 2018;115(5):986-91.

42. O'Connell GD, Johannessen W, Vresilovic EJ, Elliott DM. Human internal disc strains in axial compression measured noninvasively using magnetic resonance imaging. *Spine.* 2007;32(25):2860-8.

43. Winter DA. Biomechanical motor patterns in normal walking. *Journal of motor behavior.* 1983;15(4):302-30.

44. Sakai D, Nakai T, Mochida J, Alini M, Grad S. Differential phenotype of intervertebral disc cells: microarray and immunohistochemical analysis of canine nucleus pulposus and anulus fibrosus. *Spine.* 2009;34(14):1448-56.

45. Clouet J, Grimandi G, Pot-Vaucel M, Masson M, Fellah HB, Guigand L, Cherel Y, Bord E, Rannou F, Weiss P, Guicheux J. Identification of phenotypic discriminating markers for intervertebral disc cells and articular chondrocytes. *Rheumatology.* 2009;48(11):1447-50.

46. Shapiro IM, Risbud MV. Transcriptional profiling of the nucleus pulposus: say yes to notochord.

47. Minogue BM, Richardson SM, Zeef LA, Freemont AJ, Hoyland JA. Characterization of the human nucleus pulposus cell phenotype and evaluation of novel marker gene expression to define adult stem cell differentiation. *Arthritis & Rheumatism.* 2010;62(12):3695-705.

48. Wallin J, Wilting J, Koseki H, Fritsch R, Christ B, Balling R. The role of Pax-1 in axial skeleton development. *Development.* 1994;120(5):1109-21.

49. Seki S, Kawaguchi Y, Chiba K, Mikami Y, Kizawa H, Oya T, Mio F, Mori M, Miyamoto Y, Masuda I, Tsunoda T. A functional SNP in CILP, encoding cartilage intermediate layer protein, is associated with susceptibility to lumbar disc disease. *Nature genetics.* 2005;37(6):607.

50. Veras MA, McCann MR, Tenn NA, Séguin CA. Transcriptional profiling of the murine intervertebral disc and age-associated changes in the nucleus pulposus. *Connective tissue research.* 2019:1-9.

51. Hinz, B., Celetta, G., Tomasek, J. J., Gabbiani, G., & Chaponnier, C. (2001). Alpha-smooth muscle actin expression upregulates fibroblast contractile activity. *Molecular biology of the cell*, 12(9), 2730-2741.

52. Tillmanns, J., Hoffmann, D., Habbaba, Y., Schmitto, J. D., Sedding, D., Fraccarollo, D., ... & Bauersachs, J. (2015). Fibroblast activation protein alpha expression identifies activated fibroblasts after myocardial infarction. *Journal of molecular and cellular cardiology*, *87*, 194-203.

53. Li S, Jia X, Duance VC, Blain EJ. The effects of cyclic tensile strain on the organisation and expression of cytoskeletal elements in bovine intervertebral disc cells: an in vitro study. *Eur Cell Mater.* 2011;21:508-22.

54. Tjandrawinata RR, Vincent VL, Hughes-Fulford M. Vibrational force alters mRNA expression in osteoblasts. *The FASEB journal.* 1997;11(6):493-7.

55. Wadhwa S, Godwin SL, Peterson DR, Epstein MA, Raisz LG, Pilbeam CC. Fluid flow induction of cyclo-oxygenase 2 gene expression in osteoblasts is dependent on an extracellular signal-regulated kinase signaling pathway. *Journal of Bone and Mineral Research.* 2002;17(2):266-74.

56. Ikeda S, Yoshida A, Matayoshi S, Tanaka N. Repetitive stretch induces c-fos and myogenin mRNA within several hours in skeletal muscle removed from rats. *Archives of physical medicine and rehabilitation.* 2003;84(3):419-23.

57. Heikkila R, Schwab G, Wickstrom E, Loke SL, Pluznik DH, Watt R, Neckers LM. A c-myc antisense oligodeoxynucleotide inhibits entry into S phase but not progress from G0 to G1. *Nature.* 1987;328(6129):445.

58. O'Conor, C. J., Leddy, H. A., Benefield, H. C., Liedtke, W. B., & Guilak, F. (2014). TRPV4-mediated mechanotransduction regulates the metabolic response of chondrocytes to dynamic loading. *Proceedings of the National Academy of Sciences*, *111*(4), 1316-1321.

59. Tanigawa, H., Maeda, T., Kubo, M., Kumagai, K., & Imai, S. (2017). Functional expression of purinergic p2X7 receptors in rabbit articular chondrocyte. *Osteoarthritis and Cartilage*, *25*, S156.

60. Shi, J., Folwaczny, M., Wichelhaus, A., & Baumert, U. (2019). Differences in RUNX 2 and P2 RX 7 gene expression between mono-and coculture of human periodontal ligament cells and human osteoblasts under compressive force application. *Orthodontics & craniofacial research*, *22*(3), 168-176.

61. Kariya, T., Tanabe, N., Shionome, C., Manaka, S., Kawato, T., Zhao, N., ... & Shimizu, N. (2015). Tension force-induced ATP promotes osteogenesis through P2X7 receptor in osteoblasts. *Journal of cellular biochemistry*, *116*(1), 12-21.

62. Schneider, T. O., Mueller, S. M., Shortkroff, S., & Spector, M. (1999). Expression of α-smooth muscle actin in canine intervertebal disc cells in situ and in collagen-glycosaminoglycan matrices in vitro. *Journal of orthopaedic research*, *17*(2), 192-199.

63. Hastreiter, D., Ozuna, R. M., & Spector, M. (2001). Regional variations in certain cellular characteristics in human lumbar intervertebral discs, including the presence of α-smooth muscle actin. *Journal of Orthopaedic Research*, *19*(4), 597-604.

64. Buckley, I. K., & Porter, K. R. (1967). Cytoplasmic fibrils in living cultured cells. *Protoplasma*, *64*(4), 349-380.

65. Desmoulière, A., Rubbia-Brandt, L., Grau, G., & Gabbiani, G. (1992). Heparin induces alpha-smooth muscle actin expression in cultured fibroblasts and in granulation tissue myofibroblasts. *Laboratory investigation; a journal of technical methods and pathology*, *67*(6), 716-726.

66. Sowa G, Coelho P, Vo N, Bedison R, Chiao A, Davies C, Studer R, Kang J. Determination of annulus fibrosus cell response to tensile strain as a function of duration, magnitude, and frequency. *Journal of Orthopaedic Research.* 2011;29(8):1275-83.

67. Balestrini JL, Chaudhry S, Sarrazy V, Koehler A, Hinz B. The mechanical memory of lung myofibroblasts. *Integrative Biology.* 2012;4(4):410-21.

68. Matheson LA, Maksym GN, Santerre JP, Labow RS. Cyclic biaxial strain affects U937 macrophage-like morphology and enzymatic activities. *Journal of Biomedical Materials Research Part A.* 2006;76(1):52-62.

69. Williams JL, Chen JH, Belloli DM. Strain fields on cell stressing devices employing clamped circular elastic diaphragms as substrates. *J Biomech Eng.* 1992;114 (3): 377-384.

70. Gilbert JA, Weinhold PS, Banes AJ, Link GW, Jones GL. Strain profiles for circular cell culture plates containing flexible surfaces employed to mechanically deform cells in vitro. *Journal of biomechanics.* 1994;27(9):1169-77.

71. Hughes-Fulford M. Signal transduction and mechanical stress. Sci. STKe. 2004;2004(249):re12-.

72. Yavropoulou MP, Yovos JG. The molecular basis of bone mechanotransduction. *Journal of musculoskeletal & neuronal interactions*. 2016;16(3):221.

73. Ziegler ME, Jin YP, Young SH, Rozengurt E, Reed EF. HLA class I-mediated stress fiber formation requires ERK1/2 activation in the absence of an increase in intracellular Ca2+ in human aortic endothelial cells. *American Journal of Physiology-Cell Physiology*. 2012;303(8):C872-82.

74. Hirata H, Gupta M, Vedula SR, Lim CT, Ladoux B, Sokabe M. Actomyosin bundles serve as a tension sensor and a platform for ERK activation. *EMBO reports.* 2015;16(2):250-7.

75. Swann DA, Silver FH, Slayter HS, Stafford W, Shore E. The molecular structure and lubricating activity of lubricin isolated from bovine and human synovial fluids. *Biochemical Journal.* 1985;225(1):195.

76. Ruan MZ, Erez A, Guse K, Dawson B, Bertin T, Chen Y, Jiang MM, Yustein J, Gannon F, Lee BH. Proteoglycan 4 expression protects against the development of osteoarthritis. *Science translational medicine*. 2013;5(176):176ra34-.

77. Shine KM, Spector M. The presence and distribution of lubricin in the caprine intervertebral disc. *Journal of Orthopaedic Research.* 2008;26(10):1398-406.

78. Ogawa H, Kozhemyakina E, Hung HH, Grodzinsky AJ, Lassar AB. Mechanical motion promotes expression of Prg4 in articular cartilage via multiple CREB-dependent, fluid flow shear stress-induced signaling pathways. *Genes & development.* 2014;28(2):127-39.

79. Medzhitov R. Origin and physiological roles of inflammation. Nature. 2008;454(7203):428.

80. Sun Z, Zhang M, Zhao XH, Liu ZH, Gao Y, Samartzis D, Wang HQ, Luo ZJ. Immune cascades in human intervertebral disc: the pros and cons. *International journal of clinical and experimental pathology.* 2013;6(6):1009.

81. Kurakawa, T., Kakutani, K., Morita, Y., Kato, Y., Yurube, T., Hirata, H., ... & Doita, M. (2015). Functional impact of integrin α5β1 on the homeostasis of intervertebral discs: a study of mechanotransduction pathways using a novel dynamic loading organ culture system. *The Spine Journal*, *15*(3), 417-426.

82. Le Maitre, C. L., Frain, J., Millward-Sadler, J., Fotheringham, A. P., Freemont, A. J., & Hoyland, J. A. (2009). Altered integrin mechanotransduction in human nucleus pulposus cells derived from degenerated discs. *Arthritis & Rheumatism: Official Journal of the American College of Rheumatology*, *60*(2), 460-469.

83. Walter, B. A., Purmessur, D., Moon, A., Occhiogrosso, J., Laudier, D. M., Hecht, A. C., & Iatridis, J. C. (2016). Reduced tissue osmolarity increases TRPV4 expression and pro-inflammatory cytokines in intervertebral disc cells. *European cells & materials*, *32*, 123.

84. Gonzales, S., Rodriguez, B., Barrera, C., & Huang, C. Y. C. (2014). Measurement of ATP-induced membrane potential changes in IVD cells. *Cellular and molecular bioengineering*, *7*(4), 598-606.

Chapter 3

3 Spatiotemporal and Functional Characterization of TRPV4 in the Murine Intervertebral Disc

3.1 Co-Authorship Statement

All data presented in this chapter were collected and analyzed by Kim, M.K.M. in the laboratory of Dr. Séguin, C.A. Drs. Ramachandran, R. provided the *Trpv4*$^{LacZ/LacZ}$ mouse strain. Dr. Pest, M. and Ryan Beach provided technical assistance with embryo imaging and live cell calcium imaging, respectively. Drs. Ramachandran, R. and Séguin, C.A. contributed to study design.

3.2 Chapter Summary

The process of mechanotransduction in intervertebral disc cells are not well understood. The aim of this study was to determine the expression pattern and function of TRPV4 in the IVD. A novel transgenic reporter mouse, in which the endogenous *Trpv4* locus drives expression of the lacZ reporter, was used to localize *Trpv4* expression in the spine. We characterized *Trpv4* expression during embryonic spine development (embryonic day (E) 8.5, 12.5, 17.5, postnatal day (PN)1) and at time points following skeletal maturity (2.5, 6, 9 months of age). The response of AF cells to the TRPV4-specific agonist GSK1016790A and antagonist GSK2193874 was assessed using epifluorescence imaging with Ca^{2+}-sensitive Fura-2-AM dye and cytoskeletal morphology was assessed using F-actin staining. The effect of TRPV4 agonism and antagonism in mechanically stimulated AF cells were quantified at the level of gene expression. We showed that *Trpv4* expression in the spine was specific to developing notochord and intervertebral mesenchyme at E12.5. In contrast, in mice at 2.5, 6, and 9 months of age, *Trpv4* expression was detected in cells of nucleus

pulposus, inner annulus fibrosus, cartilage endplate, and vertebral growth plate. AF cells treated with the TRPV4-specific agonist demonstrated heterogeneous Ca^{2+} responses: no response, calcium oscillation, or a sustained response. TRPV4-induced Ca^{2+} signalling was associated with actin cytoskeleton remodeling and stress fibre formation, dependent on Rho/ROCK signalling. In AF cells, mechanically induced changes in *Acan* and *Prg4* gene expression were mediated by TRPV4 activity. These studies show that *Trpv4* is expressed in the cells of developing notochord and intervertebral mesenchyme, then subsequently detected within multiple cell types of the mature IVD. The functional activity of TRPV4 was validated in murine AF cells, where it was found to regulate cytoskeletal remodelling and the expression of matrix genes.

3.3 Introduction

Low back pain, recently reported to be one of the leading causes of disability worldwide[1], is typically associated with intervertebral disc (IVD) degeneration[2]. The lack of disease-modifying treatments for IVD degeneration is linked to our incomplete understanding of cellular pathways that contribute to disc development, function, and degeneration. The IVD is a fibrocartilaginous connective tissue structure located between the vertebral bodies responsible for spine load bearing and movement. IVDs are composite structure consisting of distinct tissue types that work in concert to absorb and dissipate mechanical load throughout the spine. During axial load, the central nucleus pulposus (NP), due to its high water content, experiences compressive and hydrostatic loading, creating an intradiscal pressure that deforms the outer annulus fibrosus (AF) which in turn experiences multi-directional tensile strain[3–6]. Similar to other musculoskeletal tissues, biomechanical factors are important contributors to the IVD microenvironment and play a role in both tissue

homeostasis and the initiation of disc degeneration[7–10]. Specifically, physiological levels of mechanical load produce an anabolic response in the IVD marked by increased expression of extracellular matrix (ECM) genes, such as aggrecan and collagen, and decreased expression of catabolic enzymes, such as matrix metalloproteinases (MMPs) [11–15]. In contrast, aberrant mechanical loading (either under- or over-loading) can contribute to altered ECM homeostasis through the initiation of tissue degeneration[7,10,16]. Despite numerous studies characterizing on the effects of mechanical stimulation on IVD tissues, information regarding the mediators of IVD mechanotransduction – *i.e.* how cells sense mechanical forces and convert them into biochemical signals – remains limited.

Previous reports on the mechano-sensing mechanism in AF cells have focused on the role of integrins as mechanoreceptors. Expression profiling of integrin subunits in the human IVD showed tissue-type and regional variance in their expression pattern. Notably, the RGD-integrin, α5β1, was highly expressed in cells of human NP and inner AF compared to the outer AF[17], and was shown to mediate the cellular response to mechanical loading[18–20]. Exposure of non-degenerate human NP cells to compressive load (0.35 – 0.95 MPa, 1 Hz for 2 h) decreased aggrecan gene expression, which was inhibited by pre-treatment of cells with an RGD peptide that competitively blocked integrin ligand binding. This effect, however, was not detected in NP cells derived from degenerative human IVDs[19]. In non-degenerate human AF cells exposed to cyclic tensile strain (CTS) (10%, 1.0 Hz for 20 min) pre-treatment with RGD peptide prevented the mechanically induced decrease in aggrecanase-1 (ADAMTS4) gene expression and increased focal adhesion kinase phosphorylation. Similar to NP cells, the RGD pre-treatment failed to inhibit the mechanoresponse in degenerative AF cells[20]. These findings suggest that IVD

mechanotransduction pathways and effectors of mechano-response vary depending on the cell type and degenerative state. To date, however, the role and expression pattern of other mechanoreceptors in the IVD have not been fully elucidated.

The transient receptor potential vanilloid 4 (TRPV4) channel is a multi-modally activated Ca^{2+}-permeable non-selective cation channel involved in transducing various external environmental cues into specific cellular responses by generating intracellular Ca^{2+} transients[21,22]. In mammals, TRPV4 was first reported to regulate cellular functions in response to changes in osmolarity in murine heart, liver, and kidney[21,23,24], but was recently demonstrated to mediate mechano-response in musculoskeletal tissues. In porcine chondrocytes, chemical and mechanical activation of TRPV4 was shown to regulate the expression of the type II collagen and transforming growth factor β 3 genes[25]. Furthermore, studies using mice with global deletion of *Trpv4* showed that mechanically regulated bone formation and resorption[26], as well as mechanically induced intracellular Ca^{2+} oscillation in osteoblasts, were TRPV4-dependent[27]. In the context of the IVD, studies using a bovine *ex vivo* IVD organ culture model showed that reduced tissue osmolarity increased TRPV4 protein expression and channel activation, which correlated with increased interleukin-1β and interleukin-6 gene expression in cells of the IVD[28]. Furthermore, previous work by our group showed increased *Trpv4* gene expression in murine AF cells following acute exposure to CTS (6% CTS, 2.0 Hz for 30 min). However, the *in situ* expression pattern of TRPV4 and its role in transducing and regulating the IVD mechano-response is unclear.

The goal of this study was to characterize the expression and function of TRPV4 in murine IVD. Using a novel *Trpv4* reporter mouse model, the current study resolved the spatiotemporal expression profile of *Trpv4* during murine embryonic spine development

and aging. Using both pharmacological and mechanical assays, the role of TRPV4 in AF cells was interrogated, focusing on intracellular calcium response, cytoskeletal adaptation, and changes in gene expression.

3.4 Methods

3.4.1 Mice

All animal experiments were performed in accordance with the policies and guidelines set forth by the Canadian Council on Animal Care and were approved by the Animal Use Subcommittee of the University of Western Ontario (protocol 2017-154, **Appendix A**). The EUCOMM "knockout-first" gene trap strategy was used to generate *Trpv4*$^{tm1a(KOMP)Wtsi}$ mice. Embryonic stem cells with the *Trpv4*$^{tm1a(KOMP)Wtsi}$ allele from Wellcome Trust Sanger Institute (produced for the Knockout Mouse Project; MGI:4460277) were injected to C57BL/6NCrl host blastocysts. The resultant chimeric offspring contained the L1L2_Bact_P cassette inserted upstream of exon 6 in the *Trpv4* locus. The cassette includes 2 FRT sites flanking an IRES:lacZ trapping cassette and a floxed human beta actin promoter-driven neo cassette inserted upstream, with an additional loxP site downstream of exon 6, the critical exon (**Figure 3.1A**). Sperm from *Trpv4*$^{tm1a(KOMP)Wtsi}$ mice were used for *in vitro* fertilization with oocytes from C57BL/6N mice. The resulting embryos were incubated with TATCre to remove the neomycin resistance cassette and exon 6, to generate the *Trpv4*$^{tm1b(KOMP)Wtsi}$ reporter mice where the *Trpv4* gene was rendered null, and the gene locus drives the expression of *lacZ* (*Trpv4*$^{LacZ/LacZ}$; **Figure 3.1A**). Wild-type C57BL/6N mice (Charles River: Wilmington, MA, USA) were used for gene expression analysis and cell culture experiments. Mice were housed in standard cages and maintained on a 12-hour

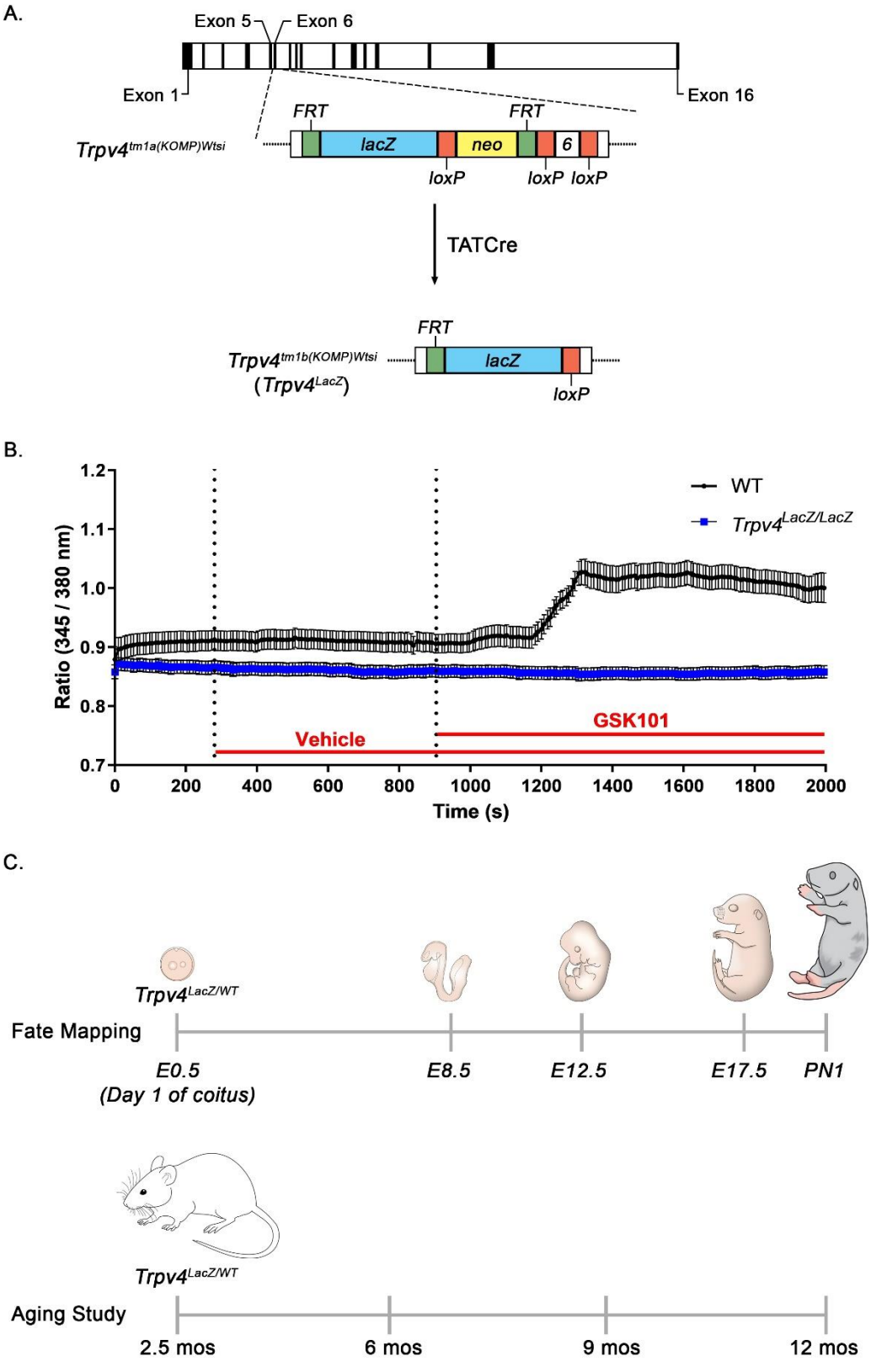
A.
Exon 5
Exon 6
Exon 1
Exon 16
FRT
FRT
Trpv4tm1a(KOMP)Wtsi
lacZ
neo
6
loxP
loxP
loxP
TATCre
FRT
Trpv4tm1b(KOMP)Wtsi
(Trpv4LacZ)
lacZ
loxP
B.
WT
Trpv4LacZ/LacZ
Ratio (345 / 380 nm)
1.2
1.1
1.0
0.9
0.8
0.7
Vehicle
GSK101
0
200
400
600
800
1000
1200
1400
1600
1800
2000
Time (s)
C.
Trpv4LacZ/WT
Fate Mapping
E0.5
(Day 1 of coitus)
E8.5
E12.5
E17.5
PN1
Trpv4LacZ/WT
Aging Study
2.5 mos
6 mos
9 mos
12 mos

Figure 3.1. Generation of *Trpv4*^{tm1b} reporter mouse and schematic overview of experimental workflow.

A) EUCOMM "knock-out first" gene trap strategy used to generate the *Trpv4* reporter mouse. The L1L2_Bact_P cassette was inserted upstream of the critical exon (exon 6) in the *Trpv4* locus. The cassette includes FRT site, *lacZ* sequence and a loxP site. This first loxP site is followed by a neomycin resistance gene, a second FRT site and a second loxP site. A third loxP site is inserted downstream of the targeted exon 6. The resulting construct has exon 6 of *Trpv4* gene flanked by loxP sites (tm1a). The tm1a mice were then Cre-excised to remove neomycin resistance cassette and exon 6, to generate reporter mice (tm1b) where the *Trpv4* locus drives expression of the *lacZ* gene (*Trpv4*$^{LacZ/LacZ}$). B) Calcium traces of AF cells isolated from 2.5 month-old WT and *Trpv4*$^{LacZ/LacZ}$ mice treated with to the TRPV4 agonist GSK101 (100 nM). After incubation with Fura 2-AM, AF cells were imaged during 5 min of calibration, 10 min following administration of vehicle (0.1% v/v DMSO), and then 20 min following administration of GKS101 (100 nM). Calcium response induced by GSK101, indicative of TRPV4 activation, was detected in WT AF cells, but was absent in *Trpv4*$^{LacZ/LacZ}$ AF cells (n=3 per genotype). C) *Trpv4*$^{LacZ/WT}$ embryos at E8.5, E12.5, E17.5 and postnatal day 1 were harvested for fate mapping experiments. Mice at 2.5, 6, 9, 12 months-of-age were used to characterize *Trpv4* expression in the murine IVD over time.

light/dark cycle, with rodent chow and water available *ad libitum*. Mice were euthanized by CO_2 asphyxiation or by lethal injection of sodium pentobarbital.

Trpv4$^{LacZ/LacZ}$ mice were mated with wild-type C57BL/6N mice to generate *Trpv4*$^{LacZ/WT}$ mice. For fate mapping experiments, *Trpv4*$^{LacZ/LacZ}$ male mice were bred with wild-type C57BL/6N females. For timed matings, insemination was confirmed by the presence of vaginal sperm plug, which was counted as embryonic day (E) 0.5. Pregnant female mice were sacrificed at E8.5, E12.5 and E17.5 to harvest embryos. Thoracic, lumbar, and caudal spines were isolated by dissection from mice at 2.5-, 6-, 9-, 12-months-of-age.

NP and AF tissues were isolated by microdissection from the lumbar and caudal spines of C57BL/6N mice at 2.5-, 6-, 9-, 12-months-of-age and immediately placed in TRIzol reagent (Life Technologies, Carlsbad, CA, USA) for subsequent RNA extraction.

3.4.2 β-Galactosidase Staining

Embryos were fixed for 40 min (E<10.5) or 1 h (E>10.5) in 2% paraformaldehyde, 0.2% glutaraldehyde, 0.02% IGEPAL® CA-630 in Phosphate Buffered Saline (PBS) on ice. Embryos were washed in detergent rinse buffer (0.01% sodium deoxycholate, 2 mM $MgCl_2$, 0.02% IGEPAL® CA-630) for 3 times 10 min each prior to overnight incubation in X-gal staining solution (1 mg/mL X-Gal, 2 mM $MgCl_2$, 5 mM EGTA, 0.02% IGEPAL® CA-630, 5 mM $K_3Fe(CN)_6$, 5 mM $K_4Fe(CN)_6$) at 37°C with agitation. Embryos were then washed 3 times with PBS (10 min each) and stored in PBS overnight to allow stain to develop. Embryos were imaged using a Leica M165FC stereo microscope (Leica Microsystems Inc. Canada, Richmond Hill, ON, Canada) and the staining reaction was

stopped by placing embryos in 4% paraformaldehyde overnight at room temperature (post-fixed).

To visualize β-galactosidase staining in embryos >E10.5 (including postnatal day 1; PN1), a clearing step was performed as previously described[29,30]. Briefly, embryos were cleared using a series of solutions containing decreasing KOH and increasing glycerol concentrations (100:0, 80:20, 50:50, 20:80, and 0:100%, respectively, for 3 days each) following post fixation. β-galactosidase staining of isolated thoracic, lumbar and caudal spinal segments was conducted as outlined above for mice >2.5 months-of-age. Following staining, tissues were decalcified using Shandon's TBD-2 (Thermo Fisher Scientific, Waltham, MA, USA) for 5 days at room temperature with continuous agitation.

3.4.3 Histology

For histological analysis, tissues were dehydrated in a graded series of ethanol, cleared in xylene, and embedded in paraffin as previously described[30]. Paraffin-embedded samples were sectioned sagittally at a thickness of 5 μm. Mid-sagittal sections of whole embryos and spinal regions of skeletally mature mice (thoracic, lumbar, and caudal) were counterstained with Eosin-Y (Sigma-Aldrich, St. Louis, MO, USA) and mounted with DAKO Faramount aqueous mounting medium (DAKO/Agilent, Santa Clara, CA, USA). Embryo sections were imaged using BioTek Cytation 5 Cell Imaging Multi-Mode Reader and BioTek Gen5 Microplate Reader and Imaging Software (BioTek, Winooski, VT, USA). Spine sections were imaged using a Leica DM1000 Microscope with Leica Application Suite Software.

3.4.4 Immunohistochemistry

Heat-induced antigen retrieval was performed in sodium citrate buffer (10 mM sodium citrate, 0.05% Tween-20, pH 6.0) at 95°C for 12 min and tissue sections were blocked for 1 h with 5% goat serum in PBS containing 0.1% Triton X-100 (PBS-T; Sigma Aldrich). Tissue sections were incubated with a primary antibody directed against β-galactosidase (1:500 in blocking solution; Abcam, Cambridge, MA, USA) in a humidified chamber overnight at 4°C. The next day, slides were washed with PBS-T, and tissue sections were incubated with goat anti-rabbit Alexa Fluor 488 secondary antibody (1:500 in PBS; Thermo Fisher Scientific) for 1 h, washed three times in PBS, and coverslipped with Fluoroshield Mounting Medium with DAPI (Abcam), and imaged using the BioTek Cytation 5.

3.4.5 Primary cell isolation and culture

AF tissues were isolated by microdissection from 2.5-month-old C57BL/6N mice (cervical to caudal spines) using Leica M165 FC stereo microscope (Leica). Isolated tissues were digested with Type II collagenase (3 mg/mL; Worthington, NJ, USA) in Dulbecco's modified Eagle's medium/Ham's F-12 medium (DMEM/F12) for 20 min at 37°C. AF tissues were then minced and further digested for 1 h at 37°C. Tissue digests were filtered using a 70 micron cell strainer and cells were pelleted by centrifugation (1,100 rpm for 5 min). Cells were plated at an initial density of ~400,000 cells/cm^2 in DMEM/F12 supplemented with 10% Fetal Bovine Serum (FBS) and 1% penicillin and streptomycin (Thermo Fisher Scientific) at 37°C in a humidified atmosphere of 5% CO_2. Media was changed every 2 days until cells reached 80% confluency.

All cell culture experiments were conducted with primary AF cells at passage 1. Cells were treated with the following compounds: TRPV4 antagonist GSK2193874 (Sigma Aldrich), TRPV4 agonist GSK1016790A (Sigma Aldrich), the pan ROCK inhibitor Y-27632 (Stemcell Technologies, Vancouver, BC, Canada).

3.4.6 Live cell calcium imaging

Primary AF cells were passaged onto 14 mm glass bottom microwell dishes (Thermo Fisher Scientific; Cat. # NC9069930) at a density of ~5,000 cells/cm^2 and allowed to adhere for 2 h, and cultured in DMEM/F12 containing 10% FBS and 1% Penstrep for 24 hr. On the day of the experiment, cells were loaded with calcium sensitive Fura-2 by incubation with 2.5 μM Fura-2-acetoxymethyl ester (Fura-2 AM, Thermo Fisher Scientific, MA, USA; Cat. # F1221) in culture media for 40 min at 37°C in 5% CO_2. After loading, cells were rinsed once and medium was replaced with warmed (37°C) HEPES buffer containing 135 mM NaCl, 5 mM KCl, 1 mM $MgCl_2$, 1 mM $CaCl_2$, 10 mM D(+)-glucose, and 20 mM HEPES (buffer adjusted to 290 ± 5 mOsm/L and pH 7.30 ± 0.02). Dishes were placed on a stage warmer (35°C) mounted on a Nikon inverted microscope (Nikon Eclipse TE2000-U, Tokyo, Japan) and imaged using a Plan Fluor 40x/1.3 NA oil/water immersion objective for fluorescence. Cells were excited with alternating wavelengths of 345/380 nm using a DeltaRAM™ X Illuminator (Horiba Photon Technology International (PTI) Inc., NJ, USA) and the emission was acquired using a bandpass filter (510 ± 20 nm)[31]. Ratio images were acquired every 5 s with a pco.edge 4.2 LTsCMOS camera (PCO AG, Kelheim, Germany) and EasyRatioPro 2.3 Software (Horiba PTI). For all of the calcium imaging experiments, the following protocol was used: 5 min incubation for baseline measurement, 10 min incubation following addition of either TRPV4 antagonist GSK2193874 (GSK219; 250

nM) or vehicle control (0.1% v/v DMSO diluted in HEPES buffer), 20 min of TRPV4 agonist GSK1016790A (GSK 101; 100 nM). The ratiometric calcium measurements (345 nm / 380 nm ratio) were determined using a manually defined regions of interest (ROIs) corresponding to individual cells in the field of view (approximately 14-22 cells per experiment) and each experimental condition was repeated three times from different cell preparations established from different mice (3 biological replicates). In the vehicle + GSK101 treated group, the proportions of cells eliciting intracellular calcium response was quantified by categorizing each cell (n=67) into one of three groups according to changes in 345/380 nm ratio upon TRPV4 activation: no response (ratio at 0.76-0.92), oscillation (ratio fluctuating above and below 1.0), sustained (ratio above 1.0).

3.4.7 Cytoskeleton Staining

Primary AF cells were seeded at a density of 48,000 cells/cm^2 onto a standard 35 mm dish and cultured for 2 days. Following expansion, AF cells were treated with GSK 101 (10 nM or 100 nM) in culture media to activate TRPV4 for 30 min. AF cells treated with vehicle (0.1% DMSO v/v diluted in culture media) for 30 min served as a control. Following acute TRPV4 activation, cells were fixed with 4% paraformaldehyde for 10 min, permeabilized with 0.1% Triton X-100 (PBS-T) for 10 min at room temperature, and blocked with Bovine Serum Albumin (in PBS) for 30 min. Alexa Fluor 488 Phalloidin (Life Technologies) was used to detect F-actin according to manufacturer's protocol and Hoeschst stain (Thermo Fisher) was used to visualize the nuclei. Images were acquired using a Leica DMI6000 inverted microscope and Leica Application Suite Software (Leica). For each of the 3 biological replicates, 3 non-overlapping ROIs were imaged for each treatment group.

To determine the role of Rho-kinase/ROCK signalling, AF cells were pretreated with the pan ROCK inhibitor Y-27632 (10 μM; Stemcell Technologies, Vancouver, BC, Canada) or vehicle (equal volume of sterile water) in culture media for 24 h prior to 30 min incubation with 100 nM of GSK 101. Following acute exposure of TRPV4 agonist, cells were processed, stained for F-actin, and imaged as described above.

3.4.8 Mechanical stimulation

The MechanoCulture B1 (MCB1) device (CellScale Biomaterials Testing, Waterloo, Ontario, Canada) was used to deliver bi-axial multi-directional cyclic tensile strain (CTS) to AF cell cultures, as previously described[32]. Briefly, primary AF cells were seeded at a density of 48,000 cells/cm^2 onto FBS-coated silicone membranes and cultured for 2 days in culture media. AF cells were exposed to 10% CTS, at a sinusoidal frequency of 1.0 Hz, for 30 min in the presence or absence of the TRPV4 antagonist GSK219 (250 nM). To measure the direct effects of TRPV4 channel activation on AF cell gene expression, AF cells were treated with 100 nM GSK101 for 30 min in the absence of CTS. AF cells cultured on FBS-coated silicone membranes treated with vehicle (0.1% DMSO) in static culture served as time-matched unloaded vehicle controls. After 30 min of treatment (CTS, CTS + GSK219, or GSK101 only), cells were incubated for additional 6 hours before harvesting for total RNA. To limit the exposure of cells to the pharmacological TRPV4 modulators, following 30 min treatment, cells were rinsed, media was replaced, and cells were incubated for additional 6 hours before harvest.

3.4.9 RNA extraction and gene expression analysis

Total RNA was extracted from NP and AF tissues harvested at 2.5-, 6-, 9-, and 12-months-of-age (n=3), and CTS-treated AF cells (n=3) using Trizol reagent (Life Technologies),

according to the manufacturer's protocol. RNA was quantified using a NanoDrop 2000 spectrophotometer (Thermo Fisher Scientific). Complementary DNA was synthesized from 150 ng of RNA using the Bio-Rad iScript cDNA synthesis kit (Bio-Rad, Hercules, CA, USA). Gene expression was determined by SYBR-based real-time PCR using the Bio-Rad CFX384 thermocycler. PCR reactions were run in triplicate using 470 nM forward and reverse primers (primer sequences in **Table 3.1**) with 2x SsoFast EvaGreen Supermix (Bio-Rad). The PCR program consisted of the following: initial 2 min enzyme activation at 95^{o}C, 10 sec denaturation at 95^{o}C, 30 sec annealing/elongation at 60^{o}C, for a total of 40 cycles. *Trpv4* transcript levels in NP and AF tissues were quantified relative to a six-point standard curve made from pooled cDNA generated from wild-type murine heart, brain, kidney, and IVDs. For CTS experiments, gene expression was quantified using ΔΔCt, normalized for input based on hypoxanthine quinine phosphoribosyl transferase (*Hprt*) expression and expressed relative to time-matched unloaded controls.

3.4.10 Statistical analyses

Statistical analyses were performed using GraphPad Prism 8. qPCR analyses comparing IVD gene expression over time or in mechanically stimulated AF cells were assessed using two-way ANOVA with Tukey's multiple comparison test. qPCR analyses comparing GSK101 treated AF cells and vehicle control were assessed by two-tailed, unpaired t-test. $P < 0.05$ was considered statistically significant. Biological replicates (n) correspond to experiments performed in different animals or cell preparations from different animals.

3.5 Results

3.5.1 *Trpv4LacZ/LacZ* mice have non-functional TRPV4 channel

The EUCOMM gene trap strategy used to generate *Trpv4*$^{tm1b(KOMP)Wtsi}$ reporter mice involved targeting the endogenous *Trpv4* gene locus with a *LacZ* reporter gene (**Figure 3.1A**). To validate this mouse model, calcium response was examined in primary AF cells from mice homozygous for the transgene insertion (*Trpv4*$^{LacZ/LacZ}$) treated with the TRPV4 agonist GSK101. Acute stimulation of AF cells with GSK101 (100 nM) elicited a rise in

Table 3.1. Sequences of the primers used in the real-time PCR analysis.

Gene	Forward (5' → 3')	Reverse (5' → 3')
Acan	CCTGCTACTTCATCGACCCC	AGATGCTGTTGACTCGAACCT
Col1a1	CTGGCGGTTCAGGTCCAAT	TCCAGGCAATCCAGGAGC
Col2a1	GCACATCTGGTTTGGAGAGACC	TAGCGGTGTTGGGAGCCA
Prg4	GGGTGGAAAATACTTCCCGTC	CAGGACAGCACTCCATGTAGT
Trpv4	TTCGTAGGGATCGTTGGTCCT	TACAGTGGGGCATCGTCCGT

intracellular calcium in WT AF cells, but not in *Trpv4*$^{LacZ/LacZ}$ AF cells, confirming the absence of functional TRPV4 channel in the homozygous reporter mouse (**Figure 3.1B**). Previous studies reported that mice with global knockout of *Trpv4* showed accelerated osteoarthritis detectable at 9 months-of-age, and increased bone mass due to impaired osteoclast activity[33,34]. To avoid detrimental effects due to complete loss of TRPV4 function, all subsequent studies were conducted using *Trpv4*$^{LacZ/WT}$ reporter mice.

3.5.2 *Trpv4* is expressed in the notochord and primitive annulus fibrosus

Using heterozygous reporter mice (*Trpv4*$^{LacZ/WT}$), experiments were conducted to localize *Trpv4* expression during IVD development. At E8.5 no β-galactosidase staining was detected in embryos, suggesting that *Trpv4* is not expressed during early stages of notochord formation and elongation (**Figure 3.2A**; E8.5). At E12.5, β-galactosidase expression indicative of *Trpv4* expression was detected in the developing limb buds, regions of alar plate of myelencephalon, primitive axial skeleton, and notochord (**Figure 3.2A**; E12.5). To better resolve β-galactosidase expression within the developing spine, stained embryos were sectioned for histological analysis. Consistent with the whole mount examination, patchy β-galactosidase staining was detected in the notochord at E12.5. In addition to notochord, immunofluorescence staining for β-galactosidase demonstrated expression in regions of intervertebral mesenchyme, highlighting the metameric patterning between the developing IVD and prevertebral structure (**Figure 3.2B**). At E17.5 and PN1, the cartilage primordium of mandible, limbs, ribs, and spine showed β-galactosidase expression indicative of *Trpv4* expression (**Figure 3.2A**). At both E17.5 and PN1, β-galactosidase expression was detected in cells of NP and AF, as well as the developing bone (**Figure 3.2C, D**).

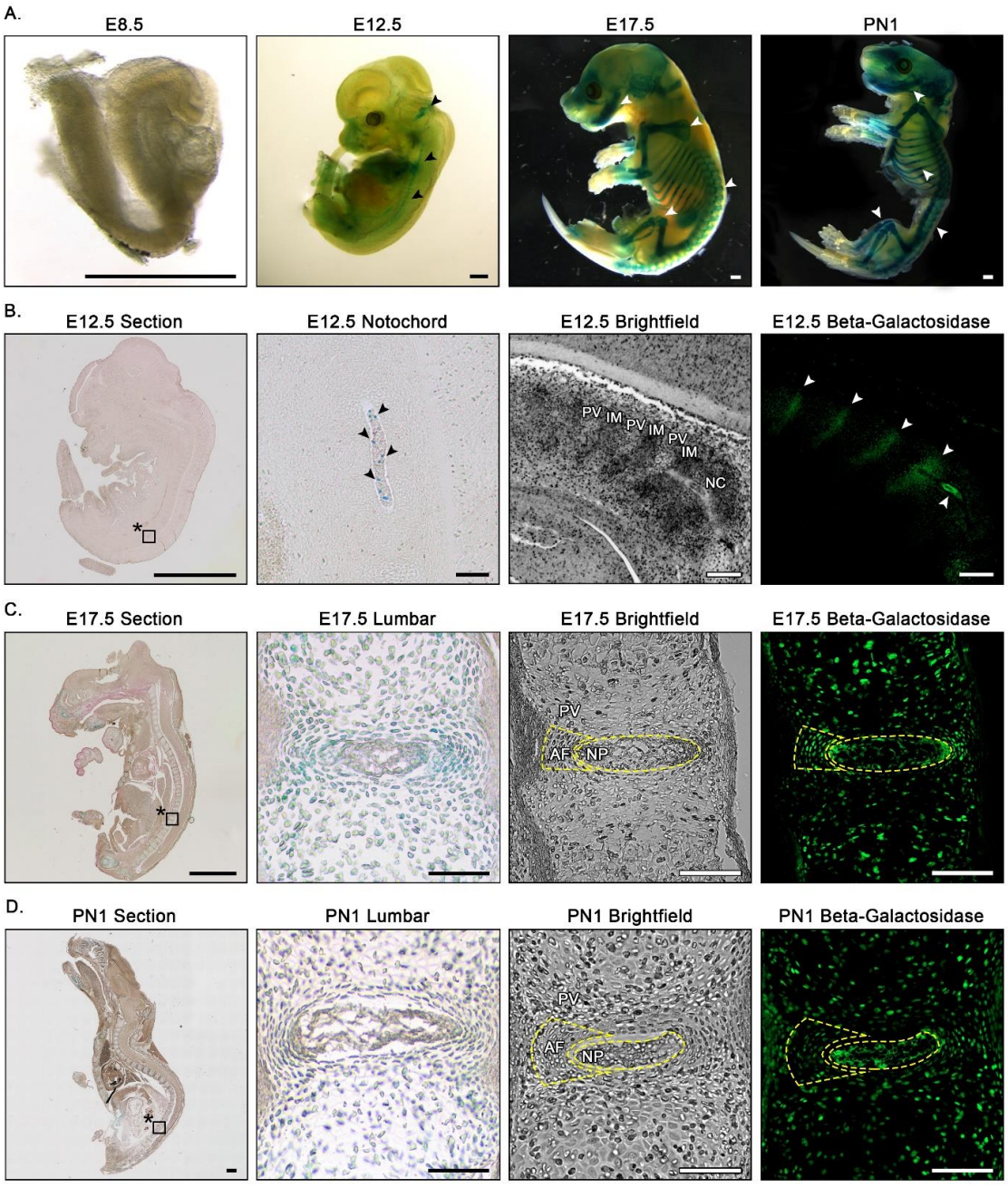
A.
E8.5
E12.5
E17.5
PN1
B.
E12.5 Section
E12.5 Notochord
E12.5 Brightfield
E12.5 Beta-Galactosidase
PV
IM
PV
IM
PV
IM
NC
C.
E17.5 Section
E17.5 Lumbar
E17.5 Brightfield
E17.5 Beta-Galactosidase
PV
AF
NP
D.
PN1 Section
PN1 Lumbar
PN1 Brightfield
PN1 Beta-Galactosidase
PV
AF
NP

Figure 3.2. Localization of *Trpv4* expressing cells during mouse spinal development.

A) Representative images of *Trpv4*$^{lacZ/WT}$ mice at embryonic day (E) 8.5, E12.5, E17.5, and Postnatal day (PN)1. Embryos were cleared and X-Gal stain was used to detect β-galactosidase activity. *Trpv4* expression, indicated by blue β-galactosidase staining (arrows), is not detected in embryos at E8.5, but was detected in the developing limb buds, structure of medulla oblongata, and notochord at E12.5. At E17.5 and PN1, the cartilage primordium of mandible, limbs, ribs, and spine were positive for β-galactosidase. B) Midsagittal section of the *Trpv4*$^{lacZ/WT}$ embryos at E12.5 either counterstained with Eosin or assessed by immunofluorescence using β-galactosidase antibody (1:500). β-Galactosidase activity was patchy in the notochord (asterisk) at E12,5; however, immunofluorescence-based detection showed localization to the notochord (NC) as well as the intervertebral mesenchyme (IM), but not at the prevertebral (PV) region of the developing spine. β-galactosidase was detected in primitive AF, NP, and pre-vertebrae (PV) at both E17.5 and PN1 using both staining methods (C, D). Scale bar = 1 mm, n = 3-5 embryos/ timepoint derived from at least 2 different litters.

3.5.3 *Trpv4* expression in the IVD differs based on anatomical region, tissue type and age

In skeletally mature mice, *Trpv4* expression was examined in midsagittal sections from the thoracic, lumbar and caudal spine. At 2.5 months-of-age, β-galactosidase expression indicative of *Trpv4* expression was detected in the lumbar spine in cells of NP and inner AF (IAF), using both β-galactosidase colorimetric detection and immunofluorescence staining (**Figure 3.3A, B**). In keeping with previous reports, staining was also detected in chondrocytes throughout the vertebral growth plates[35–37]. Interestingly, β-galactosidase staining was more intense in the tail IVDs compared to thoracic and lumbar IVDs. In addition, β-galactosidase staining decreased with increasing age. At 6 months-of-age, less β-galactosidase staining was detected in the NP and IAF compared to 2.5 months-of-age. β-galactosidase staining was further reduced at 9 months-of-age, and by 12 months-of-age, few cells were positive for β-galactosidase staining (**Figure 3.3B**).

To further quantify age-related changes in *Trpv4* expression, we performed gene expression analysis using NP and AF tissues isolated from lumbar and caudal IVDs of wild-type mice. Although no significant difference in *Trpv4* expression levels was detected with age in the lumbar IVDs, a significant decrease in *Trpv4* gene expression levels was detected with age in both the NP and AF of the caudal IVDs. In the lumbar IVDs, expression levels of *Trpv4* gene was more robust in the AF compared to the NP, with significant differences detected in tissues isolated at 6 months-of-age (**Figure 3.3C**).

3.5.4 TRPV4 is functionally active in AF cells

To correlate *Trpv4* expression to functional receptor activation, intracellular calcium measurements were performed in primary AF cells isolated from mice at 2.5 months-of-

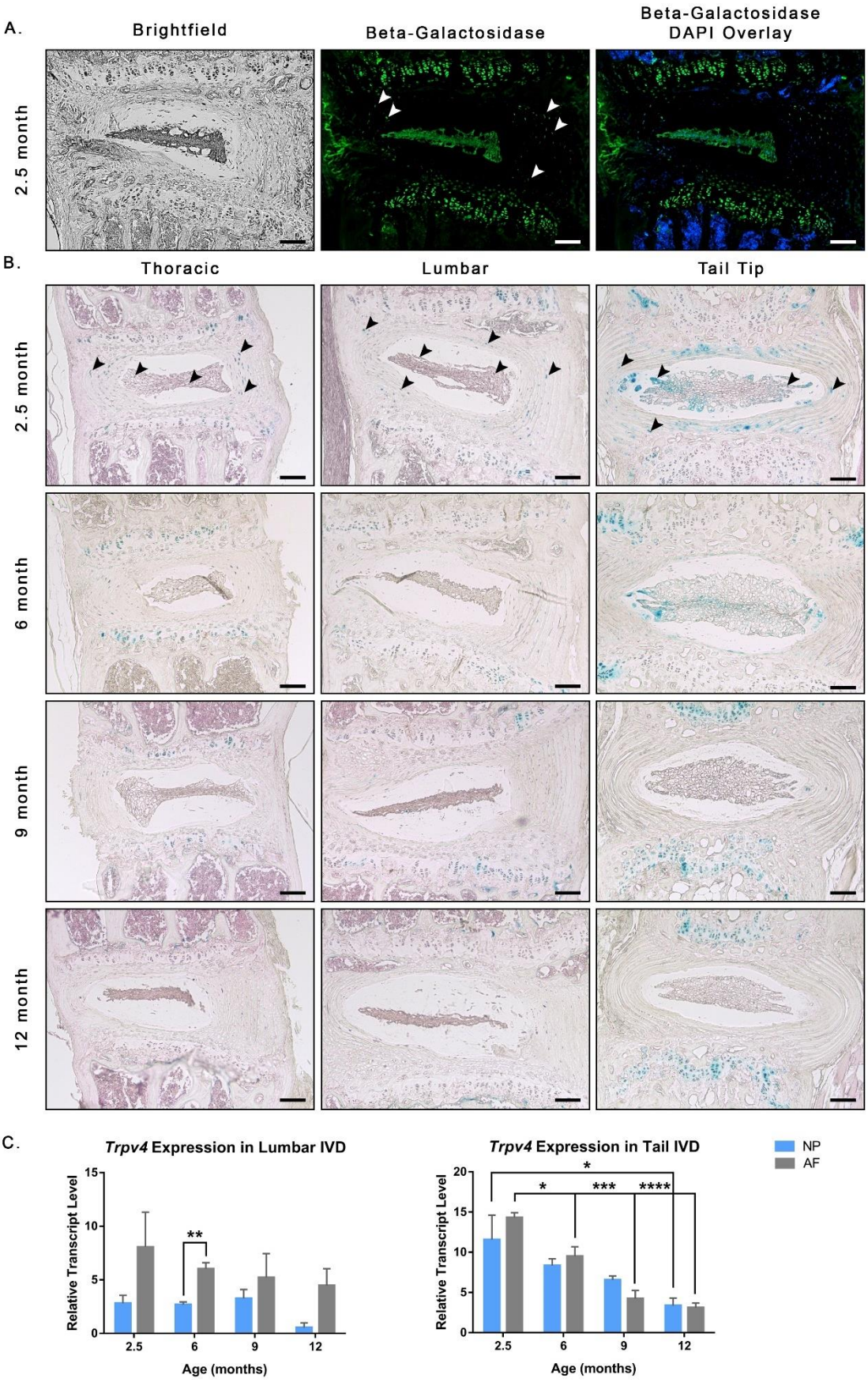
A.
Brightfield
Beta-Galactosidase
Beta-Galactosidase
DAPI Overlay
2.5 month
B.
Thoracic
Lumbar
Tail Tip
2.5 month
6 month
9 month
12 month
C.
Trpv4 Expression in Lumbar IVD
Relative Transcript Level
Age (months)
Trpv4 Expression in Tail IVD
NP
AF
Relative Transcript Level
Age (months)

Figure 3.3. Characterization of *Trpv4* expression in the IVD over time.

Midsagittal histological sections of different spinal regions (thoracic, lumbar, or tail) from *Trpv4*$^{lacZ/WT}$ mice at 2.5, 6, 9, and 12-months-of-age. A) Representative images of immunofluorescence-based detection of β-galactosidase in lumbar IVDs of *Trpv4*$^{lacZ/WT}$ mice at 2.5-months-of-age. The cells of nucleus pulposus and inner AF were positive for β-galactosidase, indicative of *Trpv4* expression (white arrows). B). Representative midsagittal sections of IVDs of thoracic, lumbar, or tail regions isolated from the *Trpv4*$^{lacZ/WT}$ reporter mice at 2.5, 6, 9, and 12-months of age. X-Gal stain was used to detect β-galactosidase activity, indicative of *Trpv4* expression. β-galactosidase staining was detected in the nucleus pulposus and inner annulus fibrosus of the IVD (black arrows). Hypertrophic chondrocytes of the vertebral growth plate served as an internal positive control for each spine segments. Scale bar = 100 μm, n = 3-4 mice/timepoint. C) SYBR-based real time qPCR quantifying the expression of *Trpv4* in AF and NP tissues isolated from lumbar and tail IVDs at each time point. Transcript levels were expressed relative to the six-point standard curve. No significant changes in *Trpv4* expression were detected in lumbar IVDs, except at 6 mos where *Trpv4* expression was increased in the AF compared to the NP. A significant decrease in *Trpv4* gene expression was detected with advancing age in both NP and AF tissues of tail IVDs. Data were analyzed using two-way ANOVA with Tukey's multiple comparisons. * = $p < 0.05$; ** = $p < 0.01$; *** = $p < 0.001$; **** = $p < 0.0001$. Data presented in mean ± SEM. n = 3.

age. Activation of TRPV4 channels in AF cells using the TRPV4 agonist GSK1016790A (GSK101; 100 nM) elicited an increase in intra-cellular calcium (**Figure 3.4A**), confirming functional receptor expression. The GSK101-induced calcium response in AF cells was inhibited when cells were pre-treated with TRPV4 antagonist GSK2193874 (GSK219; 250 nM; **Figure 3.4B**). Interestingly, AF cells treated with GSK101 demonstrated heterogeneity in the TRPV4-dependent calcium responses detected, with cells showing a mixture of sustained, oscillatory, or no calcium responses (**Figure 3.4C**). To quantify the proportion of cells exhibiting each of the distinct calcium responses, fluorescence was assessed in regions of interest corresponding to individual cells and thresholds were set to represent each calcium response: no response (340/380 ratio 0.76-0.92), oscillation (340/380 ratio fluctuating above and below 1.0), sustained (340/380 ratio above 1.0). When all the cells were assessed over 3 biological replicates (n=67), 27% of cells showed no response, 54% of cells showed an oscillation response, and 19% of cells showed a sustained response to TRPV4 agonism (**Figure 3.4D**).

3.5.5 TRPV4 activation is associated with cytoskeletal remodelling in AF cells

Having confirmed functional activation of TRPV4 in murine AF cell cultures, the downstream effects of TRPV4-mediated calcium signalling were assayed. TRPV4-mediated calcium signalling regulates cytoskeletal rearrangement in other cell types, including chondrocytes and trabecular meshwork cells[38,39]. Moreover, in many cell types, including chondrocyte and cancer cells, Rho-kinase/ROCK signalling regulates cytoskeletal remodelling in both physiological and pathological states [40–42]. AF cells showed increased stress fibre formation compared to untreated controls following acute

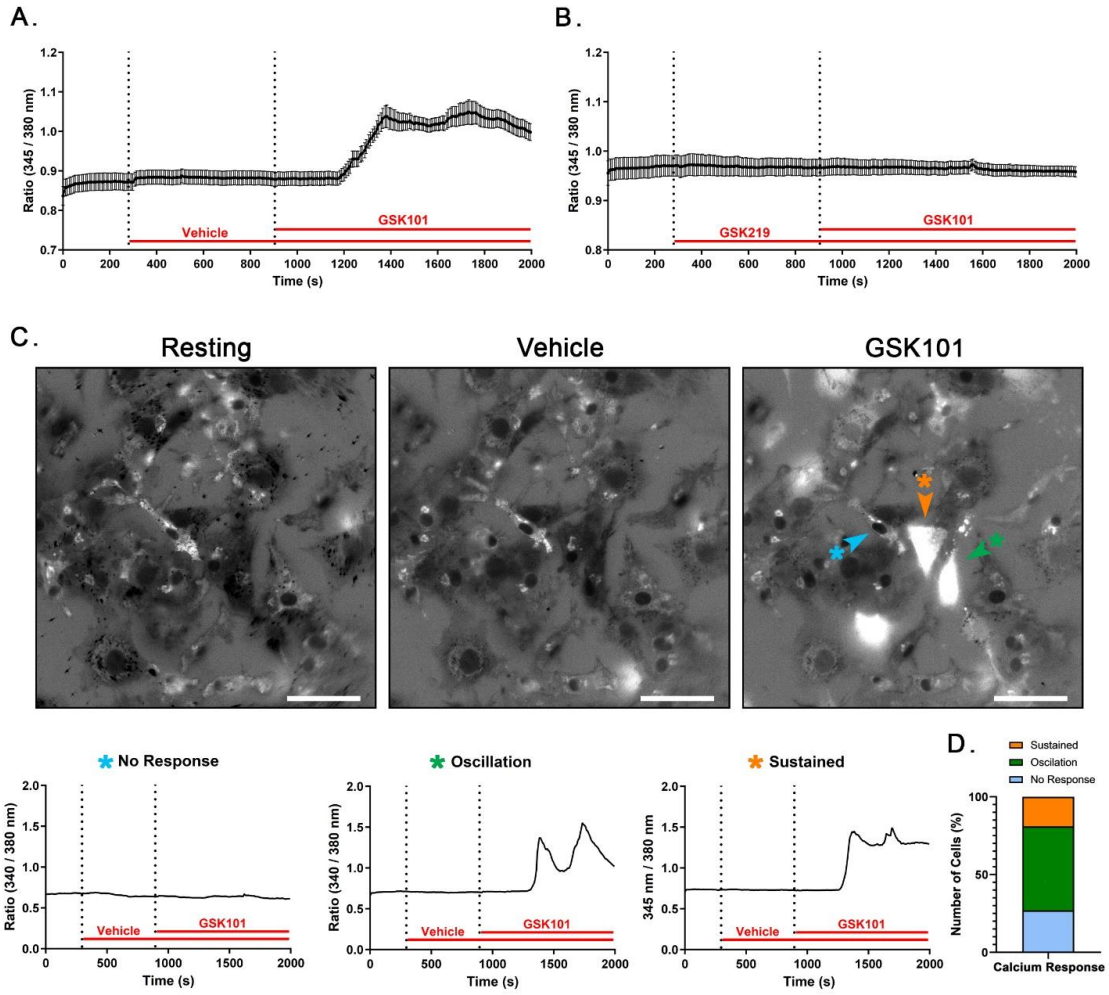

Figure 3.4. TRPV4 activity in primary AF cells.

A) Calcium traces of AF cells isolated from 2.5- month-old WT mice in response to the TRPV4 agonist GSK101 (100 nM), confirming the expression and functionality of TRPV4. Following incubation with Fura 2-AM, AF cells were imaged for: 5 min of calibration, 10 min following administration of vehicle (0.1% v/v DMSO), and then 20 min following administration of GKS101 (100 nM). Graph represents the average calcium response of all cells in the field of view from 3 biological replicates (n = 67). B) The calcium response induced by GSK101 was inhibited by pre-treatment of AF cells with the TRPV4 antagonist GSK219 (250 nM). C) Representative images of fluorescence signals at distinct stages of treatment. TRPV4 activation by GSK101 yielded one of three calcium responses in AF cells: sustained, oscillation, and no response. D) Stacked histogram showing the proportions of AF cells showing the distinct calcium responses following TRPV4 activation. Cells were categorized based on their response to the TRPV4 agonist as defined by their specific fluorescence ratio: 27% of cells showed no response (340/380 ratio 0.76-0.92), 54% of cells showed oscillation (340/380 ratio fluctuating above and below 1.0), and 19% of cells showed a sustained response (340/380 ratio above 1.0). Scale bar = 100 μm; n = 67 cells assessed from a total of 3 independent cell preparations.

treatment with increasing concentrations of the TRPV4 agonist GSK101 (**Figure 3.5A**). Moreover, pre-treatment of AF cells with the ROCK inhibitor Y-27632 inhibited GSK101-induced stress fibre formation (**Figure 3.5B**).

3.5.6 TRPV4 activation mediates the response of AF cells to cyclic tensile loading

To assess the contribution of TRPV4 activation in mediating the mechano-response of AF cells, cells were exposed to 10% CTS at 1.0 Hz for 30 min in the presence or absence of the TRPV4 antagonist, GSK219. Cells were harvested 6 h post CTS and gene expression analysis was performed to detect changes in the expression of aggrecan (*Acan*), type I collagen (*Col1a1*), type II collagen (*Col2a1*), and lubricin (*Prg4*). The expression of *Col1a1* and *Col2a1* by AF cells were not affected by CTS (**Figure 3.6**). Interestingly, AF cells exposed to CTS in the presence of GSK219 showed significantly reduced *Col1a1* gene expression compared to unloaded control and CTS only group. In keeping with our previous findings[32], CTS significantly increased *Acan* (1.5 ± 0.1 fold) and *Prg4* (1.7 ± 0.2) expression compared to unloaded vehicle control. CTS-induced increases in both *Acan* and *Prg4* expression were inhibited by the presence of GSK219 during mechanical stimulation (**Figure 3.6**). These findings suggest that TRPV4 mediates, at least in part, the response of AF cells to CTS.

To measure the direct effects of TRPV4 activation on AF cell gene expression, cells were exposed to the TRPV4 agonist GSK101 using a protocol designed to mimic that used for CTS. AF cells were treated with GSK101 for 30 min in static culture, cells were rinsed, media was replaced, and cells were incubated for 6 h post-stimulation prior to harvest. Similar to the effects of CTS, treatment of AF cells with GSK101 induced a significant

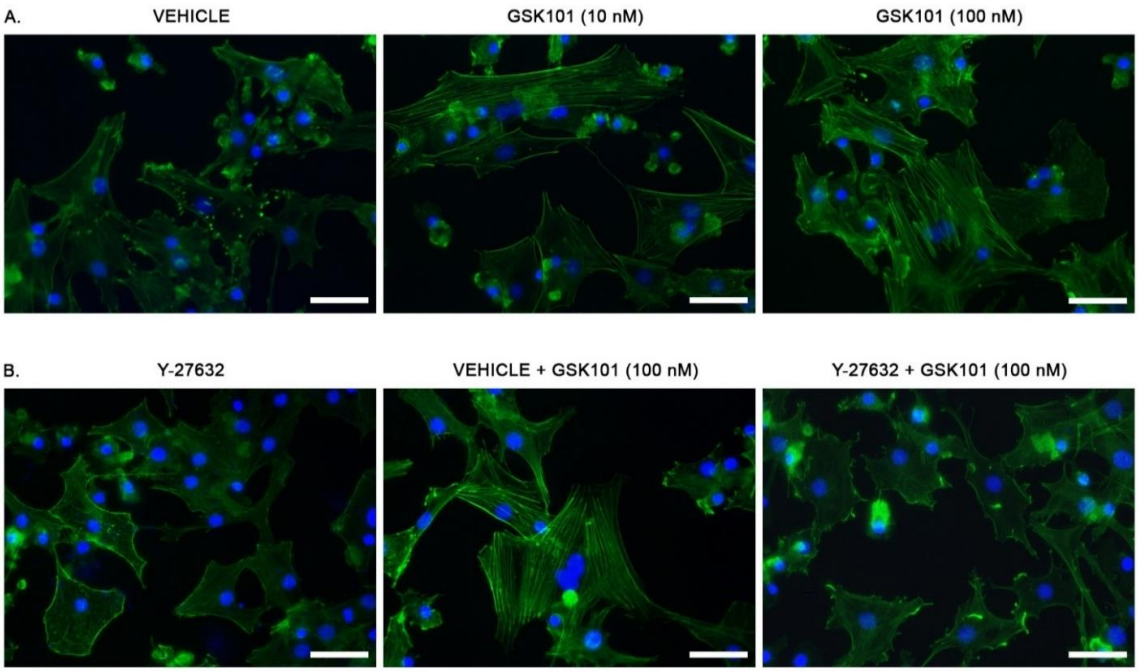

Figure 3.5. Effect of TRPV4 activation on cytoskeleton remodelling in annulus fibrosus cells.

A) AF cells were incubated with increasing concentrations of GSK101 for 30 minutes, fixed, and stained with Alexa 488 Phalloidin to visualize the actin cytoskeleton. Increased stress fibre formation was detected with increasing concentrations of GSK101, suggesting the cytoskeletal network of the AF cells are changing following acute activation of TRPV4. B) GSK101-induced stress fibre formation was inhibited when cells were pretreated with Y-27632 (ROCK inhibitor). Scale bar = 50 μm; n = 3 independent cell preparations derived from 3 different mice at 2.5 months-of-age.

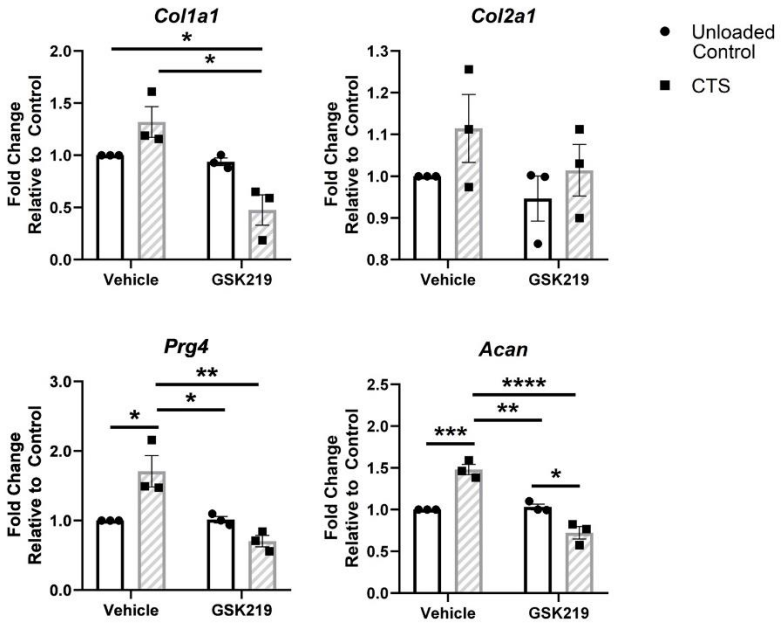

Figure 3.6. TRPV4-dependent gene expression in mechanically stimulated AF cells.

AF cells were subjected to 10% cyclic tensile strain (CTS) at 1.0 Hz for 30 min in the presence or absence of TRPV4-specific antagonist, GSK219. 6 h post CTS, cells were harvested for gene expression analysis to detect changes in the expression of candidate ECM genes. Mechanical loading induced an upregulation of *Acan* and *Prg4* expression, which was blocked by treatment of cells with the TRPV4 antagonist GSK219. Relative gene expression was calculated using ΔΔCt, normalized for input using the housekeeping gene *Hprt* and expressed relative to time-matched unloaded vehicle control. Data presented as mean ± SEM; n = 3 cell preparations. Data were analyzed using two-way ANOVA with Tukey's multiple comparisons. * = $P < 0.05$; ** = $P < 0.01$; *** = $P < 0.001$; **** = $P < 0.0001$

increase in the expression of *Acan* (1.8 ± 0.3 fold) and *Prg4* (2.1 ± 0.1 fold) compared to vehicle control (**Figure 3.7**). TRPV4 agonism did not alter the expression of *Col1a1* or *Col2a1*.

3.6 Discussion

The IVD represents a mechanically dynamic environment, in which the cells receive mechanical cues from their surrounding microenvironment and transduce this information into intracellular biochemical signals that regulate cellular processes. Although there is growing evidence of the effects of different types of mechanical stimulation on IVD biology, information on mechanoreceptor molecules that sense and transduce the mechanical signals remains limited. In this study, we utilized a novel transgenic reporter mouse model to characterize the spatiotemporal pattern of TRPV4 expression in the murine IVD during development and in skeletally mature IVD tissues. We demonstrated that TRPV4 activation in AF cells elicits intracellular calcium response and regulates cytoskeleton remodelling. Using a mechanically dynamic bioreactor system and pharmacological modulation of TRPV4 activation, we showed that TRPV4-dependent response of AF cells to CTS alters extracellular matrix gene expression. The characterization of the TRPV4 ion channel provide evidence for the role of TRPV4 as a mechanoreceptor regulating IVD mechanobiology.

Our findings in the mouse are consistent with previous studies describing *Trpv4* expression during zebrafish embryogenesis[35]. In the zebrafish, *Trpv4* was first detected during notochord elongation and subsequently in other chondrogenic tissues in later developmental stages. Similarly, in our reporter mouse, *Trpv4* expression was detected in the notochord as well as the condensed segments of intervertebral mesenchyme,

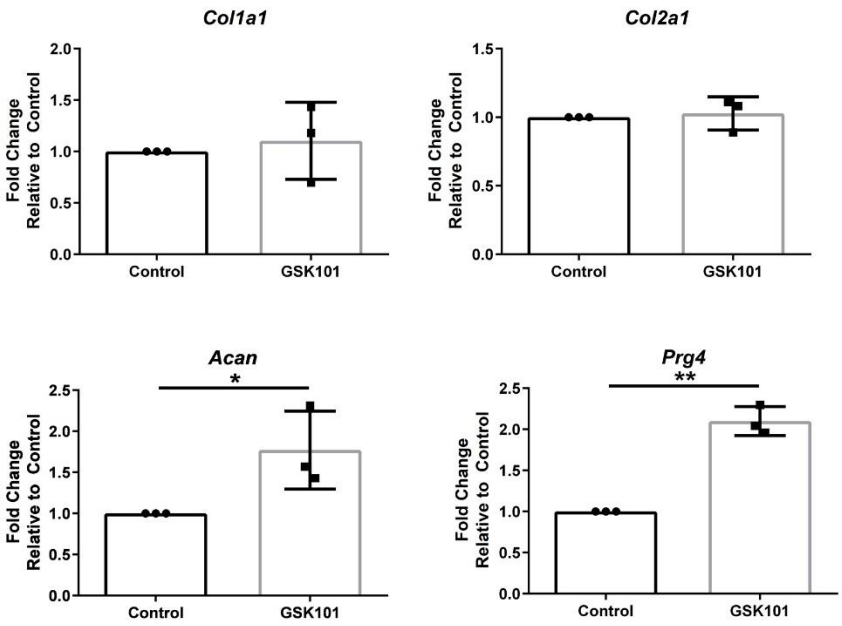

Figure 3.7. TRPV4-mediated changes in AF cell gene expression.

Primary AF cells were treated with the TRPV4 agonist GSK101 (100 nM) for 30 min and after 6 h, cells were harvested for gene expression analysis to detect changes in the expression of candidate ECM genes. Treatment of AF cells with the TRPV4 agonist induced a significantly increase in the expression of *Acan* and *Prg4*. Relative gene expression was calculated using ΔΔCt, normalized for input using the housekeeping gene *Hprt* and expressed relative to time-matched vehicle control. Data presented as mean ± SEM; n = 3 cell preparations. Data were analyzed using unpaired t-tests. * = $P < 0.05$; ** = $P < 0.01$.

highlighting the metameric patterning at E12.5. Anatomically, the notochord is a continuous rod-like structure that creates the primitive longitudinal and bilateral axes of the embryo. Functionally, the notochord provides both mechanical and morphogenic signals to the developing embryo. During development, elongation of the notochord is thought to happen through two complementary mechanisms: i) through convergent extension guided along the tension generated by expanding amniotic cavity along the anterior/posterior axis[43–45], and ii) through vacuole expansion within the notochord cells distributed along the embryonic axis by the rigid ECM of the notochordal sheath restricting bilateral cell volume expansion[46–50]. TRPV4 has been shown to regulate cell volume during cellular osmoregulation[51,52] and respond to both compressive and tensile load in multiple cell types[25,53–56]. Importantly, TRPV4 expression was detected in the notochord of zebrafish at the time of vacuole inflation[35,57]. As such, *Trpv4* expression in the notochord may be evidence for TRPV4 mediating notochord development as mechanoreceptor and osmosensor, transducing the directionality of mechanical signals and regulating the notochord cell volume expansion, respectively. Furthermore, intracellular calcium signalling has been shown to regulate embryogenesis in other animal models. Previous studies investigating calcium signalling in the developing zebrafish showed high intracellular calcium transients in the trunk region during early and late segmentation[58]. Additionally, intracellular calcium signals were found to regulate cell proliferation, migration, and shape during zebrafish embryogenesis[59–63]. *Trpv4* expression detected in the condensed mesenchymal segments at E12.5 in the mouse suggests that TRPV4-mediated calcium signalling may contribute to the regulation of cell proliferation and migration required for metameric patterning along the longitudinal axis.

In skeletally mature mice, *Trpv4* expression was preserved in the cells of NP and inner AF, with differential expression detected based on anatomical region and age. The differences in *Trpv4* expression in spinal regions may result from differences in mechanical load experienced in these tissues. Previous studies by our group showed that *Trpv4* expression was upregulated in AF cells following mechanical stimulation[32]. Accordingly, increased *Trpv4* expression detected in lumbar and tail IVDs compared to thoracic IVDs may be due to greater mechanical load experienced at these sites. Moreover, the current study demonstrated decreased *Trpv4* expression with increasing age. Tissue osmolarity and pH within the IVD decrease as aggrecan and other glycosaminoglycans are degraded with advancing age or degeneration. Previous studies investigating the role of TRPV4 in human IVDs reported that culturing IVD explants in hypotonic conditions, thereby increasing the osmotic pressure, leads to increased TRPV4 protein expression[28]. Notably, the studies used mechanically dynamic organ culture system delivering cyclic compression to IVD explants (0.0-0.8 MPa at 0.1 Hz for 8h; 0.2 MPa for 16 h), which may also influence TRPV4 expression. In keeping with these studies, the decrease observed in *Trpv4* expression with increasing age may be due to age-associated changes in tissue osmolarity. Our work suggests cell type, anatomical region, and age as factors that regulate *Trpv4* expression in the murine IVD.

Our studies show that pharmacological activation of TRPV4 elicited one of three calcium responses in AF cells: sustained, oscillation, and no response. These findings may relate to the heterogeneity of the primary cell culture system used which contained cells of both inner and outer AF. The cells that did not respond to TRPV4 agonism may be outer AF cells, in which *Trpv4* expression was not detected in our reporter mouse. Our results are

consistent with previous findings reporting sustained intracellular calcium response in AF and NP tissues upon direct activation of TRPV4 ion channel[28]. Interestingly, we observed intracellular calcium oscillation. Calcium oscillation following TRPV4 activation has been reported to drive matrix production in chondrocytes and regulate cell-matrix adhesion and alignment in mesenchymal stem cells[25,64]. The presence of both sustained and oscillatory calcium response in our cell culture system may be due to agonist concentration and differences in receptor density on cell subpopulations. Previous studies on receptor activation in glial cells concluded that lower agonist concentration elicits calcium oscillation, while high concentration lead to sustained responses[65,66]. In mesenchymal stem cells, TRPV4 activation with lower agonist concentration (1 or 10 nM) led to short oscillatory calcium transients, while high agonist concentration (100 nM) induced sustained calcium response[64]. Furthermore, studies investigating the relationship between intracellular calcium and receptor density showed that changes in receptor density influences intracellular calcium response following receptor activation[67,68]. Given the differences between cells of the inner and outer AF in terms of ECM components, cell shape, and mechanical environment[69], we postulate that differential expression of the TRPV4 receptor in these cells may account for the different cellular responses we detected. Differences in TRPV4 expression in AF cells based on anatomical location from which the IVDs were isolated may likewise contribute to cell heterogeneity in our model and influence the cellular responses detected.

One of the earliest cellular adaptations to mechanical stimulation is the formation of stress fibres[70–72], and TRPV4-mediated calcium signalling has been shown to regulate cytoskeletal rearrangement in other cell types, including chondrocytes and trabecular

meshwork cells[38,39]. In primary AF cells, pharmacological activation of TRPV4 increased stress fibre formation, which was blocked with Rho/ROCK inhibition. In many cell types, including chondrocyte and cancer cells, Rho /ROCK signalling regulate cytoskeletal remodelling in both physiological and pathological states [40–42]. The crosstalk between TRPV4 and Rho-kinase/ROCK has been studied in endothelial cells. In normal endothelial cells, TRPV4 senses mechanical force and induces RhoA/ROCK activation necessary for migration, stiffening, and contraction[73]. However, in the pathological state, Rho/ROCK activation and cell stiffening caused decreased TRPV4 expression, and pharmacological activation of TRPV4 supressed Rho/ROCK mediated signalling[74], suggesting that Rho/ROCK can act as both an effector and target of TRPV4. Our findings likewise suggest the involvement of both TRPV4 and Rho/ROCK signalling in cytoskeleton remodelling and AF cell mechanotransduction.

In other musculoskeletal cell types, intracellular calcium signalling is believed to be one of the earliest mechano-response events[75–78]. Specifically in chondrocytes, TRPV4 mediates the mechano-response, including gene expression and proteoglycan synthesis[25]. Using a previously characterized culture system, we assessed the role of TRPV4 in the response of AF cells to cyclic tensile loading. TRPV4 activation was both necessary and sufficient for the induction of *Col1a1*, *Acan*, and *Prg4* expression in response to CTS. Previous studies investigating the effects of both extracellular osmolarity and mechanical stimulation showed that in human and bovine AF cells, type I collagen gene expression decreased with increasing osmolarity, while aggrecan gene expression increased[79]. Mechanical stimulation to AF cells inhibited osmotically induced increase in these gene expression, with the exception of increased aggrecan gene expression in hypertonic environment[79]. Given that

TRPV4 is well-established osmosensor, future studies should investigate the role of TRPV4 in regulating mechano-response of AF cells in different osmotic conditions.

3.7 Conclusions

Our findings show that *Trpv4* is first expressed in primitive IVD structures during development and persists in cells of the mature NP and inner AF. Specifically, in AF cells, we demonstrated that TRPV4 activation is a key mechanism of mechanical signal transduction. In addition to previous evidence of TRPV4 as an osmosensor in the IVD, our data highlights TRPV4 as a mechanoreceptor regulating cytoskeletal architecture and ECM gene expression. These findings highlight the role of ion channel receptors in modulating cellular function via intracellular calcium transients. Understanding the mechanism of mechanoreception and mechanotransduction in IVD cells will help delineate cell-type specific mediators of mechano-response that regulate IVD health and degeneration.

3.8 Supplementary Figure

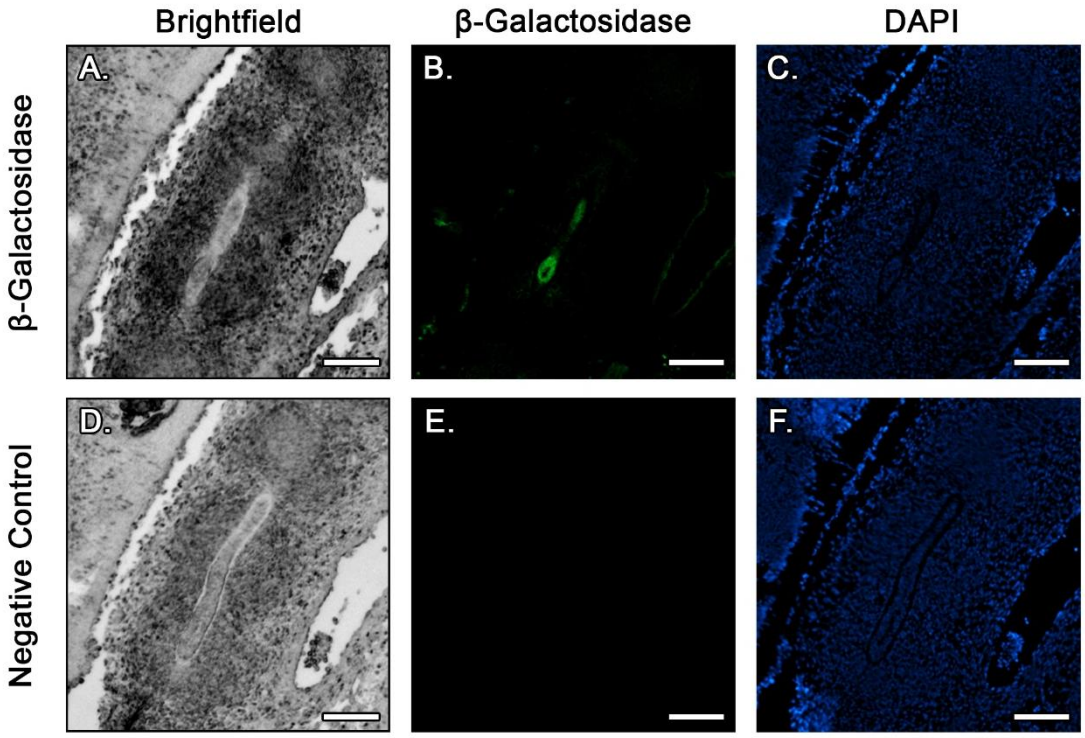

Supplementary Figure 3.1. β-Galactosidase immunofluorescence staining of the lumbar region at the notochord at E12.5.

The lumbar region within midsagittal sections of *Trpv4*$^{LacZ/WT}$ embryos at E12.5 were assessed by immunofluorescence using a β-galactosidase antibody (1:500). β-galactosidase, indicative of *Trpv4* expression, was detected at the notochord (B), but not at the intervertebral mesenchyme (pattern less pronounced in the lumbar region as shown in brightfield images of A, D). E) No primary antibody negative control. (C, F) DAPI staining of the nuclei. Scale bar = 100 μm; n = 2 embryos from 2 different litters.

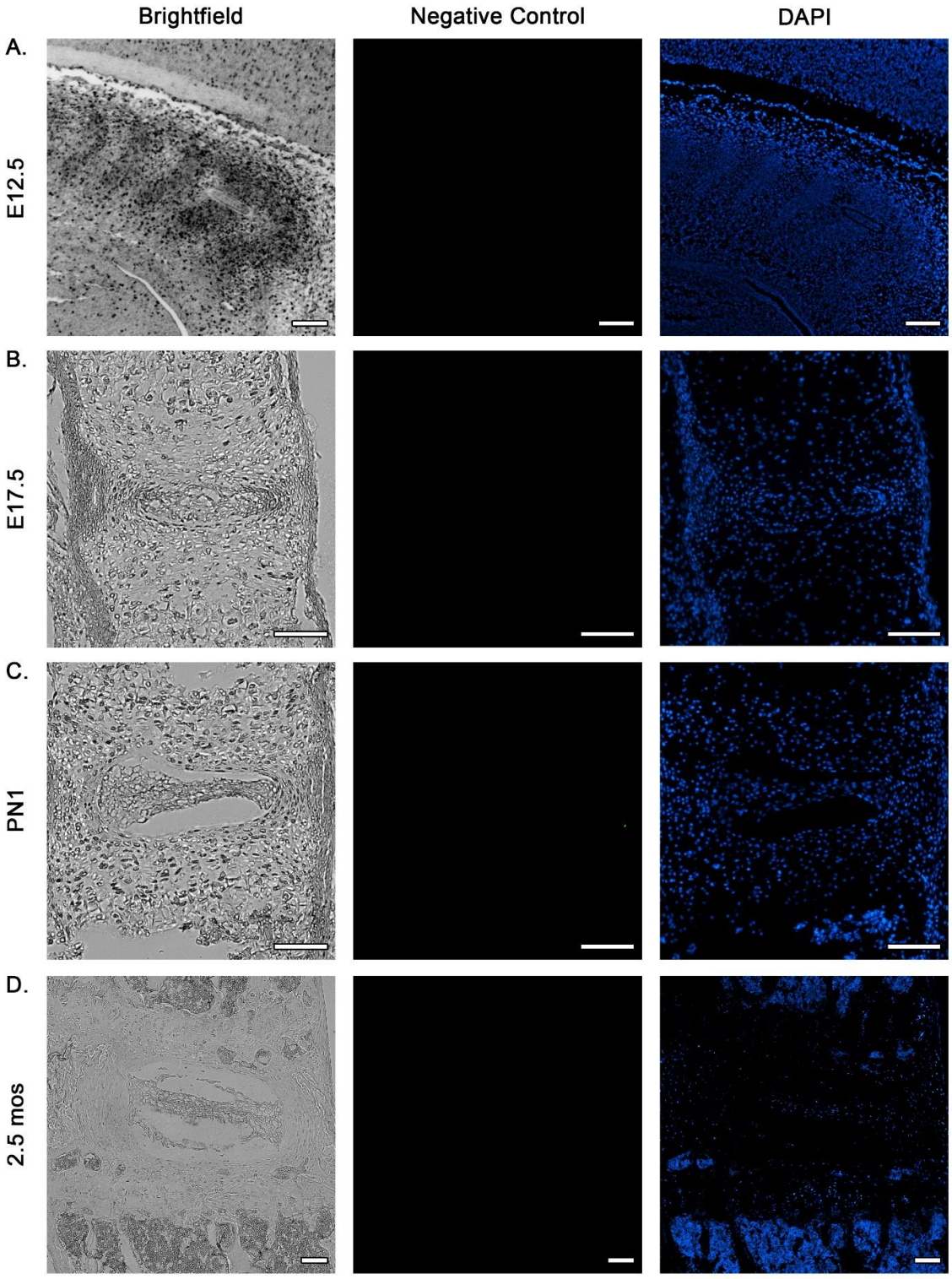
Brightfield
Negative Control
DAPI
A.
E12.5
B.
E17.5
C.
PN1
D.
2.5 mos

Supplementary Figure 3.2. Negative control immunofluorescence images of mouse spine sections at different time points.

Midsagittal sections of the *Trpv4*$^{lacZ/WT}$ embryos at (A) E12.5, (B) E17.5, (C) PN1, and (D) 2 mos treated with no primary antibody as negative control parallel to immunofluorescence using β-galactosidase antibody (1:500). DAPI was used to stain the nuclei. Scale bar = 100 μm; n = 3 embryos/ timepoint derived from at least 2 different litters.

3.9 References

1. James SL, Abate D, Abate KH, et al. Global, regional, and national incidence, prevalence, and years lived with disability for 354 Diseases and Injuries for 195 countries and territories, 1990-2017: A systematic analysis for the Global Burden of Disease Study 2017. *Lancet*. 2018:1789-1858. doi:10.1016/S0140-6736(18)32279-7

2. Arnbak B, Jensen TS, Egund N, et al. Prevalence of degenerative and spondyloarthritis-related magnetic resonance imaging findings in the spine and sacroiliac joints in patients with persistent low back pain. *Eur Radiol*. 2016;26(4):1191-1203. doi:10.1007/s00330-015-3903-0

3. Adams MA, Mcnally S, Dolan P, Mcnally DS. *"STRESS" DISTRIBUTIONS INSIDE INTERVERTEBRAL DISCS THE EFFECTS OF AGE AND DEGENERATION*. Vol 78.; 1996.

4. Shirazi-Adl SA, Shrivastava SC, Ahmed AM. Stress analysis of the lumbar disc-body unit in compression. A three-dimensional nonlinear finite element study. *Spine (Phila Pa 1976)*. 1984;9(2):120-134. doi:10.1097/00007632-198403000-00003

5. Neidlinger-Wilke C, Galbusera F, Pratsinis H, et al. Mechanical loading of the intervertebral disc: From the macroscopic to the cellular level. *Eur Spine J*. 2014;23(SUPPL. 3):333-343. doi:10.1007/s00586-013-2855-9

6. Gregory DE, Callaghan JP. A Comparison of Uniaxial and Biaxial Mechanical Properties of the Annulus Fibrosus: A Porcine Model. 2011. doi:10.1115/1.4003327

7. Iatridis JC, Maclean JJ, Roughley PJ, Alini M. Effects of Mechanical Loading on Intervertebral Disc Metabolism In Vivo. *J Bone Jt Surg Am*. 2006;88(2):41-46. doi:10.2106/JBJS.E.01407

8. Gawri R, Moir J, Ouellet J, et al. Physiological loading can restore the proteoglycan content in a model of early IVD degeneration. *PLoS One*. 2014;9(7). doi:10.1371/journal.pone.0101233

9. Setton LA, Chen J. Cell Mechanics and Mechanobiology in the Intervertebral Disc. *Spine (Phila Pa 1976)*. 2004;29(23):2710-2723. doi:10.1097/01.brs.0000146050.57722.2a

10. Videman TA, Nurminen MA TJ. Volvo Award in clinical sciences. Lumbar spinal pathology in cadaveric material in relation to history of back pain, occupation, and physical loading. *Spine (Phila Pa 1976)*. 1990;15(8):728-740.

11. Chan SCW, Ferguson SJ, Gantenbein-Ritter B. The effects of dynamic loading on the intervertebral disc. *Eur Spine J*. 2011;20(11):1796-1812. doi:10.1007/s00586-011-1827-1

12. Wuertz K, Godburn K, MacLean JJ, et al. In vivo remodeling of intervertebral discs in response to short- and long-term dynamic compression. *J Orthop Res*. 2009;27(9):1235-1242. doi:10.1002/jor.20867

13. Walsh AJL, Lotz JC. Biological response of the intervertebral disc to dynamic loading. *J Biomech*. 2004;37:329-337. doi:10.1016/S0021-9290(03)00290-2

14. Wuertz K, Urban JPG, Klasen J, et al. Influence of extracellular osmolarity and mechanical stimulation on gene expression of intervertebral disc cells. *J Orthop Res*. 2007;25(11):1513-1522. doi:10.1002/jor.20436

15. Neidlinger-Wilke C, Würtz K, Liedert A, et al. A three-dimensional collagen matrix as a suitable culture system for the comparison of cyclic strain and hydrostatic pressure effects on intervertebral disc cells. *J Neurosurg Spine*. 2005;2(4):457-465. doi:10.3171/spi.2005.2.4.0457

16. Gawri R, Rosenzweig DH, Krock E, et al. High mechanical strain of primary intervertebral disc cells promotes secretion of inflammatory factors associated with disc degeneration and pain. *Arthritis Res Ther*. 2014;16(1):R21. doi:10.1186/ar4449

17. Nettles DL, Richardson WJ, Setton LA. Integrin expression in cells of the intervertebral disc. *J Anat*. 2004;204(6):515-520. doi:10.1111/j.0021-8782.2004.00306.x

18. Kurakawa T, Kakutani K, Morita Y, et al. Functional impact of integrin a5b1 on the homeostasis of intervertebral discs: a study of mechanotransduction pathways using a novel dynamic loading organ culture system. *Spine J*. 2015;15(3):417-426. doi:10.1016/j.spinee.2014.12.143

19. Le Maitre CL, Frain J, Millward-Sadler J, Fotheringham AP, Freemont AJ, Hoyland JA. Altered integrin mechanotransduction in human nucleus pulposus cells derived from degenerated discs. *Arthritis Rheum*. 2009;60(2):460-469. doi:10.1002/art.24248

20. Gilbert HTJ, Nagra NS, Freemont AJ, Millward-Sadler SJ, Hoyland JA. Integrin - Dependent Mechanotransduction in Mechanically Stimulated Human Annulus Fibrosus Cells: Evidence for an Alternative Mechanotransduction Pathway Operating with Degeneration. *PLoS One*. 2013;8(9). doi:10.1371/journal.pone.0072994

21. Strotmann R, Harteneck C, Nunnenmacher K, Schultz G, Plant TD. *OTRPC4, a Nonselective Cation Channel That Confers Sensitivity to Extracellular Osmolarity*. Vol 2.; 2000. http://cellbio.nature.com. Accessed June 10, 2020.

22. Watanabe, H., Vriens, J., Prenen, J., Droogmans, G., Voets, T. and Nilius B. Anandamide and arachidonic acid use epoxyeicosatrienoic acids to activate TRPV4 channels. *Nature*. 2003;424(6947):434-438. doi:10.1038/nature01844

23. Liedtke W, Choe Y, Martí-Renom MA, et al. Vanilloid receptor-related osmotically activated channel (VR-OAC), a candidate vertebrate osmoreceptor. *Cell*. 2000;103(3):525-535. doi:10.1016/S0092-8674(00)00143-4

24. Liedtke W, Kim C. Review Functionality of the TRPV subfamily of TRP ion channels: add mechano-TRP and osmo-TRP to the lexicon! *Cell Mol Life Sci*. 2005;62:2985-3001. doi:10.1007/s00018-005-5181-5

25. O'Conor CJ, Leddy HA, Benefield HC, Liedtke WB, Guilak F. TRPV4-mediated mechanotransduction regulates the metabolic response of chondrocytes to dynamic loading. *Proc Natl Acad Sci*. 2014;111(4):1316-1321. doi:10.1073/pnas.1319569111

26. Mizoguchi F, Mizuno A, Hayata T, et al. Transient receptor potential vanilloid 4 deficiency suppresses unloading-induced bone loss. *J Cell Physiol*. 2008;216(1):47-53. doi:10.1002/jcp.21374

27. Suzuki T, Notomi T, Miyajima D, et al. Rapid Communication Osteoblastic differentiation enhances expression of TRPV4 that is required for calcium oscillation induced by mechanical force. 2013. doi:10.1016/j.bone.2013.01.001

28. Walter BA, Purmessur D, Moon A, et al. Reduced tissue osmolarity increases trpv4 expression and pro-inflammatory cytokines in intervertebral disc cells. *Eur Cells Mater*. 2016;32:123-136. doi:10.22203/eCM.v032a08

29. Schatz O, Golenser E, Ben-Arie N. Clearing and photography of whole mount X-gal stained mouse embryos. *Biotechniques*. 2005;39(5):650-656. doi:10.2144/000112034

30. McCann MR, Tamplin OJ, Rossant J, Seǵuin CA. Tracing notochord-derived cells using a Noto-cre mouse: Implications for intervertebral disc development. *DMM Dis Model Mech*. 2012;5(1):73-82. doi:10.1242/dmm.008128

31. Kovac JR, Chrones T, Sims SM. Temporal and spatial dynamics underlying capacitative calcium entry in human colonic smooth muscle. *Am J Physiol Gastrointest Liver Physiol*. 2008;294:88-98. doi:10.1152/ajpgi.00305.2007

32. Kim MKM, Burns MJ, Serjeant ME, Séguin CA. The mechano-response of murine annulus fibrosus cells to cyclic tensile strain is frequency dependent. *JOR Spine*.

33. Clark AL, Votta BJ, Kumar S, Liedtke W, Guilak F. Chondroprotective role of the osmotically sensitive ion channel transient receptor potential vanilloid 4: Age- and sex-dependent progression of osteoarthritis in Trpv4-deficient mice. *Arthritis Rheum*. 2010;62(10):2973-2983. doi:10.1002/art.27624

34. Masuyama R, Vriens J, Voets T, et al. Cell Metabolism TRPV4-Mediated Calcium Influx Regulates Terminal Differentiation of Osteoclasts. doi:10.1016/j.cmet.2008.08.002

35. Mangos S, Liu Y, Drummond IA. Dynamic expression of the osmosensory channel trpv4 in multiple developing organs in zebrafish. doi:10.1016/j.modgep.2006.10.011

36. Muramatsu S, Wakabayashi M, Ohno T, et al. Functional Gene Screening System Identified TRPV4 as a Regulator of Chondrogenic Differentiation *. 2007. doi:10.1074/jbc.M706158200

37. Phan MN, Leddy HA*, Votta BJ, et al. Functional Characterization of TRPV4 As an Osmotically Sensitive Ion Channel in Articular Chondrocytes. doi:10.1002/art.24799

38. Trompeter N, Gardinier JD, Debarros ; Victor, et al. Insulin-like Growth Factor-1 Regulates the Mechanosensitivity of Chondrocytes by Modulating TRPV4. doi:10.1101/2020.03.10.985713

39. Ryskamp DA, Frye AM, Phuong TTT, et al. TRPV4 regulates calcium homeostasis, cytoskeletal remodeling, conventional outflow and intraocular pressure in the mammalian eye. 2016. doi:10.1038/srep30583

40. Woods A, Wang G, Beier F. Regulation of chondrocyte differentiation by the actin cytoskeleton and adhesive interactions. *J Cell Physiol*. 2007;213(1):1-8. doi:10.1002/jcp.21110

41. Bhadriraju K, Yang M, Ruiz SA, Pirone D, Tan J, Chen CS. *ACTIVATION OF ROCK BY RHOA IS REGULATED BY CELL ADHESION, SHAPE, AND CYTOSKELETAL TENSION*.

42. Amano M, Nakayama M, Kaibuchi K. Rho-Kinase/ROCK: A Key Regulator of the Cytoskeleton and Cell Polarity. doi:10.1002/cm.20472

43. Imuta Y, Koyama H, Shi D, Eiraku M, Fujimori T, Sasaki H. Mechanical control of notochord morphogenesis by extra-embryonic tissues in mouse embryos. *Mech Dev*. 2014;132(1):44-58. doi:10.1016/j.mod.2014.01.004

44. Koyama H, Fujimori T. Isotropic expansion of external environment induces tissue elongation and collective cell alignment. *J Theor Biol*. 2020;496:110248. doi:10.1016/j.jtbi.2020.110248

45. Wallingford JB, Fraser SE, Harland RM. Convergent extension: The molecular control of polarized cell movement during embryonic development. *Dev Cell*. 2002;2(6):695-706. doi:10.1016/S1534-5807(02)00197-1

46. Jurand A. *Some Aspects of the Development of the Notochord in Mouse Embryos*. Vol 32.; 1974.

47. Ellis K, Hoffman BD, Bagnat M. The vacuole within. *Bioarchitecture*. 2013;3(3):64-68. doi:10.4161/bioa.25503

48. Adams DS, Koehu MAR. *The Mechanics of Notochord Elongation, Straightening and Stiffening in the Embryo of Xenopus Laevis*. Vol 110.; 1990.

49. Paavola LG, Wilson DB, Center EM. *Histochemistry of the Developing Notochord, Perichordal Sheath and Vertebrae in Danforth's Short-Tail (Sd) and Normal C57BL/6 Mice*. Vol 55.; 1980.

50. Koehl MAR, Quillin KJ, Pell CA. *Mechanical Design of Fiber-Wound Hydraulic Skeletons: The Stiffening and Straightening of Embryonic Notochords 1*. Vol 40.; 2000. https://academic.oup.com/icb/article-abstract/40/1/28/2139725. Accessed June 20, 2020.

51. Becker D, Blase C, Bereiter-Hahn J, Jendrach M. TRPV4 exhibits a functional role in cell-volume regulation. *J Cell Sci*. 2005;118(11):2435-2440. doi:10.1242/jcs.02372

52. Liedtke W, Friedman JM. Abnormal osmotic regulation in trpv4-/- mice. *Proc Natl Acad Sci U S A*. 2003;100(23):13698-13703. doi:10.1073/pnas.1735416100

53. Du G, Li L, Zhang X, et al. Roles of TRPV4 and piezo channels in stretch-evoked Ca 21 response in chondrocytes. *Exp Biol Med*. 2020;245:180-189. doi:10.1177/1535370219892601

54. Pairet N, Mang S, Fois G, et al. TRPV4 inhibition attenuates stretch-induced inflammatory cellular responses and lung barrier dysfunction during mechanical ventilation. *PLoS One*. 2018;13(4). doi:10.1371/journal.pone.0196055

55. Mochizuki T, Sokabe T, Araki I, et al. The TRPV4 Cation Channel Mediates Stretch-evoked Ca 2 Influx and ATP Release in Primary Urothelial Cell Cultures □ S. 2009. doi:10.1074/jbc.M109.020206

56. Thodeti CK, Matthews B, Ravi A, et al. TRPV4 channels mediate cyclic strain-induced endothelial cell reorientation through integrin-to-integrin signaling. *Circ Res*. 2009;104(9):1123-1130. doi:10.1161/CIRCRESAHA.108.192930

57. Ellis K, Bagwell J, Bagnat M. Notochord vacuoles are lysosome-related organelles that function in axis and spine morphogenesis. *J Cell Biol*. 2013;200(5):667-679. doi:10.1083/jcb.201212095

58. Tsuruwaka Y, Shimada E, Tsutsui K, Ogawa T. Ca2+ dynamics in zebrafish morphogenesis. *PeerJ*. 2017;2017(1):e2894. doi:10.7717/peerj.2894

59. Webb SE, Miller AL. Calcium signalling during zebrafish embryonic development. *BioEssays*. 2000;22(2):113-123. doi:10.1002/(SICI)1521-1878(200002)22:2<113::AID-BIES3>3.0.CO;2-L

60. Reinhard E, Yokoe H, Niebling KR, Allbritton NL, Kuhn MA, Meyer T. Localized Calcium Signals in Early Zebrafish Development. *Dev Biol*. 1995;170(1):50-61.

doi:10.1006/dbio.1995.1194

61. Blaser H, Reichman-Fried M, Castanon I, et al. Migration of Zebrafish Primordial Germ Cells: A Role for Myosin Contraction and Cytoplasmic Flow. *Dev Cell*. 2006;11(5):613-627. doi:10.1016/j.devcel.2006.09.023

62. Bonneau B, Popgeorgiev N, Prudent J, Gillet G. Cytoskeleton dynamics in early zebrafish development. *Bioarchitecture*. 2011;1(5):216-220. doi:10.4161/bioa.18116

63. Sahu SU, Visetsouk MR, Garde RJ, Hennes L, Kwas C, Gutzman JH. Calcium signals drive cell shape changes during zebrafsh midbrain-hindbrain boundary formation. *Mol Biol Cell*. 2017;28(7):875-882. doi:10.1091/mbc.E16-08-0561

64. Gilchrist CL, Leddy HA, Kaye L, et al. TRPV4-mediated calcium signaling in mesenchymal stem cells regulates aligned collagen matrix formation and vinculin tension. doi:10.1073/pnas.1811095116

65. Verkhratsky A, Orkand RK, Kettenmann H. Glial calcium: Homeostasis and signaling function. *Physiol Rev*. 1998;78(1):99-141. doi:10.1152/physrev.1998.78.1.99

66. Kawano S, Shoji S, Ichinose S, Yamagata K, Tagami M, Hiraoka M. Characterization of Ca 2+ signaling pathways in human mesenchymal stem cells. *Cell Calcium*. 2002;32(4):165-174. doi:10.1016/S0143-4160(02)00124-0

67. Dickson EJ, Falkenburger BH, Hille B. Quantitative properties and receptor reserve of the IP3 and calcium branch of Gq-coupled receptor signaling. *J Gen Physiol*. 2013;141(5):521-535. doi:10.1085/jgp.201210886

68. Ochsenbein RM, Inaebnit SP, Luethy CM, Wiesmann UN, Oetliker OH, Honegger UE. *Differential Regulation of Bradykinin Receptor Density, Intracellular Ca2+, and Prostanoid Release in Skin and Foreskin Fibroblasts. Effects of Cell Density and Interleukin-1α*. http://www.stockton-press.co.uk/bjp. Accessed June 24, 2020.

69. Fearing B V, Hernandez PA, Setton LA, Chahine NO. Mechanotransduction and cell biomechanics of the intervertebral disc HHS Public Access. 2018;1(3). doi:10.1002/jsp2.1026

70. Ziegler ME, Jin YP, Young SH, Rozengurt E, Reed EF. HLA class I-mediated stress fiber formation requires ERK1/2 activation in the absence of an increase in intracellular Ca2+ in human aortic endothelial cells. *Am J Physiol - Cell Physiol*. 2012;303(8):C872. doi:10.1152/ajpcell.00199.2012

71. Hayakawa K, Sato N, Obinata T. Dynamic reorientation of cultured cells and stress fibers under mechanical stress from periodic stretching. *Exp Cell Res*. 2001;268(1):104-114. doi:10.1006/excr.2001.5270

72. Yavropoulou MP, Yovos JG. The molecular basis of bone mechanotransduction. *J Musculoskelet Neuronal Interact*. 2016;16(3):221-236. /pmc/articles/PMC5114345/?report=abstract. Accessed June 24, 2020.

73. Liu J, Wada Y, Katsura M, et al. Rho-associated coiled-coil kinase (ROCK) in molecular regulation of angiogenesis. *Theranostics*. 2018;8(21):6053-6069. doi:10.7150/thno.30305

74. Yang, Xiao, Arun Bhaskaran, Harry Scott, Soroush Ardekani, Jun Xu, Umar Mohideen, Timothy S. Kern and KG. Rho/ROCK-mediated Retinal Endothelial Stiffening Impairs TRPV4 Signaling and Promotes Diabetic Retinal Inflammation. *Invest Ophthalmol Vis Sci*. 2016;57(12):3220-3220.

75. Raizman I, Amritha JN, Croos D, Pilliar R, Kandel RA. Calcium regulates cyclic compression-induced early changes in chondrocytes during in vitro cartilage tissue formation. *Cell Calcium*. 2010;48:232-242. doi:10.1016/j.ceca.2010.09.006

76. Han S-K, Wouters W, Clark A, Herzog W. Mechanically induced calcium signaling in chondrocytes in situ. *J Orthop Res*. 2012;30(3):475-481. doi:10.1002/jor.21536

77. Godin LM, Suzuki S, Jacobs CR, Donahue HJ, Donahue SW. Mechanically induced intracellular calcium waves in osteoblasts demonstrate calcium fingerprints in bone cell mechanotransduction. *Biomech Model Mechanobiol*. 2007;6(6):391-398. doi:10.1007/s10237-006-0059-5

78. Morrell AE, Brown GN, Robinson ST, et al. Mechanically induced Ca2+ oscillations in osteocytes release extracellular vesicles and enhance bone formation. *Bone Res*. 2018;6(1):6. doi:10.1038/s41413-018-0007-x

79. Wuertz K, Urban JPG, Klasen J, et al. Influence of extracellular osmolarity and mechanical stimulation on gene expression of intervertebral disc cells. *J Orthop Res*. 2007;25(11):1513-1522. doi:10.1002/jor.20436

Chapter 4

4 Transient Receptor Potential Vanilloid 4 Mediates Load-Induced Intervertebral Disc Degeneration in a Percutaneous Tail Disc Puncture Model

4.1 Co-Authorship Statement

All data presented in this chapter were collected and analyzed by Kim, M.K.M. in the laboratory of Dr. Séguin, C.A. Drs. Ramachandran, R. and Beier, F. provided *Trpv4*$^{fl/fl}$ and *Col2-Cre* mouse strains, respectively. Heather Cadieux-Pitre and Diana Quinonez provided technical assistance with tail puncture procedures. Drs. Ramachandran, R. and Séguin, C.A. contributed to study design.

4.2 Chapter Summary

Transient receptor potential vanilloid 4 (TRPV4) is a multi-modally activated cation channel that mediates mechanotransduction pathways by which musculoskeletal tissues respond to mechanical load and regulate tissue health. Using *Col2Cre;Trpv4*$^{fl/fl}$ (*Trpv4* KO) mice, we investigated the role of *Trpv4* in an injury-induced model of IVD degeneration. While loss of *Trpv4* did not significantly alter vertebral bone length or histopathological IVD health compared to age-matched wild-type mice at 4 or 8 months-of-age, *Trpv4* KO mice showed decreased proteoglycan staining in the inner AF compared to IVDs of age-matched wild-type mice. Following AF puncture, both *Trpv4* KO and wild-type mice showed similar signs of degeneration at the site of injury. Interestingly, loss of *Trpv4* prevented mechanically-induced degeneration in IVDs adjacent to sites of injury. These studies suggest a role for *Trpv4* in regulating extracellular matrix synthesis and mediating the response of IVD tissues to mechanical stress.

4.3 Introduction

Low back pain is one of the most disabling conditions worldwide, identified as the leading cause of years lived with disability in 65% of the world (126 out of 195 countries)[1]. Although multifaceted in its cause, in at least 30% of patients low back pain is associated with radiographic signs of intervertebral disc (IVD) degeneration[2,3]. IVDs are complex connective tissue structures located between the vertebrae of the spine that serve as load bearing joints. The induction of IVD degeneration is thought to be associated with decreased cellularity and proteoglycan content in the central nucleus pulposus (NP)[4,5]. These changes lead to decreased water content, reducing the ability of the tissue to absorb load. Reduced load absorption in the NP introduces aberrant levels of mechanical load on the surrounding annulus fibrosus (AF), leading to altered AF cellular processes and disruption of the lamellar structure[3,5]. This cascade of degenerative changes ultimately impairs IVD biomechanical function, leading to structural failures that can precipitate disc herniation, spondylosis, and spinal stenosis[6,7]. Although the etiology of IVD degeneration is unclear, multiple factors are thought to contribute to its onset and progression, including mechanical loading[6,8,9], genetics[10,11], nutrient supply[12–14], and trauma[15,16].

In addition to age-associated IVD degeneration, injury models have been widely used to study IVD degeneration in both large (bovine[17], porcine[18], and dog[19]) and small (rabbit[20], rat[21], and mouse[22,23]) animals. The acute injury induced to the IVD in these models produces mechanical instability and altered load distribution within the injured IVD and consequently also within adjacent IVDs. Previous studies in mice adopted an AF puncture procedure, where a needle inserted through the AF penetrates into the central NP, causing NP depressurization[22]. In both lumbar and caudal IVDs, AF puncture induced immediate

NP herniation followed by progressive degeneration of adjacent tissues, exhibiting histomorphological signs of mild to advanced degeneration depending on the size of the needle used and subsequent extent of NP depressurization[22–26]. Most often, AF injury is conducted using a surgical approach where an incision and soft tissue dissections are used to expose the disc space for puncture. More recently, methods have been developed to allow for percutaneous AF puncture in the caudal spine, an approach that minimizes inflammation and injury to surrounding tissues, decreases morbidity, and increases reproducibility of the induced injury[27,28].

Although altered mechanical loading is a well-established risk factor for IVD degeneration[29–33], the cell-type specific mediators of mechanotransduction in the IVD are not fully understood. Transient receptor potential vanilloid 4 (TRPV4) is a cation channel responsive to multiple extracellular signals, including osmolarity[34,35], temperature[36–38], pH[39], and mechanical loading (i.e. membrane stretch activation)[37,40,41]. TRPV4 is expressed and functionally relevant in musculoskeletal tissues, mediating mechano-response of chondrocytes and osteoblasts to dynamic compressive load and fluid flow, respectively[42,43]. In chondrocytes, mechanical and pharmacological activation of TRPV4 elicits intracellular calcium transients that serve to regulate matrix synthesis and chondrogenic differentiation[42,44]. In bone, mechanically induced TRPV4-mediated calcium signalling regulates the terminal differentiation of osteoclasts as well as osteoblastic differentiation, eliciting oscillatory calcium response[43,45,46]. In the context of the IVD, TRPV4 expression and activation has been shown to be regulated by changes in extracellular osmolarity in human NP and AF cells[47]. In the mouse, we recently demonstrated that TRPV4 is expressed in the NP and inner AF, and serves to regulate cytoskeletal remodelling and mechano-

sensitive gene expression in AF cells. Nonetheless, the role of TRPV4 as a regulator of IVD mechanobiology requires further investigation.

Previous studies demonstrated that TRPV4 function is critical to the maintenance of musculoskeletal tissues. Whole-body deletion of *Trpv4* in mice accelerates age-associated osteoarthritis and impairs bone turnover, owing to altered mechanotransduction pathways in chondrocytes, osteoblasts, and osteoclasts[48,49]. In contrast, conditional deletion of *Trpv4* in cartilaginous tissues of skeletally mature mice was shown to attenuate age-associated but not injury-induced osteoarthritis[50]. Together, these findings suggest a regulatory role of TRPV4-mediated signalling in joint health.

The goal of this study was to assess the role of TRPV4-mediated mechanotransduction in the maintenance of IVD health. Using a newly established 'knockout ready' mouse strain, we targeted *Trpv4* expression in the majority of the IVD using *Col2-Cre* to generate a knockout mouse model, which was then used to investigate the role of TRPV4 in IVD health, vertebral bone length, and in an injury-induced model of IVD degeneration.

4.4 Methods

4.4.1 Mice

The EUCOMM "knockout-first" strategy was used to generate *Trpv4*$^{tm1a(KOMP)Wtsi}$ mice, containing the L1L2_Bact_P cassette inserted upstream of exon 6 in the *Trpv4* locus. Conditional knockout-ready mice were generated by breeding the *Trpv4*$^{tm1a(KOMP)Wtsi}$ mice with *Gt(ROSA)26Sor*$^{tm2(CAG-flpo,-EYFP)Ics}$ mice to excise the selection cassette, generating *Trpv4*$^{tm1c(KOMP)Wtsi}$ mice (**Figure 4.1A**). Homozygous *Trpv4*$^{tm1c(KOMP)Wtsi}$ mice (*Trpv4*$^{fl/fl}$) were bred to mice carrying Cre recombinase under control of the type IIα1 collagen

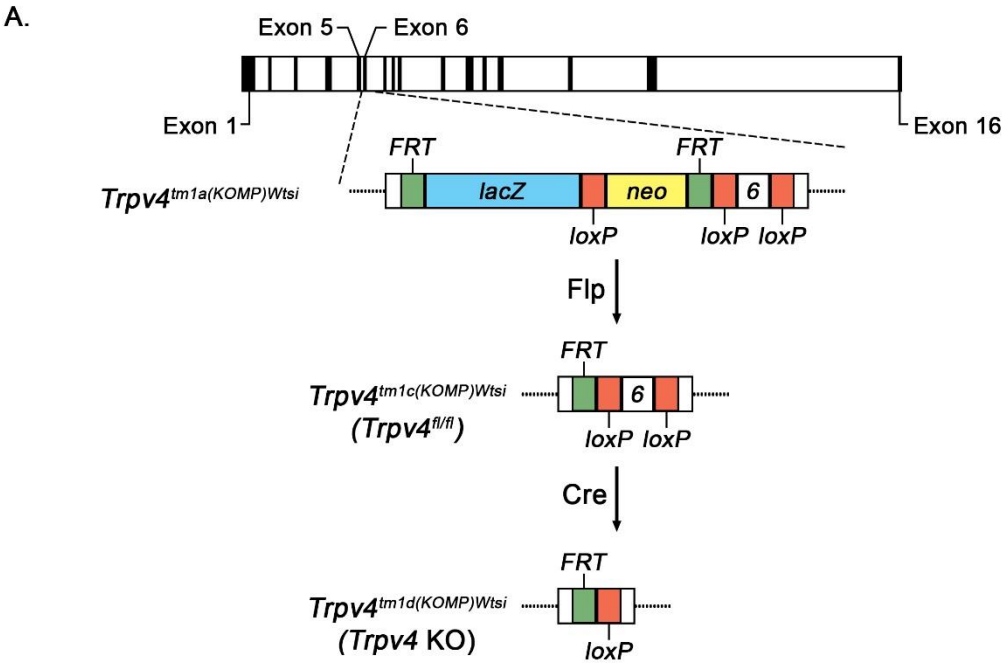
A.
Exon 5
Exon 6
Exon 1
Exon 16
FRT
FRT
Trpv4tm1a(KOMP)Wtsi
lacZ
neo
6
loxP
loxP
loxP
Flp
FRT
Trpv4tm1c(KOMP)Wtsi
(Trpv4fl/fl)
6
loxP
loxP
Cre
FRT
Trpv4tm1d(KOMP)Wtsi
(Trpv4 KO)
loxP

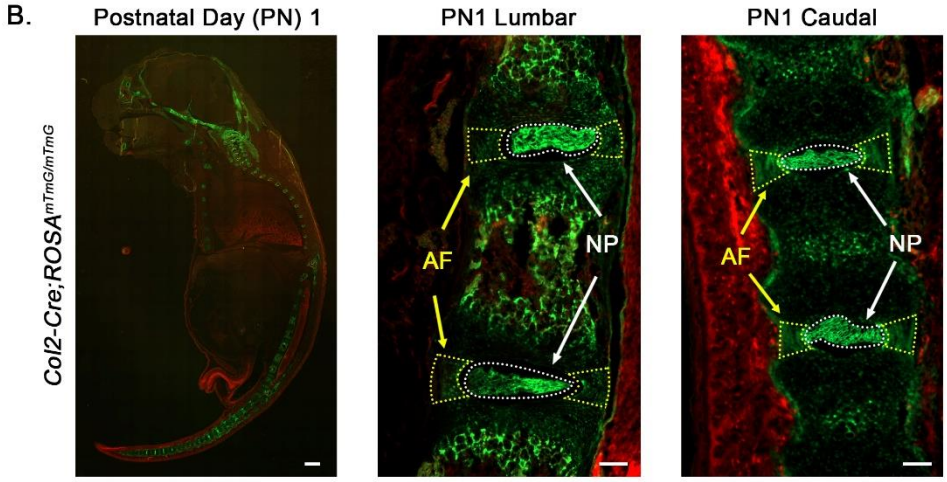
B.
Postnatal Day (PN) 1
PN1 Lumbar
PN1 Caudal
Col2-Cre;ROSAmTmG/mTmG
AF
NP
AF
NP

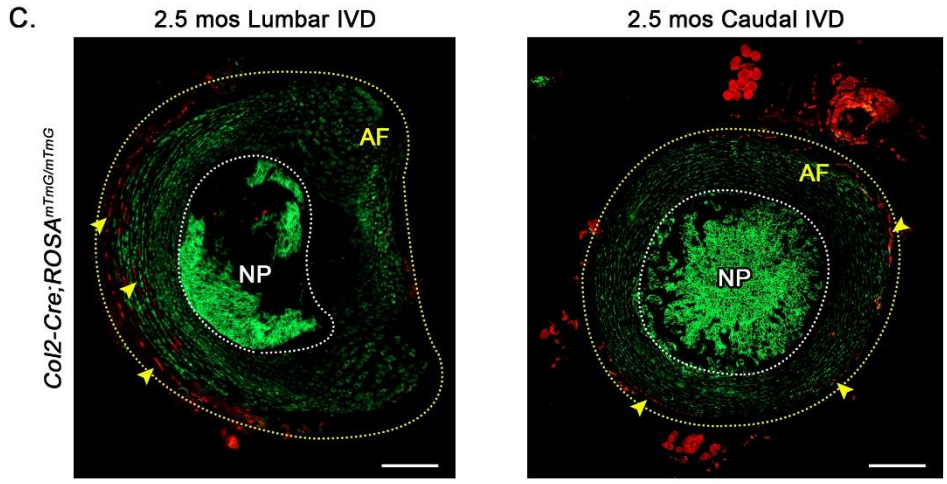
C.
2.5 mos Lumbar IVD
2.5 mos Caudal IVD
Col2-Cre;ROSAmTmG/mTmG
AF
NP
AF
NP

Figure 4.1. Transgenic mouse models.

A) Gene trap strategy used to generate *Trpv4* floxed mice. The EUCOMM "knockout-first" strategy was used to generate *Trpv4*$^{tm1a(KOMP)Wtsi}$ mouse. The L1L2_Bact_P cassette was inserted upstream of the critical exon (exon 6) in the *Trpv4* locus. The cassette includes FRT site followed by *lacZ* sequence and a loxP site. The first loxP site is followed by a neomycin resistance gene, a second FRT site and a second loxP site. A third loxP site is inserted downstream of exon 6. The resulting construct has exon 6 of *Trpv4* gene flanked by loxP sites (tm1a). A "conditional ready" (floxed) allele was generated by breeding the *Trpv4*$^{tm1a(KOMP)Wtsi}$ mice with *Gt(ROSA)26Sor*$^{tm2(CAG-flpo,-EYFP)Ics}$ mice to excise the selection cassette, generating *Trpv4*$^{tm1c(KOMP)Wtsi}$ (*Trpv4*$^{fl/fl}$) mice. Subsequent Cre excision leads to *Trpv4*$^{tm1d(KOMP)Wtsi}$ (*Trpv4* KO) mice B) Fluorescent images of midsagittal sections of *Col2-Cre;ROSA*$^{mTmG/mTmG}$ mice at postnatal day1 (B) and transverse sections of IVDs from mice at 2.5-moths-of-age (C) to localize Cre activity within the IVD. Expression of GFP indicates Cre activity. The images demonstrate that Col2Cre targets all cells within the nucleus pulposus (white label and dotted lines) as well as the inner and middle regions of the annulus fibrosus (yellow label and dotted lines). Tomato expressing cells (Cre-negative) were detected in the outer region of the annulus fibrosus (yellow solid arrow at C) Scale bar = 100 μm. n = 3 mice per time point.

promoter and its 3-kb chondrocyte-specific enhancer region (*Col2-Cre* mice)[51–54]. Mice without Cre-recombinase were used as controls (*Col2Cre*$^{-}$*;Trpv4*$^{fl/fl}$, hereinafter referred to as WT) for comparison to Cre-positive mice (*Col2Cre*$^{+}$*;Trpv4*$^{fl/fl}$, hereinafter referred to as *Trpv4* KO).

To localize Col2-Cre activity within the IVD, *Col2-Cre* mice were mated with the conditional *ROSA26 (R26) mT/mG* reporter mouse (*Gt(ROSA)26Sor*$^{tm4(ACTB-tdTomato,-EGFP)Luo}$/J)[55] to generate *Col2Cre*$^{+}$*;ROSA*$^{mTmG/mTmG}$ mice (**Figure 4.1B**).

All mice were housed in conventional cages and maintained on a 12-hour light/dark cycle, with rodent chow and water available *ad libitum.* Mice were euthanized by intraperitoneal injection of a lethal dose of sodium pentobarbital. All procedures were conducted in accordance with the policies and guidelines set by the Canadian Council on Animal Care and approved by the Animal use Subcommittee of Western University, London, ON (protocol 2017-154, **Appendix A**).

4.4.2 Percutaneous AF Needle Puncture

To induce IVD degeneration, 2.5-month-old and 6.5-month-old WT and *Trpv4* KO mice (n=5 at 2.5 months-of-age and n=3 for 6.5 months-of-age per genotype) were anesthetized using 1.75% isofluorane gas and dorsoventral X-ray images were used to locate caudal IVDs in reference to a custom-made electron-dense landmarking guide (**Figure 4.2A**). Using the landmarking tool, caudal IVDs 7/8 (Co7/Co8) and 8/9 (Co8/Co9) were marked on the dorsal side of the tail. Using aseptic technique, the Co7/Co8 and Co8/Co9 IVDs were sequentially punctured with a 30-guage needle inserted through the skin into the centre of the disc (**Figure 4.2C**). The depth of needle puncture was standardized using a

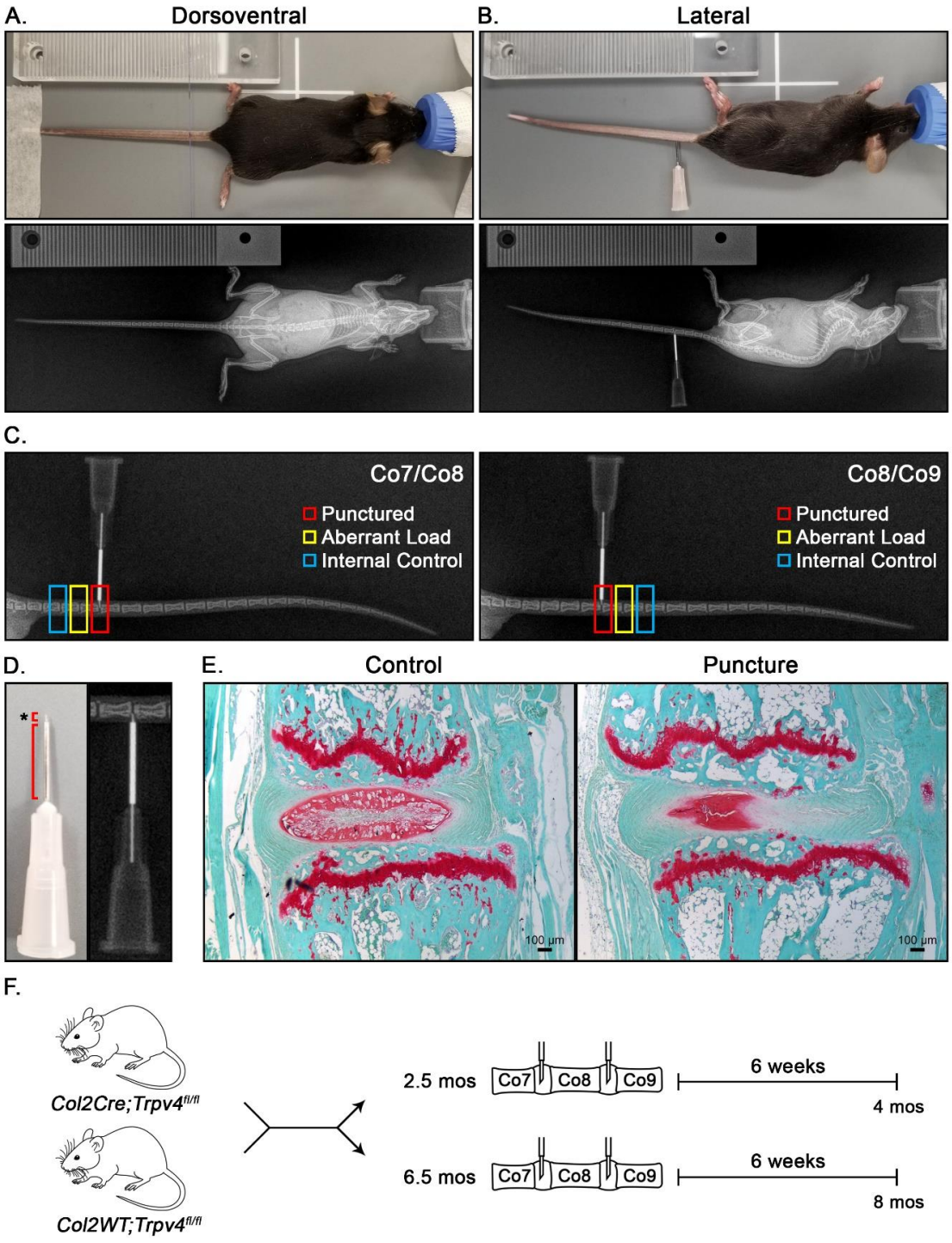
A.
Dorsoventral
B.
Lateral
C.
Co7/Co8
Punctured
Aberrant Load
Internal Control
Co8/Co9
Punctured
Aberrant Load
Internal Control
D.
E.
Control
Puncture
100 µm
100 µm
F.
Col2Cre;Trpv4fl/fl
Col2WT;Trpv4fl/fl
2.5 mos
Co7
Co8
Co9
6 weeks
4 mos
6.5 mos
Co7
Co8
Co9
6 weeks
8 mos

Figure 4.2. Injury-induced model of IVD degeneration using percutaneous tail IVD puncture.

Dorsoventral (A) and lateral (B) view of a 2.5-month-old wild-type mouse undergoing percutaneous IVD puncture. A) Dorsoventral X-rays with an electron dense measuring tool are used to locate and mark caudal IVDs 7/8 and 8/9. D) Guided by a 22-gauge sleeve (asterisk) to standardize depth of puncture, a 30-gauge needle is used to puncture and depressurize the IVDs, confirmed using lateral X-ray (B). E) Mid-sagittal sections of internal control (Co5/Co6) and punctured IVDs (Co7/Co8) harvested 48 hours following needle puncture stained with safranin-O/fast green demonstrating depressurization of the NP and evidence of fibrous tissue formation in the punctured IVD. F) Experimental workflow. To induce IVD degeneration, 2.5-month-old and 6.5-month-old WT and *Trpv4* KO mice (n=5 per genotype for 2.5 mos; n=3 per genotype for 6.5 mos) were subjected to tail puncture. Six weeks post-disc puncture (mice 4-months-of-age and 8-months-of-age at sacrifice) IVD health was assessed using histopathological scoring. Scale bar = 100 μm.

22-guage needle sleeve designed to expose 1.4 mm of the 30-guage needle for puncture (**Figure 4.2D**). Once the IVD was punctured, the needle was held in position for 45 s to standardize NP depressurization. The puncture location and depth were confirmed by lateral X-ray images (**Figure 4.2B**). Uninjured IVDs adjacent to the punctured IVDs (Co6/Co7 and Co9/Co10) were assayed to look for changes in response to aberrant loading. Uninjured IVDs two levels above or below the punctured IVDs (Co5/Co6 and Co10/Co11) served as internal controls. Following the procedure, mice were returned to normal cage activity and were euthanized 48 h or 6 weeks following disc puncture (**Figure 4.2F**).

4.4.3 Histological Analyses

Col2Cre^{+}*;ROSA*$^{mTmG/mTmG}$ pups at postnatal day 1 (PN1) and microdissected lumbar and caudal IVDs from mice at 2.5 months-of-age were fixed and embedded in optimal cutting temperature (OCT) compound (VWR International, Mississauga, ON, Canada) for cryosectioning. Tissues sections were coverslipped with Fluoroshield Mounting Medium with DAPI (Abcam) and imaged using the BioTek Cytation 5 Cell Imaging Multi-Mode Reader and BioTek5 Microplate Reader and Imaging Software (BioTek, Winooski, VT, USA).

Lumbar and caudal spines of WT and *Trpv4* KO mice were harvested and fixed overnight with 4% (w/v) paraformaldehyde in phosphate buffered saline (PBS). Fixed tissues were decalcified using Shandon's TBD-2 (Thermo Fisher Scientific, Waltham, MA, USA) for 5 days at room temperature with continuous agitation. Following standard histological processing, tissues were embedded in paraffin and sectioned sagittally at a thickness of 5 μm. Midsagittal sections of lumbar and caudal spines were deparaffinized and rehydrated as previously described[56,57], and stained with 0.05% Safranin-O/0.05% fast green. Stained

sections were imaged using a Leica DM1000 Microscope with Leica Application Suite Software (Leica Microsystems).

Stained sections of the lumbar spine were assessed for both proteoglycan staining and vertebral bone length using ImageJ software. Briefly, for each lumbar IVD, a region of interest (ROI) was manually defined to include the entire anterior AF and the area of corresponding to red pixels within the ROI was normalized to the total ROI area. To assess vertebral bone length, the distance between the superior and inferior growth plates of each lumbar vertebrate was measured at the anterior edge, mid-line, and posterior edge and values were averaged out to generate overall length measurements.

Caudal spine sections stained with Safranin-O/fast green were assessed for IVD degeneration using an established mouse IVD histopathological scoring system[58]. For the purposes of this study, the scoring system included Part (I), Part B(I), and Part C of the reported criteria, with modifications made in Part (I) ("score 4: mineralized matrix in NP" omitted). For each caudal IVD, degeneration was scored by two individuals blinded to both genotype and age of mice in the NP, AF, and NP/AF boundary. Scores from these 3 regions were summed to provide the overall degeneration score, where the maximum score of 9 reflects the highest degree of degeneration.

4.4.4 Statistical Analyses

All statistical analyses were performed using GraphPad Prism version 8.0.1. Proteoglycan staining and vertebral bone length measurements were analyzed using two-way ANOVA followed by Bonferroni multiple comparisons. Grubb's outlier test was used to identify outliers in proteoglycan staining quantification. Histopathological scores were compared

between strains of mice at each time point using a Mann-Whitney U nonparametric test. $P < 0.05$ were considered statistically significant.

4.5 Results

4.5.1 *Col2-Cre* targets the NP and most of the AF

Conditional knockout-ready *Trpv4*$^{fl/fl}$ mice were generated to examine the role of *Trpv4* in the IVD. The *Col2-Cre* transgenic strain allows constitutive Cre-recombinase expression under the control of the type IIα1 collagen promoter and its 3-kb chondrocyte-specific enhancer[51]. Type II collagen (*Col2a1*) has been shown to be expressed in cells of the NP and AF in mice and other species[59–61]. Other *Col2-Cre* strains have been previously characterized with differences in the genomic location of and regulatory elements driving Cre recombinase expression[62,63]. The *Col2a1-Cre* transgene developed by Ovchinnikov *et al* consisted of 3-kb of the *Col2a1* promoter region, exon 1 with a mutated initiation codon, and 3.02-kb fragment of intron 1, followed by an internal ribosome-entry site, and Cre recombinase coding region[62]. In this mouse strain, Cre activity was detected in the entire NP, AF and cartilage endplate (CEP) at 6 weeks-of-age[59]. Long *et al* subsequently modified the *Col2a1-Cre* construct, adding the G.S.S.-Cre-polyA cassette inserted between the promoter and enhancer region of *Col2a1* gene[63]. In this *Col2a1-Cre* mouse line, Cre-mediated recombination was detected in 75% of NP, 73% in inner AF, 10.6% of outer AF, and the entire CEP at 2 months-of-age[64]. To characterize the spatial distribution of *Col2Cre* expression in the IVD, *Col2-Cre* mice were bred with the *ROSA*$^{mTmG/mTmG}$ double reporter mice. In *Col2-Cre;ROSA*$^{mTmG/mTmG}$ mice at PN1, GFP expression indicative of Cre activity was detected in the NP and AF of both lumbar and caudal IVDs (**Figure 4.1B**). Transverse sections of IVD tissues from mice at 2.5 months-of-age demonstrated robust expression of

GFP in the NP, in all the cells of the inner and middle regions of the AF, and a mixture of GFP and Tomato expression in the outer 1-3 AF lamellar layers of both lumbar and tail IVDs (**Figure 4.1C**). The spatial distribution of *Col2-Cre* matches our previous work on the expression profile of *Trpv4* in the murine IVD, showing *Trpv4* expression in the cells of the NP and inner half of the AF. As such, *Col2-Cre;Trpv4*$^{fl/fl}$ mice were generated to target all Trpv4-expressing cells in the IVD.

4.5.2 *Trpv4* deletion leads to decreased proteoglycan staining in the lumbar IVDs

Using the conditional knockout *Col2-Cre;Trpv4*$^{fl/fl}$ mice (*Trpv4* KO), we investigated the role of TRPV4 in the IVD. Lumbar spines were harvested for histological analysis from WT and *Trpv4* KO mice at 4 and 8 months-of-age. No gross morphological changes or overt signs of degeneration were detected in the IVDs of *Trpv4* KO mice compared to age-matched WT mice (**Figure 4.3A**). Interestingly, decreased proteoglycan staining was detected in the inner AF of IVDs from *Trpv4* KO mice compared to WT at both timepoints (**Figure 4.3A**). Safranin-O staining was therefore quantified within the anterior AF of lumbar IVDs. No significant difference was detected in the percent area of Safranin-O staining averaged over all lumbar IVDs between WT and *Trpv4* KO mice (**Figure 4.3B**) at either time point. However, when assessed at each individual lumbar IVD level, a significant decrease in proteoglycan staining was detected at L5/L6 in *Trpv4* KO mice compared to WT at 4 months-of-age (**Figure 4.3C**). At 8 months-of-age, a similar trend was observed at L5/L6. Decreased proteoglycan staining in *Trpv4* KO mice suggests potential role of TRPV4 as a regulator of matrix synthesis in AF cells.

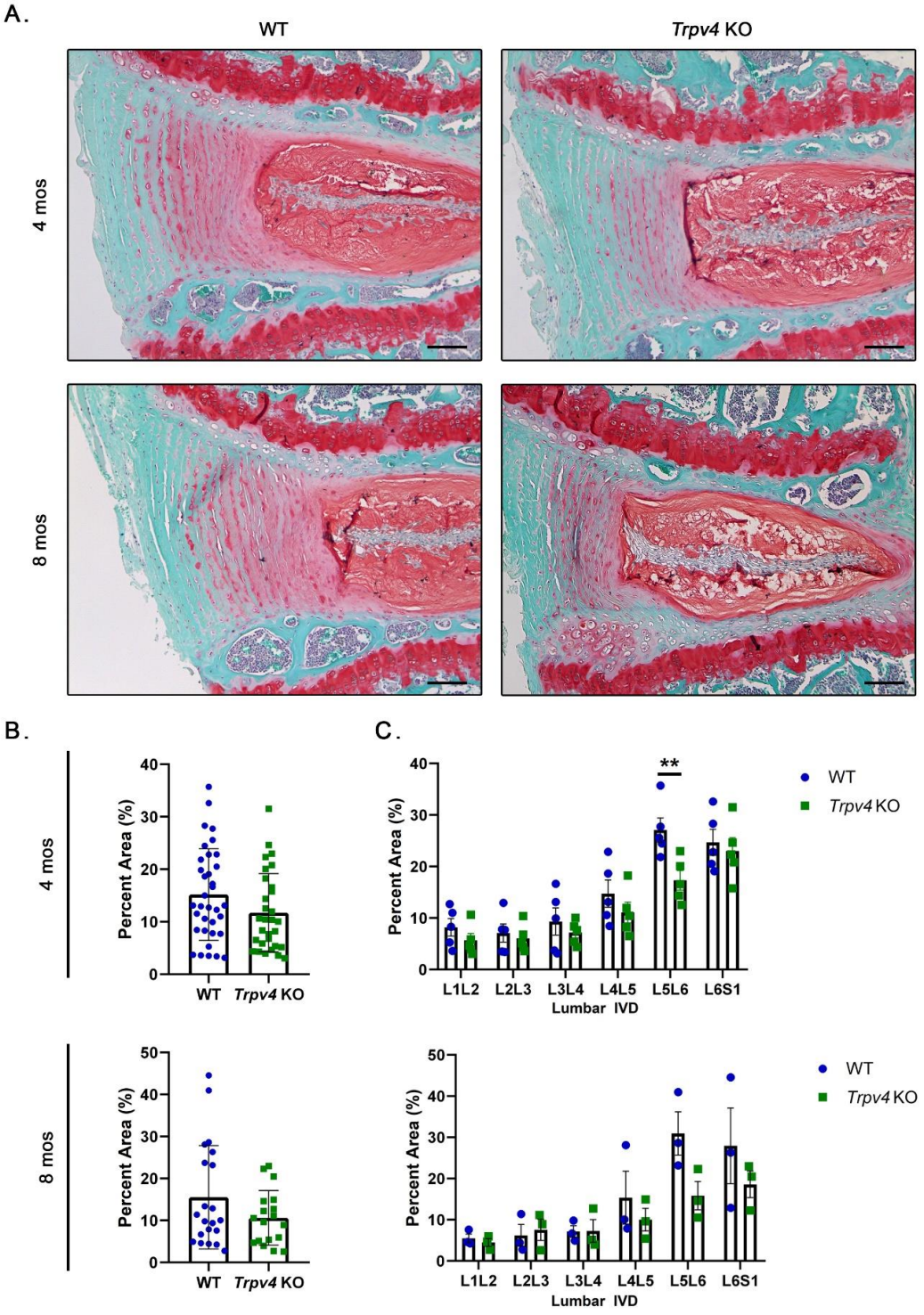
A.
WT
Trpv4 KO
4 mos
8 mos
B.
4 mos
Percent Area (%)
WT
Trpv4 KO
8 mos
C.
**
WT
Trpv4 KO
L1L2
L2L3
L3L4
L4L5
L5L6
L6S1
Lumbar IVD

Figure 4.3. Loss of *Trpv4* does not alter gross IVD morphology.

A) Representative midsagittal sections of lumbar IVDs stained with Safranin-O/fast green from wild-type and *Trpv4* KO mice at 4 and 8 months-of-age. No overt differences were detected in overall IVD morphology following deletion of *Trpv4*. To quantify sulphated proteoglycan levels in the AF, Safranin-O staining was quantified within a region of interest (ROI) capturing the entire anterior AF and expressed as a percentage of the total ROI. B) Average percentage of AF area stained by Safranin-O for all lumbar IVDs in WT and *Trpv4* KO. C) Percentage of AF area stained by Safranin-O for each lumbar IVD based on anatomical location. At 4 months-of-age, *Trpv4* KO mice showed decreased Safranin-O staining in the AF of L5/L6 compared to wild-type mice. Data presented as mean ± SEM, analyzed by two-way ANOVA with Bonferroni multiple comparisons test. No outliers were detected using Grubb's outlier test. ** = $P < 0.01$. Scale bar = 100 μm. 4 mos n=5 per genotype; 8 mos n=3 per genotype.

4.5.3 Loss of *Trpv4* does not affect vertebral bone growth

Since the cartilaginous and bony elements of the spine were likewise targeted by *Col2-Cre* (**Figure 4.1B**), we investigated the effects of *Trpv4* deletion on vertebral bone length. Midsagittal sections of the lumbar spine were used to measure the vertebral bone length, defined as length of bone between the superior and inferior growth plates of the vertebral body along the craniocaudal axis (**Figure 4.4A**). No differences in vertebral bone length were detected in any lumbar vertebrae between *Trpv4* KO and age-matched WT mice at either 4 or 8 months-of-age.

4.5.4 Percutaneous AF needle puncture induces degeneration of caudal IVDs

Using a minimally invasive percutaneous AF needle puncture protocol previously optimized by our group[65], we targeted the Co7/Co8 and Co8/Co9 IVDs to induce acute IVD injury via NP depressurization. In this model, caudal IVDs adjacent to the punctured IVDs (Co6/Co7 and Co9/Co10) were investigated to assess the tissue response to the injury-induced aberrant load, and uninjured IVDs two levels above or below punctured IVDs (Co5/Co6 and Co10/Co11) served as the internal control. To validate this model, wild-type mice at 2.5 months-of-age underwent percutaneous AF puncture and IVD tissues were assessed following 48 h. At the site of puncture, IVDs showed histomorphological changes consistent with the loss of NP tissue volume (due to puncture) and signs of NP tissue fibrosis compared to adjacent uninjured IVDs (**Figure 4.2E**).

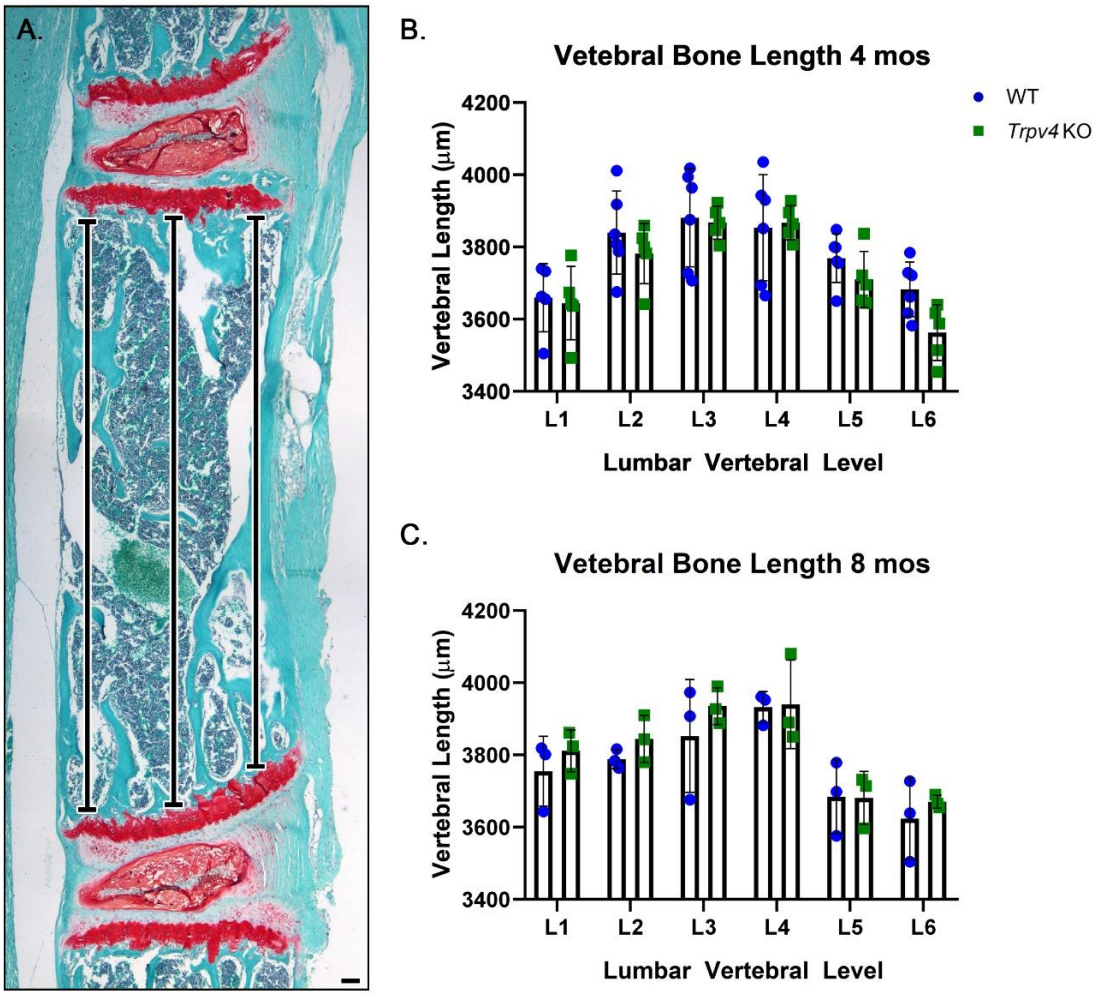

Figure 4.4. Vertebral bone length is not altered in *Trpv4* KO mice.

A) Representative midsagittal sections of L4 vertebra of WT mice annotated with location of vertebral bone length measurements. Vertebral bone length was measured at three different points across the vertebrae (black lines) and averaged for each lumbar vertebrae. B, C) Average bone lengths for each lumbar vertebral level in wild-type and *Trpv4* KO mice at 4 (B) and 8 months-of-age (C). Vertebral bone length was not altered by loss of *Trpv4*. Data presented as mean ± SEM analyzed by two-way anova with Bonferroni multiple comparisons test. Scale bar = 100 μm. 4 mos n=5 per genotype; 8 mos n=3 per genotype.

4.5.5 Loss of *Trpv4* protects from degeneration induced in IVDs adjacent to sites of injury

We then investigated the role of TRPV4 in regulating the response to injury induced IVD degeneration. *Trpv4* KO and age-matched WT mice at 2.5 and 6.5 months-of-age were subject to percutaneous AF puncture and sacrificed 6 weeks post puncture (at 4 and 8 months-of-age) for histopathological analysis. At both 4 and 8 months-of-age *Trpv4* KO and wild-type mice showed similar degenerative changes at the sites of puncture, including loss of NP tissue structure and cellularity, NP tissue fibrosis, and disorganization and reversal of AF lamellae (**Figures 4.5 & 4.6** - Co7/Co8; Co8/Co9). Although degenerative changes induced by puncture were not different between *Trpv4* KO and WT mice, loss of TRPV4 altered the response of adjacent IVDs to the aberrant mechanical load induced by IVD puncture. In wild-type mice, the Co6/Co7 IVDs adjacent to the sites of puncture showed signs of advanced degeneration marked by decreased NP cellularity, and NP fibrosis, and disorganization and reversal of the AF lamellar structure. In contrast, IVDs at the same level in *Trpv4* KO mice showed minimal histopathological signs of degeneration. Similarly, in wild-type mice Co9/Co10 IVDs (distal to punctured Co8/Co9 IVDs) showed signs of accelerated NP degeneration, including cell cluster formation, reduced cellularity, and increased matrix density localized specifically to the side of the needle insertion in the adjacent punctured IVDs. These degenerative changes were not observed at the same IVD level in *Trpv4* KO mice. The differences observed in both Co6/Co7 and Co9/Co10 were associated with histopathological scores that were significantly higher in wild-type mice compared to *Trpv4* KO mice at 4 months-of-age (**Figure 4.5**), but not at 8 months-of-age (**Figure 4.6**).

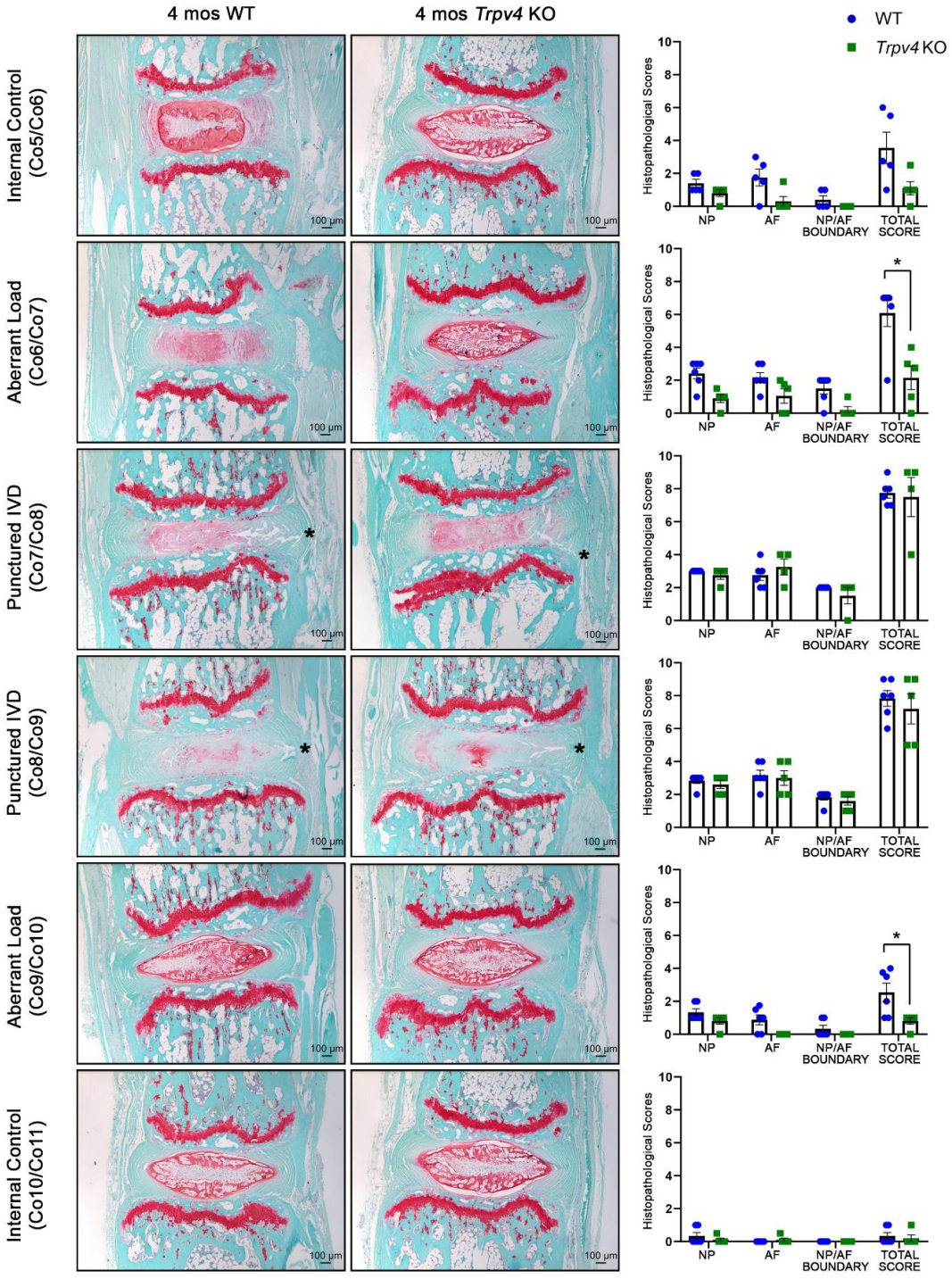
4 mos WT
4 mos Trpv4 KO
WT
Trpv4 KO
Internal Control (Co5/Co6)
Aberrant Load (Co6/Co7)
Punctured IVD (Co7/Co8)
Punctured IVD (Co8/Co9)
Aberrant Load (Co9/Co10)
Internal Control (Co10/Co11)
100 µm
Histopathological Scores
NP
AF
NP/AF BOUNDARY
TOTAL SCORE
*

Figure 4.5. Loss of *Trpv4* protects from IVD degeneration adjacent to sites of injury at 2.5-months-of-age.

Representative mid-sagittal sections of caudal IVDs from wild-type and *Trpv4* KO mice harvested 6 weeks following AF puncture at 2.5-months-of-age (site of puncture indicated by *). Caudal IVDs Co6/Co5 and Co10/Co11 served as controls while IVDs immediately adjacent to punctured IVDs were assessed as sites experiencing aberrant load (Co6/Co7 and Co9/Co10). Sections were stained with safranin-o/fast green. IVDs from both wild-type and *Trpv4* KO mice showed signs of advanced degeneration following puncture. Caudal IVDs experiencing aberrant load (Co6/Co7 and Co9/Co10) showed significantly increased degeneration in wild-type mice compared to *Trpv4* KO mice, as reflected by increased histopathological scores. Data presented as mean ± SD, analyzed by Mann-Whitney test. * = $P < 0.05$. Scale bar = 100 μm. n = 5 mice per genotype.

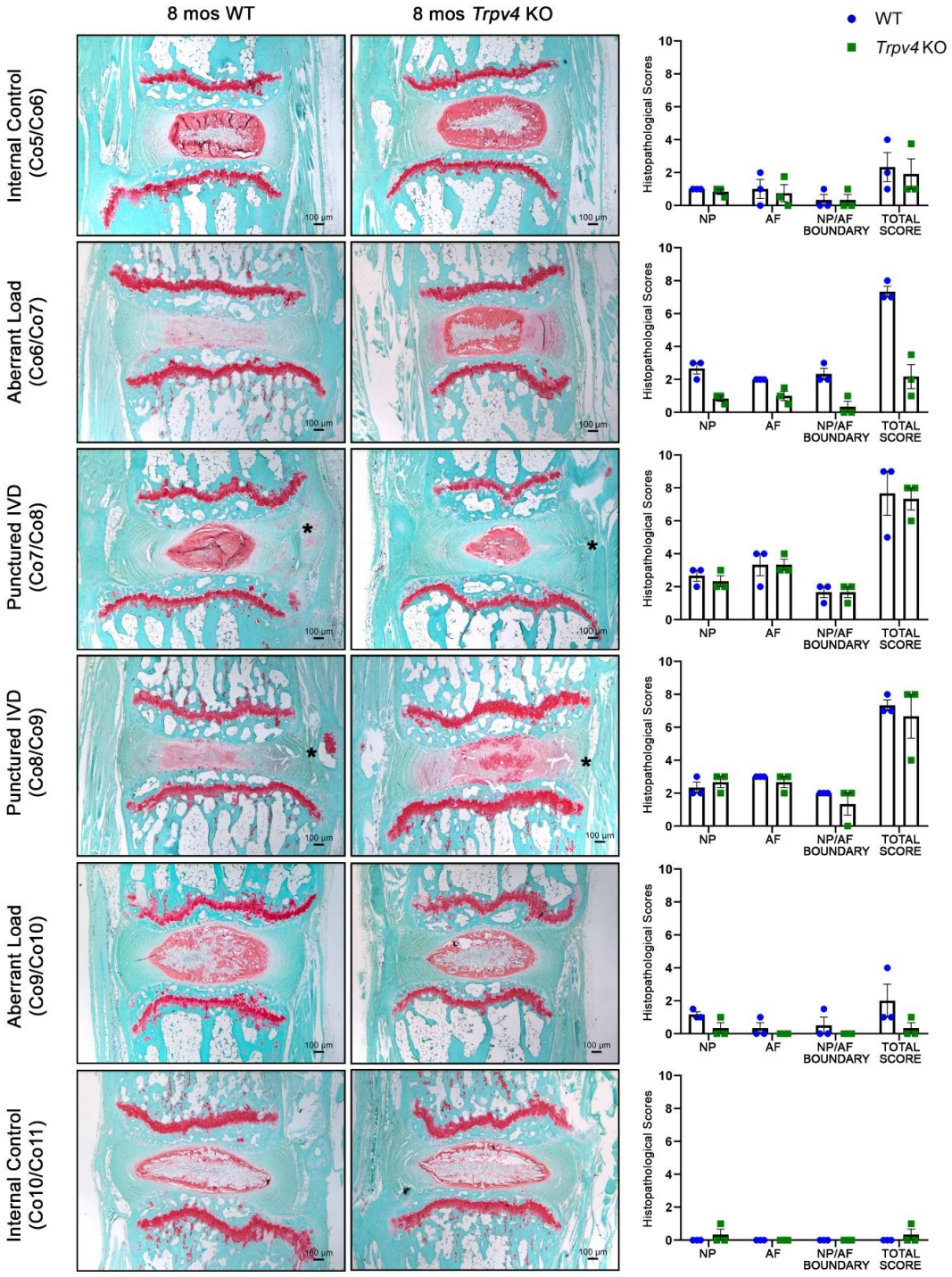
8 mos WT
8 mos Trpv4 KO
WT
Trpv4 KO
Internal Control (Co5/Co6)
Aberrant Load (Co6/Co7)
Punctured IVD (Co7/Co8)
Punctured IVD (Co8/Co9)
Aberrant Load (Co9/Co10)
Internal Control (Co10/Co11)
100 µm
Histopathological Scores
NP
AF
NP/AF BOUNDARY
TOTAL SCORE

Figure 4.6. Loss of *Trpv4* alters IVD degeneration adjacent to sites of injury at 6.5-months-of-age.

Representative mid-sagittal sections of caudal IVDs from wild-type and *Trpv4* KO mice harvested 6 weeks following needle puncture injury at 6.5-months-of-age (site of puncture indicated by *). Caudal IVDs Co5/Co6 and Co10/11 served as controls, while IVDs immediately adjacent to punctured IVDs were assessed as sites experiencing aberrant load (Co6/Co7 and Co9/Co10). Sections were stained with safranin-o/fast green. IVDs from both wild-type and *Trpv4* KO mice showed signs of advanced degeneration following puncture. In the caudal IVDs experiencing aberrant load (Co6/Co7 and Co9/Co10), WT mice showed a trend towards higher degeneration scores compared to *Trpv4* KO mice. Data presented as mean ± SD analyzed by Mann-Whitney test. Scale bar = 100 μm. n= 3 mice per genotype.

4.6 Discussion

Given that IVDs serves as the major load bearing structures for the spine, mechanotransduction pathways in its resident cells are likely key regulators of IVD homeostasis. In this study, we used a conditional knockout mouse model to evaluate the role of the TRPV4 ion channel as a mechanoreceptor regulating IVD health and degeneration. Using *Col2-Cre* to target cells of the NP and the majority of the AF, the effect of *Trpv4* deletion was investigated in the IVDs at different spinal regions: lumbar spines were used to assess vertebral bone length and IVD tissue morphology, while caudal spines were used to assess the response of IVD tissues to acute injury. Although loss of *Trpv4* in cartilaginous cells did not affect the vertebral bone length, a significant decrease in proteoglycan staining was detected in the AF of *Trpv4* KO mice compared to WT. In the caudal AF puncture model, loss of *Trpv4* significantly decreased the severity of degeneration in IVDs adjacent to the site of injury, but did not alter injury-induced IVD degeneration. These findings support the overall importance of mechanical load as a key factor regulating IVD degeneration and the specific role of TRPV4 in facilitating the response of IVD tissues to aberrant mechanical load.

Tissue or cell-type specific knockout mouse models enable targeted gene deletion to understand the role of specific genes in development, cell function, and disease. Several Cre strains have been reported to target specific cell types of the IVD. Cre strains such as *Noto-Cre*[56], *Shh-Cre*[66], and *Hif1a-Cre*[67], are commonly used notochord-Cre mouse to target the NP, while *Gdf5-Cre*[68] and *Col1a2-CreERT*[69] strains have been used to target the AF. Previous studies have used different *Col2a1-Cre* strains to target both NP and AF for gene deletion[70–73]. Critical to our experiments was the verification of Cre activity in the

IVD, to ensure that our genetic strategy would appropriately target *Trpv4*-expressing cells of the IVD. To achieve this, we bred *Col2-Cre* mice with *ROSA*$^{mTmG/mTmG}$ double reporter mice and demonstrated Cre activity in the entire NP and most of the AF (excluding outer 1-3 lamellar layers of AF), in mice at post-natal day 1 and 2.5 months-of-age. This pattern of transgene activity coincides with our previous characterization of *Trpv4* expression (**Chapter** 3), which localized *Trpv4* expression to cells of the NP and inner AF. Previous studies reported the Cre activity of *Col2-Cre*[62] and *Col2-CreER* mice using tdTomato as the reporter[59]. Similar to our findings, *Col2Cre;Rosa26TdTomato* mice showed Cre activity in the entire NP and AF at 6 weeks-of-age, in both lumbar and caudal IVDs. Interestingly, in *Col2CreERT;Rosa26TdTomato* mice following tamoxifen-induction at postnatal day 7, Cre activity was limited to the inner regions of the AF at 6 weeks-of-age. In contrast, studies using *Col1a2-Cre(ER)T;ROSAmTmG* mice showed that 100 days following tamoxifen-induction at 3 weeks-of-age, Cre activity was detected in cells of the outer AF, but not in the inner AF or the NP. Use of these Cre strains in future studies would allow for a more detailed examination of the role of *Trpv4* in specific cell types of the IVD.

TRPV4 has been shown to be essential in maintaining musculoskeletal tissue health and function, serving as a regulator of matrix synthesis. In porcine chondrocytes, TRPV4-mediated mechanotransduction regulates the cellular response to dynamic loading; TRPV4 antagonism blocked mechanically-induced regulation of *TGF-β3* and *ADAMTS5* gene expression as well as the loading-induced enhancement of matrix accumulation[42]. In the context of mesenchymal stem cells (MSC) osteogenesis, TRPV4 antagonism inhibited loading-induced early osteogenic gene expression while prolonged pharmacological activation promoted osteogenic differentiation, as evidenced by increased collagen and

mineral deposition[74]. Similarly, previous work by our group demonstrated that TRPV4 mediates loading-induced increase in type I collagen, aggrecan, and lubricin gene expression in the primary AF cells (**Chapter 3**). These findings suggest that TRPV4 contributes to the regulation of matrix synthesis in AF cells, findings further strengthened by the current study demonstrating that loss of *Trpv4* led to decreased proteoglycan staining in the AF.

Growing evidence suggests that TRPV4 is crucial for joint and bone health. Studies using pan-*Trpv4* knockout and cartilage-specific inducible *Trpv4* knockout mouse models showed distinct alterations in the progression of osteoarthritis: pan-*Trpv4* knockout mice show accelerated age-associated osteoarthritis, while cartilage-specific deletion of *Trpv4* at 10 weeks-of-age reduces the severity of age-associated osteoarthritis[48,50]. The observed discrepancy in disease progression in these models may be related to *Trpv4* deletion in multiple joint tissues in the pan-*Trpv4* knockout mice. TRPV4 expression was detected in the human fibroblast-like synoviocyte line MH7A, as well as primary synovial cells derived from rheumatoid arthritis (RA) patients and control patients[75]. In human synoviocytes, activation of TRPV4 increased intracellular Ca^{2+}, which was inhibited by TRPV antagonist. Interestingly, the pro-inflammatory cytokine interleukin-1 alpha (IL-1α) activated the production of IL-8, a response that was suppressed in the presence of TRPV4 agonist in synoviocytes from RA patients but not from control patients. Furthermore, pan-*Trpv4* knockout mice fed a high-fat diet (41.9% kcal from fat) for 3 months had reduced weight gain and increased expression of genes related to energy metabolism (i.e. peroxisome proliferator-activated receptor α, phosphoenolpyruvate carboxykinase, and lipoprotein lipase) in oxidative skeletal muscle compared to wild-type mice fed the same

diet[76]. Additionally, although pan-*Trpv4* knockout mice did not show altered longitudinal bone growth[45], these mice showed increased subchondral bone volume, bone mass and decreased trabecular bone volume, potentially due to insensitivity to mechanical loading and decreased osteoblast/osteoclast activity[48,49].

The roles of TRPV4 in numerous musculoskeletal tissues provided a clear rationale to examine the role of TRPV4 in multiple spinal tissues. We, therefore, investigated the effects of *Trpv4* deletion on vertebral bone length in our *Col2-Cre* driven *Trpv4* KO model. No differences in vertebral bone length were detected in *Trpv4* KO mice within the lumbar spine, confirming that changes detected in our model are not due to gross alterations in vertebral bone. Interestingly, TRPV4 gain-of-function mutation, clinically associated with skeletal dysplasia, have been shown to increase osteoclast number and activity, leading to bone loss and decreased bone mass[49,78]. For example, TRPV4 gain-of-function mutation has been shown to be associated with brachyolmia, a form of skeletal dysplasia of unknown etiology that primarily affect the spine. Type 1 brachyolmia, one of three identified types, is characterized by scoliosis, elongated vertebral bodies, overfaced pedicles, and narrow IVD spaces[79]. These studies suggest increased TRPV4 activity is associated with vertebral bone development.

Using a percutaneous IVD puncture model, we investigated the effect of *Trpv4* deletion on the IVD tissue response to injury. Consistent with previous studies[27,28], we showed advanced degeneration of caudal IVDs marked by decreased cellularity and fibrotic changes in the NP as well as disruption of the AF lamellar structure 4 weeks after puncture. Conditional deletion of *Trpv4* did not alter IVD degeneration at the site of AF puncture. It is important to note that AF puncture associated with NP depressurization more accurately

models IVD herniation resulting in more severe IVD degeneration than models of progressive age-related or mechanically induced IVD degeneration. Since AF puncture induces a severe injury with drastic degenerative changes, the modulation of a single mechanoreceptor may not affect the degenerative process due to injury. Interestingly, loss of *Trpv4* protected from degeneration in IVDs adjacent to sites of injury. Following puncture, the biomechanical properties of the injured IVD are immediately compromised, which in turn introduces abnormal levels of mechanical load to the adjacent IVDs. A similar scenario occurs in the clinical setting in adjacent segment disease, characterized by degenerative changes occurring in the IVD at a spinal level adjacent to sites of surgical intervention in the spine[80]. Previous studies reported increased intradiscal pressure at adjacent IVDs after single level spinal fusion[81]. The protective effect of *Trpv4* deletion may be explained by the magnitude-dependent nature of TRPV4 activation. In chondrocytes, repetitive cyclical mechanical load evoked increased intracellular calcium response in a strain magnitude-dependent manner[82]. Furthermore, increased basal calcium influx through genetic alterations or pharmacological activation of TRPV4 has been shown to cause cell toxicity and cell death in different cell types[83–86]. In the context of our injury model, increased mechanical load experienced by the adjacent IVDs may increase TRPV4-mediated intracellular calcium influx, leading to degenerative changes. Together, these studies demonstrate that while *Trpv4* deletion did not alter degenerative changes at the site of injury, in a less severe more progressive model (i.e. adjacent discs with aberrant loading) or in a model where mechanical loading is the driver of degeneration, TRPV4 plays an important role.

It is important to acknowledge limitations associated with the current study. First, murine caudal IVDs are different in geometry, biomechanical properties, and surrounding tissue environment compared to lumbar IVDs of both human and mice[87–89]. Mouse tails are more circular in geometry, contain less musculature surrounding the IVD, and experience greater motion compared to lumbar IVDs. Future studies should adopt the needle puncture procedure developed to target lumbar IVDs[24,25]. Furthermore, other parameters of the AF puncture, such as needle size and depth of puncture can be adjusted to modulate the severity of injury. An injury model with less severe injury may be appropriate to better study the role of TRPV4 during injury induced IVD degeneration.

Another limitation of our study is the use of *in vivo* models. While transgenic mouse models allow for studies on a protein of interest within the native IVD environment, the small size of the murine IVD and heterogeneity in IVD cell types within limit our ability to interrogate mechanistic questions. Future *in vitro* studies using primary AF cells derived from WT and *Trpv4 KO* mice could be conducted using mechanically dynamic bioreactor systems (i.e. cell stimulators or organ culture) to examine the cellular pathways modulated by loss of TRPV4. Furthermore, by implementing multi-omics approaches, unbiased studies may be conducted to examine the effects of *Trpv4* deletion in IVD tissues. Lastly, the current study did not assess sex as biological variable. In the pan-*Trpv4* knockout mouse model, male mice exhibited more severe osteoarthritis and bone abnormalities than female mice. Consideration of sex-related differences should therefore be incorporated in future studies, including investigation of the effect of *Trpv4* deletion in age-associated IVD degeneration.

4.7 Conclusions

In the present study, we conditionally knocked out *Trpv4* gene in the IVD tissues to investigate the role of TRPV4 in IVD health and degeneration. Loss of *Trpv4* was found to decrease proteoglycan staining in the AF, suggesting the involvement of TRPV4-mediated signalling in proteoglycan synthesis. Using percutaneous AF puncture model, we demonstrated that *Trpv4* deletion did not alter injury-induced degeneration, but protected from loading-induced degeneration in adjacent IVDs. Taken together, our findings suggest regulatory roles of TRPV4 in both tissue homeostasis and injury, mediating matrix production and mechanically-induced IVD degeneration. Understanding the role of TRPV4 in IVD mechanobiology may contribute to the development of disease modifying treatments for IVD degeneration.

4.8 References

1. James SL, Abate D, Abate KH, et al. Global, regional, and national incidence, prevalence, and years lived with disability for 354 Diseases and Injuries for 195 countries and territories, 1990-2017: A systematic analysis for the Global Burden of Disease Study 2017. *Lancet*. 2018:1789-1858. doi:10.1016/S0140-6736(18)32279-7

2. Arnbak B, Jensen TS, Egund N, et al. Prevalence of degenerative and spondyloarthritis-related magnetic resonance imaging findings in the spine and sacroiliac joints in patients with persistent low back pain. doi:10.1007/s00330-015-3903-0

3. Luoma K, Riihimäki H, Luukkonen R, Raininko R, Viikari-Juntura E, Lamminen A. Low back pain in relation to lumbar disc degeneration. *Spine (Phila Pa 1976)*. 2000;25(4):487-492. doi:10.1097/00007632-200002150-00016

4. Buckwalter JA, Roughley PJ, Rosenberg LC. Age-Related Changes in Cartilage Proteoglycans : Quantitative Electron Microscopic Studies. *Micosc Res Tech*. 1994;28(5):398-408.

5. Adams MA, Roughley PJ. What is Intervertebral Disc Degeneration , and What Causes It ? *Spine (Phila Pa 1976)*. 2006;31(18):2151-2161.

6. Oichi T, Taniguchi Y, Oshima Y, Tanaka S, Saito T. Pathomechanism of intervertebral disc degeneration. *JOR SPINE*. 2020;3(1). doi:10.1002/jsp2.1076

7. Sakai D. Future perspectives of cell-based therapy for intervertebral disc disease. In: *European Spine Journal*. Vol 17. Springer; 2008:452. doi:10.1007/s00586-008-0743-5

8. Setton LA, Chen J. Cell Mechanics and Mechanobiology in the Intervertebral Disc. *Spine (Phila Pa 1976)*. 2004;29(23):2710-2723. doi:10.1097/01.brs.0000146050.57722.2a

9. Zhu Q, Gao X, Gu W. Temporal changes of mechanical signals and extracellular composition in human intervertebral disc during degenerative progression. *J Biomech*. 2014;47(15):3734-3743. doi:10.1016/j.jbiomech.2014.09.004

10. Wang S, Rui Y, Lu J, Wang C. Cell and molecular biology of intervertebral disc degeneration: Current understanding and implications for potential therapeutic strategies. *Cell Prolif*. 2014;47(5):381-390. doi:10.1111/cpr.12121

11. Feng Y, Egan B, Wang J. Genetic factors in intervertebral disc degeneration. *Genes Dis*. 2016;3(3):178-185. doi:10.1016/j.gendis.2016.04.005

12. Urban JPG, Smith S, Fairbank JCT. Nutrition of the Intervertebral Disc. *Spine (Phila Pa 1976)*. 2004;29(23):2700-2709. doi:10.1097/01.brs.0000146499.97948.52

13. Urban JPG, Roberts S. Degeneration of the intervertebral disc. *Arthritis Res Ther*. 2003;5(3):120-130. doi:10.1186/ar629

14. Grunhagen T, Shirazi-Adl A, Fairbank JCT, Urban JPG. Intervertebral Disk Nutrition: A Review of Factors Influencing Concentrations of Nutrients and Metabolites. *Orthop Clin North Am*. 2011;42(4):465-477. doi:10.1016/j.ocl.2011.07.010

15. Carragee EJ, Don AS, Hurwitz EL. Erratum: ISSLS prize winner: Does discography cause accelerated progression of degeneration changes in the lumbar disc: A ten-year matched cohort study (Spine (2009) 34 (2338-2345). *Spine (Phila Pa 1976)*. 2010;35(14):1414. doi:10.1097/BRS.0b013e3181e234b5

16. Russo S, Belli A, Eynon A, Nader-Sepahi A. Post-traumatic Spinal Hygroma Causing Cord Compression in Type III Odontoid Fracture with Vertical Atlantoaxial Instability. *Spine (Phila Pa 1976)*. 2017;42(18):E1092-E1094. doi:10.1097/BRS.0000000000002081

17. Melrose J, Shu C, Young C, et al. Mechanical destabilization induced by controlled annular incision of the intervertebral disc dysregulates metalloproteinase expression and induces disc degeneration. *Spine (Phila Pa 1976)*. 2012;37(1):18-25. doi:10.1097/BRS.0b013e31820cd8d5

18. Acosta FL, Metz L, Adkisson HD, et al. Porcine intervertebral disc repair using allogeneic juvenile articular chondrocytes or mesenchymal stem cells. *Tissue Eng - Part A*. 2011;17(23-24):3045-3055. doi:10.1089/ten.tea.2011.0229

19. Ganey T, Hutton WC, Moseley T, Hedrick M, Meisel HJ. Intervertebral disc repair using adipose tissue-derived stem and regenerative cells: Experiments in a canine model. *Spine (Phila Pa 1976)*. 2009;34(21):2297-2304. doi:10.1097/BRS.0b013e3181a54157

20. Masuda K, Aota Y, Muehleman C, et al. A novel rabbit model of mild, reproducible disc degeneration by an anulus needle puncture: Correlation between the degree of disc injury and radiological and histological appearances of disc degeneration. *Spine (Phila Pa 1976)*. 2005;30(1):5-14. doi:10.1097/01.brs.0000148152.04401.20

21. Zhang Y, Liu L, Wang S, et al. Production of CCL20 on nucleus pulposus cells recruits IL-17-producing cells to degenerated IVD tissues in rat models. *J Mol Histol*. 2016;47(1):81-89. doi:10.1007/s10735-015-9651-2

22. Yang F, Leung VY, Luk KD, Chan D, Cheung KM. Injury-induced sequential transformation of notochordal nucleus pulposus to chondrogenic and fibrocartilaginous phenotype in the mouse. *J Pathol*. 2009;218(1):113-121. doi:10.1002/path.2519

23. Martin JT, Gorth DJ, Beattie EE, Harfe BD, Smith LJ, Elliott DM. Needle puncture injury causes acute and long-term mechanical deficiency in a mouse model of

intervertebral disc degeneration. *J Orthop Res*. 2013;31(8):1276-1282. doi:10.1002/jor.22355

24. Millecamps M, Stone LS. Delayed onset of persistent discogenic axial and radiating pain after a single-level lumbar intervertebral disc injury in mice. *Pain*. 2018;159(9):1843-1855. doi:10.1097/j.pain.0000000000001284

25. Lee S, Millecamps M, Foster DZ, Stone LS. Long-term histological analysis of innervation and macrophage infiltration in a mouse model of intervertebral disc injury–induced low back pain. *J Orthop Res*. 2020;38(6):1238-1247. doi:10.1002/jor.24560

26. Iatridis JC, Michalek AJ, Purmessur D, Korecki CL. Localized intervertebral disc injury leads to organ level changes in structure, cellularity, and biosynthesis. *Cell Mol Bioeng*. 2009;2(3):437-447. doi:10.1007/s12195-009-0072-8

27. Tian Z, Ma X, Yasen M, et al. Intervertebral Disc Degeneration in a Percutaneous Mouse Tail Injury Model. *Am J Phys Med Rehabil*. 2018;97(3):170-177. doi:10.1097/PHM.0000000000000818

28. Piazza M, Peck SH, Gullbrand SE, et al. Quantitative MRI correlates with histological grade in a percutaneous needle injury mouse model of disc degeneration. *J Orthop Res*. 2018;36(10):2771-2779. doi:10.1002/jor.24028

29. Adams MA, Freeman BJC, Morrison HP, Nelson IW, Dolan P. Mechanical initiation of intervertebral disc degeneration. *Spine (Phila Pa 1976)*. 2000;25(13):1625-1636. doi:10.1097/00007632-200007010-00005

30. Stokes IAF, Iatridis JC. Mechanical conditions that accelerate intervertebral disc degeneration: Overload versus immobilization. *Spine (Phila Pa 1976)*. 2004;29(23):2724-2732. doi:10.1097/01.brs.0000146049.52152.da

31. Urban JPG, Roberts S. Development and degeneration of the intervertebral discs. *Mol Med Today*. 1995;1(7):329-335. doi:10.1016/S1357-4310(95)80032-8

32. Vergroesen PPA, Kingma I, Emanuel KS, et al. Mechanics and biology in intervertebral disc degeneration: A vicious circle. *Osteoarthr Cartil*. 2015;23(7):1057-1070. doi:10.1016/j.joca.2015.03.028

33. Galbusera F, Van Rijsbergen M, Ito K, Huyghe JM, Brayda-Bruno M, Wilke HJ. Ageing and degenerative changes of the intervertebral disc and their impact on spinal flexibility. *Eur Spine J*. 2014;23(SUPPL. 3):324-332. doi:10.1007/s00586-014-3203-4

34. Liedtke W, Choe Y, Martí-Renom MA, et al. Vanilloid receptor-related osmotically activated channel (VR-OAC), a candidate vertebrate osmoreceptor. *Cell*. 2000;103(3):525-535. doi:10.1016/S0092-8674(00)00143-4

35. Strotmann R, Harteneck C, Nunnenmacher K, Schultz G, Plant TD. OTRPC4, a nonselective cation channel that confers sensivity to extracellular osmolarity. *Nat Cell Biol*. 2000;2(10):695-702. doi:10.1038/35036318

36. Güler AD, Lee H, Iida T, Shimizu I, Tominaga M, Caterina M. Heat-evoked activation of the ion channel, TRPV4. *J Neurosci*. 2002;22(15):6408-6414. doi:10.1523/jneurosci.22-15-06408.2002

37. Chung MK, Lee H, Caterina MJ. Warm temperatures activate TRPV4 in mouse 308 keratinocytes. *J Biol Chem*. 2003;278(34):32037-32046. doi:10.1074/jbc.M303251200

38. Shibasaki K. TRPV4 activation by thermal and mechanical stimuli in disease progression. *Lab Investig*. 2020;100(2):218-223. doi:10.1038/s41374-019-0362-2

39. Suzuki M, Mizuno A, Kodaira K, Imai M. Impaired pressure sensation in mice lacking TRPV4. *J Biol Chem*. 2003;278(25):22664-22668. doi:10.1074/jbc.M302561200

40. Loukin S, Zhou X, Su Z, Saimi Y, Kung C. Wild-type and brachyolmia-causing mutant TRPV4 channels respond directly to stretch force. *J Biol Chem*. 2010;285(35):27176-27181. doi:10.1074/jbc.M110.143370

41. Liedtke W, Kim C. Functionality of the TRPV subfamily of TRP ion channels: Add mechano-TRP and osmo-TRP to the lexicon! *Cell Mol Life Sci*. 2005;62(24):2985-3001. doi:10.1007/s00018-005-5181-5

42. O'Conor CJ, Leddy HA, Benefield HC, Liedtke WB, Guilak F. TRPV4-mediated mechanotransduction regulates the metabolic response of chondrocytes to dynamic loading. *Proc Natl Acad Sci U S A*. 2014;111(4):1316-1321. doi:10.1073/pnas.1319569111

43. Suzuki T, Notomi T, Miyajima D, et al. Osteoblastic differentiation enhances expression of TRPV4 that is required for calcium oscillation induced by mechanical force. *Bone*. 2013;54(1):172-178. doi:10.1016/j.bone.2013.01.001

44. Muramatsu S, Wakabayashi M, Ohno T, et al. Functional gene screening system identified TRPV4 as a regulator of chondrogenic differentiation. *J Biol Chem*. 2007;282(44):32158-32167. doi:10.1074/jbc.M706158200

45. Masuyama R, Vriens J, Voets T, et al. TRPV4-Mediated Calcium Influx Regulates Terminal Differentiation of Osteoclasts. *Cell Metab*. 2008;8(3):257-265. doi:10.1016/j.cmet.2008.08.002

46. Hu F, Zhao Y, Hui Z, et al. Regulation of intracellular Ca2+/CaMKII signaling by TRPV4 membrane translocation during osteoblastic differentiation. *Biophys Reports*. 2019;5(5-6):254-263. doi:10.1007/s41048-019-00100-y

47. Walter BA, Purmessur D, Moon A, et al. Reduced tissue osmolarity increases trpv4 expression and pro-inflammatory cytokines in intervertebral disc cells. *Eur Cells Mater*. 2016;32:123-136. doi:10.22203/eCM.v032a08

48. Clark AL, Votta BJ, Kumar S, Liedtke W, Guilak F. Chondroprotective role of the osmotically sensitive ion channel transient receptor potential vanilloid 4: Age- and sex-dependent progression of osteoarthritis in Trpv4-deficient mice. *Arthritis Rheum*. 2010;62(10):2973-2983. doi:10.1002/art.27624

49. Masuyama R, Mizuno A, Komori H, et al. Calcium/calmodulin-signaling supports TRPV4 activation in osteoclasts and regulates bone mass. *J Bone Miner Res*. 2012;27(8):1708-1721. doi:10.1002/jbmr.1629

50. O'Conor CJ, Ramalingam S, Zelenski NA, et al. Cartilage-Specific Knockout of the Mechanosensory Ion Channel TRPV4 Decreases Age-Related Osteoarthritis. *Sci Rep*. 2016;6. doi:10.1038/srep29053

51. Terpstra L, Prud'Homme J, Arabian A, et al. Reduced chondrocyte proliferation and chondrodysplasia in mice lacking the integrin-linked kinase in chondrocytes. *J Cell Biol*. 2003;162(1):139-148. doi:10.1083/jcb.200302066

52. Wang G, Woods A, Agoston H, Ulici V, Glogauer M, Beier F. Genetic ablation of Rac1 in cartilage results in chondrodysplasia. *Dev Biol*. 2007;306(2):612-623. doi:10.1016/j.ydbio.2007.03.520

53. Solomon LA, Li JR, Bérubé NG, Beier F. Loss of ATRX in chondrocytes has minimal effects on skeletal development. *PLoS One*. 2009;4(9). doi:10.1371/journal.pone.0007106

54. Pest MA, Russell BA, Zhang YW, Jeong JW, Beier F. Disturbed cartilage and joint homeostasis resulting from a loss of mitogen-inducible gene 6 in a mouse model of joint dysfunction. *Arthritis Rheumatol*. 2014;66(10):2816-2827. doi:10.1002/art.38758

55. Muzumdar MD, Tasic B, Miyamichi K, Li N, Luo L. A global double-fluorescent cre reporter mouse. *Genesis*. 2007;45(9):593-605. doi:10.1002/dvg.20335

56. McCann MR, Tamplin OJ, Rossant J, Seǵuin CA. Tracing notochord-derived cells using a Noto-cre mouse: Implications for intervertebral disc development. *DMM Dis Model Mech*. 2012;5(1):73-82. doi:10.1242/dmm.008128

57. Bedore J, Sha W, McCann MR, Liu S, Leask A, Séguin CA. Impaired intervertebral disc development and premature disc degeneration in mice with notochord-specific deletion of CCN2. *Arthritis Rheum*. 2013;65(10):2634-2644. doi:10.1002/art.38075

58. Tam V, Chan WCW, Leung VYL, et al. Histological and reference system for the analysis of mouse intervertebral disc. *J Orthop Res*. 2017;36(1):233-243. doi:10.1002/jor.23637

59. Wei Y, Tower RJ, Tian Z, et al. Spatial distribution of type II collagen gene expression in the mouse intervertebral disc. *JOR SPINE*. 2019;2(4). doi:10.1002/jsp2.1070

60. Lee CR, Sakai D, Nakai T, et al. A phenotypic comparison of intervertebral disc and articular cartilage cells in the rat. *Eur Spine J*. 2007;16(12):2174-2185. doi:10.1007/s00586-007-0475-y

61. Minogue BM, Richardson SM, Zeef LAH, Freemont AJ, Hoyland JA. Transcriptional profiling of bovine intervertebral disc cells: Implications for identification of normal and degenerate human intervertebral disc cell phenotypes. *Arthritis Res Ther*. 2010;12(1):1-20. doi:10.1186/ar2929

62. Ovchinnikov DA, Deng JM, Ogunrinu G, Behringer RR. Col2a1-directed expression of Cre recombinase in differentiating chondrocytes in transgenic mice. *Genesis*. 2000;26(2):145-146. doi:10.1002/(SICI)1526-968X(200002)26:2<145::AID-GENE14>3.0.CO;2-C

63. Long F, Zhang XM, Karp S, Yang Y, McMahon AP. Genetic manipulation of hedgehog signaling in the endochondral skeleton reveals a direct role in the regulation of chondrocyte proliferation. *Development*. 2001;128(24):5099-5108.

64. Zheng Y, Fu X, Liu Q, et al. Characterization of Cre recombinase mouse lines enabling cell type-specific targeting of postnatal intervertebral discs. *J Cell Physiol*. 2019;234(9):14422-14431. doi:10.1002/jcp.28166

65. Serjeant, Meaghan; Moon, Paxton; Penuela, Silvia; Laird, Dale; Beier, Frank; Séguin C. The role of Pannexin 3 in age-associated and injury-induced intervertebral disc degeneration.

66. Harfe BD, Scherz PJ, Nissim S, Tian H, McMahon AP, Tabin CJ. Evidence for an expansion-based temporal Shh gradient in specifying vertebrate digit identities. *Cell*. 2004;118(4):517-528. doi:10.1016/j.cell.2004.07.024

67. Merceron C, Mangiavini L, Robling A, et al. Loss of HIF-1α in the notochord results in cell death and complete disappearance of the nucleus pulposus. *PLoS One*. 2014;9(10):110768. doi:10.1371/journal.pone.0110768

68. Mundy C, Yasuda T, Kinumatsu T, et al. Synovial joint formation requires local Ext1 expression and heparan sulfate production in developing mouse embryo limbs and spine. *Dev Biol*. 2011;351(1):70-81. doi:10.1016/j.ydbio.2010.12.022

69. Bedore J, Quesnel K, Quinonez D, Séguin CA, Leask A. Targeting the annulus fibrosus of the intervertebral disc: Col1a2-Cre(ER)T mice show specific activity of Cre recombinase in the outer annulus fibrosus. *J Cell Commun Signal*. 2016;10(2):137-142. doi:10.1007/s12079-016-0329-7

70. Behrens, A., Haigh, J., Mechta-Grigoriou, F., Nagy, A., Yaniv, M., & Wagner EF.

Impaired intervertebral disc formation in the absence of Jun. *Development*. 2003;130(1):103-109. doi:10.1242/dev.00186

71. Baffi MO, Slattery E, Sohn P, Moses HL, Chytil A, Serra R. Conditional deletion of the TGF-β type II receptor in Col2a expressing cells results in defects in the axial skeleton without alterations in chondrocyte differentiation or embryonic development of long bones. *Dev Biol*. 2004;276(1):124-142. doi:10.1016/j.ydbio.2004.08.027

72. Roughley PJ, Lamplugh L, Lee ER, Matsumoto K, Yamaguchi Y. The role of hyaluronan produced by Has2 gene expression in development of the spine. *Spine (Phila Pa 1976)*. 2011;36(14). doi:10.1097/BRS.0b013e3181f1e84f

73. Wang M, Tang D, Shu B, et al. Conditional activation of β-catenin signaling in mice leads to severe defects in intervertebral disc tissue. *Arthritis Rheum*. 2012;64(8):2611-2623. doi:10.1002/art.34469

74. Corrigan MA, Johnson GP, Stavenschi E, Riffault M, Labour MN, Hoey DA. TRPV4-mediates oscillatory fluid shear mechanotransduction in mesenchymal stem cells in part via the primary cilium. *Sci Rep*. 2018;8(1):1-13. doi:10.1038/s41598-018-22174-3

75. Itoh Y, Hatano N, Hayashi H, Onozaki K, Miyazawa K, Muraki K. An environmental sensor, TRPV4 is a novel regulator of intracellular Ca^{2+} in human synoviocytes. *Am J Physiol Physiol*. 2009;297(5):C1082-C1090. doi:10.1152/ajpcell.00204.2009

76. Kusudo T, Wang Z, Mizuno A, Suzuki M, Yamashita H. TRPV4 deficiency increases skeletal muscle metabolic capacity and resistance against diet-induced obesity. *J Appl Physiol*. 2012;112(7):1223-1232. doi:10.1152/japplphysiol.01070.2011

77. Shinohara H. *The Mouse Vertebrae: Changes in the Morphology of Mouse Vertebrae Exhibit Specific Patterns Over Limited Numbers of Vertebral Levels*. Vol 76.; 1999.

78. Han X, Kato H, Sato H, Hirofuji Y, Fukumoto S, Masuda K. Accelerated osteoblastic differentiation in patient-derived dental pulp stem cells carrying a gain-of-function mutation of TRPV4 associated with metatropic dysplasia. *Biochem Biophys Res Commun*. 2020;523(4):841-846. doi:10.1016/j.bbrc.2019.12.123

79. Rock MJ, Prenen J, Funari VA, et al. Gain-of-function mutations in TRPV4 cause autosomal dominant brachyolmia. *Nat Genet*. 2008;40(8):999-1003. doi:10.1038/ng.166

80. Saavedra-Pozo FM, Deusdara RAM, Benzel EC. Adjacent segment disease perspective and review of the literature. *Ochsner J*. 2014;14(1):78-83. /pmc/articles/PMC3963057/?report=abstract. Accessed July 3, 2020.

81. Dmitriev AE, Cunningham BW, Hu N, Sell G, Vigna F, McAfee PC. Adjacent Level Intradiscal Pressure and Segmental Kinematics Following A Cervical Total Disc Arthroplasty. *Spine (Phila Pa 1976)*. 2005;30(10):1165-1172. doi:10.1097/01.brs.0000162441.23824.95

82. Du G, Li L, Zhang X, et al. Roles of TRPV4 and piezo channels in stretch-evoked Ca2+ response in chondrocytes. *Exp Biol Med*. 2020;245(3):180-189. doi:10.1177/1535370219892601

83. Olivan-Viguera A, Garcia-Otin AL, Lozano-Gerona J, et al. Pharmacological activation of TRPV4 produces immediate cell damage and induction of apoptosis in human melanoma cells and HaCaT keratinocytes. Slominski AT, ed. *PLoS One*. 2018;13(1):e0190307. doi:10.1371/journal.pone.0190307

84. Alenmyr L, Uller L, Greiff L, Högestätt ED, Zygmunt PM. TRPV4-Mediated Calcium Influx and Ciliary Activity in Human Native Airway Epithelial Cells. *Basic Clin Pharmacol Toxicol*. 2014;114(2):210-216. doi:10.1111/bcpt.12135

85. Amin AK, Huntley JS, Bush PG, Simpson AHRW, Hall AC. Chondrocyte death in mechanically injured articular cartilage-the influence of extracellular calcium. *J Orthop Res*. 2009;27(6):778-784. doi:10.1002/jor.20809

86. Landouré G, Zdebik AA, Martinez TL, et al. Mutations in TRPV4 cause Charcot-Marie-Tooth disease type 2C. *Nat Genet*. 2010;42(2):170-174. doi:10.1038/ng.512

87. Alini M, Eisenstein SM, Ito K, et al. Are animal models useful for studying human disc disorders/degeneration? *Eur Spine J*. 2008;17(1):2-19. doi:10.1007/s00586-007-0414-y

88. Sarver JJ, Elliott DM. Mechanical differences between lumbar and tail discs in the mouse. *J Orthop Res*. 2005;23(1):150-155. doi:10.1016/j.orthres.2004.04.010

89. Daly C, Ghosh P, Jenkin G, Oehme D, Goldschlager T. A Review of Animal Models of Intervertebral Disc Degeneration: Pathophysiology, Regeneration, and Translation to the Clinic. *Biomed Res Int*. 2016;2016. doi:10.1155/2016/5952165

90. Ohnishi T, Sudo H, Iwasaki K, Tsujimoto T, Ito YM, Iwasaki N. In Vivo mouse intervertebral disc degeneration model based on a new histological classification. *PLoS One*. 2016;11(8). doi:10.1371/journal.pone.0160486

91. Yang F, Leung VY, Luk KD, Chan D, Cheung KM. Injury-induced sequential transformation of notochordal nucleus pulposus to chondrogenic and fibrocartilaginous phenotype in the mouse. *J Pathol*. 2009;218(1):113-121. doi:10.1002/path.2519

Chapter 5

5 Conclusions and General Discussion

5.1 Thesis Summary

"How do annulus fibrosus cells respond/adapt to mechanical load?"

The research presented in this thesis was designed to address this question and aimed to characterize the mechanotransduction pathways mediating the response of annulus fibrosus (AF) cells. Specifically, these studies investigated the effects of cyclic tensile strain (CTS) on AF cells (**Chapter 2**), the spatiotemporal expression pattern of the candidate mechanoreceptor, transient receptor potential vanilloid 4 (TRPV4) in spine development and aging (**Chapter 3**), the function of TRPV4 in AF cell mechanotransduction (**Chapter 3**), and the role of TRPV4 in regulating intervertebral disc (IVD) health and injury-induced degeneration (**Chapter 4**). Using a mechanically dynamic bioreactor system, we demonstrated that *in vitro* exposure of CTS to AF cells led to cytoskeletal remodelling, MAPK pathway activation, and gene expression changes in a frequency-dependent manner. Among the panels of genes assessed, we showed that expression of mechanoreceptors, including *Trpv4*, was mechanically regulated, suggesting a potential role of TRPV4 in IVD mechanobiology. Next, using the novel *Trpv4*-reporter mouse ($Trpv4^{LacZ/WT}$), we showed that *Trpv4* is expressed during early stages of spine development and its expression is maintained in mature IVD tissues. Using pharmacological modulation of TRPV4, we then demonstrated that TRPV4 signalling mediates cytoskeletal remodelling and CTS- induced changes in extracellular matrix (ECM) genes. Lastly, using *Col2-Cre;*$Trpv4^{fl/fl}$ conditional knock-out mouse we investigated the role of TRPV4 in regulating IVD health and degeneration. These studies demonstrated that TRPV4 regulates matrix

homeostasis and tissue response to aberrant load. The specific objectives and findings of each data chapter are summarized below.

5.1.1 Chapter 2: Quantify the Effects of Mechanical Loading on Annulus Fibrosus Cells

Objective 1: Validate mechanically-dynamic culture using the *MechanoCulture B1* bioreactor

Objective 2: Quantify the effects of acute exposure to CTS on AF cells

Objective 3: Identify mechanosensitive pathway(s) in AF cells following acute exposure to CTS

Summary of Findings

1. Validation of our culture system involved two steps. First, motion tracking analysis was used to ensure that strain profiles on the silicone membrane were uniform during mechanical stretch. Second, genetic labeling using the $Noto^{Cre};ROSA^{mTmG/mTmG}$ conditional reporter mouse and gene expression analysis demonstrated that primary murine AF cells maintained an AF-like phenotype in culture on the bioreactor.
2. AF cells exposed to CTS showed increased stress fibre formation with increasing loading frequency.
3. Exposure of AF cells to CTS at 2.0 Hz induced a transient phosphorylation of extracellular signal-regulated kinase1/2 (ERK1/2), but not p38.
4. Acute exposure of AF cells to CTS induced frequency-dependent changes in gene expression (**Table 5.1**).

Table 5.1. Synopsis of gene expression changes induced by CTS protocols in AF cells.

Acan: aggrecan; *Col1a1*: type I collagen; *Cox2*: cytochrome c oxidase subunit 2; *Fos*: FOS proto-oncogene AP-1 transcription factor subunit; *Mmp3*: matrix metallopeptidase 3; *Myc*: MYC proto-oncogene; *P2rx7*: purinoreceptor x subtype 7; *Prg4*: lubricin; *Itga5*: integrin subunit alpha 5; *Itgb1*: integrin subunit beta 1; *Tnfα*: tumor necrosis factor alpha; *Trpv4*: transient receptor protein vanilloid 4. N.S. = No significant differences detected.

CTS Protocol **Gene Group**	6% Strain **0.1 Hz** 30 min	6% Strain **1.0 Hz** 30 min	6% Strain **2.0 Hz** 30 min
Extracellular Matrix Genes	*Col1a1* *Acan* *Prg4*	*Acan*	*Acan* *Prg4*
Matrix Remodelling Genes	*Mmp3*	*N.S.*	*N.S.*
Inflammatory Cytokine Genes	*N.S.*	*Tnfα*	*Tnfα*
Candidate Mechano-sensitive Genes	*N.S.*	*Myc*	*Cox2* *Myc* *Fos*
Cell Surface Receptor Genes	*Not quantified*	*Not quantified*	*Itga5* *Itgb1* *Trpv4* *P2rx7*

5.1.2 Chapter 3: Characterize the Expression Pattern and Function of Transient Receptor Potential Vanilloid 4 in the Murine Intervertebral Disc

Objective1: Determine the spatiotemporal expression profile of *Trpv4* in the murine spine

Objective 2: Determine the function of TRPV in AF cell mechano-response

Summary of Findings

1. *Trpv4* expression was detected in the elongated notochord and condensed regions of mesenchyme at embryonic day (E)12.5, and subsequently in the NP, AF, and prevertebral structure at E 17.5 and postnatal day 1.
2. At 2.5 months-of-age, *Trpv4* expression was detected in the NP and inner AF. Expression varied between anatomical regions (thoracic, lumbar, caudal IVDs) and decreased with age.
3. Pharmacological agonism confirmed the functional activity of TRPV4, and demonstrated heterogeneous calcium responses in primary AF cells.
4. Activation of TRPV4 in AF cells promoted cytoskeletal remodelling and increased stress fibre formation, inhibited by Rho-associated protein kinase (ROCK) inhibition.
5. Pharmacological inhibition of TRPV4 in AF cells prevented CTS-induced increases in ECM gene expression (*Col1a1*, *Acan*, *Prg4*).
6. In static culture, pharmacological activation of TRPV4 in AF cells induced *Acan* and *Prg4* gene expression.

5.1.3 Chapter 4: Determine the Role of Transient Receptor Potential Vanilloid 4 in Intervertebral Disc Health and Injury

Objective 1: Determine the effects of *Trpv4* deletion on lumbar IVD health and vertebral bone growth

Objective 2: Determine the role of *Trpv4* in an injury-induced model of IVD degeneration

Summary of Findings

1. Using a transgenic reporter mouse, *Col2-Cre* activity was localized to the NP and most of the AF, identifying the cells targeted in *Col2-Cre;Trpv4*$^{fl/fl}$ (*Trpv4* KO) mice.
2. *Trpv4* KO mice did not show alterations in vertebral bone length or histopathological signs of lumbar IVD degeneration compared to age-matched wild-type mice at 4 or 8 months-of-age; however, *Trpv4* KO mice showed decreased proteoglycan staining in the inner AF compared to IVDs of age-matched WT mice.
3. In the AF puncture model, loss of *Trpv4* did not alter degenerative changes at the site of injury but prevented mechanically-induced degeneration in IVDs adjacent to sites of injury.

5.2 Relevance and Contributions to the Field

Mechanotransduction is the cellular mechanism by which physical forces are translated into biochemical impulses and signals[1,2]. These biochemical signals include changes to intracellular concentrations of molecules and elements (i.e. intracellular calcium transient) as well as the activation of intracellular signalling pathways, each of which may regulate

changes to cellular and extracellular structures. The idea of applying mechanics to biology was first postulated by Wilhelm Roux, who proposed that proper embryogenesis occurs as a result of "formative forces[3]." Roux's contribution to the mechanobiology field was the concept of "form follows function[3,4]." This concept is relevant in IVD mechanobiology, as the tissue architecture of the NP, AF, and cartilage endplate (CEP) tissues that form the IVD enable them to work interdependently to function as a load bearing joint. Although mechanical loading has been established as a key regulators of tissue homeostasis, it is paradoxically also established as an initiator of IVD degeneration. As such, studies investigating the effects of both physiological and pathological parameters of mechanical loading on IVD cells report mechano-regulation of ECM synthesis and/or degradation[5–12]. Nevertheless, information on the cell type-specific response to mechanical loading and mechanisms mediating this response in the IVD is limited. The contributions and interpretations of the findings presented in this thesis are discussed below in the context to three general principles of mechanotransduction.

5.2.1 Mechanoreception

Recent studies have reported the expression of different mechanoreceptors, including integrins[13], toll-like receptors[5,14], purinoreceptors[15], proteinase activated receptors[16], and transient receptor potential ion channels[17,18] in the IVDs of different species including human, porcine, and rat. Among these, previous studies investigating mechano-sensitive pathway activation in the IVD have been limited to characterization of the α5β1 integrin receptor[6]. This knowledge gap highlights the need for in-depth characterization of the expression pattern and function of the mechanically sensitive "receptorome" of the IVD.

The data presented in **Chapter 3** demonstrate that *Trpv4* is expressed during spine development, detected as early as E12.5 in the notochord and condensed regions of mesenchymal cells, and maintained in the NP and inner AF of skeletally mature mice. Given that both embryonic development and homeostasis of the IVD are regulated by dynamic mechanical cues, it is tempting to speculate that TRPV4 may act as a mediator of physiologic mechanical signals in both contexts (**Figure 5.1**). Moreover, *Trpv4* expression in the IVD differed based on anatomical region in the spine and age. The differences in *Trpv4* expression based on anatomical region may be related to differences in mechanical load experienced in each spinal region. Consistent with this notion, in **Chapter 2** we demonstrate that *Trpv4* expression is mechanically regulated. Previous studies comparing IVD mechanical properties in mice reported that lumbar IVDs were more stiff than caudal IVDs by nearly two fold; lumbar IVDs compressed by 64% of their original height compared to tail IVDs which compressed by 98% after static creep compression[19]. The authors of this study proposed that these differences were due to the increased motion experienced by the tail compared to the lumbar spine. Furthermore, we found that *Trpv4* expression in both lumbar and caudal IVDs decreased with age. The age-associated decrease in *Trpv4* gene expression may be part of normal IVD aging, potentially contributing to age-induced changes in biochemical and biomechanical properties of IVD. Our studies characterizing the spatiotemporal expression of *Trpv4* in the IVD suggest that TRPV4 may play a role in IVD development, homeostasis, and aging.

5.2.2 Mechano-transmission

Mechano-transmitters are molecules that mediate specific intracellular biochemical signalling cascade upon receptor activation. In **Chapters 2 & 3**, we showed activation and

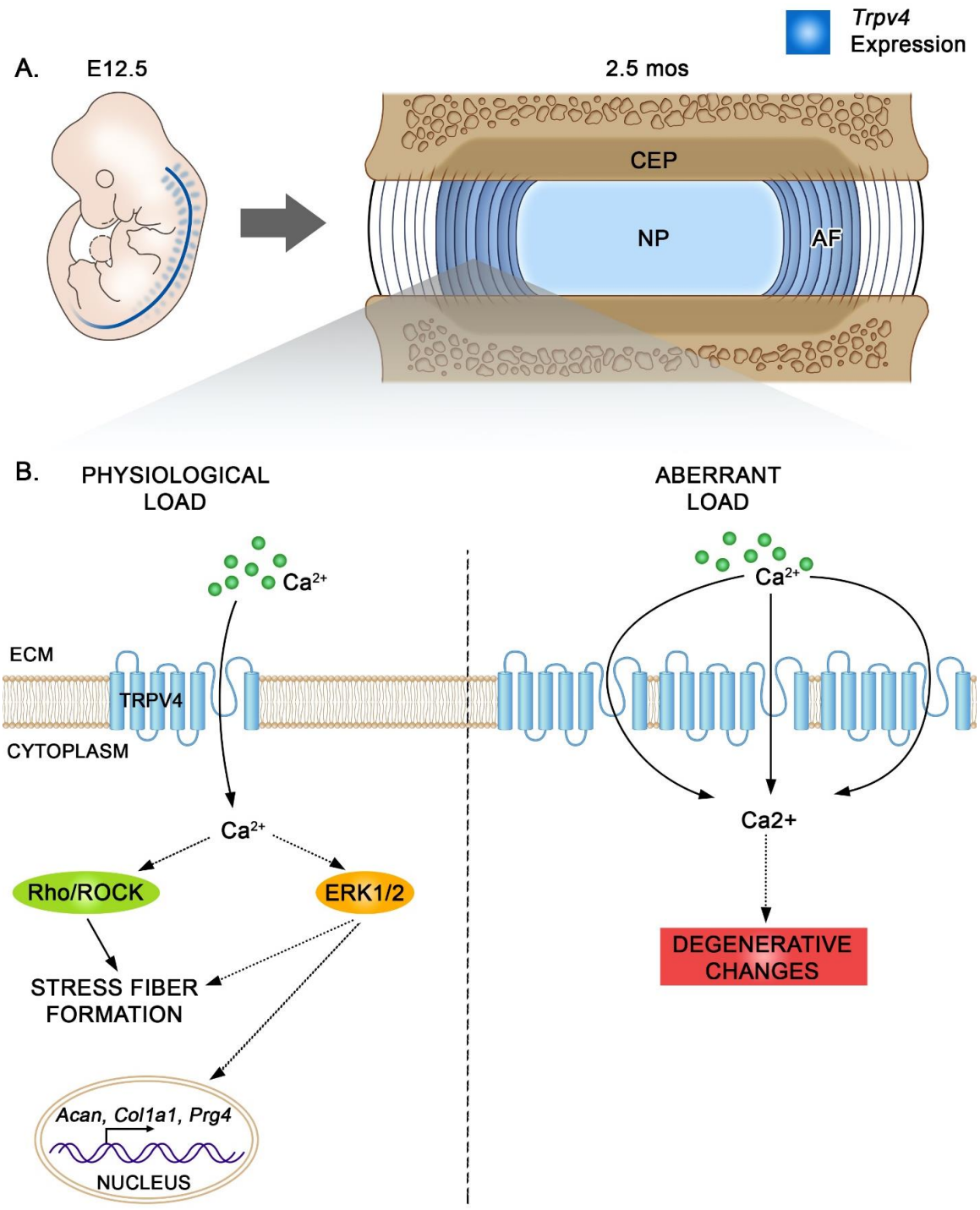
Trpv4
Expression
A.
E12.5
2.5 mos
CEP
NP
AF
B.
PHYSIOLOGICAL
LOAD
ABERRANT
LOAD
Ca2+
ECM
TRPV4
CYTOPLASM
Ca2+
Rho/ROCK
ERK1/2
STRESS FIBER
FORMATION
Acan, Col1a1, Prg4
NUCLEUS
Ca2+
Ca2+
DEGENERATIVE
CHANGES

Figure 5.1. Proposed model of TRPV4 signalling in AF cells.

A) *Trpv4* expression is detected as early as embryonic day (E) 12.5 and is maintained in the NP and inner AF of mature IVDs (blue gradient = *Trpv4* expression). B) Proposed mechanism of TRPV4 function in AF cell mechantransduction. In normal loading, TRPV4 and Rho/ROCK signalling are involved in stress fibre formation and regulation of extracellular matrix (ECM) gene expression. Mechanical load also activates the ERK1/2 pathway. In response to aberrant loading, increased TRPV4 receptor expression leads to increased TRPV4 function, facilitating degenerative changes and inducing IVD degeneration. Solid arrows = observed; Dotted arrows = proposed. NP = nucleus pulposus. AF = annulus fibrosus. CEP = cartilage endplate.

involvement of different signalling pathways downstream of mechanical load or TRPV4 activation. Specifically, we showed that exposure of AF cells to CTS at 2.0 Hz to AF cells produced a transient increase in ERK1/2 phosphorylation. One of the upstream signalling events that can influence ERK activation is a rise in free intracellular calcium concentrations. Calcium is a versatile second messenger that affects signalling processes, thereby regulating numerous cellular processes. In **Chapter 3**, pharmacological activation of TRPV4 induced both sustained and oscillating calcium signalling in AF cells. Interestingly, in rat fibroblasts, elevated calcium concentrations activate ERK signalling cascade by altering ERK2 binding affinity. In cells treated with high concentration of calcium (1 mM), more proteins were bound to ERK2 compared to untreated cells[20]. Moreover, ERK2 nuclear translocation was delayed with increased calcium, suggesting that intracellular calcium regulates signalling specificity and spatiotemporal regulation of ERK2 localization[20,21]. Although speculative, we postulate that the increase in ERK1/2 phosphorylation induced by tensile stretch is regulated by TRPV4-mediated calcium transients, similar to those we characterized using pharmacological receptor agonists (**Figure 5.1**).

Another mechano-transmitter we identified was Rho/ROCK and its role in regulating load-induced stress fibre formation in AF cells. In many cell types, one of the earliest adaptations to mechanical stimulation is stress fibre formation[20,21]. In chondrocytes, TRPV4-mediated calcium signalling has been shown to regulate cytoskeletal rearrangement[22]. Our data in **Chapter 3** demonstrates that pharmacological activation of TRPV4 in AF cells led to increased stress fibre formation, which was inhibited when cells were pre-treated with the ROCK inhibitor. Although not studied in musculoskeletal cell types, the cross-talk between

TRPV4 and Rho/ROCK signalling has been demonstrated in endothelial cells[23–25]. In healthy endothelial cells, mechanically-induced TRPV4 activates Rho/ROCK signalling to regulate cell migration, stress fibre formation, and contraction[26]. However, in pathological state, Rho/ROCK-mediated cell stiffening caused a decrease in TRPV4 expression, and pharmacological activation of TRPV4 suppressed Rho/ROCK signalling[27]. These studies suggest that Rho/ROCK signalling can act as both an effector and target of TRPV4. In keeping with these findings, our data suggests that both TRPV4-mediated and Rho/ROCK signalling pathways are involved in stress fibre formation in AF cells in response to mechanical load (**Figure 5.1**).

5.2.3 Mechano-response

The current thesis used both *in vitro* and *in vivo* models to study the IVD mechano-response under physiological and pathological conditions. In **Chapter 2**, we showed that the cellular response of AF cells to CTS is frequency-dependent. It is important to note that all CTS loading protocols used in this study had constant tensile strain (6%) and duration (30 min) with frequencies falling within the range that was considered physiologically relevant (0.1 Hz, 1.0 Hz, 2.0 Hz). Interestingly, even within the physiological range, changes in cytoskeleton remodelling, pathway activation, and gene expression were different for each of the loading protocols. In keeping with previous studies[6,28,29], mechanical loading increased ECM gene expression, which we subsequently showed to be mediated by TRPV4 signalling (**Chapter 3**). This was further supported by data presented in **Chapter 4** where conditional deletion of *Trpv4* was associated with decreased proteoglycan staining in AF (compared to WT controls). These data suggest that mechanically-induced TRPV4 signalling is involved in proteoglycan synthesis in AF cells.

Interestingly, among the ECM genes assessed, lubricin (*Prg4*), which was recently identified as an AF-enriched gene by our group[30], showed frequency-dependent changes in gene expression, significantly upregulated in AF cells exposed to CTS at 0.1 Hz and 2.0 Hz. Lubricin is a surface-active mucinous glycoprotein found in the synovial joint that functions to lubricate the cartilage surface and reduce joint friction[31,32]. A recent study examining the distribution of lubricin in the IVD showed that in AF, lubricin is present in the interlamellar space of the annular lamellae[33]. In the IVD, the lamellar structure of the AF lengthens and shortens upon loading and unloading, respectively. Accordingly, there is a relative motion between the lamellae during dynamic load, and lubricin may be one of the mechanically regulated proteins that contribute to this internal tissue tribology. Nevertheless, the precise function of lubricin within the IVD and its role in AF mechanotransduction are unknown.

Notably, other than *Trpv4*, AF cells exposed to CTS at 2.0 Hz showed increased expression of *Itga5* and *Itgb1*, suggesting that mechanically stimulated AF cells increase mechanoreceptor gene expression, thereby potentially perpetuating the activation of mechanotransduction signalling pathways.

Next, we investigated the role of TRPV4 in regulating the tissue response to IVD injury (**Chapter 4**). Using a percutaneous AF puncture model, we demonstrated that deletion of *Trpv4* did not protect from degeneration induced at the site of IVD injury. However, loss of *Trpv4* prevented degeneration due to aberrant load in IVDs adjacent to sites of injury. These data suggest that although modulation of TRPV4 function does not alter degeneration following severe acute IVD injury (resulting in complete NP depressurization), TRPV4-mediated signalling is upstream of the degenerative changes

induced by aberrant mechanical load in the IVD (**Figure 5.**1). One possible mechanism for this may be increased mechanical loading upregulating *Trpv4* expression, leading to increased TRPV4 activity within the IVD cells, contributing to degenerative changes.

In summary, our findings demonstrate that TRPV4 is a mechanoreceptor in AF cells and regulates ECM synthesis during physiological loading as well as the tissue response to aberrant mechanical load (**Figure 5.1**). The current work reinforces the theory suggesting the existence of a "window" of loading parameters that promote IVD health.

5.3 Limitations and Future Directions

Although specific limitations are addressed within each chapter, it is important to address important limitations that apply to our overall study design. First, while *in vitro* bioreactor systems enable the design of controlled experiments, they do not recapitulate the innate mechanical loading environment experienced by AF cells *in vivo*. The IVD represents a complex loading environment diverse in the type, direction, magnitude, and frequency of mechanical load experienced. To model the radial strain that is predominantly experienced by cells of the AF, we chose a bioreactor system that delivered bi-axial multi-directional CTS. In addition, given the limited number of cells that can be isolated from each of the murine IVD, primary AF cell cultures were established by pooling AF tissues from all spinal levels. As such, we acknowledge that our reported findings correspond to a mixed AF cell population, with variability in cell phenotype introduced by the presence of both inner and outer AF cells with additional differences related to the anatomical region of the spine from which the tissue was isolated.

To address these limitations, future studies could capitalize on the validated bioreactor system to further characterize the effects of varying tensile strain and loading duration of CTS on cellular mechano-response to better understand AF mechanobiology. Mechanistically, CTS experiments could be conducted with pharmacological modulators of TRPV4 to investigate if TRPV4 mediates mechanical-induction of genes associated with matrix remodelling, mechano-sensitive genes, or inflammatory cytokine genes. Furthermore, *ex vivo* organ culture models allow for reproducible cost-effective studies to investigate IVD mechanobiology and degeneration in an innate tissue structure. IVD organ culture systems can help develop treatment strategies, as they have the potential to bridge the gap between *in vitro* and *in vivo* systems.

Recent studies have used *ex vivo* organ culture bioreactors to deliver diurnal loading cycle to more accurately model daily activity[34–37]. Adopting such protocols coupled with cyclic strain may help recapitulate mechanical environment *in vivo.* Building upon our findings, future studies using these model systems should investigate the mechano-response of IVD tissues under physiological and pathological loading conditions. Given the established discrepancy between gene expression and protein expression[38,39], changes in both gene and protein expression should be quantified in tissue as well as assessing levels of secreted proteins in conditioned media. For assessment of changes in IVD tissues, omics technologies can be used to gain a global understanding of the tissue response to normal and aberrant load. Notably, using IVDs from large animals (i.e. bovine, porcine) in these studies may be useful in characterizing the mechano-response of AF cells residing in the inner and outer regions of AF tissue. Although not yet fully characterized, the two regions of AF differ in cell morphology and matrix composition. Determining the differential

responses of inner and outer AF cells to mechanical load may contribute to understanding IVD tissue anatomy, function, and degeneration.

A second limitation is the use of mouse models. Although mouse models are invaluable to study genes of interest within the native environment through genetic manipulation, there are certain differences between mouse and human IVDs that must be acknowledged. One of the main differences is the cellular composition in the central NP tissue. In mice, notochordal cells persist in the NP throughout life, while in humans, notochordal cells are present at birth, but typically disappear by 10 years-of-age[40]. Notochordal cells are large vacuolated cells that persists from the notochord structure during development, responsible for sulphated glycosaminoglycan production in the NP[41], and their disappearance is thought to precede IVD degeneration in humans[42]. In addition, given the differences in musculature and increased degree of motion of tails, mouse caudal IVDs have different mechanical properties compared to both murine and human lumbar IVDs[19,43,44]. Despite such differences, both humans and mice have similar lumbar IVD geometry, tissue architecture, matrix compositions, and biomechanical properties[43–45].

An important limitation specific to the mouse models reported in this thesis is the Cre-driver used to target *Trpv4*. Using *Col2a1Cre;ROSA*$^{mTmG/mTmG}$ reporter mice, we showed that *Col2-Cre* targets the whole NP and most of the AF (inner 2/3). However, it is important to note that *Col2-Cre* is not specific for the IVD, but also targets other tissues, including chondrocytes, osteoblasts, synovial fibroblasts, and suture mesenchymal cells in the calvaria[46]. The loss of TRPV4 in these numerous musculoskeletal cell types could contribute to alterations in joint function that may impact the phenotype of the knockout mouse generated. Alterations in other joints tissues in the *Trpv4* KO mouse may influence

the mechanical behaviours of mice (i.e. sedentary or altered gait), thereby impairing our ability draw conclusions about the precise role of TRPV4 in IVD mechanobiology. Accordingly, future studies should utilize additional complementary Cre strains to target *Trpv4* deletion in specific tissues of the IVD. For example, previous studies reported that tamoxifen induction of *Col2CreERT* (at PN7) and *Col1a2-Cre(ER)T* (at 3 weeks-of-age) showed Cre activity in the inner AF and outer AF, respectively. Furthermore, *Noto*-Cre mice can be used to target cells of notochordal origin (i.e. NP).

In addition, to further investigate the expression and function of TRPV4 in murine IVD, mice at advanced ages should be included in future studies. Previous studies reported that in C57BL/6 mice, both histomorphological and radiological signs of age-induced IVD degeneration were detected starting at 14 months-of-age, progressing to a moderate to severe degeneration by 22 months-of-age[47]. Accordingly, both the *Trpv4*-reporter (*Trpv4*$^{LacZ/WT}$) and *Trpv4* KO mice should be examined at later time points up to 2 years of age to characterize expression profile and function of *Trpv4* during age-associated IVD degeneration.

Lastly, another limitation to the work presented in **Chapter 4** is the use of tail injury model. Although the percutaneous AF needle puncture model used is less invasive and highly reproducible compared to surgical AF puncture, the loading environment of caudal IVDs, and perhaps the phenotype of cells within the IVD are different from those of lumbar IVDs. The caudal spine generally has little musculature, and has a greater range of motion compared to the lumbar spine due to the absence of dorsal bony structures and facet joints[43–45]. Furthermore, caudal IVDs have different geometry than lumbar IVDs, which may influence the loading environment and biomechanical properties[19,43,44]. As such, the

tail injury model does not accurately model NP herniation in the clinical context in humans. Future studies could carry out a detailed investigation of the role of *Trpv4* using an IVD injury model as reported by recent studies, which involves needle AF puncture to lumbar IVDs in mice[48,49].

5.4 References

1. Pruitt BL, Dunn AR, Weis WI, Nelson WJ. Mechano-Transduction: From Molecules to Tissues. doi:10.1371/journal.pbio.1001996

2. Ingber DE. Cellular mechanotransduction: putting all the pieces together again. *FASEB J*. 2006;20(7):811-827. doi:10.1096/fj.05-5424rev

3. Hamburger V. Wilhelm Roux: visionary with a blind spot. *J Hist Biol*. 1997;30(2):229-238. doi:10.1023/a:1004231618837

4. Wall M, Butler D, Haj A El, Bodle JC, Loboa EG, Banes AJ. Key developments that impacted the field of mechanobiology and mechanotransduction. *J Orthop Res*. 2017;36(2):605-619. doi:10.1002/jor.23707

5. Gawri R, Rosenzweig DH, Krock E, et al. High mechanical strain of primary intervertebral disc cells promotes secretion of inflammatory factors associated with disc degeneration and pain. *Arthritis Res Ther*. 2014;16(1):R21. doi:10.1186/ar4449

6. Gilbert HTJ, Nagra NS, Freemont AJ, Millward-Sadler SJ, Hoyland JA. Integrin – Dependent Mechanotransduction in Mechanically Stimulated Human Annulus Fibrosus Cells: Evidence for an Alternative Mechanotransduction Pathway Operating with Degeneration. Tsilibary EC, ed. *PLoS One*. 2013;8(9):e72994. doi:10.1371/journal.pone.0072994

7. Gilbert HTJ, Hoyland JA, Freemont AJ, Millward-Sadler SJ. The involvement of interleukin-1 and interleukin-4 in the response of human annulus fibrosus cells to cyclic tensile strain: An altered mechanotransduction pathway with degeneration. *Arthritis Res Ther*. 2011;13(1):R8. doi:10.1186/ar3229

8. Le Maitre CL, Frain J, Millward-Sadler J, Fotheringham AP, Freemont AJ, Hoyland JA. Altered integrin mechanotransduction in human nucleus pulposus cells derived from degenerated discs. *Arthritis Rheum*. 2009;60(2):460-469. doi:10.1002/art.24248

9. Li P, Gan Y, Wang H, et al. Dynamic compression effects on immature nucleus pulposus: A study using a novel intelligent and mechanically active bioreactor. *Int J Med Sci*. 2016;13(3):225-234. doi:10.7150/ijms.13747

10. Neidlinger-Wilke C, Würtz K, Liedert A, et al. A three-dimensional collagen matrix as a suitable culture system for the comparison of cyclic strain and hydrostatic pressure effects on intervertebral disc cells. *J Neurosurg Spine*. 2005;2(4):457-465. doi:10.3171/spi.2005.2.4.0457

11. Neidlinger-Wilke C, Galbusera F, Pratsinis H, et al. Mechanical loading of the intervertebral disc: From the macroscopic to the cellular level. *Eur Spine J*. 2014;23(SUPPL. 3). doi:10.1007/s00586-013-2855-9

12. Rannou F, Richette P, Benallaoua M, et al. Cyclic tensile stretch modulates proteoglycan production by intervertebral disc annulus fibrosus cells through production of nitrite oxide. *J Cell Biochem*. 2003;90(1):148-157. doi:10.1002/jcb.10608

13. Nettles DL, Richardson WJ, Setton LA. Integrin expression in cells of the intervertebral disc. *J Anat*. 2004;204(6):515-520. doi:10.1111/j.0021-8782.2004.00306.x

14. Klawitter M, Hakozaki M, Kobayashi H, et al. Expression and regulation of toll-like receptors (TLRs) in human intervertebral disc cells. *Eur Spine J*. 2014;23(9):1878-1891. doi:10.1007/s00586-014-3442-4

15. Gonzales S, Rodriguez B, Barrera C, Huang CYC. Measurement of ATP-Induced Membrane Potential Changes in IVD Cells. *Cell Mol Bioeng*. 2014;7(4):598-606. doi:10.1007/s12195-014-0355-6

16. Richards J, Tang S, Gunsch G, et al. Mast cell/proteinase activated receptor 2 (PAR2) mediated interactions in the pathogenesis of discogenic back pain. *Front Cell Neurosci*. 2019;13. doi:10.3389/fncel.2019.00294

17. Sadowska A, Touli E, Hitzl W, et al. Inflammaging in cervical and lumbar degenerated intervertebral discs: analysis of proinflammatory cytokine and TRP channel expression. *Eur Spine J*. 2018;27(3):564-577. doi:10.1007/s00586-017-5360-8

18. Sadowska A, Hitzl W, Karol A, et al. Differential regulation of TRP channel gene and protein expression by intervertebral disc degeneration and back pain. *Sci Rep*. 2019;9(1):1-16. doi:10.1038/s41598-019-55212-9

19. Sarver JJ, Elliott DM. Mechanical differences between lumbar and tail discs in the mouse. *J Orthop Res*. 2005;23(1):150-155. doi:10.1016/j.orthres.2004.04.010

20. Chuderland D, Marmor G, Shainskaya A, Seger R. Calcium-mediated interactions regulate the subcellular localization of extracellular signal-regulated kinases. *J Biol Chem*. 2008;283(17):11176-11188. doi:10.1074/jbc.M709030200

21. Rubinfeld H, Hanoch T, Seger R. Identification of a cytoplasmic-retention sequence in ERK2. *J Biol Chem*. 1999;274(43):30349-30352. doi:10.1074/jbc.274.43.30349

22. Trompeter N, Gardinier JD, Debarros ; Victor, et al. Insulin-like Growth Factor-1 Regulates the Mechanosensitivity of Chondrocytes by Modulating TRPV4. doi:10.1101/2020.03.10.985713

23. Woods A, Wang G, Beier F. Regulation of chondrocyte differentiation by the actin cytoskeleton and adhesive interactions. *J Cell Physiol*. 2007;213(1):1-8. doi:10.1002/jcp.21110

24. Bhadriraju K, Yang M, Ruiz SA, Pirone D, Tan J, Chen CS. *ACTIVATION OF ROCK BY RHOA IS REGULATED BY CELL ADHESION, SHAPE, AND CYTOSKELETAL TENSION*.

25. Amano M, Nakayama M, Kaibuchi K. Rho-Kinase/ROCK: A Key Regulator of the Cytoskeleton and Cell Polarity. doi:10.1002/cm.20472

26. Liu J, Wada Y, Katsura M, et al. Rho-associated coiled-coil kinase (ROCK) in molecular regulation of angiogenesis. *Theranostics*. 2018;8(21):6053-6069. doi:10.7150/thno.30305

27. Yang, Xiao, Arun Bhaskaran, Harry Scott, Soroush Ardekani, Jun Xu, Umar Mohideen, Timothy S. Kern and KG. Rho/ROCK-mediated Retinal Endothelial Stiffening Impairs TRPV4 Signaling and Promotes Diabetic Retinal Inflammation. *Invest Ophthalmol Vis Sci*. 2016;57(12):3220-3220.

28. Sowa G, Coelho P, Vo N, et al. Determination of annulus fibrosus cell response to tensile strain as a function of duration, magnitude, and frequency. *J Orthop Res*. 2011;29(8):1275-1283. doi:10.1002/jor.21388

29. Molladavoodi S, McMorran J, Gregory D. Mechanobiology of annulus fibrosus and nucleus pulposus cells in intervertebral discs. *Cell Tissue Res*. 2020;379(3):429-444. doi:10.1007/s00441-019-03136-1

30. Veras MA, McCann MR, Tenn NA, Séguin CA. Transcriptional profiling of the murine intervertebral disc and age-associated changes in the nucleus pulposus. *Connect Tissue Res*. 2020;61(1):63-81. doi:10.1080/03008207.2019.1665034

31. Swann DA, Silver FH, Slayter HS, Stafford W, Shore E. The molecular structure and lubricating activity of lubricin isolated from bovine and human synovial fluids. *Biochem J*. 1985;225(1):195-201. doi:10.1042/bj2250195

32. Ogawa H, Kozhemyakina E, Hung HH, Grodzinsky AJ, Lassar AB. Mechanical motion promotes expression of Prg4 in articular cartilage via multiple CREB-dependent, fluid flow shear stress-induced signaling pathways. *Genes Dev*. 2014;28(2):127-139. doi:10.1101/gad.231969.113

33. Shine KM, Spector M. The presence and distribution of lubricin in the caprine intervertebral disc. *J Orthop Res*. 2008;26(10):1398-1406. doi:10.1002/jor.20614

34. Gantenbein B, Illien-Jünger S, Chan S, et al. Organ Culture Bioreactors – Platforms to Study Human Intervertebral Disc Degeneration and Regenerative Therapy. *Curr Stem Cell Res Ther*. 2015;10(4):339-352. doi:10.2174/1574888x10666150312102948

35. Walter BA, Illien-Jünger S, Nasser PR, Hecht AC, Iatridis JC. Development and validation of a bioreactor system for dynamic loading and mechanical characterization of whole human intervertebral discs in organ culture. *J Biomech*.

2014;47(9):2095-2101. doi:10.1016/j.jbiomech.2014.03.015

36. Korecki CL, MacLean JJ, Iatridis JC. Characterization of an in vitro intervertebral disc organ culture system. *Eur Spine J*. 2007;16(7):1029-1037. doi:10.1007/s00586-007-0327-9

37. Le Maitre CL, Fotheringham AP, Freemont AJ, Hoyland JA. Development of an in vitro model to test the efficacy of novel therapies for IVD degeneration. *J Tissue Eng Regen Med*. 2009;3(6):461-469. doi:10.1002/term.180

38. Koussounadis A, Langdon SP, Um IH, Harrison DJ, Smith VA. Relationship between differentially expressed mRNA and mRNA-protein correlations in a xenograft model system. *Sci Rep*. 2015;5(1):1-9. doi:10.1038/srep10775

39. Edfors F, Danielsson F, Hallström BM, et al. Gene-specific correlation of RNA and protein levels in human cells and tissues . *Mol Syst Biol*. 2016;12(10):883. doi:10.15252/msb.20167144

40. Trout JJ, Buckwalter JA, Moore KC, Landas SK. Ultrastructureofthe human intervertebral disc. I. Changes in notochordal cells with age. *Tissue Cell*. 1982;14(2):359-369. doi:10.1016/0040-8166(82)90033-7

41. Souter WA, Taylor TK. Sulphated acid mucopolysaccharide metabolism in the rabbit intervertebral disc. *J Bone Jt Surg - Ser B*. 1970;52(2):371-384. doi:10.1302/0301-620X.52B2.371

42. Butler, D; Trafimow, J H; Andersson, G B; McNeill, T W; Huckman MS. Disc degenerate before facets. *Spine (Phila Pa 1976)*. 1990;15(2):111-113.

43. Daly C, Ghosh P, Jenkin G, Oehme D, Goldschlager T. A Review of Animal Models of Intervertebral Disc Degeneration: Pathophysiology, Regeneration, and Translation to the Clinic. *Biomed Res Int*. 2016;2016. doi:10.1155/2016/5952165

44. Alini M, Eisenstein SM, Ito K, et al. Are animal models useful for studying human disc disorders/degeneration? *Eur Spine J*. 2008;17(1):2-19. doi:10.1007/s00586-007-0414-y

45. Elliott DM, Sarver JJ. Young Investigator Award Winner: Validation of the Mouse and Rat Disc as Mechanical Models of the Human Lumbar Disc. *Spine (Phila Pa 1976)*. 2004;29(7):713-722. doi:10.1097/01.BRS.0000116982.19331.EA

46. Sakagami N, Ono W, Ono N. Diverse contribution of Col2a1-expressing cells to the craniofacial skeletal cell lineages. *Orthod Craniofacial Res*. 2017;20(Suppl 1):44-49. doi:10.1111/ocr.12168

47. Ohnishi T, Sudo H, Tsujimoto T, Iwasaki N. Age-related spontaneous lumbar intervertebral disc degeneration in a mouse model. *J Orthop Res*. 2017;36(1):224-232. doi:10.1002/jor.23634

48. Millecamps M, Stone LS. Delayed onset of persistent discogenic axial and radiating pain after a single-level lumbar intervertebral disc injury in mice. *Pain*. 2018;159(9):1843-1855. doi:10.1097/j.pain.0000000000001284

49. Lee S, Millecamps M, Foster DZ, Stone LS. Long-term histological analysis of innervation and macrophage infiltration in a mouse model of intervertebral disc injury–induced low back pain. *J Orthop Res*. 2020;38(6):1238-1247. doi:10.1002/jor.24560

Appendices

Appendix A. Animal Protocol Notice of Approval

Western

2017-154:9:

AUP Number: 2017-154
AUP Title: Mouse Models to Characterize Intervertebral Disc Development and Disc Disease
Yearly Renewal Date: 11/01/2020

The YEARLY RENEWAL to Animal Use Protocol (AUP) 2017-154 has been approved by the Animal Care Committee (ACC), and will be approved through to the above review date.

Please at this time review your AUP with your research team to ensure full understanding by everyone listed within this AUP.

As per your declaration within this approved AUP, you are obligated to ensure that:

1) Animals used in this research project will be cared for in alignment with:
a) Western's Senate MAPPs 7.12, 7.10, and 7.15

http://www.uwo.ca/univsec/policies_procedures/research.html
b) University Council on Animal Care Policies and related Animal Care Committee procedures

http://uwo.ca/research/services/animalethics/animal_care_and_use_policies.html
2) As per UCAC's Animal Use Protocols Policy,
a) this AUP accurately represents intended animal use;
b) external approvals associated with this AUP, including permits and scientific/departmental peer approvals, are complete and accurate;
c) any divergence from this AUP will not be undertaken until the related Protocol Modification is approved by the ACC; and
d) AUP form submissions - Annual Protocol Renewals and Full AUP Renewals - will be submitted and attended to within timeframes outlined by the ACC.

http://uwo.ca/research/services/animalethics/animal_use_protocols.html

3) As per MAPP 7.10 all individuals listed within this AUP as having any hands-on animal contact will

a) be made familiar with and have direct access to this AUP;

b) complete all required CCAC mandatory training ([training@uwo.ca] training@uwo.ca); and

c) be overseen by me to ensure appropriate care and use of animals.

4) As per MAPP 7.15,

a) Practice will align with approved AUP elements;

b) Unrestricted access to all animal areas will be given to ACVS Veterinarians and ACC Leaders;

c) UCAC policies and related ACC procedures will be followed, including but not limited to:

i) Research Animal Procurement
ii) Animal Care and Use Records
iii) Sick Animal Response
iv) Continuing Care Visits

5) As per institutional OH&S policies, all individuals listed within this AUP who will be using or potentially exposed to hazardous materials will have completed in advance the appropriate institutional OH&S training, facility-level training, and reviewed related (M)SDS Sheets, http://www.uwo.ca/hr/learning/required/index.html

Submitted by: Copeman, Laura
on behalf of the Animal Care Committee
University Council on Animal Care

The University of Western Ontario
Animal Care Committee / University Council on Animal Care
London, Ontario Canada N6A 5C1
519-661-2111 x 88792
Fax 519-661-2028
[auspc@uwo.ca]auspc@uwo.caï¿½
http://www.uwo.ca/research/services/animalethics/index.html

Curriculum Vitae

Min Kyu, Mark Kim

I. Post-secondary Education and Degrees

2014-Present **Doctor of Philosophy in Physiology and Pharmacology (Collaborative Training Program in Musculoskeletal Health Research)**
Schulich School of Medicine & Dentistry
Bone and Joint Institute
The University of Western Ontario
London, Ontario, Canada
Supervisor: Dr. Cheryle Séguin, Ph.D.

2010-2014 **Bachelor of Medical Science (BMSc 2014)**
Honours Specialization in Medical Science
Schulich School of Medicine & Dentistry
The University of Western Ontario
London, Ontario, Canada

II. Honours and Awards

2014-Present NSERC Collaborative Research and Training Experience Program Scholarship (Ph.D.)

2018 Cell Biology Poster Award: Physiology and Pharmacology Research Day

2017-2018 The Queen Elizabeth II Graduate Scholarship in Science and Technology

2016-2018 The Ontario Graduate Scholarship (Ph.D.)

2015 Travel Award: 2015 Canadian Connective Tissue Conference

2014-2018 The Western Graduate Research Scholarship

2010 The Western Scholarship of Excellence

III. Contributions to Teaching and Education

2018-2019 Graduate teaching assistant
PHYSIOLOGY 1021: Introduction to Human Physiology

The University of Western Ontario

2014-2016 Graduate teaching assistant
PHYSIOLOGY 2130: Human Physiology
The University of Western Ontario

IV. Student Supervision

Summer 2019 Yevin Cha
Summer NSERC Undergraduate Student Research Awards

2016-2017 Marisa Burns
PHYSIOLOGY 4980: Seminar and Research Project
4th year thesis supervision
The University of Western Ontario

2015-2016 Meaghan Serjeant
PHYSIOLOGY 4980: Seminar and Research Project
4th year thesis supervision
The University of Western Ontario

V. Publications

1) **Kim, M. M.,** Séguin, C. A. (2020) The mechano-response of murine annulus fibrosus cells to cyclic tensile strain is frequency-dependent. Journal of Orthopedic Research Spine. *Accepted July, 2020.*

2) Kerr, G. J., Veras, M. A., **Kim, M. M.,** Séguin, C. A. (2016) Decoding the intervertebral disc: Unravelling the complexities of cell phenotypes and pathways associated with degeneration and mechanotransduction. Seminars in Cell and Developmental Biology.

3) **Kim, M. M.,** Ramachandran, R., Séguin, C. A. (2020) Spatiotemporal and functional characterization of TRPV4 in the murine intervertebral disc. *In preparation.*

VI. Conferences & Internship Presentations

Presentation type underlined

1) **Kim, M. M.,** Ramachandran, R., Séguin, C. A. (November 2019) Spatiotemporal and functional characterization of TRPV4 in the murine intervertebral disc. 2019 Orthopaedic Research Society Philadelphia Spine Research Symposium Skytop, Pennsylvania. Poster Presentation.

2) **Kim, M. M.,** Ramachandran, R., Séguin, C. A. (April 2019) Spatiotemporal and functional characterization of TRPV4 in the murine intervertebral disc. 2019 London Health Research Day, London, Ontario. Poster Presentation.

3) **Kim, M. M.,** Burns, M., Serjeant, M., Séguin, C. A. (May 2018) Characterizing mechanotransduction in annulus fibrosus cells. 2018 NSERC CREATE Annual General Meeting, Kingston, Ontario. Podium Presentation.

4) **Kim, M. M.,** Burns, M., Serjeant, M., Séguin, C. A. (November 2018) Characterization of the cellular response of annulus fibrosus cells to cyclic tensile strain. 2018 Physiology and Pharmacology Research Day, London, Ontario. Poster Presentation. (*recipient of poster award*)

5) **Kim, M. M.,** Burns, M., Serjeant, M., Séguin, C. A. (November 2018) Characterization of the cellular response of annulus fibrosus cells to cyclic tensile strain. CellScale, Waterloo, Ontario. Scientific Internship Presentation.

6) **Kim, M. M.,** Burns, M., Serjeant, M., Séguin, C. A. (May 2018) Characterization of the cellular response of annulus fibrosus cells to cyclic tensile strain. 2018 NSERC CREATE Annual General Meeting, Kingston, Ontario. Podium Presentation.

7) **Kim, M. M.,** Burns, M., Serjeant, M., Séguin, C. A. (May 2018) Characterization of the cellular response of annulus fibrosus cells to cyclic tensile strain. 2018 Canadian Bone and Joint Conference, London, Ontario. Poster Presentation.

8) **Kim, M. M.,** Burns, M., Serjeant, M., Séguin, C. A. (November 2017) Characterization of the cellular response of annulus fibrosus cells to cyclic tensile strain. 2017 Physiology and Pharmacology Research Day, London, Ontario. Poster Presentation.

9) **Kim, M. M.,** Burns, M., Serjeant, M., Séguin, C. A. (May 2017) Characterization of the cellular response of annulus fibrosus cells to cyclic tensile strain. 2017 NSERC CREATE Annual General Meeting, Toronto, Ontario. Podium Presentation.

10) **Kim, M. M.,** Burns, M., Serjeant, M., Séguin, C. A. (April 2017) Characterization of the cellular response of annulus fibrosus cells to cyclic tensile strain. 2017 Gordon Research Seminar – Cartilage Biology and Pathology, Tuscany, Italy. Podium Presentation.

11) **Kim, M. M.,** Burns, M., Serjeant, M., Séguin, C. A. (April 2017) Characterization of the cellular response of annulus fibrosus cells to cyclic tensile strain. 2017 Gordon Research Conference – Cartilage Biology and Pathology, Tuscany, Italy. Poster Presentation.

12) **Kim, M. M.,** Burns, M., Serjeant, M., Séguin, C. A. (January 2017) Characterization of the cellular response of annulus fibrosus cells to cyclic tensile strain. CellScale, Waterloo, Ontario. Scientific Internship Presentation.

13) **Kim, M. M.,** Serjeant, M., Cadieux, C., Tenn N. A., Séguin, C. A. (November 2016) Characterization of the cellular response of annulus fibrosus cells to cyclic tensile strain. 2016 Physiology and Pharmacology Research Day, London, Ontario. Poster Presentation.

14) **Kim, M. M.,** Serjeant, M., Cadieux, C., Tenn N. A., Séguin, C. A. (June 2016) Characterization of the cellular response of annulus fibrosus cells to cyclic tensile strain. 2016 Canadian Connective Tissue Conference, Hamilton, Ontario. Poster Presentation.

15) **Kim, M. M.,** Serjeant, M., Cadieux, C., Tenn N. A., Séguin, C. A. (April 2016) Characterization of the cellular response of annulus fibrosus cells to cyclic tensile strain. 2016 Canadian Bone and Joint Conference, London, Ontario. Poster Presentation.

16) **Kim, M. M.,** Serjeant, M., Cadieux, C., Tenn N. A., Séguin, C. A. (March 2016) Characterization of the cellular response of annulus fibrosus cells to cyclic tensile strain. 2016 London Health Research Day, London, Ontario. Poster Presentation.

17) **Kim, M. M.,** Cadieux, C., Tenn N. A., Séguin, C. A. (November 2015) Characterization of the cellular response of annulus fibrosus cells to cyclic tensile strain. ORS 3rd International Philadelphia Spine Research Symposium, Philadelphia, USA. Poster Presentation.

18) **Kim, M. M.,** Cadieux, C., Tenn N. A., Séguin, C. A. (November 2015) Characterization of the cellular response of annulus fibrosus cells to cyclic tensile strain. 2015 Physiology and Pharmacology Research Day, London, Ontario. Poster Presentation.

19) **Kim, M. M.,** Cadieux, C., Tenn N. A., Séguin, C. A. (May 2015) Characterization of the cellular response of annulus fibrosus cells to cyclic tensile strain. 2015 Bone and Joint Retreat, London, Ontario. Panel Presentation.

20) **Kim, M. M.,** Cadieux, C., Tenn N. A., Séguin, C. A. (May 2015) Characterization of the cellular response of annulus fibrosus cells to cyclic tensile strain. 2015 Canadian Connective Tissue Conference, Québec City, Québec. Poster Presentation. (*recipient of travel award*)